



TECHNISCHE
UNIVERSITÄT
WIEN
Vienna University of Technology

Dissertation

Novel Iron PNP Pincer Complexes in Catalysis

ausgeführt zum Zwecke der Erlangung des akademischen Grades eines
Doktors der technischen Wissenschaften (Dr. techn.)

unter Leitung von

Univ. Prof. Dipl.-Ing. Dr. techn. Karl Kirchner

Institut für Angewandte Synthesechemie E163

eingereicht an der Technischen Universität Wien

Fakultät für Technische Chemie

Von

Dipl.-Ing. Wolfgang Eder

[Redacted]

[Redacted]

[Redacted]

Wien, im Mai 2024



TECHNISCHE
UNIVERSITÄT
WIEN
Vienna University of Technology

Ich habe zur Kenntnis genommen, dass ich zur Drucklegung meiner Arbeit unter der Bezeichnung

Dissertation

nur mit Bewilligung der Prüfungskommission berechtigt bin.

Ich erkläre an Eides statt, dass die vorliegende Arbeit nach den anerkannten Grundsätzen für wissenschaftliche Abhandlungen von mir selbstständig ausgeführt habe und alle verwendeten Hilfsmittel, insbesondere die zugrunde gelegte Literatur, genannt habe.

Weiters erkläre ich, dass ich diese Arbeit bisher weder im In- noch Ausland (einer Beurteilerin/einem Beurteiler zur Begutachtung) in irgendeiner Form als Prüfungsarbeit vorgelegt habe und dass diese Arbeit mit der von den Begutachterinnen/Begutachtern beurteilten Arbeit übereinstimmt.

Wien, im Mai 2024

Danksagung

Als erstes gilt mein Dank **Karl Kirchner**, dass ich meine Dissertation in seiner Forschungsgruppe durchführen durfte. Besonders sein unaufgeregter Führungsstil und die Freiheiten, die er mir während meiner Forschung gegeben hat, werden mir dabei in Erinnerung bleiben. Weiters sei sein noch immer vorhandener Enthusiasmus für die Forschung und seine unermüdliche Rechenarbeit erwähnt, die eine Inspiration für uns alle sein sollten.

Außerdem gilt mein besonderer Dank allen Kolleginnen und Kollegen in der FGKK, für die vielen unvergesslichen Momente während der letzten Jahre und für das beste Arbeitsklima, das man sich wünschen kann. **Ines Blaha** danke ich für die Hilfe bei NMR-Fragen und Gespräche über die Ungereimtheiten der Siliciumchemie. Weiters bleiben mir so manche gemeinsame Synthesen in Erinnerung, bei der explosive Entdeckungen betreffend des pH-Wertes unseres Wassers gemacht wurden. **Nikolaus Gorgas** möchte ich für die Unterstützung mit der PNP-Chemie und die mir (un)vergessenen Abende im Bendl danken. **Daniel Himmelbauer** danke ich für die vielen produktiven Gespräche und lustigen Abende, an denen auch kulturelle Unternehmungen wie lange Nächte bei Museen und gemeinsame Theaterbesuche nicht fehlen durften. Dein Sinn für Gerechtigkeit und deine Würdigung von (schlechten) Wortwitzen sind legendär. Bei **Matthias „Schurl“ Käfer** möchte ich mich für die vielen bereichernden Gespräche über eine Vielzahl unterschiedlicher Themen bedanken. Sein Enthusiasmus für Musik vom Balkan und österreichischer Kartenspielkultur ist ansteckend. Bei **Claudia Rabijasz** bedanke ich mich für ihre Ehrlichkeit und ihre klare Meinung, die sie stets geäußert hat. Dein gelegentliches Probekosten diverser Pizzen gaben mir Sicherheit nie an der Qualität des Mittagessens zu zweifeln. **Heiko Schratzberger** danke ich für die vielen Fachdiskussionen des Team Eisens zu späterer Stunde, welche auch mit Bier- oder Cocktailbegleitung zu dem einen oder anderen Aha-Moment geführt haben. **Florian Thurnher**, meinem Platznachbarn, danke ich für die immer lustige Stimmung in der Bench. Die zahlreichen Ohrwürmer, die du mir gegeben hast und deine manchmal interessante Verwendung des Marltls waren echte Highlights. **Daniel Zobernig** danke ich für zahlreiche Diskussionen und Einblicke über Katalysen und der Manganchemie. Auch wenn du manchmal Wortwitze berechtigter Weise nur mit einem Augenrollen quittiert hast, so waren wir uns in vielen Sachen aufgrund unserer „südösterreichischen Mentalität“ doch einig.

Weiters möchte ich mich bei **Sebastian Rücker**, **Oliver Lugmayr** und **Gergana Sotirova** für diverse Wandertage und gesellige Abende, bei denen ab und zu auch das Busfahren nicht zu kurz kam, bedanken.

Gerald Tomsu danke ich für die Hilfestellung in diversen synthetischen Fragen und, dass er mir nähergebracht hat, wie vielseitig Übersetzungsapps im Internet einsetzbar sind. Weiters waren deine Zeichnungen immer gern gesehener Schmuck auf meiner Abzugsscheibe. **Stefan Weber** möchte ich für seine Unterstützung in vielen Bereichen der Chemie und für eine Vielzahl an Gesprächen über alle möglichen Themen an so manchem geselligen Abend danken. **Matthias Mastalir** und **Mathias Glatz**, durch euch konnte ich viele Dinge in Sachen Synthesechemie und Metallorganische Chemie lernen. Außerdem will ich euch für die zahlreichen lustigen und denkwürdigen Abende, die wir auf der Uni verbracht haben, danken. **Julian Brünig** möchte ich für die vielen netten Unterhaltungen danken, deine mit trockenem Humor dargebrachten Pointen haben mich stets sehr unterhalten. **Dina Iebed** danke ich für die schöne Zeit als meine Sitznachbarin und für die große Unterstützung die sie mir beim Lösen von Kreuzworträtseln gegeben hat.

Mein Dank gilt weiters **Jan Pecak** und **Sarah Fleissner** für viele sachliche Diskussionen und der Messung von HRMS. Unsere gegenseitige Wertschätzung alpiner Likörspezialitäten wird mir auch in Erinnerung bleiben. Außerdem möchte ich mich bei **Flora Jessl**, **Felix Seitz**, **Lukas Eigenschink** und **Michael Luxner** für viele lustige Abende sowie **Julia Bubenik** für einige zündende Synthesen bedanken. Danke auch an **Ronald Alvaro Farrar Tobar** für ein paar Hinweise über die Eigenheiten der spanischen Sprache und für einen neuen Spitznamen. **Berthold Stöger** möchte ich für das Messen und die Hilfe beim Auswerten meiner Kristallstrukturen und für viele interessante Gespräche, nicht zuletzt über das Tauchen, danken.

Peter Weinberger danke ich für viele lustige Geschichten und Unterhaltungen. Weiters möchte ich der gesamten Forschungsgruppe FGPW, im speziellen **Martin Huber**, **Matthias Schöbinger**, **Willi Zeni**, **Sophia Mundigler**, **Jakob Werner** und **Frieda Kapsamer** für lustige Abende und die gute Zusammenarbeit danken. Großer Dank gebührt auch dem nicht-wissenschaftlichen Personal des IAS.

Meinen Eltern und meiner Familie bin ich für ihre große Unterstützung und ihre Geduld sehr dankbar. Abschließend möchte ich **Julia** von tiefstem Herzen danken, dass sie für mich eine so große Stütze, auch während der Durchführung dieser Arbeit, war. Ohne dich wäre vieles nicht möglich gewesen und ich danke dir, dass du immer für mich da bist. Te amo muchísimo!!

Table of Content

Abstract.....	I
Kurzfassung.....	II
1. Introduction	1
1.1. Hydrosilylation.....	2
1.2. The Chalk-Harrod Mechanism.....	3
1.3. Transition Metal Silyl Complexes.....	4
1.4. Hydrosilylation of Alkenes facilitated by Fe Pincer Complexes	7
1.5. Transition metal acetylide complexes	18
1.6. Iron catalyzed alkene dimerization reactions	19
2. Results and Discussion.....	30
2.1. Synthesis of Fe PNP Silyl Complexes	30
2.2. Catalytic Activity of the Fe PNP Silyl Complexes.....	39
2.3. Mechanistic Studies.....	43
2.4. Ligand Exchange Reactions	46
2.5. Fe PNP Acetylide Complexes and their Role in the Dimerization of Alkynes	58
2.6. Fe PNP Pincer Hydride Complexes for the Activation of Carbon Dioxide	67
2.7. Reaction of the Fe PNP Hydride Complexes with Carbon Dioxide	81
3. Conclusion.....	84
4. Experimental	85
4.1. General Procedure for the Hydrosilylation of Alkenes	86
4.2. General Procedure for the Dimerization of Alkynes.....	86
4.3. Syntheses of PNP Fe Silyl Complexes.....	87
4.4. Syntheses of Fe PNP Mono- and Tris(acetylide) Complexes	99
4.5. Synthesis of Fe PNP Acetylide Hydride Complexes.....	102
4.6. Spectroscopic Data of Hydrosilylation Products	114

5.	References	124
6.	List of Abbreviations	138
7.	Curriculum Vitae	140
8.	Published Papers and Conference Contributions	142

Abstract

The synthesis of novel transition metal catalysts is, due to their great importance in synthetic chemistry as well as their indispensability in many industrial processes, an important field of research in organometallic chemistry. In this context, catalytic systems based on precious metals are still ubiquitous. However, due to their scarce natural abundance, leading to supply risks, environmental issues in the extraction process as well as their high prices, recently, research has shifted towards employing base metals in these processes. Thus, iron, as the most abundant transition metal in Earth's crust, plays a key role in the development of more sustainable catalysts. This work is centered on the synthesis and characterization of novel iron PNP pincer complexes and a special focus is laid on their potential as catalysts for transformations such as hydrosilylation of alkenes, Z-selective dimerization of alkynes and activation of CO₂.

In the first part of this study, novel Iron(II)-PNP silyl complexes, featuring η^2 -dihydrogen or η^2 -dialkylsilane ligands are synthesized and $[(\text{PNP}^{\text{NMe}})\text{Fe}(\text{H})(\eta^2\text{-SiEt}_2\text{H}_3)]$ (**4**) was successfully employed for the anti-markovnikov hydrosilylation of allylic and aliphatic alkenes. Moreover, with the help of computational studies, ligand exchange reactions and stoichiometric reactions, a mechanism based on the classical Chalk-Harrod mechanism is proposed.

The second part of this work describes the synthesis and characterization of novel mono- and tris(acetylide) iron-PNP pincer complexes. Their catalytic activity towards the Z-selective dimerization of alkynes is tested and compared to the reactivity of the previously published bis(acetylide) complex. The studies indicate that the spin-state of the employed complex plays a critical role in its ability to perform this transformation.

In the final part of this thesis, based on DFT calculation, a correlation between the hydricity of a series of iron-PNP pincer complexes and their reactivity towards the insertion of CO₂ into the iron-hydride bond of the complex is presented. This correlation shows that the choice of the ancillary ligand plays a crucial role in this transformation. In a next step, the complexes used in this correlation were synthesized and experimentally probed for the activation of CO₂, indicating an excellent agreement between the calculations and the experimental data.

Kurzfassung

Wegen ihrer großen Bedeutung in der Synthesechemie und durch ihre Unabdingbarkeit in vielen industriellen Prozessen ist die Synthese neuer Übergangsmetallkatalysatoren ein wichtiges Forschungsfeld der metallorganischen Chemie. In diesem Kontext sind Systeme, die auf Edelmetallen basieren, noch immer weit verbreitet. Aufgrund ihrer Seltenheit in der Natur, die zu Versorgungsunsicherheiten, zu Umweltproblemen bei der Schürfung und dadurch zu hohen Preisen führen können, wurde jedoch neuer Fokus auf die Erforschung von auf unedlen Metallen basierenden Systemen gelegt. Eisen, als das häufigste Element in der Erdkruste, spielt hierbei eine große Rolle in der Entwicklung von neuen nachhaltigen Katalysatoren. Diese Arbeit konzentriert sich auf die Synthese und Charakterisierung neuer Eisen-PNP-Pincer-Komplexe. Hierbei wird ein besonderes Augenmerk auf das Potential der Verbindungen als Katalysatoren, für Transformationen wie die Hydrosilylierung von Alkenen, die Z-selektive Dimerisierung von Alkinen und die Aktivierung von Kohlendioxid zu fungieren, gelegt.

Der erste Teil der Arbeit beschreibt die Synthese neuer Eisen(II) PNP-Silyl-Komplexe, die η^2 -Diwasserstoff und η^2 -Dialkylsilan Liganden aufweisen. Der Komplex $[(\text{PNP}^{\text{NMe}})\text{Fe}(\text{H})(\eta^2\text{-SiEt}_2\text{H}_3)]$ (**4**) wurde hierbei erfolgreich als Katalysator für die Anti-Markownikow-Hydrosilylierung von allylischen und aliphatischen Alkenen angewendet. Zusätzlich wurde unter Einbeziehung von DFT-Berechnungen, Ligandensubstitutionsreaktionen und stöchiometrischer Reaktionen ein Katalysezyklus basierend auf dem Chalk-Harrod Mechanismus vorgeschlagen.

Der zweite Teil dieser Arbeit beschreibt die Synthese neuartiger Eisen-PNP mono- und tris(Acetylid) Komplexe. Im Verlauf der Studie wurde ihre katalytische Aktivität in der Z-selektiven Dimerisierung von Alkinen getestet und mit den Resultaten des literaturbekannten bis(Acetylid) Komplexes verglichen. Hierbei wurde ein wesentlicher Einfluss des Spin-Zustandes des Komplexes in dessen Fähigkeit die Reaktion zu katalysieren gefunden.

Im letzten Teil der Arbeit wird, basierend auf DFT-Berechnungen, eine Korrelation zwischen der Hydridizität, einer Serie neuer Eisen-PNP-Pincer-Komplexen und deren Reaktivität für die Insertion von CO_2 in die Eisen-Hydrid-Bindung vorgestellt. Diese Korrelation zeigt auf, dass die Wahl des Co-Liganden eine wesentliche Rolle in dieser Transformation spielt. In einem nächsten Schritt wurden die Komplexe, die für die Berechnungen verwendet wurden, synthetisiert, und ihre Reaktivität hinsichtlich der Aktivierung von CO_2 wurde experimentell

getestet. Hierbei zeigte sich, dass sich die experimentellen Daten hervorragend mit den Berechnungen deckte.

1. Introduction

Catalytic transformations are an integral part in synthetic chemistry. Their efficiency as well as selectivity, particularly compared to stoichiometric reactions, is crucial for the sustainable synthesis of fine and bulk chemicals. Thus, catalysis, particularly mediated by transition metals, is widely employed in the industry for a multitude of processes.¹

In this context, platinum group metals (PGM) were predominantly used in the industry. However, recently interests shifted towards employing more abundant, cheaper, and more sustainable first row transition metals. A rationalizing factor would be the overall scarcity of the PGMs, making their extraction difficult and expensive, thereby causing a considerably higher environmental impact. This can be illustrated for example by comparing the global warming potential (GWP) for the extraction of PGMs in contrast to first row transition metals. While the GWP to produce 1 kg of iron is about 1.5 kg equivalents of CO₂ (e-CO₂) and the extraction of 1 kg of nickel amounts to a GWP of 6.5 kg e-CO₂, the GWPs of PGMs are significantly higher, culminating to e.g., 35.100 kg CO₂ equivalents for 1 kg of rhodium mined.^{2,3}

As the most abundant transition metal in the Earth's crust, application of iron in catalysis garnered much interest and extensive research was devoted to the development of iron-based catalysts in recent years.⁴ However, in contrast to the second- and third-row transition metals, the coordination chemistry of first-row transition metals is more complex. These metals tend to undergo facile one-electron redox processes, they are inclined to react uncontrolled with dioxygen and feature complex spin-state interplay, that can lead to facile ligand dissociation and redistribution reactions. Thus, great emphasis has to be given to ligand design to mitigate these drawbacks.^{5,6}

Due to their great stability and modifiability pincer ligands have been established as suitable platforms to gain entry into base metal coordination chemistry. In case of iron, pincer complexes have been successfully introduced to catalyze a multitude of different transformations such as hydrogenation reactions,^{7–14} hydrofunctionalization reactions^{15–18} and small molecule activation.^{19–26} Thus, this work focuses on the implementation of the Fe-PNP Pincer platform in novel fields of catalysis to gain further insight into the reactivity and applicability of novel iron based base metal catalysts.

1.1. Hydrosilylation

Hydrosilylation, i.e. the addition of silicon hydrides across C-C multiple bonds, is an important reaction in silicon chemistry and is widely used for the synthesis of silicon polymers, such as oils and resins, as well as in the synthesis of chemicals utilized in organic synthesis, such as for example in cross-coupling reactions.²⁷ The first known catalysts being employed in this reaction were organic peroxides, which necessitated high catalyst loadings while suffering from low selectivity.²⁸ The discovery of Speier's catalyst ($[\text{H}_2\text{PtCl}_6] \cdot x \text{H}_2\text{O}$) in 1956 greatly improved selectivity, while also requiring drastically decreased catalyst loadings, thus demonstrating the great potential of transition metals in hydrosilylation.²⁹ This was further highlighted by the introduction of Karstedt's catalyst, a Pt(0) vinylsiloxane complex (Figure 1), in 1973, which showed drastically increased solubility as well as activity and selectivity for the hydrosilylation of alkenes.³⁰

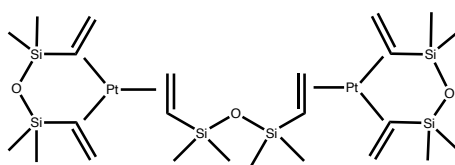


Figure 1 Karstedt's catalyst

These Pt-based siloxanes continue to be widely employed in the industrial synthesis of organo-silicon compounds. However, recently, efforts to obtain effective catalysts utilizing earth abundant base metals such as Fe and Co were made, showing promising results and comparable reactivity to Pt-based catalysts.³¹

In order to stabilize the metal center and control the reactivity of the formed complexes, pincer ligands were successfully employed in the synthesis of novel base metal catalysts. In case of Fe, NNN and PNN pincer showed excellent reactivity for the hydrosilylation of alkenes and alkynes, thus constituting an important class of base metal catalysts.³² However, as of yet, there are no reports in literature on the successful application of Fe complexes, based on the common PNP pincer scaffold, in the hydrosilylation chemistry of alkenes and alkynes. This detail served as motivation to investigate the reactivity of these complexes with silanes, alkenes and alkynes in order to establish novel catalytic pathways and expanding the knowledge in base metal hydrosilylation chemistry.

1.2. The Chalk-Harrod Mechanism

Transition metal mediated hydrosilylation of alkenes is generally proposed to proceed through the Chalk-Harrod mechanism, which was first proposed by Chalk and Harrod in their groundbreaking study of 1965.³³

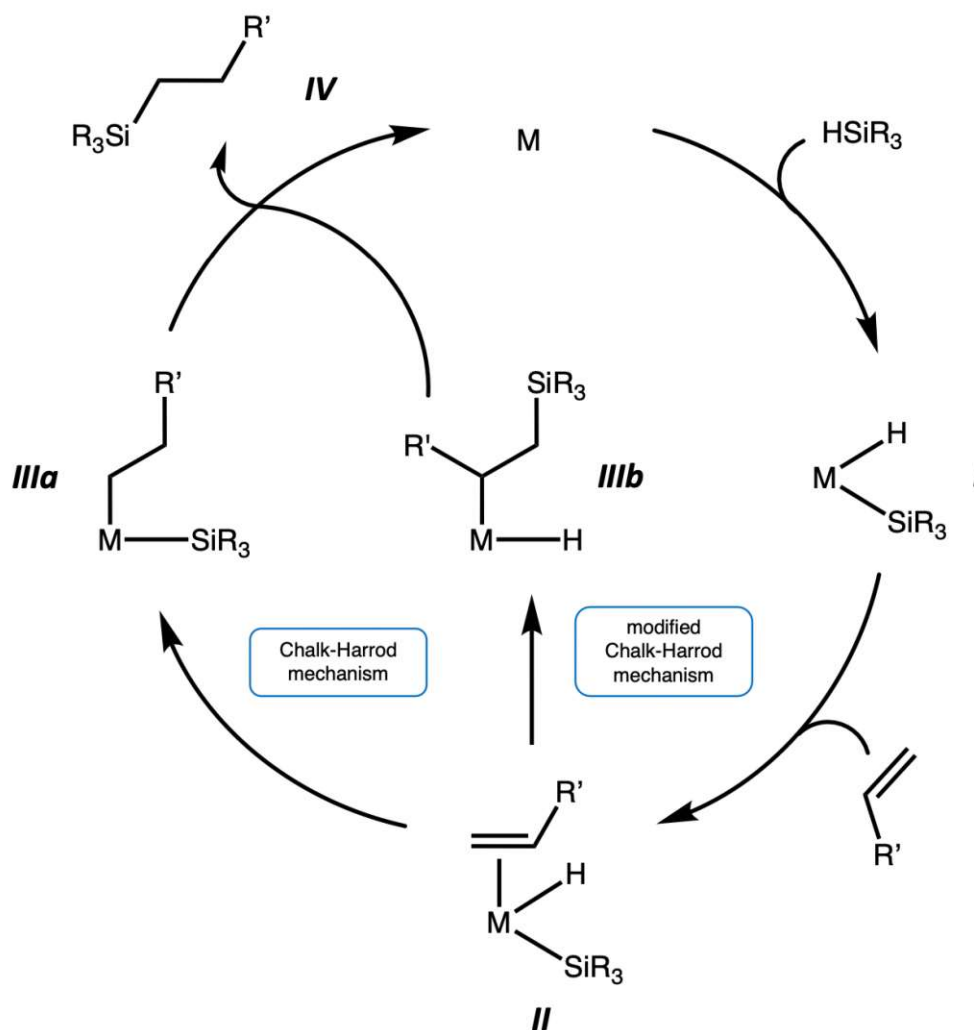


Figure 2 Catalytic cycle of hydrosilylation of alkenes based on the Chalk and Harrod mechanisms

As illustrated in Figure 2, in the first step of the catalytic cycle, low valent transition metal complexes are thought to undergo oxidative addition with silicon-hydrides affording complexes. The oxidative addition is proposed to occur in intermediacy of η^2 -Si-H- σ -complexes (*vide infra*). (**I**) These complexes can then react with olefines to form the corresponding saturated transition metal-alkene π -complexes. (**II**). In the original Chalk-Harrod mechanism, migratory insertion of the coordinated alkene into the metal-hydride bond leads to silyl-alkyl complexes. (**IIIa**) However, as vinyl- or allylsilanes are a common side

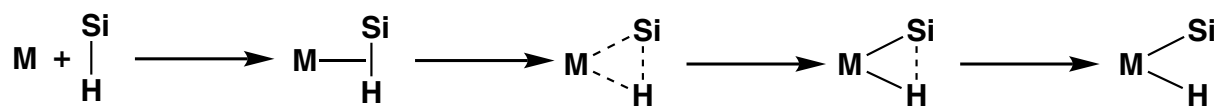
product of catalytic hydrosilylation, a modified Chalk-Harrod mechanism was also proposed, explaining possible isomerization and/or formation of unsaturated hydrosilylation products. In this modified mechanism, migratory insertion of the coordinated alkene into the metal-silyl bond occurs, affording alkyl-hydride complexes. (*IIIb*) In the final step of the cycle, reductive elimination leads to the liberation of the hydrosilylated product, regenerating the low valent metal catalyst. (*IV*)

1.3. Transition Metal Silyl Complexes

Since transition metal complexes with silane ligands are often encountered during hydrosilylation processes they are ubiquitous in literature and much research was devoted to them.^{34–36} The biggest group among transition metal silane complexes constitute metal silyl complexes that are formed *via* the oxidative addition of hydrosilanes onto low valent transition metal fragments.³⁵

The oxidative addition of silicon hydrides is initiated by the interaction of the transition metal with the hydrosilane forming a weak σ -complex. This σ -complex can be regarded to feature a two electron-three center bond. Sufficient back bonding by the low valent transition metal into the antibonding Si-H σ^* -orbital leads to cleavage of the Si-H bond thus forming a silicon-metal σ -bond and creating a transition metal silyl hydride complex. (Scheme 11)

If the electron density of the transition metal is not sufficient to complete the oxidative addition reaction, the η^2 -Si-H- σ -complexes can also be isolated and characterized.³⁵

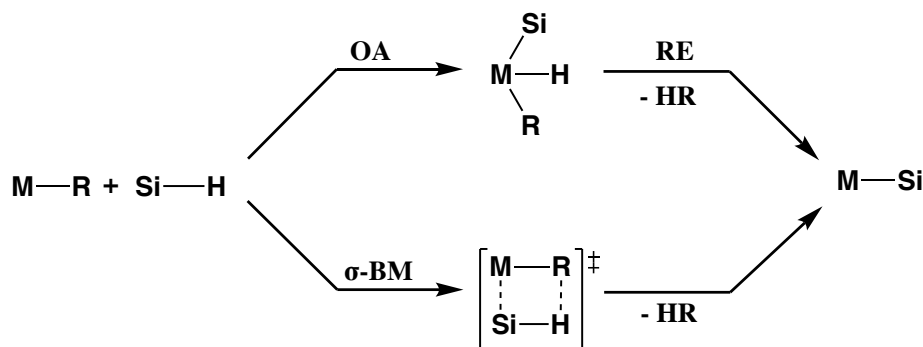


Scheme 11 Idealized sequence for the oxidative addition of a hydrosilane to a transition metal

In some cases, this oxidative addition reaction is followed by the rapid reductive elimination of the formed hydride with another coordinated ligand, eliminating small molecules such as H_2 , alkanes or hydrogen halides, thus affording transition metal silyl complexes instead of silyl hydrides.

Early transition metals, generally lacking the electron density needed for the oxidative addition reaction, also can form transition metal silyl complexes *via* σ -bond metathesis reactions. The σ -bond metathesis is thought to proceed in a concerted fashion *via* a four

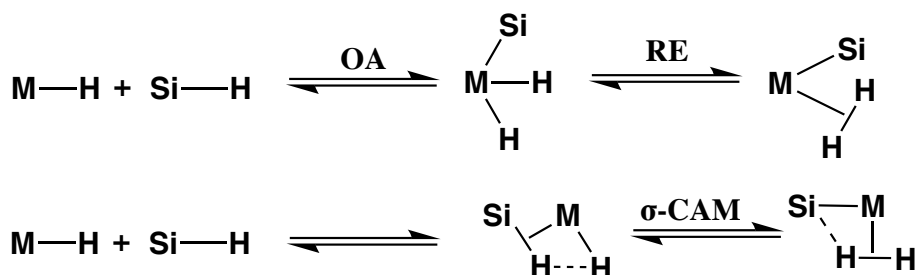
centered transition state, and formally constitutes a $[2\sigma + 2\sigma]$ cycloaddition of a metal ligand bond with the silane. Subsequently, the metal silyl complex is generated in addition to elimination of small molecules such as H_2 or alkanes. (Scheme 12)^{35,37}



Scheme 12 Oxidative addition (OA) of a hydrosilane and subsequent reductive elimination (RE) as well as σ -bond metathesis (σ -BM)

To allow for an alternative reaction mechanism in which silyl complexes are formed with late transition metals, without the need of the metal to change its oxidation state, σ -complex assisted metathesis (σ -CAM) was introduced by *Perutz and Sabo-Etienne* in 2007.³⁸ This mechanism was based on previous observations showing that transition metal hydride-dihydrogen complexes showed fluxional behavior in solution. This behavior was shown to not occur due to oxidative addition of dihydrogen to the metal center, but rather *via* the rapid dynamic rearrangement of discrete σ -complexes on the metal center.^{39,40} Similar behavior was later also observed in dihydrogen silyl complexes, inspiring the proposal of a general σ -CAM mechanism.^{38,41}

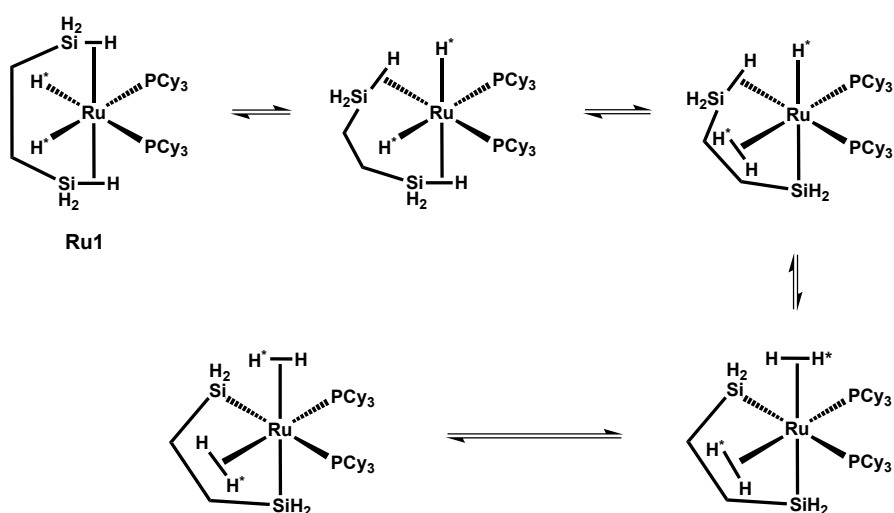
The proposed σ -CAM mechanism differs from traditional σ -bond metathesis by the presence of discrete σ -complex intermediates, which are not observed in traditional σ -bond metathesis, as the four centered state in the traditional σ -bond metathesis reaction is not an intermediate but rather a transition state. The formation of the silyl complex is then achieved by dynamic rearrangement of the initially formed η^2 -Si-H- σ -complex into a η^2 -H₂- σ -complex, forming a metal silane σ -bond. While a mechanism based on oxidative addition/reductive elimination also features discrete σ -complexes, it differs from σ -CAM by its need for the change of the oxidation state of the metal.^{35,37} (Scheme 13)



Scheme 13 Oxidative addition (OA) and subsequent reductive elimination (RE) of a silane to form dihydrogen-silyl complexes compared to σ -complex assisted metathesis (σ -CAM)

During studies of distribution processes of Ru-Silane σ -complexes, short interactions of silicon to ancillary hydride ligands were observed in X-ray diffraction studies. These secondary interactions were shown to stabilize the complex while the proximity of the silicon atom of the η^2 -Si-H moiety to hydride ligands provide the possibility of intramolecular exchange processes, thus providing a pathway for σ -CAM pathways.

These secondary interactions were coined SISHA (secondary interactions between silicon and hydrogen atoms) and were deemed crucial for the ligand metathesis of silanes and hydrides on the ruthenium bisphosphine complex **Ru1**. (Scheme 14) It was shown that the SISHA interactions provide a pathway for the formation of new σ -bonds without the need of decoordination of the ligands.^{42–44} These secondary interactions are also in line with silicon being able to form hypervalent compounds.^{45,46}



Scheme 14 Rapid intramolecular metathesis of ligands via σ -CAM mechanism facilitated by SISHA interactions.

Generally, SISHA interactions are designated by the measured distance of the silicon atom to the coordinated hydride ligands. Non-coordinated Si-H bond lengths generally are in the

range of 140-150 pm^[47], while η^2 -Si-H coordination of the silane bond to form σ -complexes increases the bond length to 170-180 pm.^[36,47] A bond distance of 190-240 pm is characteristic for SISHA and related secondary interactions of silicon to hydrides.^{46,48} Silicon hydrogen bond distances that are greater than 250 pm are regarded as non-binding.^{35,47}

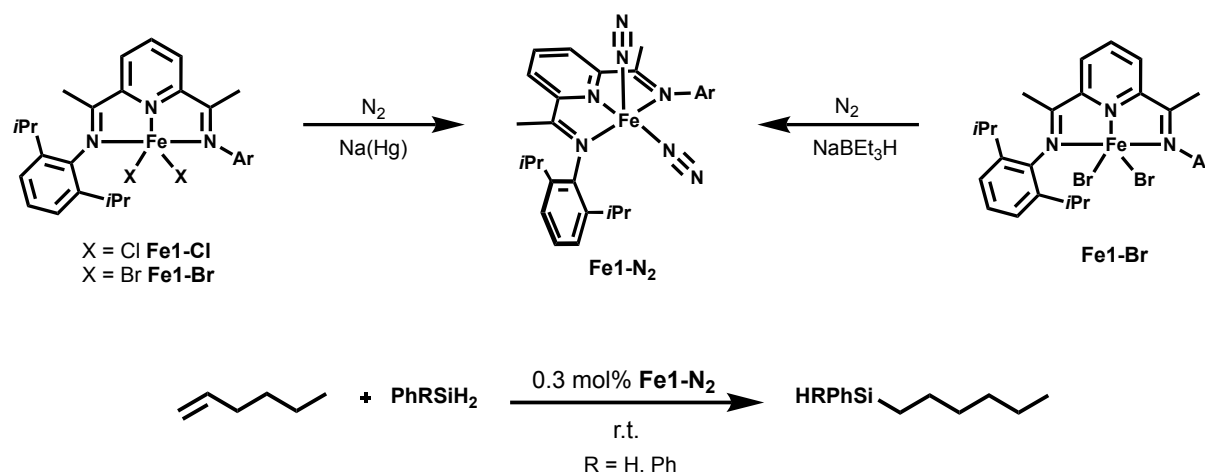
1.4. Hydrosilylation of Alkenes facilitated by Fe Pincer Complexes

The first reports of alkene hydrosilylation facilitated by an Fe complex were reported in 1962. Treatment of terminal alkenes and tertiary silanes in presence of $[\text{Fe}(\text{CO})_5]$ at 100-140 °C yielded a mixture of hydrosilylation as well as dehydrogenative silylation products.⁴⁹ Further studies utilizing UV radiation, established the active catalyst to be $[\text{Fe}(\text{CO})_3]$, which is generated *in situ*.^{50,51}

These findings inspired *Chirik* in 2004 to utilize dihalide Fe-complexes featuring NNN pincer ligands based on substituted bis(imino)pyridine scaffolds (PDI^{Ar}), which previously were successfully employed in the polymerization of ethylene.^{31,52}

The strongly π -acidic PDI^{Ar} ligands were chosen to function as a modifiable substitute for carbonyl ligands. The unsaturated 14-electron fragment $[\text{Fe}(\text{CO})_3]$ was intended to be mirrored by the isolobal $[\text{PDI}^{\text{Ar}}\text{Fe}]$ fragment, generated by reduction of the $\text{PDI}^{\text{Ar}}\text{Fe}$ -dihalide species.³¹

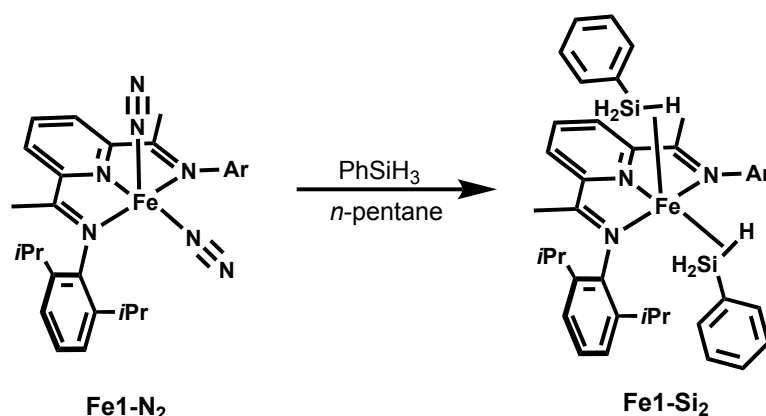
The reduction was achieved under N_2 atmosphere by treating the dihalide complexes $[(\text{PDI}^{\text{Ar}})\text{FeBr}_2]$ **Fe1-Br** and $[(\text{PDI}^{\text{Ar}})\text{FeCl}_2]$ **Fe1-Cl** with sodium amalgam, or by treating the dibromo complex **Fe1-Br** with two equivalents of NaBEt_3H , creating the complex $[(\text{PDI}^{\text{Ar}})\text{Fe}(\text{N}_2)_2]$ **Fe1-N₂**.⁵³ (Scheme 1)



Scheme 2 Synthesis of NNN Fe complex **Fe1-N₂** and catalytic hydrosilylation of 1-hexene

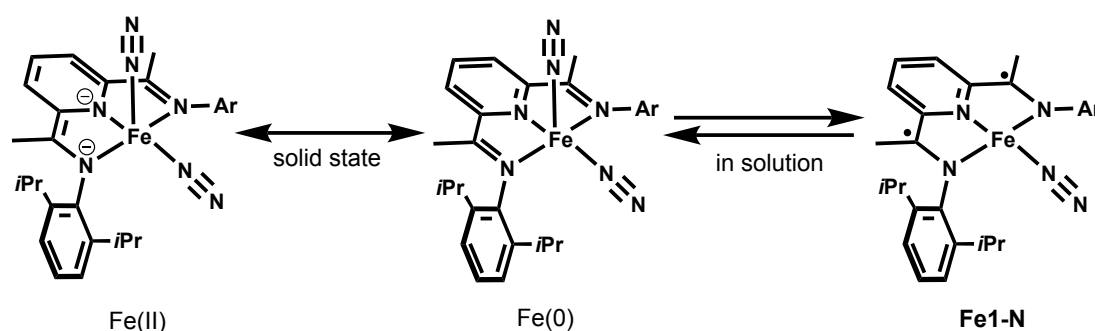
Fe1-N₂ was shown to be active for the hydrogenation of various terminal and substituted alkenes as well as internal alkynes under mild conditions.

Furthermore, **Fe1-N₂** was also shown to be an active precatalyst for the hydrosilylation of olefines. Utilizing phenylsilane and diphenylsilane, terminal as well as internal and *gem*-disubstituted alkenes were readily converted with a catalyst loading of 0.3 mol% at room temperature, achieving TOFs of up to 364 h⁻¹. The reaction selectively produced only the anti-markovnikov hydrosilylation products, while no products arising from dehydrogenative hydrosilylation were observed. Treatment of **Fe1-N₂** with an excess of phenylsilane gave the complex [(PDI^{Ar})Fe(η²-SiH₃Ph)₂] **Fe1-Si₂** (Scheme 2), which also proved to be an active precatalyst for the hydrosilylation of 1-hexene.⁵³



Scheme 2 Synthesis of NNN Fe complex **Fe1-Si₂**

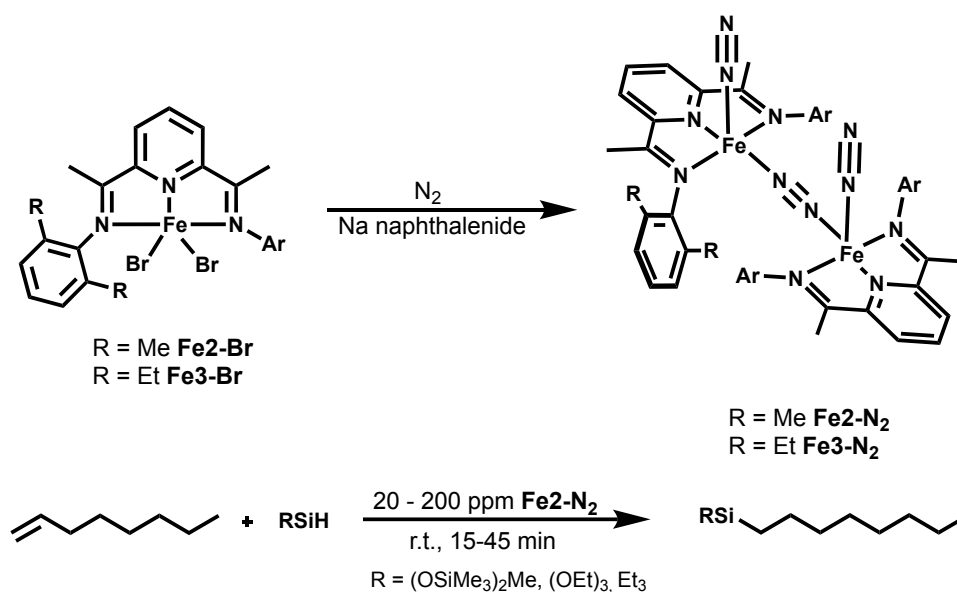
Both **Fe1-N₂** and **Fe1-Si₂** were preliminarily assigned as Fe(0) species. However, given their unusual properties in NMR spectroscopy, indicating accessible $S = 1$ states, further detailed studies utilizing Mössbauer and NMR spectroscopy, single crystal X-ray diffraction studies as well as DFT calculations were conducted. It was determined, that complex **Fe1-N₂** is best described as a hybrid between the Fe(0) and Fe(II) canonical forms. The temperature dependent, unusual NMR shift of **Fe1-N₂** can be explained by thermal population of a triplet excited state. In solution the complex readily loses one dinitrogen ligand yielding the four-coordinated complex **Fe1-N** (Scheme 3). This complex can be regarded as an intermediate spin Fe(II) complex, where two electrons have been transferred to the ligand, creating a triplet diradical ion that is antiferromagnetically coupled to the metal center, emphasizing the redox non-innocent character of the bis(imino)pyridine based ligand. (Scheme 3)⁵⁴



Scheme 3 Electronic structure of **Fe1-N₂** and **Fe1-N**

While **Fe1-N₂** showed excellent reactivity and selectivity in the hydrosilylation of unactivated olefins with primary and secondary silanes, no reaction was observed when using Et₃SiH. In contrast to that, tertiary silanes are commercially the most relevant class of silicon-hydride reagents in hydrosilylation. This is due to the fact that products generated by using both primary and secondary silanes still feature residual Si-H bonds after the reaction, which can function as catalyst poison and lower the stability of the generated products.⁵⁵

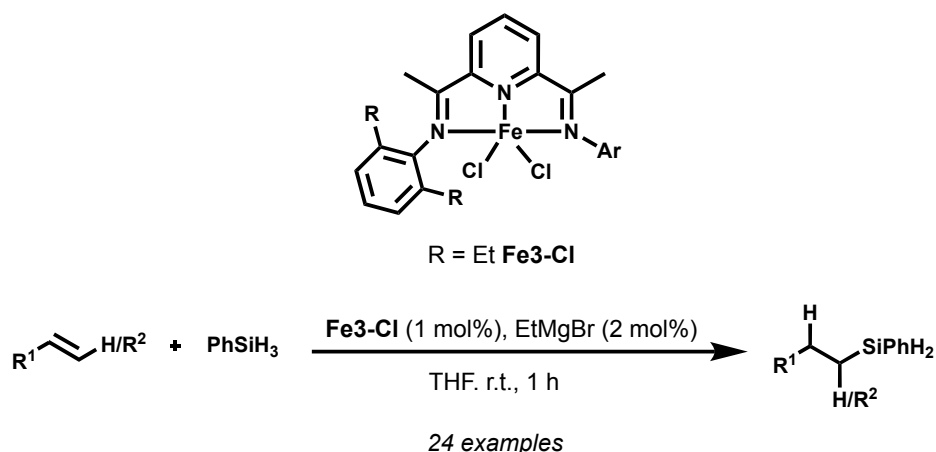
In 2012, to circumvent this problem, *Chirik* and coworkers employed Fe complexes featuring a new class of bis(imino)pyridine based NNN ligands, with smaller substituents on the aryl moieties bound to the imine groups, which previously showed increased reactivity in the catalytic hydrogenation of difficult alkene substrates.^{55,56}



Scheme 4 Synthesis of **Fe2- N_2** and **Fe3- N_2** and hydrosilylation of 1-octene with tertiary silanes by **Fe2- N_2**

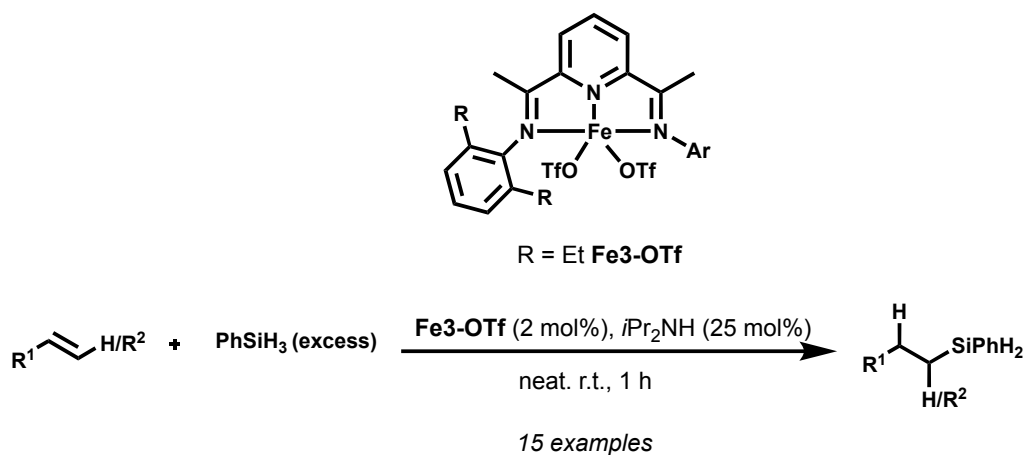
These complexes were synthesized similarly to their *i*Pr congener **Fe1- N_2** by the reduction of the corresponding dihalide complexes $[(\text{PDI}^{\text{Me}})\text{FeBr}_2]$ **Fe2-Br** and $[(\text{PDI}^{\text{Et}})\text{FeBr}_2]$ **Fe3-Br** using sodium naphthalenide in THF under nitrogen atmosphere.¹⁵ While complex $[(\text{PDI}^{\text{Et}})\text{Fe}(\text{N}_2)(\mu^2\text{-N}_2)]$ **Fe3- N_2** showed only slightly improved activity compared to **Fe1- N_2** , the sterically less encumbered complex $[(\text{PDI}^{\text{Me}})\text{Fe}(\text{N}_2)(\mu^2\text{-N}_2)]$ **Fe2- N_2** showed excellent activity and selectivity as a precatalyst for the hydrosilylation of 1-octene and styrene, even when utilizing Et_3SiH as silane. (Scheme 4) Full conversion with Et_3SiH was achieved at room temperature in 45 minutes with a catalyst loading of 200 ppm, thereby offering advantages in reactivity and selectivity to commonly used precious metal catalysts. Furthermore, it was shown that the catalyst was capable of crosslinking the two commercially important silicon fluids SilForce SL6100 and SilForce SL6020 at room temperature with a catalyst loading of 1000 ppm.⁵⁵

The group of *Thomas* showed in 2014, that catalyst **Fe3-Cl** could also be utilized for the hydrosilylation of alkenes and alkynes, without the need of reduction under nitrogen atmosphere. They showed that simple addition of EtMgBr to the reaction mixture was sufficient to activate the catalyst. The catalyst also featured good functional group tolerance, successfully converting substrates bearing ketone, ester, imine, imide as well as nitrile functionalities. (Scheme 5)⁵⁷



Scheme 5 Hydrosilylation of alkenes using **Fe3-Cl** with Grignard reagents as activator.

This concept was developed further by *Thomas* in 2016 showing that the benchstable precatalyst **Fe3-OTf** could also be activated using an excess of organic amines under aerobic conditions. It was demonstrated that the activation of the precatalyst occurs through a radical mechanism. By conducting the reaction neat and using an excess of silane, high selectivity and good functional group tolerance was achieved. (Scheme 6) It was further shown that 1-octene could be converted in gram scale with 0.25 mol% of catalyst in the presence of air in 10 minutes.⁵⁸



Scheme 6 Hydrosilylation of alkenes using **Fe3-OTf** with organic amines as activator.

In 2017 *Thomas* and coworkers showed that **Fe3-Cl** could also be directly utilized in the hydrosilylation of 1-octene with $(EtO)_3SiH$ under aerobic conditions and in gram scale. By utilizing air stable NaO^tBu as activator, full conversion to anti-markovnikov products could be achieved with a catalyst loading of merely 93 ppm.⁵⁹

In 2012, the groups of *Nakazawa* and *Chirik* published results of iron complexes based on terpyridine ligands that were effective in the anti-markonvnikov hydrosilylation of 1-hexene and 1-octene. (Figure 1) ^{60,61}

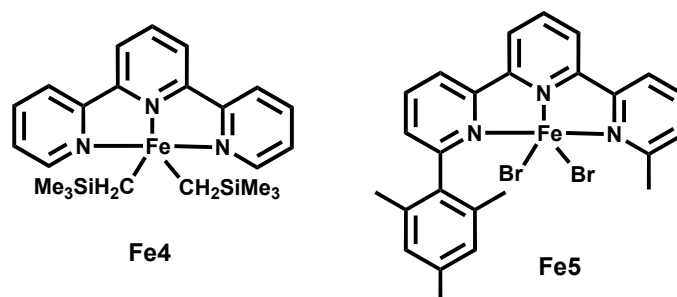


Figure. 1 Terpyridine based Fe-complexes for the hydrosilylation of 1-hexene and 1-octene

In contrast to the previously employed mostly air-sensitive catalysts based on the bis(imino)pyridine scaffold, catalysts **Fe4** and **Fe5** are air stable. **Fe4** was successfully employed in the hydrosilylation of 1-octene with methyl-bis(trimethylsilyloxy)silane (MD'M) and Et₃SiH. The catalyst loading had to be increased to 0.5 mol%, while the reaction temperature was increased to 60 °C. Moreover, the electronic structure of **Fe4** was investigated by means of Mössbauer spectroscopy and DFT calculations, revealing that the complex is best described as high-spin Fe(III) compound with antiferromagnetic coupling of a ligand radical anion.⁶⁰

The group of *Nakazawa* introduced a series of unsymmetrically substituted Fe terpyridine complexes and investigated them for the hydrosilylation of 1-hexene and 1-octene with PhSiH₃ and Ph₂SiH₂. The di-halide complexes were activated to the active species by reaction with two equivalents of NaBEt₃H, yielding tentative dihydride complexes. **Fe5** was shown to be the complex achieving highest reactivity, achieving TONs of 1533 for the hydrosilylation of 1-octene with PhSiH₃. While the catalyst loading could be reduced to 0.05 mol%, the reaction required high temperatures of 100 °C. Interestingly, the corresponding unsubstituted terpyridine dihalide complex was also probed as precatalyst in the reaction, without showing any reactivity.⁶¹

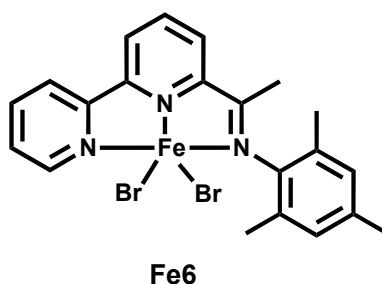
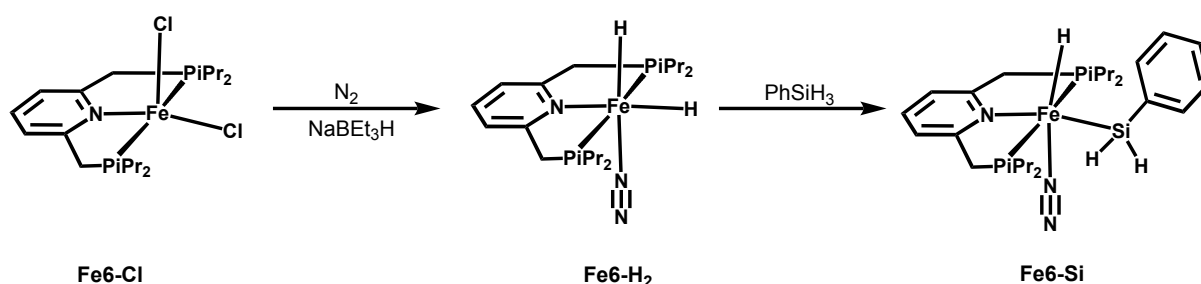


Figure. 2 (Imino)bipyridine based Fe-complexes for the hydrosilylation of cyclohexene and 1-octene

In 2015 the group of *Nakazawa* introduced catalysts based on iminobipyridine. (Figure 2) These complexes showed improved reactivity in the hydrosilylation of 1-octene, and cyclohexene compared to the systems based on terpyridine. Utilizing NaBEt_3H as an activator, **Fe6**, at a catalyst loading of 0.1 mol% at room temperature achieved TON of 1786 for the hydrosilylation of 1-octene and 1049 for the hydrosilylation of cyclohexene with phenylsilane.⁶²

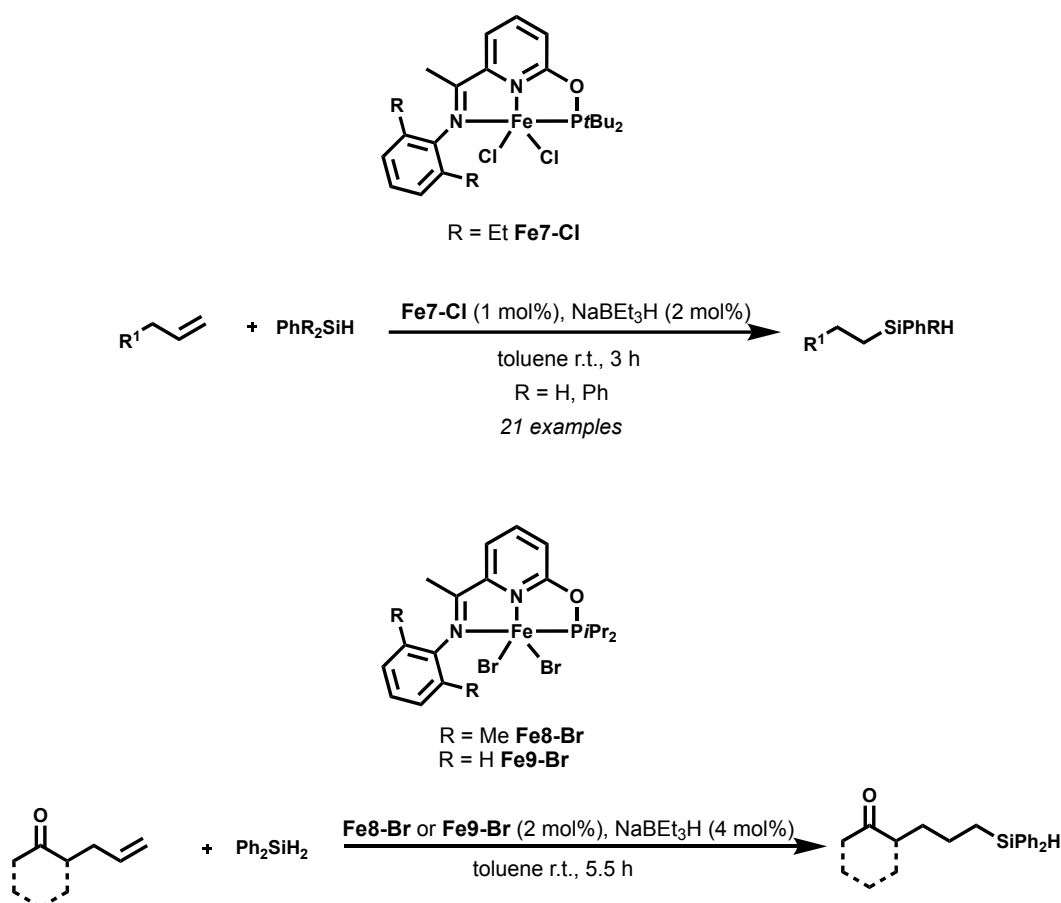


Scheme 7 Synthesis of PNP hydride and silyl complexes

Due to the successful implementation of these nitrogen-based pincer compounds, *Chirik* extended these concepts to other common pincer systems containing phosphorus donors. In 2006 a series of PNP pincer complexes were synthesized and probed for the catalytic hydrogenation and hydrosilylation of alkenes. Treatment of the complex $[(\text{PNP}^{\text{CH}_2})\text{FeCl}_2]$ (**Fe6-Cl**) with 2 equivalents of NaBEt_3H under nitrogen atmosphere yielded the ferrous dihydride complex $[(\text{PNP}^{\text{CH}_2})\text{Fe}(\text{H})_2(\text{N}_2)]$ (**Fe6-H₂**) in 36 % yield. Attempting the reduction

of **Fe6-Cl** analogously to **Fe1-N₂** did not yield any tractable products. It was reasoned that the more electron rich iron center of **Fe6-H₂**, facilitated by the phosphine donor groups, stabilizes the dihydride complex, thus preventing reductive elimination of dihydrogen and formation of a Fe(0) dinitrogen complex. **Fe6-H₂** furthermore showed drastically decreased reactivity in the hydrogenation of unactivated alkenes compared to **Fe1-N₂**.

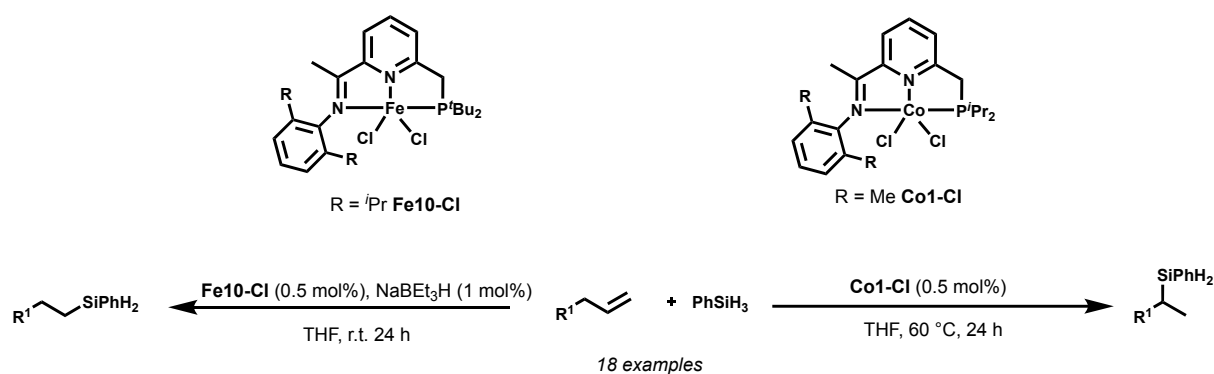
Treatment of **Fe6-H₂** with one equivalent of PhSiH₃ yielded the silyl-complex [(PNP^{CH₂})Fe(H)(SiPhH₂)(N₂)] **Fe6-Si** as the only product. (Scheme 7) This ferrous silyl hydride complex showed no reactivity in the hydrosilylation of alkenes. Treatment of **Fe6-H₂** and **Fe6-Si** with 4 atm of H₂ led to gradual replacement of the coordinated dinitrogen ligand and to the formation of tentative η^2 -dihydrogen complexes that were in rapid exchange with the iron hydride ligands in solution. These complexes could not be isolated due to the higher affinity of the iron center to dinitrogen as opposed to dihydrogen.⁶³



Scheme 8 Reactivity of Fe-PNN pincer complexes for the hydrosilylation of alkenes

Based on the findings of *Chirik* the group of *Huang* introduced a series of novel Fe-PNN pincer complexes in 2013 aiming to combine the reactivity of the bis(imino)pyridine-based ligands in hydrosilylation with the increased stability of the complexes provided by more electron-donating phosphine moieties. Complex **Fe7-Cl** was successfully employed in the hydrosilylation of a series of alkenes showing good functional group tolerance, as esters, amides and amines were readily tolerated. It was further shown that the introduction of the electron donating phosphine moieties reduced the oxophilicity of the iron center, making it possible to selectively hydrosilylate the double bond of alkenes featuring ketone-groups, while the bis(imino)pyridine based systems predominately reduced the carbonyl moieties.⁶⁴ (Scheme 8)

However, due to the relatively low stability of the reported PNN pincer complexes, which can be attributed to the easy degradation of the P-O bond, a new series of carbon linked congeneric PNN pincer complexes was reported by *Huang* in 2016 and tested in the hydrosilylation of alkenes. They showed improved activity for this transformation compared to the previously reported oxygen-linked catalysts, allowing to halve the catalyst loading for the catalysis. Moreover, it was shown that while the Fe-pincer complexes selectively promote anti-markovnikov addition of the silane, the corresponding complexes synthesized with CoCl_2 selectively promoted the markovnikov addition, highlighting the regiodivergent catalytic properties of these complexes. (Scheme 9)⁶⁵



Scheme 9 Regiodivergent hydrosilylation of alkenes promoted by Fe and Co PNN pincer complexes

The group of *Yuge* published a series of novel PNN pincer complexes in 2018 and successfully employed them in the borylation of arenes.^{66,67} Inspired by the approaches of *Thomas* (vide supra), with Fe, and *Chirik*^{68,69}, with Co, to promote hydrosilylation using air stable reagents they synthesized a series of Fe(II) alkyl and carboxylate complexes and probed

them in the hydrosilylation of alkenes in absence of activator. (Figure 3) Complexes **Fe11** and **Fe12** showed excellent reactivities for the hydrosilylation of 1-octene with phenylsilane with **Fe11** achieving TOFs of up to 90.000 h^{-1} , thus outperforming **Fe12**. (TOF: 5000 h^{-1}) However, **Fe11** showed rapid catalyst degradation when the reaction was conducted in aerobic conditions, while **Fe12** showed no decrease in reactivity. Stoichiometric studies with 1-dodecene and phenylsilane, showed no evidence for the formation of a Fe(0) species, suggesting the formation of a silyl hydride complex as catalytically active species.⁷⁰

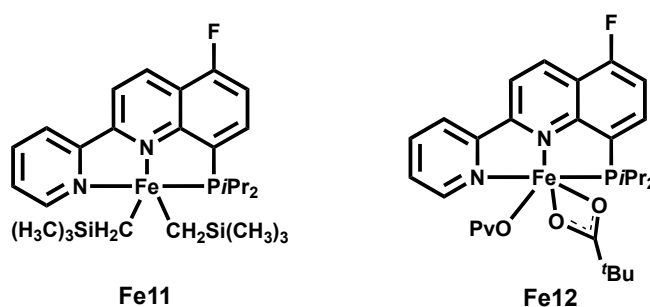
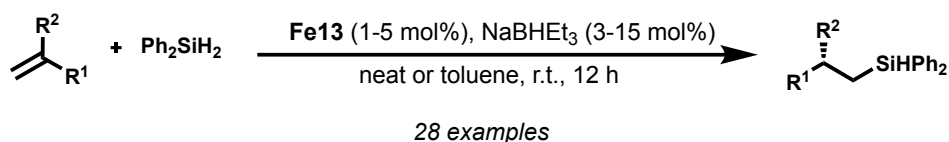
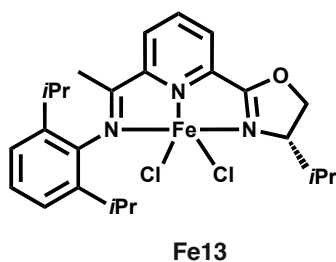


Figure. 3 PNN-Fe complexes used in the activator-free hydrosilylation of 1-octene

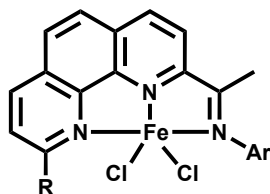
More detailed experimental and mechanistic studies were conducted in 2020, indicating a negative correlation between the steric bulk of the substituents of the phosphine donor and catalytic conversions in the series $^i\text{Pr} > \text{Ph} > \text{Cy}$. Furthermore, a catalytic cycle was proposed based on a modified Chalk-Harrod mechanism, also accounting for the formation of unwanted side products caused by isomerization and dehydrogenative hydrosilylation.⁷¹

In 2015 *Lu* reported the asymmetric hydrosilylation of 1,1-disubstituted alkenes employing a series of chiral Fe and Co NNN pincer complexes based on iminopyridine oxazoline scaffolds, that were previously employed in the enantioselective hydroboration of 1,1-disubstituted aryl alkenes by *Huang*^{72,73}

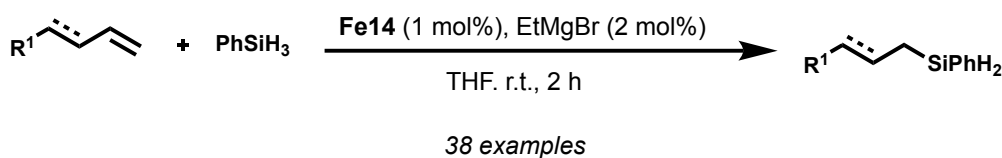


Scheme 10 Asymmetric hydrosilylation of 1,1 disubstituted alkenes using **Fe13**

Complex **Fe13**, after activation with 3 equiv. of NaBHET_3H , showed excellent reactivity for the reaction. Electron-rich styrenes featuring ortho-, meta-, and para-substitutions afforded hydrosilylated products with good yields and excellent ee values. (Scheme 11) Acetal protected aldehydes and ketones as well as imines were also readily converted with good ee, however substrates containing two alkyl substituents showed only poor enantiomeric excess.⁷³



R = Mes, Ar = 2,6 $\text{Et}_2\text{C}_6\text{H}_3$ **Fe14**



Scheme 11 Hydrosilylation of terminal alkenes and conjugated dienes using **Fe14**

In 2022, the group of *Zhu* published the iron catalyzed hydrosilylation of terminal alkenes as well as conjugated dienes employing a ligand system based on phenanthroline imines employing a catalyst loading of 1 mol%. The dihalide

complexes were transformed to the catalytically active species by the addition of EtMgBr.

The catalyst showed good selectivity for the anti-markovnikov hydrosilylation of the substrates. Mechanistic studies indicated a Chalk-Harrod mechanism involving a Fe(II)/Fe(0) redox cycle, with steric crowding induced by the bulky ligand being responsible for the excellent selectivity shown in the catalysis.⁷⁴

1.5. Transition Metal Acetylide Complexes

While alkynes can bond to transition metals in various ways e.g. in η^2 -C \equiv C or η^2 - η^2 bridging fashion⁷⁵, in this chapter the terminal bonding mode of acetylides (η^1 -alkynes) is discussed. Acetylides function as strong σ -donor ligands, however even though they are isoelectronic to cyanide and isocyanides, they are seen as only weakly π -accepting ligands, as the π^* -orbitals of the non-polarized C \equiv C triple bond have higher energy than the corresponding orbitals of the C \equiv N bond cyanide. Indeed, in some cases acetylides can be regarded as π -donor ligands, as the bonding π -orbitals of the triple bond can be energetically more accessible than their antibonding counterparts. The degree to which acetylides function as π -donor or π -acceptor ligands is dependent on the substituent bonded to the alkyne. Acetylides are thus often seen as hybrid π -donor/acceptor ligands.^{76,77}

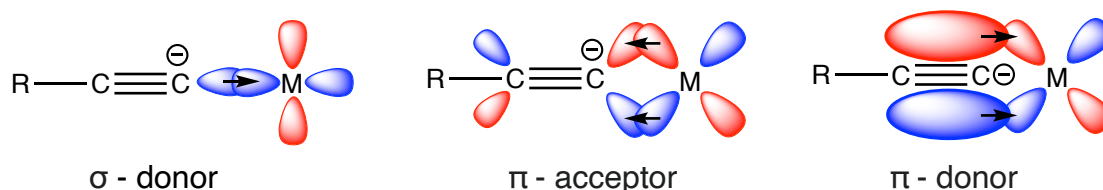


Figure 4 Simplified illustration of σ -donor and π -acceptor and π -donor properties of transition metal acetylides

In 2023, extensive experimental and computational studies were conducted comparing the donor and acceptor properties of the isoelectronic monoanionic acetylide, cyanide and κ -C-cyaphide (C \equiv P $^-$) ligands. In the study the three ligands showed similar σ -donor strengths, however the acetylide complex was determined to be in fact the weakest π -acceptor of the

series.⁷⁸ A simplified illustration of σ -donor, π -acceptor and π -donor interactions of an acetylide complex can be seen in Figure 4.

Transition metal acetylides can be prepared in a variety of ways, however salt metathesis reactions starting from magnesium or lithium acetylides as well as stannanes is most often encountered in literature. They are also accessible *via* oxidative addition reactions, or *via* reaction of the C-H-acidic alkynes with reactive ligands, in most cases alkyls or hydrides, driven by the subsequent elimination of gaseous neutral compounds.⁷⁹

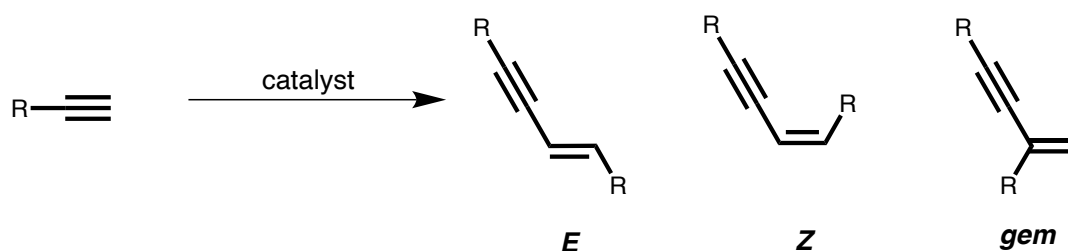
1.6. Iron catalyzed alkene dimerization reactions

1,3-enynes are an interesting class of compounds owing to the distinct reactivity of both the double and triple bond, that can be manipulated separately. This makes them ideal building blocks for various fields in organic synthesis.^{80,81}

Furthermore, several natural products feature enyne-moieties making them interesting targets for total synthesis.^{82–84} While there exist several synthetic protocols for the synthesis of enynes, catalytic dimerization of alkynes constitutes an attractive and atom economic option to gain entry into enyne chemistry.^{85,86}

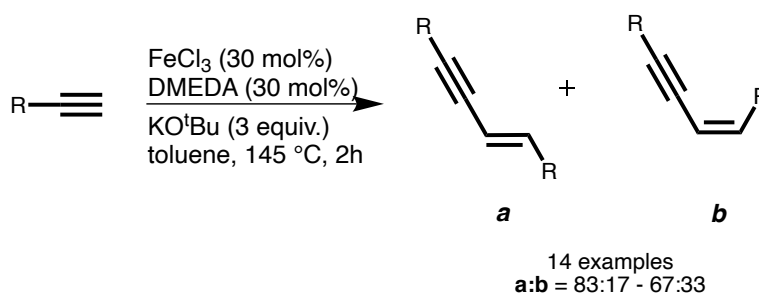
While most transition metal catalysts reported for the dimerization of alkynes are based on palladium and other precious metals, recently the focus shifted to catalysts based on base metals such as manganese, iron, cobalt and nickel.^{87–89}

In this context, the selectivity of the used catalyst is of great importance, as the homodimerization of terminal alkynes can lead to the formation of three isomers. The *E* and *Z* isomers are generated by the head-to-head dimerization of the alkynes, whereas head-to-tail isomerization affords the *gem*- isomer. (Scheme 14)



Scheme 14 Homodimerization of alkynes by a transition metal catalyst and potential isomers

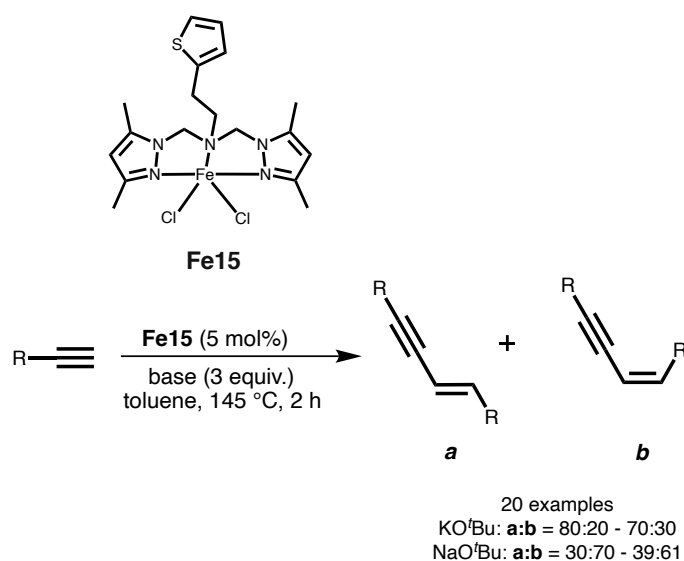
The first reported homo dimerization of alkynes with iron was reported by the group of *Dash* in 2011. Employing 30 mol% of FeCl_3 with 30 mol% of the amine ligand 1,2-dimethylethylenediamine (DMEDA) as well as 3 equivalents of KO^tBu in toluene at 145 °C gave good conversions of mixtures of *E* and *Z* enynes with aromatic acetylenes. Aliphatic acetylenes did not show any conversion. (Scheme 15)



Scheme 15 Homodimerization of alkynes by FeCl_3 with DMEDA and KO^tBu

For all substrates, the *E* isomer was preferentially formed, while no trace of the *gem* isomer was detected.⁹⁰ Later the same group showed that utilizing bisphosphines like 1,2-bis(diphenylphosphino)ethane (dppe) slightly improved the yield and selectivity. It was further shown that the reaction proceeds via radical mechanism which is initiated by the base.⁹¹

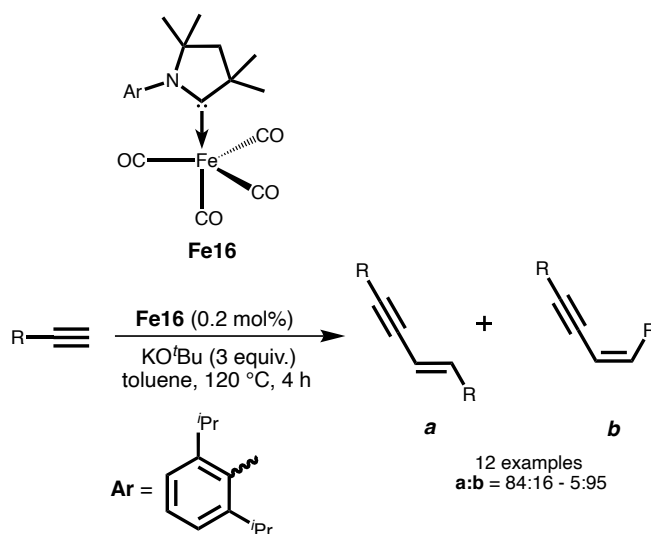
In 2018 *Zhao* and coworkers published a similar transformation employing a Fe(II) NNN tripodal complex (**Fe15**) for the homodimerization of aromatic alkynes. Utilizing 5 mol% of catalyst and 3 equivalents of base gave good yields and isomer mixtures of the *E* and *Z* enyne isomers. (Scheme 16)



Scheme 16 Homodimerization of alkynes by **Fe15** and base

Interestingly the choice of base directly influenced the selectivity of the reaction. When utilizing KO^tBu the *E* isomer was predominantly formed while switching the base to NaO^tBu afforded mainly the *Z*-isomer. Mechanistic studies were carried out and showed that a radical mechanism can most likely be excluded, as conducting the reaction with TEMPO showed no decrease in reactivity.⁹²

The group of *Mandal* showed in 2016 that Fe(0) complexes can also be utilized for the dimerization of alkynes. The complex [(CAAC)Fe(CO)₄] **Fe16** employing a cyclic(alkyl)(amino)carbene ligand (CAAC) showed excellent reactivity for the dimerization of aromatic alkynes achieving TONs of up to 6500. The catalyst exhibited for the most part a mixture of *E* and *Z* isomers. While for most substrates more of the *E*-isomer was formed, strongly electron withdrawing substituents on the aryl moieties flipped the isomeric ratio in favor of the *Z*-isomer. (Scheme 17)



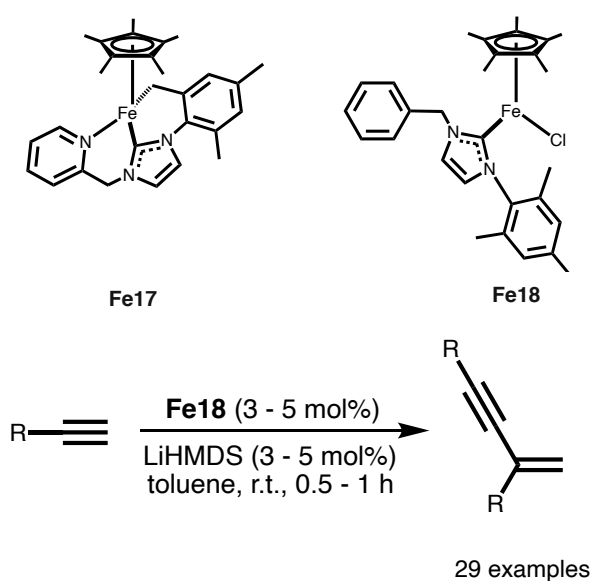
Scheme 17 Homodimerization of alkynes catalyzed by Fe(0) complex **Fe16** and base

Mechanistic studies were also conducted, indicating that preliminarily the carbonyl trans to the CAAC ligand is replaced by an alkyne, coordinating in a $\eta^2\text{-C}\equiv\text{C}$ fashion. In the next step another carbonyl ligand is replaced by a second alkyne which was previously deprotonated by the added base. This alkyne coordinates to the metal center as η^1 -acetylide, thus creating an anionic complex. The $\eta^2\text{-C}\equiv\text{C}$ and η^1 -acetylide are then perfectly aligned for a nucleophilic attack of the acetylide creating the head-to-head dimerization product, which is liberated after protonation by an incoming alkyne.⁹³

In 2017, the group of *Song* published the synthesis of an Fe(II) Cp* complex, utilizing an NHC ligand (**Fe17**) for the catalytic homodimerization and cross-dimerization of aromatic and aliphatic terminal alkynes. The complex catalyzed the selective formation of the head-to-tail dimerization product (*gem*-isomer). At a catalyst loading of 1-3 mol% in THF at 80 °C, without the use of base in 4 h full conversion with most substrates was achieved. The cross-dimerization with propargyl alcohol under the same reaction conditions showed excellent reactivity and at least a 9:1 product to homodimerization ratio was achieved for all substrates.

Mechanistic studies were conducted and showed that the mesityl group of the NHC ligand was crucial for the C-H activation of an incoming alkyne as well as the *gem*-selectivity of the reaction.

In the catalytic cycle the first step constitutes the dissociation of the pyridine ligand from the metal center following by association of an incoming acetylene. The mesityl ligand then facilitates C-H activation of the acetylene concomitant with formation of a free coordination side. Subsequently, another acetylene coordinates to the metal center in perfect alignment with the bound acetylide ligand, facilitating migratory insertion and formation of the head-to-tail dimerization isomer. Finally, C-H activation to form a metallacycle by the mesityl moiety liberates the product and reforms the catalytically active species.⁹⁴

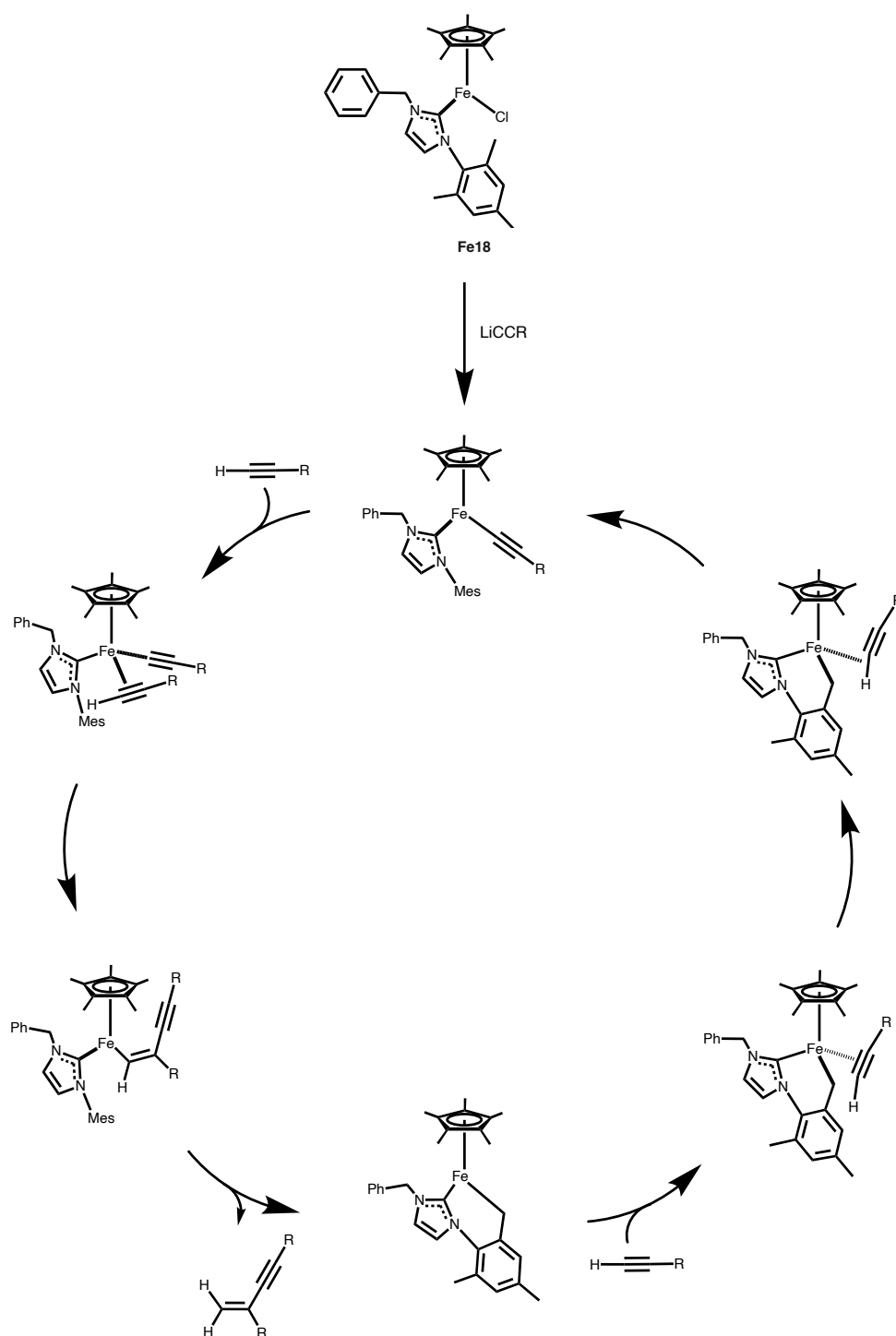


Scheme 17 *Gem*-selective dimerization of alkynes facilitated by Fe(II) Cp* complexes

Later, a new catalyst was designed in order to increase its reactivity, as reassociation of the pyridine ligand to a free coordination site leads to the formation of an 18 electron off-cycle complex, thus reducing its activity. For this reason, the pyridine substituent tethered to the backbone of the NHC moiety was replaced with a phenyl group, preventing the formation of such a complex during the catalytic cycle. **Fe18** was employed as pre-catalyst that was activated *via* addition of base, directly affording an acetylide complex by replacement of the chloride ligand due to transmetalation with an in situ formed lithium acetylide.

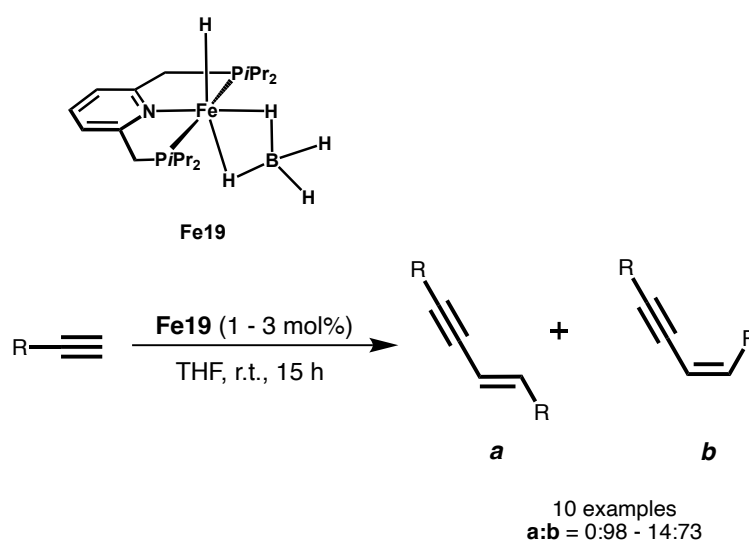
This complex showed greater reactivity achieving full *gem*-selective conversion of the substrates at ambient temperature in 1 h. (Scheme 17)

Mechanistically, the catalytic cycle proposed for the alkyne dimerization with **Fe18** closely mirrors the one proposed for **Fe17** (*vide supra*), underpinning the crucial role of the mesityl substituent of the NHC ligand stabilizing the metal during the catalytic cycle. (Scheme 18)⁹⁵



Scheme 18 Proposed catalytic cycle for the *gem*-selective dimerization of alkynes by **Fe18**

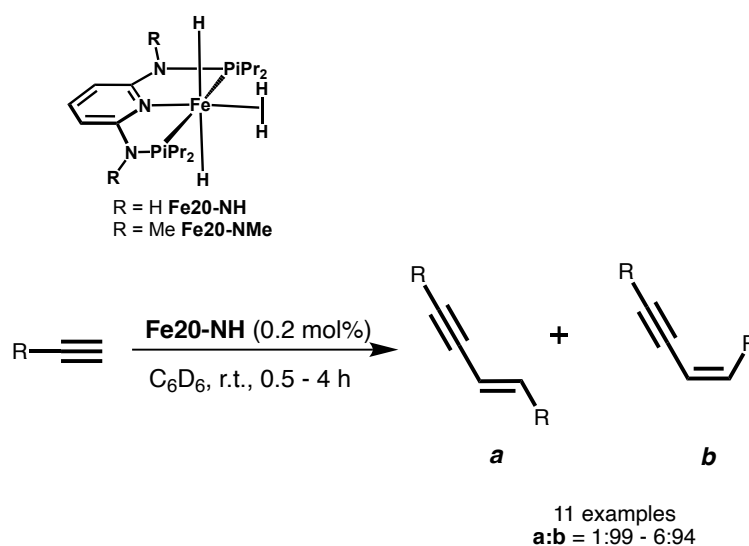
Subsequently, the effect of the used NHC donor was investigated in a new study, indicating that substitution of the imidazole based NHC-ligand with a benzimidazole based congener slightly improved the activity of the catalyst.⁹⁶



Scheme 19 Z-selective dimerization of alkynes facilitated by the pincer complex **Fe19**.

In 2016 *Milstein* and coworkers reported the Z-selective dimerization of alkynes using the PNP pincer complex $[(\text{PNP}^{\text{CH}_2})\text{Fe}(\text{H})(\eta^2\text{-BH}_4)]$ (**Fe19**). The catalyst showed excellent reactivity converting aromatic and terminal alkynes to the head-to-head dimers with excellent Z-selectivity. (Scheme 19) When aliphatic alkynes were used in the catalysis, interestingly only the *gem*-isomer was formed. The complex was also successfully employed in the cross-dimerization of aromatic alkynes with TMS-acetylene showing full conversion and good Z-selectivity for all substrates. The catalytic cycle was thought to include a vinylidene intermediate and closely resembles the catalytic cycle proposed for the complexes $[(\text{PNP}^{\text{NH}})\text{Fe}(\text{H})_2(\eta^2\text{-H}_2)]$ (**Fe20-NH**) and $[(\text{PNP}^{\text{NMe}})\text{Fe}(\text{H})_2(\eta^2\text{-H}_2)]$ (**Fe20-NMe**), which is described in more detail below.⁹⁷

In 2017, *Kirchner* and co-workers reported the synthesis of the nonclassical polyhydride complexes $[(\text{PNP}^{\text{NH}})\text{Fe}(\text{H})_2(\eta^2\text{-H}_2)]$ (**Fe20-NH**), and $[(\text{PNP}^{\text{NMe}})\text{Fe}(\text{H})_2(\eta^2\text{-H}_2)]$ (**Fe20-NMe**). These complexes showed excellent reactivity for the homo and cross-dimerization of alkynes with high Z-selectivity. At a catalyst loading of merely 0.2 mol% and a reaction time of 0.5 – 4 h, full conversion for aromatic alkynes was achieved with **Fe20-NH**. (Scheme 20) Furthermore the complexes were shown to be excellent catalysts for the Z-selective hydroboration of alkynes. (Scheme 20)⁹⁸



Scheme 20 Z-selective dimerization of alkynes facilitated by the pincer complexes **Fe20-NH** and **Fe20-NMe**.

Mechanistical and experimental studies showed that the active species for the catalysis is an intermediate spin bis(acetylide) complex generated *in situ* via reaction of the polyhydride complexes **Fe20** with alkynes. A third incoming alkyne reacts in an 1,2-H-shift to form a vinylidene intermediate. This vinylidene is subsequently attacked by a neighboring acetylide ligand, affording an alkynyl vinyl complex. Finally, proton transfer from a second incoming alkyne leads to product liberation and regeneration of species **Fe21**.

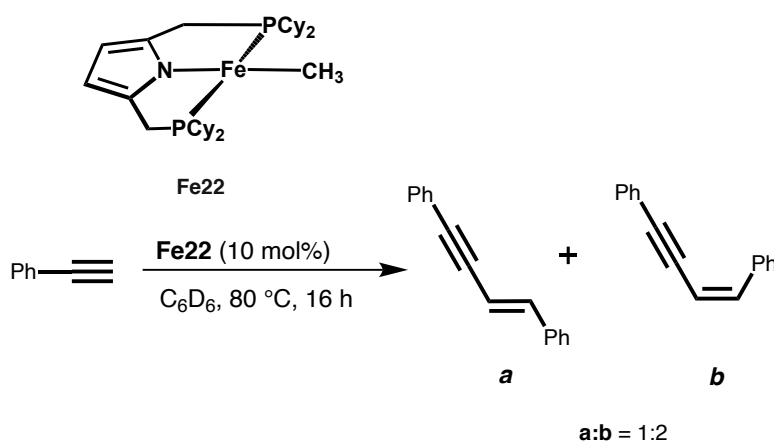
The Z-selectivity of the catalysis was explained by the fact that while the formation of the *E* and Z-selective alkynyl vinyl ligands is similar energetically, they are able to rapidly interconvert via a cumulenyl intermediate. However, the elimination of the product is energetically the highest barrier encountered in the catalytic cycle and features a lower barrier for the elimination of the Z-product compared to the *E*-product. Hence, product release is responsible for the high Z-selectivity of the reaction.⁹⁹ (Scheme 21) Trapping experiments further corroborated that product release was indeed crucial for the stereoselectivity of the reaction, as stoichiometric reactions of pre catalyst **Fe20-NMe** with 2-ethynylpyridine afforded a single species that was characterized as the *E*-alkynyl vinyl complex.⁹⁹



In 2022, *Tonzetich* and co-workers reported that the anionic PNP complex $[(\text{PNP}^{\text{Pyr,Cy}})\text{Fe}(\text{Me})]$ **Fe22** was able to catalyze the dimerization of phenylacetylene at a catalyst loading of 10 mol% and at 80 °C with a yield of 66 %. They reported that mainly the head-to-head dimerization products were formed during the reaction, with a minor amount (2 %) of *gem*-isomer being detected in the reaction mixture. (Scheme 22) Treatment of **Fe22** with an excess

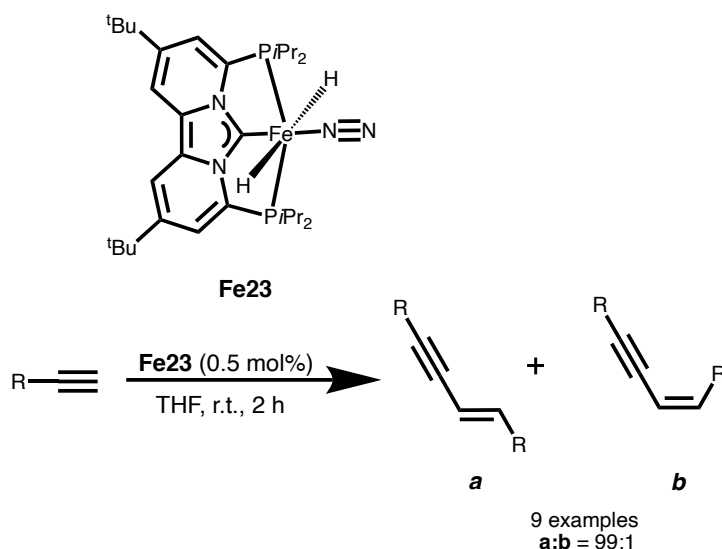
of phenylacetylene led, after elimination of methane, to the formation of a new species that was identified as the square planar *E*-alkynyl vinyl complex. It was proposed, that initially a transient square planar acetylide complex is formed. Rapid 2,1-insertion of a second alkyne then leads to the formation of primarily the *E*-alkynyl vinyl complex, in addition to only small amounts of the *gem* (formed by 1,2-insertion) and *Z*-congeners, respectively.

In contrast to the system of *Kirchner* the alkynyl-vinyl ligands are bound to the metal center on the 1-carbon, interconversion of the isomers via a cumulenyl intermediate was thus ruled out. Isomerization was proposed instead to occur *via* a zwitterionic carbene intermediate. The product release by proton transfer of an incoming alkyne was suggested to be the rate determining step of the cycle necessitating the high temperature needed for the transformation. While the *E*-alkynyl vinyl complex was determined to be the major intermediate after insertion, the high quantity of *Z*-enyne after the reaction suggests that, most likely due to reduced steric crowding, proton transfer is quicker to the *Z*-alkynyl vinyl complex.¹⁰⁰



Scheme 20 Dimerization of phenylacetylene facilitated by the pincer complexes **Fe22**

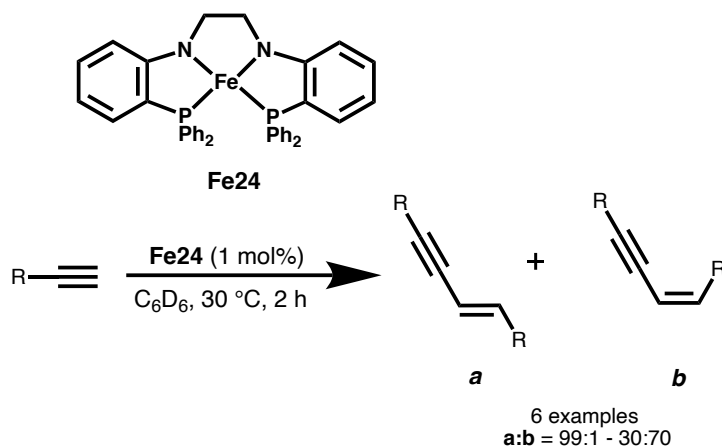
The group of *De Ruiter* published the hydroboration and *Z*-selective dimerization of aromatic terminal alkynes in 2020. The transformations were catalyzed by a NHC based Iron PCP dihydride complex, featuring a labile dinitrogen ancillary ligand (**Fe22**). The catalyst showed excellent selectivity achieving greater than 99 % *Z*-selectivity for all substrates, however aliphatic alkynes were not converted. (Scheme 21) The catalyst also showed excellent reactivity in the *Z*-selective hydroboration of the alkynes. Furthermore, it was shown that by increasing the temperature in the hydroboration reaction from room temperature to 50 °C, the stereoselectivity was reversed yielding only the *E*-vinylboronates.¹⁰¹



Scheme 21 Dimerization of aromatic alkynes by the dihydride pincer complexes **Fe23**

Very recently, *Thomas* and coworkers reported the *Z*-selective dimerization of aromatic alkynes, utilizing a square planar Fe(II) PNNP complex (**Fe24**). While the *Z*-selectivity of the reaction was good in all substrates, introduction of electron withdrawing groups in the aromatic backbone of the alkynes led to reduced yields. (Scheme 22)

Aliphatic alkynes showed no reactivity in the reaction. Stoichiometric studies showed, that in the first step of the catalysis a metal-ligand cooperative C-H activation takes place, affording an acetylide complex in concomitance with the protonation of the amide ligands in the backbone. It was further shown that aliphatic substrates were not activated due to their increased pK_a values in comparison to aromatic alkynes. In the catalytic cycles these acetylides were proposed to form vinylidenes after proton transfer back from the backbone. The α -carbon of the vinylidene is then suggested to be attacked intermolecularly by an acetylene, again protonating the backbone, followed by liberation of the product *via* a final proton transfer.¹⁰²



Scheme 22 Dimerization of aromatic alkynes by the tetradentate Fe PNNP complex **Fe24**

2. Results and Discussion

2.1. Synthesis of Fe PNP Silyl Complexes

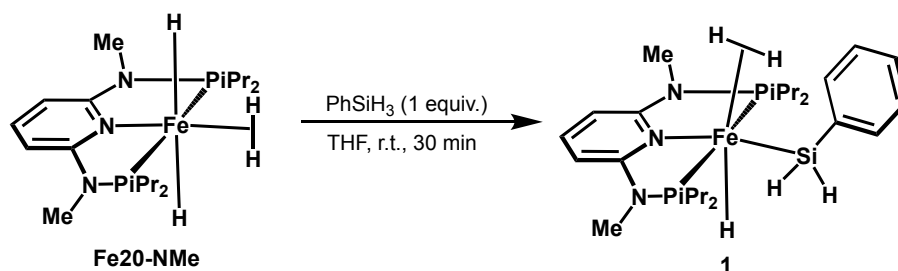
As demonstrated in chapter 1.4, iron complexes featuring pincer ligands were proven to be powerful tools in facilitating catalytic hydrosilylation of alkenes. However, no systems featuring pyridine based PNP scaffolds were yet employed in this transformation. Indeed, besides the PNP iron silyl complexes published by *Chirik* in 2006⁶³, no further reports of such complexes were reported in literature. The group of *Findlater* suggested the occurrence of η^2 -silyl iron complexes in the catalytic cycle of their reported hydrosilylation of ketones. These were proposed to form after treatment of the 2,6-dihydroxypyridine-based PNP complex $[(\text{PONOP}^{\text{tBu}})\text{FeCl}_2]$ with 2 equiv. of NaBEt_3H in the presence of $(\text{EtO})_3\text{SiH}$.¹⁰³

Tonzetich and coworkers investigated the role of Fe-PNP silyl complexes in the hydrosilylation of aldehydes and ketones with an anionic pyrrole-based system. They showed that both, Fe-hydride as well as Fe-silyl complexes are active in catalysis, proposing however different catalytic cycles for the two species. Consequently, they suggested that competitive side reactions may feature prominently in various base metal based catalytic transformations, not changing the overall product distribution of the reaction, nevertheless heavily influencing its kinetics.^[15] They previously also investigated the reactivity of these square planar PNP Fe-silyl complexes and showed that they readily form insertion products with aldehydes as well as acetylenes, corroborating their ability to participate in catalysis and highlighting their capability to partake in hydrosilylation reactions with alkynes.¹⁰⁴

These findings, combined with the successful employment of the 2,6-diaminopyridine based PNP system in the hydroboration of alkynes,⁹⁸ as well as the recent successful application of similar Fe-PNN complexes in the hydrofunctionalization of alkenes served as motivation to expand these concepts towards implementing Fe-PNP pincer complexes in hydrosilylation chemistry.

Chirik reported that treatment of $[(\text{PNP}^{\text{CH}_2})\text{Fe}(\text{H})(\text{SiPhH}_2)(\text{N}_2)]$ (**Fe6-Si**) with 4 atm of H_2 , resulted in the formation of a transient species, tentatively assigned as $[(\text{PNP}^{\text{CH}_2})\text{Fe}(\text{H})(\eta^2-$

$\text{H}_2)(\text{SiPhH}_2)]$. Based on this observation, it was envisioned that such a species can be isolated by treating $[(\text{PNP}^{\text{NMe}})\text{Fe}(\text{H})_2(\eta^2\text{-H}_2)]$ (**Fe20-NMe**) with PhSiH_3 under argon atmosphere.



Scheme 23 Synthesis of the Iron silyl polyhydride complex **1**

Gratifyingly, the reaction of a THF solution of **Fe20-NMe** with 1 equiv. of PhSiH_3 yielded after a reaction time of 30 minutes, a single product, that was identified as $[(\text{PNP}^{\text{NMe}})\text{Fe}(\text{H})(\text{SiPhH}_2)(\eta^2\text{-H}_2)]$ (**1**). (Scheme 23) In the $^{31}\text{P}\{^1\text{H}\}$ NMR spectrum, **1** features a singlet at 178.3 ppm, which represents a significant upfield shift compared to **Fe20-NMe** which can be observed at 196.8 ppm.⁹⁸ In the hydride region of the ^1H NMR complex **1** features two broad hydride resonances located at -8.20 ppm and -10.75 ppm in an integral ratio of 1:2. These signals are assignable to the hydride ligand and the η^2 -dihydrogen ligand respectively. The two remaining not coordinating hydrogen atoms located on the phenylsilyl-ligand were observed as a triplet at 5.42 ppm with a $^3J_{\text{HP}}$ coupling constant of 6.5 Hz, indicating chemical equivalence of the Si-H moieties. Additionally, an inverse gated decoupled $^{29}\text{Si}\{^1\text{H}\}$ NMR experiment was conducted in which the coordinated silyl moiety gave rise to a sharp triplet signal located at -8.9 ppm (cf. PHSiH_3 : -59.7 ppm) with a $^2J_{\text{SiP}}$ coupling constant of 25.2 Hz. To unequivocally elucidate the structure of the complex single crystal X-Ray diffraction was conducted, indicating that the hydride as well as the η^2 -dihydrogen ligand are mutually trans to each other. (Figure 5)

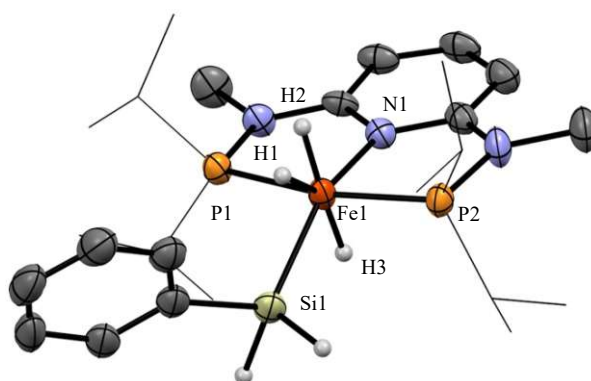


Figure 5. ORTEP view of $[(\text{PNP}^{\text{NMe}})\text{Fe}(\text{H})(\text{SiPhH}_2)(\eta^2\text{-H}_2)]$ (**1**) showing 50% thermal ellipsoids (most H omitted for clarity). Selected bond lengths (Å) and angles (deg): Fe1-N1 2.012(3), Fe1-P1 2.155(1), Fe1-P2 2.158(1), Fe1-Si1 2.258(1), Fe1-H1 1.52(5), Fe1-H2 1.42(5), Fe1-H3 1.47(5), H2-H3 0.955; N1-Fe1-Si1 151.74, P1-Fe1-P2 167.10.

The geometry of the complex can be best described as distorted octahedral, with particularly the N1-Fe1-Si1 bonds angles deviating from linearity with an angle of 151.74° . The H1-H2 bond distance is 0.955 \AA which is characteristic for coordinated η^2 -dihydrogen and similar to **Fe20-NMe** which was determined to be 0.90 \AA .⁹⁸ Interestingly, close contacts of the silyl ligand with the coordinated hydrides can be observed, with a Si1-H1 distance of 2.227 \AA and a Si1-H3 distance of 2.209 \AA , which are in the typical range of SISHA interactions. (*vide supra*) The Fe1-Si1 bond distance of $2.258(1) \text{ \AA}$ is in the range of the Fe-Si bond distances of **Fe6-Si** ($2.2718(6) \text{ \AA}$) as reported by Chirik.⁶³

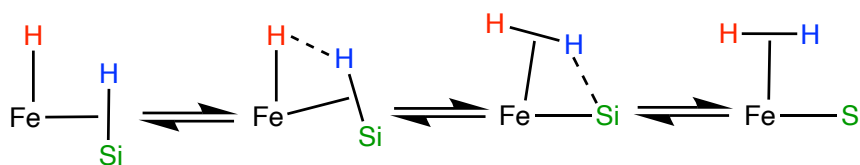
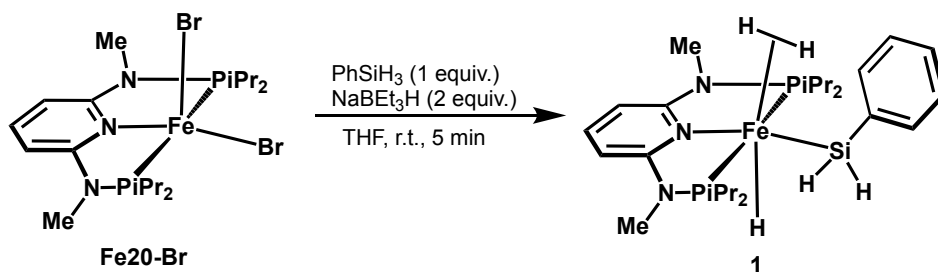


Figure 6. Proposed schematic mechanism of the formation of **1** via σ -CAM

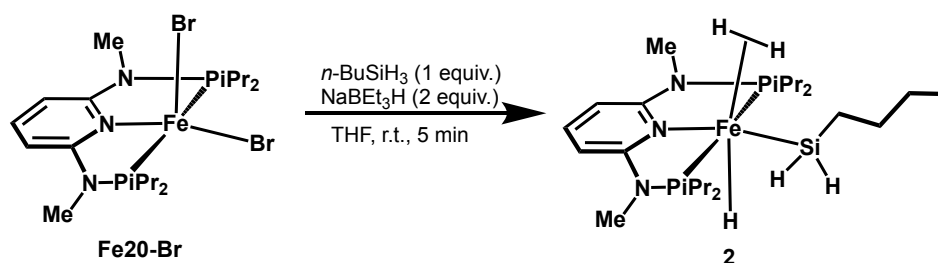
Formation of **1** is proposed to occur *via* σ -CAM mechanism. The labile η^2 -dihydrogen ligand of **Fe20-NMe** can be replaced by the incoming silane, forming a Si-H σ -complex, which subsequently can undergo sigma bond metathesis, yielding the observed silyl η^2 -dihydrogen complex. (Figure 6) Accordingly, **1** can also be synthesized in good yields by directly reacting a THF solution of $[(\text{PNP}^{\text{NMe}})\text{FeBr}_2]$ (**Fe20-Br**) with 2 equiv of NaBEt_3H in the presence of 1 equiv of PhSiH_3 . (Scheme 24)



Scheme 24 Synthesis of the Iron silyl polyhydride complex **1** directly from **Fe20-Br**

Analogously, conducting the reaction with 1 equiv. of the aliphatic primary silane $n\text{-BuSiH}_3$, afforded the corresponding complex $[(\text{PNP}^{\text{NMe}})\text{Fe}(\text{H})(\text{SiBuH}_2)(\eta^2\text{-H}_2)]$ (**2**) in good yields. (Scheme 25) **2** features similar spectroscopic characteristics to **1**, with two broad resonances

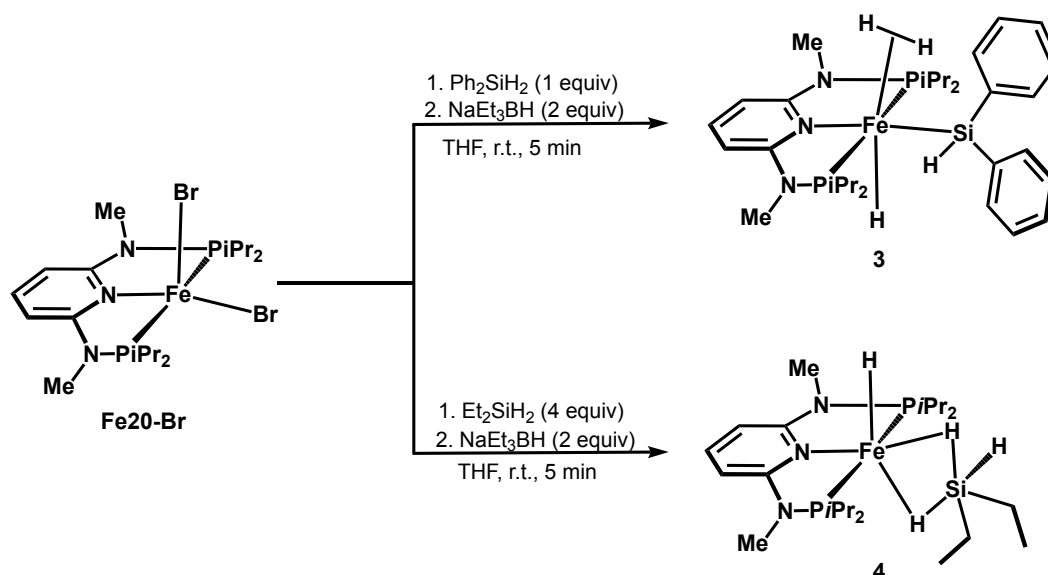
in the hydride region of the ^1H -NMR spectrum, corresponding to the hydride (-8.20 ppm) as well as the η^2 -dihydrogen ligands (-11.02 ppm) in an integral ratio of 1:2. The not coordinated silyl hydrides were located as a multiplet at 4.73 ppm.



Scheme 25 Synthesis of the Iron silyl polyhydride complex **2** from **Fe20-Br** using $n\text{-BuSiH}_3$.

In the inverse gated decoupled $^{29}\text{Si}\{^1\text{H}\}$ -NMR the complex features a broad resonance at -15.4 ppm.

Encouraged by these results the synthesis of congeneric complexes, featuring secondary and tertiary silanes, was attempted. The reaction of **Fe20-Br** in the presence of secondary silanes Ph_2SiH_2 as well as Et_2SiH_2 with NaBEt_3H led to the formation and isolation of the two well defined complexes $[(\text{PNP}^{\text{NMe}})\text{Fe}(\text{H})(\text{SiPh}_2\text{H})(\eta^2\text{-H}_2)]$ (**3**) and $[(\text{PNP}^{\text{NMe}})\text{Fe}(\text{H})(\eta^2\text{-SiEt}_2\text{H}_3)]$ (**4**) in 78% and 75% yield, respectively. (Scheme 26)



Scheme 26 Synthesis of the Iron silyl polyhydride complexes **3** and **4** from **Fe20-Br** using secondary silanes

Both complexes feature broad resonances in the hydride region of the ^1H -NMR spectrum at -11.11 ppm (**3**) and -11.00 ppm (**4**) respectively, with an integral of 3, indicative of rapid exchange of the hydride ligands. The non-coordinating silane hydrogens were observed as a

sharp triplet at 6.20 ppm with a $^3J_{\text{PH}}$ coupling constant of 9.6 Hz for **3**, while complex **4** showed a poorly resolved multiplet at 4.57 ppm. Likely due to their fluxionality no signal could be detected for both complexes in the $^{29}\text{Si}\{^1\text{H}\}$ NMR spectrum, however it was possible to locate the resonances in an ^{29}Si - ^1H HMBC experiment, with **3** showing cross peaks at 15.2 ppm, while **4** being detected at 18.5 ppm.

Crystals suitable of single crystal X-ray diffraction of both complexes were obtained from saturated *n*-pentane solutions at -30 °C.

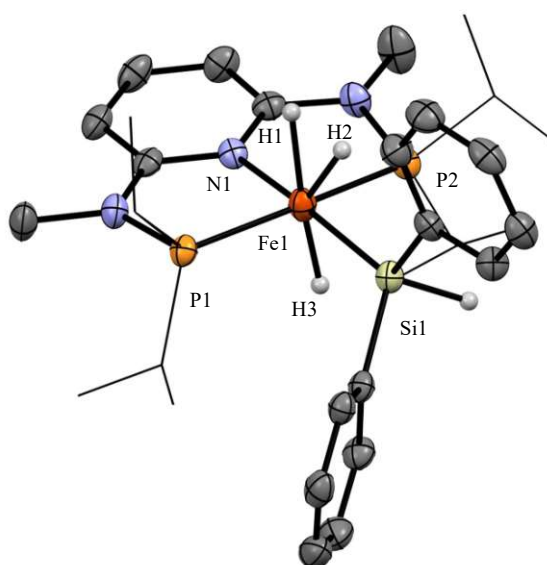


Figure 6. ORTEP view of $[(\text{PNP}^{\text{NMe}})\text{Fe}(\text{H})(\text{SiPh}_2\text{H})(\eta^2\text{-H}_2)]$ (**3**) showing 50% thermal ellipsoids (most H omitted for clarity). Selected bond lengths (Å) and angles (deg): Fe1-N1 2.006(3), Fe1-P1 2.1516(9), Fe1-P2 2.1592(9), Fe1-Si1 2.283(1), Fe1-H1 1.50(5), Fe1-H2 1.72(3), Fe1-H3 1.43(4), H1-H2 1.021; N1-Fe1-Si1 170.66, P1-Fe1-P2 164.85.

Complex **3** structurally closely resembles **1**, featuring a distorted octahedral geometry, featuring a hydride ligand and a η^2 -dihydrogen ligand that are mutually trans to each other. (Figure 6) Noticeably, the N1-Fe1-Si1 angle deviates significantly less from linearity as compared to **1** being measured at 170.66°, compared to 151.74° in **1**. The Fe1-Si1 bond distance of 2.283(1) Å is slightly longer, but comparable to **1** (2.258(1) Å) and similar to the structurally related PNP complexes of *Chirik*. (Figure 6)

The η^2 -dihydrogen ligand is elongated compared to **1** as highlighted by the H1-H2 bond distance of 1.021 Å. As with **1**, close contacts of the silyl ligand with the coordinated hydrides can be observed, with a H2-Si1 distance of 2.187 Å and a H3-Si1 distance of 2.280 Å, again showing significant SISHA interactions in the complex.

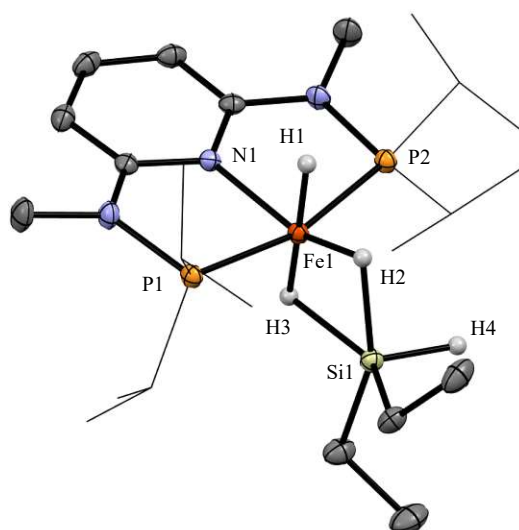


Figure 8. ORTEP view of $[(\text{PNP}^{\text{NMe}})\text{Fe}(\text{H})(\eta^2\text{-SiEt}_2\text{H}_3)]$ (**4**) showing 50% thermal ellipsoids (most H omitted for clarity). Selected bond lengths (Å) and angles (deg): Fe1-N1 2.014(2), Fe1-P1 2.1608(5), Fe1-P2 2.1483(5), Fe1-Si1 2.3066(7), Fe1-H1 1.49(2), Fe1-H2 1.46(2), Fe1-H3 1.43(2), H1-H2 1.714, Si1-H4 1.44(2); N1-Fe1-Si1 145.02, P1-Fe1-P2 165.41.

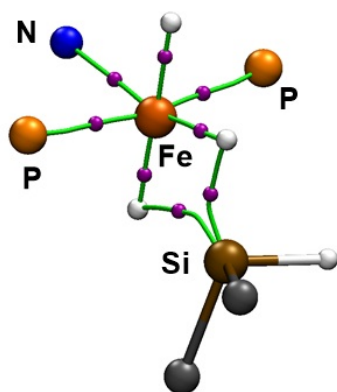
In contrast to **1** and **3**, the structure of **4** is best described as intermediate state of the σ CAM Si-H activation. The Si1-H2 and Si1-H3 distances of **4** are similar with 1.920 Å and 1.898 Å respectively, which is significantly elongated compared to non-activated Si1-H4 bond (i.e., 1.44(2) Å), however much shorter compared to the secondary interactions observed in **1** and **3**, indeed being in the lower range expected for SISHA interactions, indicating a significant σ -complex character of the bonds.³⁵ Interestingly, the bond distance of the three hydride ligands is very similar, indicating a strong interaction with the iron center. (i.e. Fe-H1 1.49(2) Å, Fe-H2 1.46(2) Å, Fe-H3 1.43(2) Å) Similar interactions of silicon and hydrogen atoms in iron complexes have been reported in literature.^{105–108}

The Fe-Si distance of the complex of 2.3066(7) Å is slightly longer when compared to **1** and **3** which are 2.258(1) Å and 2.283(1) Å respectively. This agrees with a trend observed by Lemke and coworkers. In this study, a series of ruthenium-silyl complexes was synthesized, and their metal bond strength was correlated to the substituents located on the silane ligand. It was shown that the ruthenium-silicon bond strength is highly dependent on the substituents on the silyl moiety. The introduction of electronegative Cl substituents on the silane was shown to lead to stronger Ru-Si bonds, due to increased $d(\text{Ru})\text{-}\sigma^*(\text{Si-Cl})$ π -back-bonding, while replacement of hydrogen with alkyl or aryl groups on the silane led to weaker Ru-silicon bonds. Furthermore, the replacement of alkyl substituents with aryl substituents manifested itself with a slight increase in the metal-silicon bond strength.¹⁰⁹ It has to be noted that the Fe-Si bond distances in complexes **1**, **3** and **4** is shorter than the bond lengths observed in the square planar pyrrole based pincer complexes $[(\text{PNP}^{\text{Pyr,Cy}})\text{Fe}(\text{SiPhH}_2)]$ (2.384 Å) and

$[(\text{PNP}^{\text{Pyr,tBu}})\text{Fe}(\text{SiPhH}_2)]$ (2.408 Å) published by *Tonzetich* and coworkers^{15,110}. In contrast, the structurally related complexes $[(\text{PNP}^{\text{CH}_2})\text{Fe}(\text{H})(\text{SiPhH}_2)(\text{N}_2)]$ (**Fe6-Si**) and $[(\text{PNP}^{\text{CH}_2})\text{Fe}(\text{H})(\text{SiPhH}_2)(\text{CO})]$, as reported by *Chirik* and coworkers show very similar Fe-Si bond lengths of 2.2718 Å and 2.2689 Å, respectively.⁶³

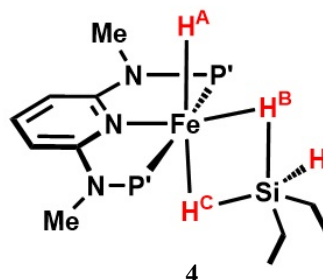
To gain further inside into the bonding modes of the complexes, DFT calculations and QTAIM¹¹¹ analyses were performed with complexes **3** and **4**.

QTAIM:

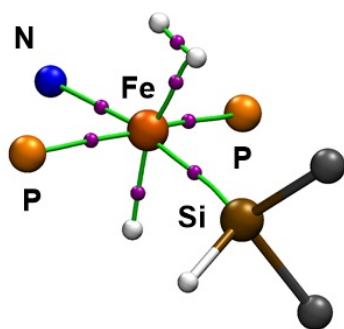


WBIs:

Fe---Si	0.28
Fe---H ^A	0.47
Fe---H ^B	0.42
Fe---H ^C	0.30
Si---H ^B	0.34
Si---H ^C	0.37
H ^A ---H ^B	0.08



QTAIM:



WBIs:

Fe---Si	0.58
Fe---H ^A	0.21
Fe---H ^B	0.18
Fe---H ^C	0.53
Si---H ^B	0.10
Si---H ^C	0.13
H ^A ---H ^B	0.60

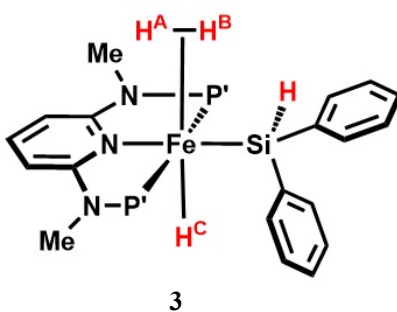


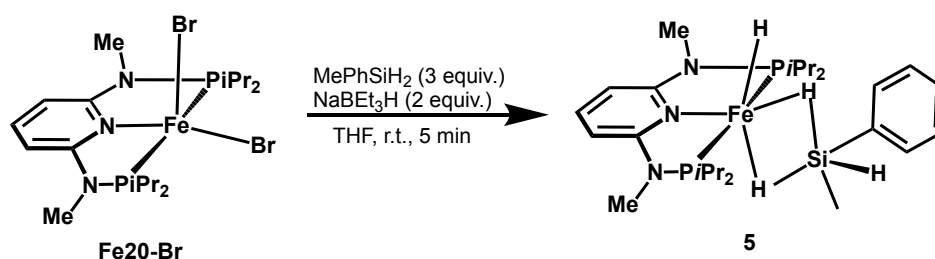
Figure 7 QTAIM analyses and list of WBIs for complexes **3** and **4**

As can be seen in Figure 7, the QTAIM analysis of **3** shows bond critical points (BCP) between the iron and silicon atoms. A Wiberg bond index (WBI) analysis shows a bond order of 0.58 for the Fe-Si bond, confirming a bonding interaction between the atoms. It is further shown that a bond critical point exists between the hydrogen atoms of the η^2 -dihydrogen ligand, which is also corroborated in the WBI analysis, showing a bond order of 0.60 between the hydrogen atoms. Furthermore, a bond critical point between the atoms of the η^2 -

dihydrogen ligand and the iron center can be observed, with WBIs of 0.21 and 0.18 respectively. The combination of these data suggests that the structure is best described as a hydrido silyl complex, featuring a coordinated η^2 -dihydrogen ligand.

In contrast, in the QTAIM plot of **4** no BPOs between the iron and silicon atom can be observed. The WBI data shows a bond order of 0.28 between Fe and Si, indicating a much weaker interaction. In contrast, BPOs between both H^b and H^c and the silicon atom can be detected, with WBIs of 0.34 and 0.37 respectively. Furthermore, only weak interactions between H^b and H^c can be observed with a WBI of 0.08. Additionally, the strong interaction of all three hydride ligands with the iron center are illustrated in the QTAIM analysis, showing BCPs between all three atoms and the central atom with WBIs of 0.47 and 0.43 for H^a and H^b and 0.30 for H^c .

These data indicate that the structure of **4** is best described as a σ -Si-H complex with significant hypervalent interaction of a coordinated hydride ligand with the silicon atom, suggesting an interaction akin to a three-center four-electron bond in the complex.



Scheme 27 Synthesis of complex **5** from **Fe20-Br**

Intrigued by these results, the synthesis of a congeneric complex, featuring both, aryl and alkyl substituents on the silicon was endeavored. Utilizing phenylmethylsilane and starting from **Fe20-Br**, $[(PNP^{NMe})Fe(H)(\eta^2-SiMePhH_2)(H)]$ (**5**) was synthesized in good yields. (Scheme 27) Spectroscopically, complex **5** closely resembles the congeners **3** and **4** with a broad resonance in the hydride region of the 1H -NMR spectrum located at -10.07 ppm with an integral of 3 as well as a multiplet located at 5.59 ppm, assignable to the hydride resonance and the non-coordinated hydrogen on the silyl moiety, respectively. In the ^{29}Si - 1H HMBC a cross peak located at 2.3 ppm was observed. The molecular structure of **5** was determined utilizing single crystal X-ray diffraction and resembles that of **4**. However, while the Si-H1 and Si-H2 bond distances of 1.872 Å and 2.002 Å are comparable to those of **4**, the H2-H3 bond distance of 1.467 Å is shorter than the one measured in **4**, which was determined to be

1.714 Å. The Si-Fe distance of 2.277(2) Å is shorter than in **4** and is similar to **3**, hinting that the structure of **5** can be seen as an intermediated state between **3** and **4**. (Figure 8)

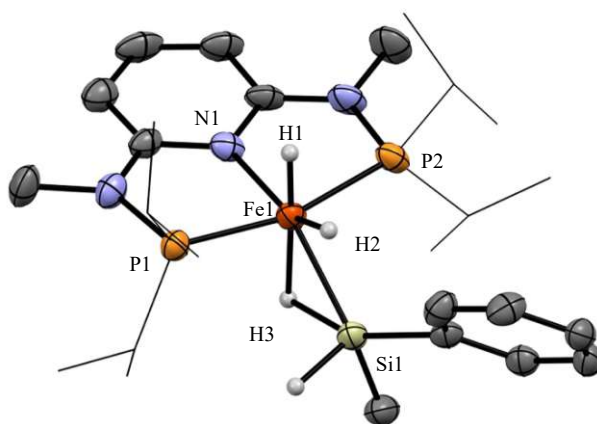
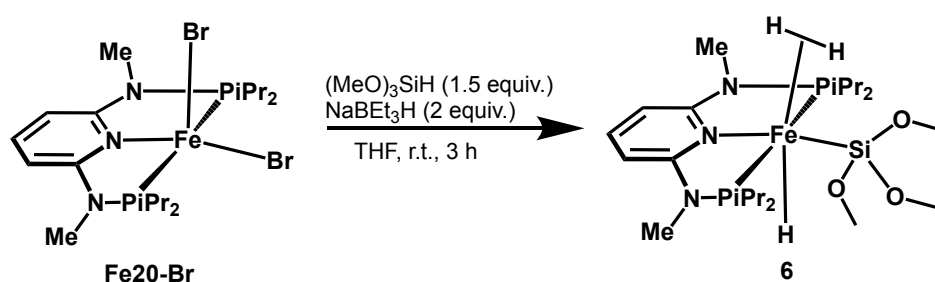


Figure 8. ORTEP view of $[(\text{PNP}^{\text{NMe}})\text{Fe}(\text{H})(\eta^2\text{-SiMePhH}_2)(\text{H})]$ (**5**) showing 50% thermal ellipsoids (most H omitted for clarity). Selected bond lengths (Å) and angles (deg): Fe1-N1 2.004(4), Fe1-P1 2.159(2), Fe1-P2 2.153(2), Fe1-Si1 2.277(2), Fe1-H1 1.44(6), Fe1-H2 1.42(7), Fe1-H3 1.72(6), H1-H2 1.467; N1-Fe1-Si1 148.28, P1-Fe1-P2 165.40.



Scheme 28 Synthesis of complex **6** from **Fe20-Br**

Attempts to synthesize PNP iron silyl complexes with the tertiary silanes Et_3SiH as well as Me_2PhSiH were unsuccessful and only intractable products were obtained. This can possibly be explained by the increased steric bulk of the tertiary silanes. It was however possible to synthesize a complex using the sterically less demanding silane $(\text{MeO})_3\text{SiH}$, which was spectroscopically identified as $[(\text{PNP}^{\text{NMe}})\text{Fe}(\text{H})((\text{MeO})_3\text{Si})(\eta^2\text{-H}_2)]$ (**6**). (Scheme 28) In contrast to complexes **1-5** which only show broad and unresolved hydride signals in the ^1H NMR spectrum, **6** exhibits two triplets located at -13.33 ($^2J_{\text{PH}} = 36.8$ Hz) and -7.19 ($^2J_{\text{PH}} = 23.3$ Hz) in an integral ratio of 2:1 respectively. The decoalescence of the hydride signals can possibly be attributed to a slower exchange in absence of hydrogens situated on the silyl moiety. In the inverse gated decoupled $^{29}\text{Si}\{^1\text{H}\}$ -NMR experiment the coordinated silicon atom can be observed as a broad resonance at -78.5 ppm.

The characteristic NMR-spectroscopic shifts and multiplicities of the complexes are listed in Table 1.

Table 1 Characteristic NMR Shifts of the described PNP Iron Hydrido Silyl Complexes

Complex	¹ H-NMR		³¹ P{ ¹ H}-NMR		²⁹ Si{ ¹ H}-NMR	
	hydrides (ppm)	² J _{PH} (Hz)	silane (ppm)	³ J _{PH} (Hz)		² J _{PSi} (Hz)
1	-10.75 (br); - 8.20 (br)	-	5.42 (t)	6.5	178.3	-8.9 (t) 25.2
2	-11.02 (br); - 8.20 (br)	-	4.73 (m)	-	179.3	-14.5 -
3	-11.11 (br)	-	6.20 (t)	9.6	177.1	15.2 -
4	-11.00 (br)	-	4.57 (m)	-	179.0	18.5 -
5	-10.07 (br)	-	5.59 (m)	-	177.9	2.3 -
6	-13.33 (t) -7.19 (t)	36.8 23.3	-	-	180.0	-78.5 -

2.2. Catalytic Activity of the Fe PNP Silyl Complexes

As the reaction of the novel Fe-silyl complexes **1-6** with alkynes only afforded the Z-selective homodimerization products, they were subsequently tested as catalysts for the hydrosilylation of alkenes.

Complexes **1** and **2** did not show any activity in the transformation, indeed treating them with excess of the respective primary silane, led to a color change from orange to red, with concomitant formation of new diamagnetic species, as observed in the ³¹P{¹H}-NMR spectrum. Similarly, when conducting the reaction employing complex **6**, no conversion could be observed.

In contrast, complexes **3** and **4** did not show degradation when treated with an excess of the respective secondary silane and were both preliminary tested for the hydrosilylation of 4-

fluorostyrene using the respective silane in THF. Initially a catalyst loading of 5 mol% was chosen. Gratifyingly, complex **4** showed full conversion of the alkene after 20 h at a temperature of 50 °C. The product mixture consisted of mainly hydrogenated alkane and anti-markovnikov hydrosilylation product. Under the same conditions, only traces of products could be observed, when utilizing complex **3** as catalyst. In attempts to increase the conversion for the catalysis with **3**, a test reaction with 2 mol% catalyst at a temperature of 80 °C, without solvent was attempted. Unfortunately, the conversion could only be improved to 36 %. The reaction yielded a mixture of products, as hydrogenated alkane, markovnikov and anti-markovnikov hydrosilylation product were all detected in a ratio of 36 %, 25 % and 39 % respectively. Moreover, a significant amount of polymerization product was found in the reaction mixture.

Subsequently, attempts were made to optimize the reaction conditions utilizing **4** as catalyst for the hydrosilylation of 4-fluorostyrene with and excess diethylsilane, however all attempts to increase the selectivity of the reaction failed, as in all attempts a mixture of hydrogenated alkane, anti-markovnikov hydrosilylation product as well as dehydrogenative silylation product was observed.

Gratifyingly, when attempting the reaction with 4-fluoroallylbenzene instead of a styrene derivative, a drastic increase in selectivity was observed, and the reaction conditions were consequently optimized.

Table 2 Optimization reactions for the hydrosilylation of alkenes

Entry	Cat.	Substrate	Cat. loading (mol %)	Solvent	T (°C)	Conversion (%)	A/B/C/D
1	4	a	2	benzene	50	94	48/27/25/0
2	4	a	2	toluene	50	95	51/27/22/0
3	4	a	2	THF	50	>99	78/6/16/0
4	4	a	2	neat	50	>99	73/13/11/3
5	4	a	1	THF	50	>99	78/16/6/0
6	4	a	1	neat	50	>99	79/8/12/1
7	4	a	0.5	THF	50	19	62/27/11/0
8	4	a	0.5	neat	50	53	75/10/14/1
9	4	a	0.1	THF	50	traces	-
10	4	a	0.1	neat	50	traces	-
11	4	a	2	THF	25	37	35/0/54/11

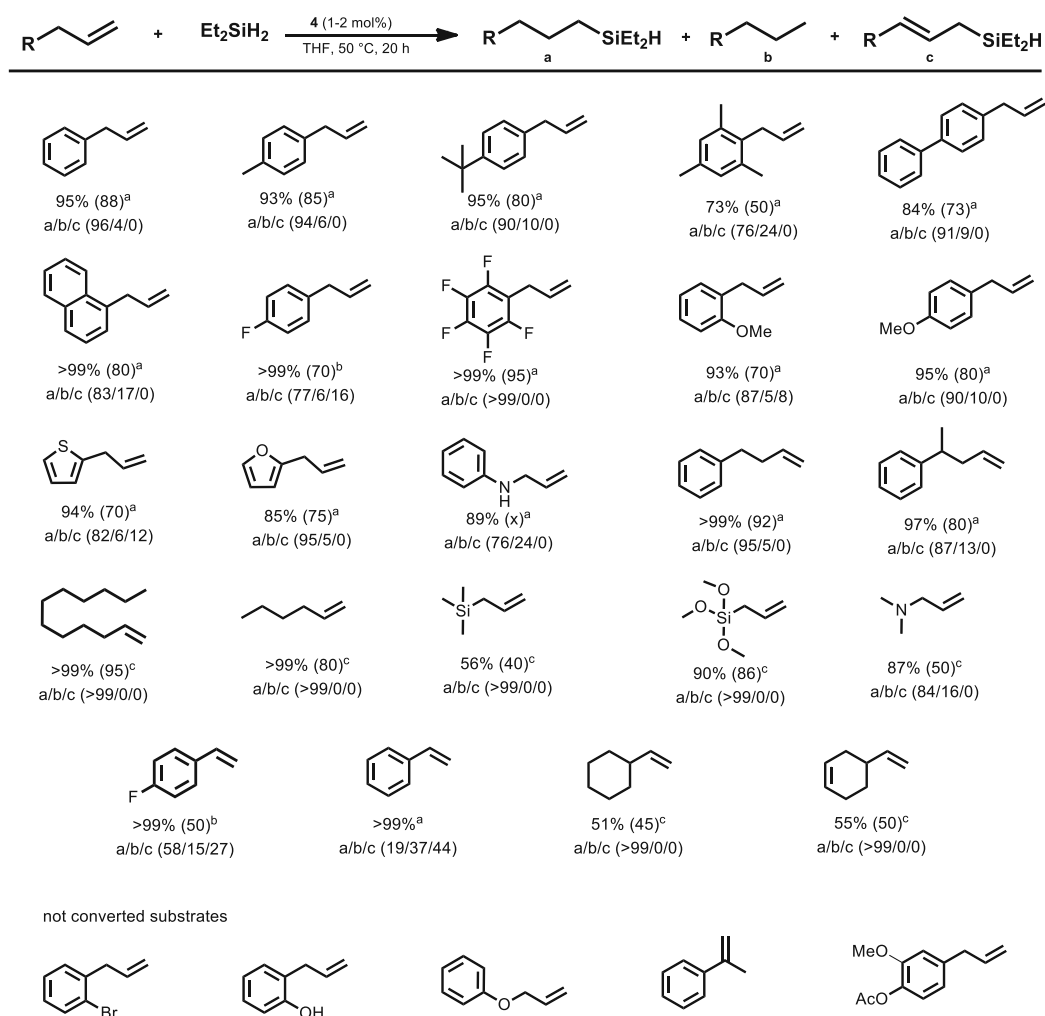
12	4	b	2	THF	50	95	96/4/0/0
13	4	b	1	THF	50	83	90/10/0/0
14	3	a	2	THF	50	13	64/27/9/0
15	5	a	2	THF	50	37	66/29/4/0

a = 4-fluoroallylbenzene, **b** = allylbenzene; product **A** = anti-markovnikov hydrosilylation product, **B**=hydrogenation product, **C** = dehydrogenative silylation product, **D** = markovnikov hydrosilylation product; reaction conditions: alkene (0.021 mmol, 1 equiv), silane (0.053 mmol, 2.5 equiv), 0.25 ml solvent if used, for **a** conversion and product ratio determined by $^{19}\text{F}\{^1\text{H}\}$ -NMR for **b** by GC MS with mesitylene as internal standard.

As can be seen in Table 2, when conducting the reaction in apolar aromatic solvents like benzene and toluene high conversions were obtained, however the selectivity of the reaction was inferior when compared to conducting the reaction in the polar solvent THF or without solvent. The selectivity in THF and under neat conditions was comparable, however THF was chosen for the reaction, as the reaction under neat conditions also yielded the markovnikov hydrosilylation product, which was absent when using THF as a solvent. The catalyst loading could be lowered to 1 mol% while maintaining full conversion for 4-fluoroallylbenzene, however when conducting the reaction with unsubstituted allylbenzene, the conversion dropped to 83%, after which the catalyst loading was retained at 2 mol% for most substrates.

Interestingly, when conducting the reaction at room temperature, an increased formation of dehydrogenative silylation as well as markovnikov hydrosilylation products was observed. Complexes **3** and **5** were then tested under optimized reaction conditions, displaying however a drastic decrease in reactivity when compared to complex **4**.

With the optimized reaction conditions in hand, catalyst **4** was employed in hydrosilylation of allylic and aliphatic alkenes. (Table 3)

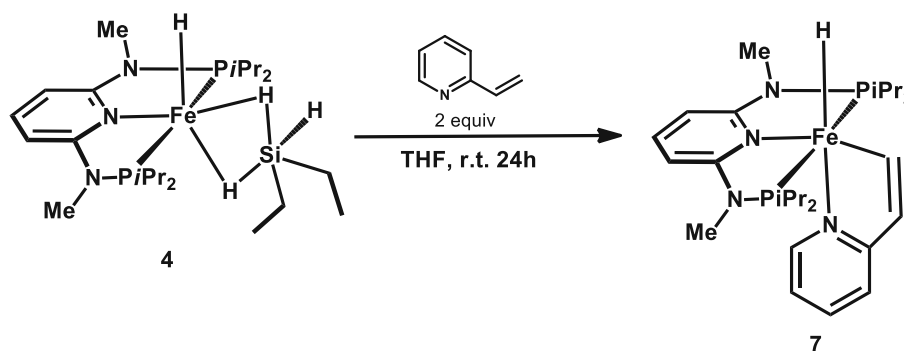
Table 3 Substrates and scope for the hydrosilylation of alkene by **4**

^a reaction conditions: alkene (0.021 mmol, 1 equiv), **4** (2 mol%), diethylsilane (69 μ l, 2.5 equiv), 0.25 ml THF, 50°C, 20 h, ^b alkene (0.021 mmol, 1 equiv), **4** (1 mol%), diethylsilane (69 μ l, 2.5 equiv), 0.25 ml THF, 50°C, 20 h, ^c alkene (0.021 mmol, 1 equiv), **4** (2 mol%), diethylsilane (69 μ l, 2.5 equiv), neat, 50°C, 20 h Conversion was determined by GC/MS with an internal standard of mesitylene, numbers in parantheses give isolated yield.

While the catalyst performed well for aromatic and aliphatic alkenes, the functional group tolerance was limited. For halides, only fluorine substituents were tolerated, and substrates containing alcohols or esters showed no conversion. Furthermore, the catalyst did also not hydrosilylate internal alkenes. Likewise, allylphenylether was not converted, which can be attributed to the fact that the substrate underwent Claisen rearrangement¹¹² under reaction conditions, with the forming allylphenol acting as catalyst poison. Nevertheless, substrates containing amine functionalities were readily tolerated.

2.3. Mechanistic Studies

To gain further insight into the mechanism of the reaction, stoichiometric studies were conducted with **4**. It could be shown that in absence of silanes, the complex readily reacts with alkenes even at room temperature, forming deep red solutions of hydrogenated alkane and paramagnetic by-products. By utilizing an excess of 2-vinylpyridine a single diamagnetic complex **7**, as well as one equivalent of 2-ethylpyridine were obtained. **7** was studied by multinuclear NMR spectroscopy as well as single crystal X-ray diffraction and identified as $[(\text{PNP}^{\text{NMe}})\text{Fe}(\text{H})(\kappa^2\text{-C,N, py-CH=CH})]$, which was formed by apparent vinylic $\text{sp}^2\text{-C-H}$ activation of the alkene. (Scheme 28)



Scheme 28 Synthesis of complex **7** from **4** via vinylic C-H activation

Complex **7** features a signal in the $^{31}\text{P}\{^1\text{H}\}$ -NMR spectrum at 162.9 ppm. In the ^1H -NMR, the hydride ligand can be observed as a triplet at -16.62 ppm with a relatively large $^2J_{\text{PH}}$ -coupling constant of 72.5 Hz. The coordinated vinyl moiety as well as the neighboring CH group can be observed as a multiplet between 7.66-7.62 ppm. In the $^{13}\text{C}\{^1\text{H}\}$ -NMR spectrum, the signal attributed to the coordinated vinyl ligand features a broad signal at 149.6 ppm.

Single crystal X-Ray diffraction shows that **7** adopts a slightly distorted octahedral geometry. The 2-vinylpyridine ligand coordinates in a κ^2 fashion, with the pyridine moiety being located trans to the hydride ligand, while the vinylic carbon is situated trans to the pyridine moiety of the pincer ligand. The Fe1-C1 bond length was measured to be 1.931(7) Å, while the C1-C2 bond length of 1.372(9) Å is indicative of a still existing double bond. (cf. ethylene 1.339 Å)¹¹³

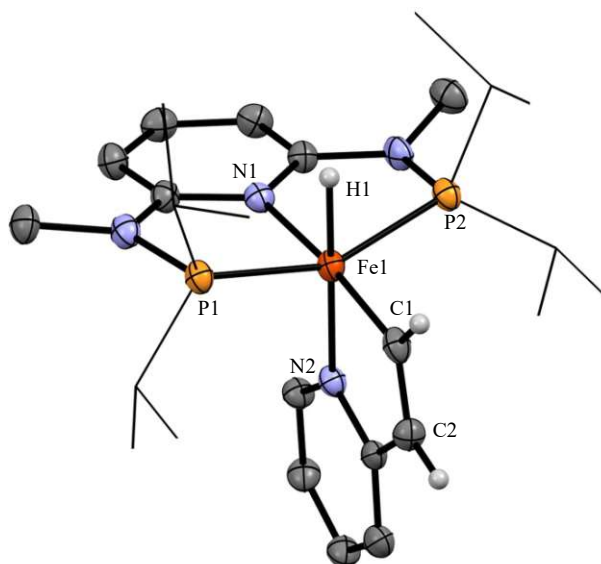


Figure 9. ORTEP view of $[(\text{PNP}^{\text{NMc}})\text{Fe}(\text{H})(\kappa^2\text{-C,N, py-CH=CH})]$ (**7**) showing 50% thermal ellipsoids (most H omitted for clarity). Selected bond lengths (Å) and angles (deg): Fe1-N1 2.012(5), Fe1-P1 2.153(2), Fe1-P2 2.160(2), Fe1-N2 2.020(5), Fe1-H1 1.55(6), Fe1-C1 1.931(7), C1-C2 1.372(9); N1-Fe1-C1 172.70, P1-Fe1-P2 155.66.

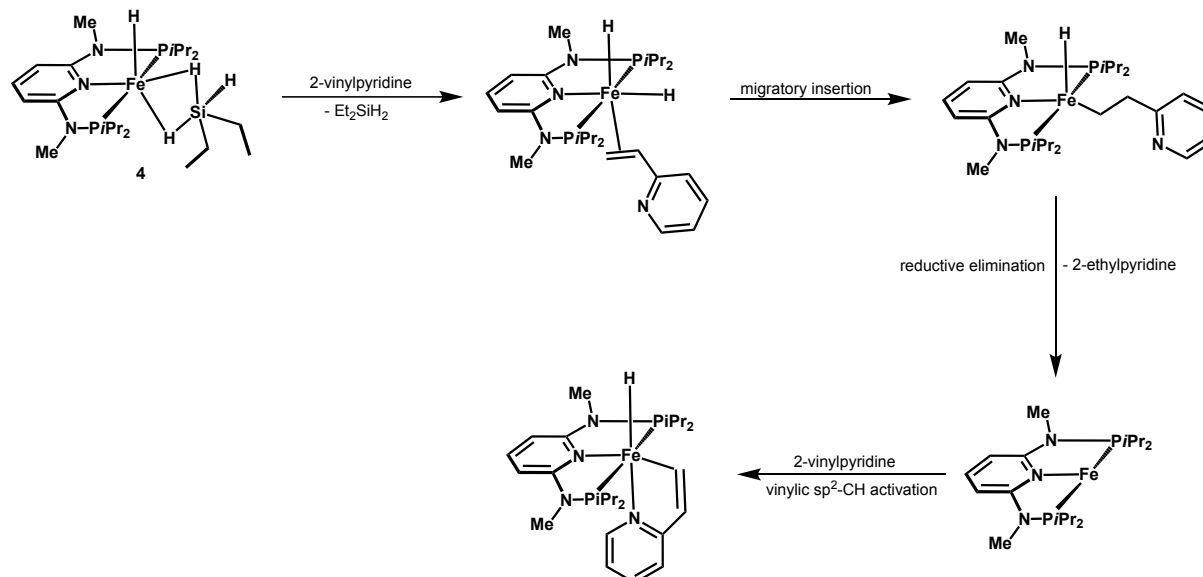
Noteworthy, complexes featuring a sp^2 -vinylic metal-carbon bond are quite rare in literature. *Bergman* studied Iridium vinyl complexes in the 1980s and found that one reason for the scarcity of sp^2 CH-activated alkene complexes are selectivity issues arising from the dominance of competitive π -coordination of the alkenes to single site metal transition complexes.^{114,115} For example, it was ruled out that a π -complex can be a viable intermediate for the vinylic CH activation, as the formation of a π -complex was thermodynamically favored compared to oxidative addition of the C-H bond.¹¹⁴

As for Fe, only two examples of single site low valent Fe(bisphosphine) complexes being capable of vinylic sp^2 -CH activation were reported by *Field*. In these studies, a Fe(0) complex generated by in situ photolysis of either dihydride or alkyl-hydride complexes showed reactivity towards alkenes to generate the C-H activated vinylic hydride complexes. These complexes were only stable at low temperatures, as allowing the reaction mixtures to warm to room temperature triggered an isomerization to the corresponding π -complexes, a reaction that was shown to not be reversible.^{116,117}

Recently, the vinylic sp^2 -CH activation of alkenes employing a bimetallic iron-aluminium complex was reported by *Crimmin* and *Gorgas*. The mechanism of this reaction was reported to proceed *via* initial binding of the alkene across the Fe-Al bond and subsequent intramolecular transition state to achieve CH activation.¹¹³

Consequently, in accordance with the reports by *Field*, a possible mechanism for the generation of **7** could be an initial replacement of the labile $\eta^2\text{-SiEt}_2\text{H}_2$ ligand of **4** by an entering alkene. After migratory insertion of the alkene into the Fe-H bond, an unsaturated

$16e^-$ alkyl-hydride complex is formed that can undergo reductive elimination to create a $Fe(0)$ complex thereby generating 1 equiv of 2-ethylpyridine. Oxidative addition of an entering 2-vinylpyridine molecule leads consequently to the formation of **7**. (Scheme 29)



Scheme 29 Plausible mechanism for the formation of **7**

It is noteworthy, that a similar deep red complex is formed when **4** is treated with an excess of 2-allylpyridine. The complex features a signal in the $^3P\{^1H\}$ NMR at 159.2 ppm and a triplet in the hydridic region of the 1H -NMR located at -16.86 ppm with an analogously large coupling constant of 77.2 Hz. However, due to impurities, the exact position of the double bond in the complex could as of yet not be established.

In contrast to that, complex **4** does not readily react with 2-phenylpyridine to yield an aromatic sp^2 -activation product, hinting to alkene instead of pyridine coordination being necessary to replace the labile η^2 - $SiEt_2H_2$ ligand, which is crucial for the observed CH-activation.

These findings suggest that insertion of alkenes into the Fe-H bond of a putative dihydride complex, featuring a side-on coordinated alkene can be plausible. Thus, a mechanism similar to the classical Chalk-Harrod cycle during the catalytic hydrosilylation of alkenes with **4** is proposed.

2.4. Ligand Exchange Reactions

To gain further insight into the differences in bonding between complexes **3** and **4** and their drastically different reactivities in catalysis, a series of ligand exchange reactions were carried out.

Treatment of complexes **3** and **4** with 1 bar of D₂ gas in a Young NMR tube led to rapid incorporation of the deuterium into both, Fe-H as well as Si-H bonds. However, as judged by ¹H-NMR spectroscopy, after incorporation of 60% deuterium in **3** and 55% deuterium incorporation in **4**, respectively, equilibria were reached. Due to deuterium incorporation, the ³¹P{¹H}-NMR spectra of both complexes showed a broadening of the signals. Furthermore, in both reactions, gradual formation of H₂ as well as HD gas was observed. (Figure 10)

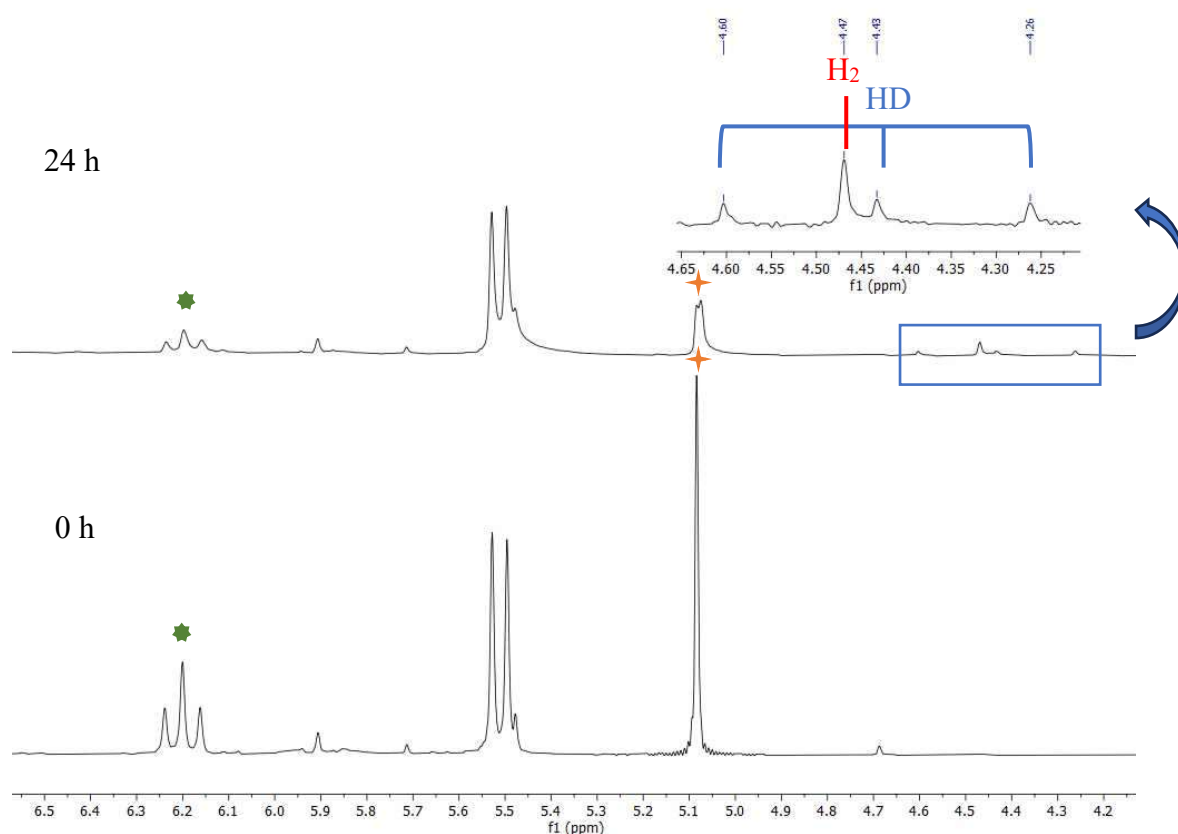


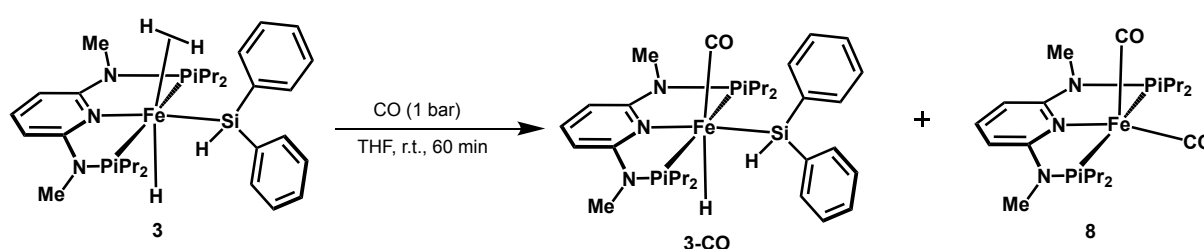
Figure 10. Section of the ¹H-NMR spectrum of **3** measured in C₆D₆. The lower part of the spectrum represents **3** before D₂ exposure the upper segment the reaction after 24 h exposure to 1 bar D₂. ★ denotes the Si-H bond on the silyl ligand ★ denotes residual Ph₂SiH₂.

Interestingly, during the reaction of D₂ with **4** two additional minor diamagnetic species were detected, of which one was identified as the partially deuterated complex **Fe20-NMe**, reinforcing the labile character of the η²-SiEt₂H₂ ligand, while the rapid incorporation of the

deuterium in all bonds suggests an equilibrium between the η^2 -dihydrogen and η^2 -alkylsilane structures, probably facilitated by σ CAM processes.

To further study the ligand exchange behavior of complexes **3** and **4**, they were treated with a series of ancillary ligands.

Treatment of a THF solution of **3** with 1 bar of CO, led to mainly the formation of the complex $[(\text{PNP}^{\text{NMe}})\text{Fe}(\text{H})(\text{SiPh}_2\text{H})(\text{CO})]$ (**3-CO**). However, due to reductive coupling of the silyl moiety with the hydride ligand, the Fe(0) complex $[(\text{PNP}^{\text{NMe}})\text{Fe}(\text{CO})_2]$ (**8**) was also formed in an integral ratio of 8:1. The identity of **8** was confirmed by comparing the spectroscopic data with those reported in literature.¹¹⁸ (Scheme 30)



Scheme 30 Treatment of **3** with CO and formation of **3-CO** and the Fe(0) complex **8**

Characteristic features of **3-CO** in the ^1H -NMR spectrum include a sharp triplet of the not coordinated Si-H bond at 5.84 ppm, with a $^3J_{\text{PH}}$ coupling constant of 9.2 Hz and a triplet in the hydride region of the spectrum at -7.57 ppm and $^2J_{\text{PH}}$ a coupling constant of 49.3 Hz, assignable to the remaining Fe-H bond. The complex features a singlet in the $^{31}\text{P}\{^1\text{H}\}$ -NMR spectrum located at 170.4 ppm. In the $^{13}\text{C}\{^1\text{H}\}$ -NMR spectrum, the carbonyl ligand can be observed as a triplet at 217.4 ppm with a $^2J_{\text{PC}}$ coupling constant of 17.3 Hz.

Furthermore, a ^{29}Si - ^1H HMBC experiment was conducted in which the coordinating silyl ligand was located at 24.1 ppm, which is a slight downfield shift when compared to **3**, where the silyl moiety was located at 15.2 ppm. In an ATR-IR experiment, a distinct carbonyl stretching band could be observed at 1889 cm^{-1} , which is comparable to the wavenumber found in $[(\text{PNP}^{\text{CH}_2})\text{Fe}(\text{H})(\text{SiPh}_2\text{H})(\text{CO})]$ (**Fe6-CO**) of 1879 cm^{-1} , reported by the group of Chirik, by treating **Fe6-Si** with 1 atm of CO gas.⁶³

Similarly, repeated freeze-pump-thaw cycles of a C_6D_6 solution of **3** in a Young NMR tube and subsequent backflushing with 1 bar N_2 gas led to the gradual replacement of the η^2 -dihydrogen ligand by dinitrogen and the formation of complex $[(\text{PNP}^{\text{NMe}})\text{Fe}(\text{H})(\text{SiPh}_2\text{H})(\text{N}_2)]$ (**3-N₂**) as judged by a combination of ^1H -NMR and $^{31}\text{P}\{^1\text{H}\}$ -NMR spectroscopy. (Figure 11)

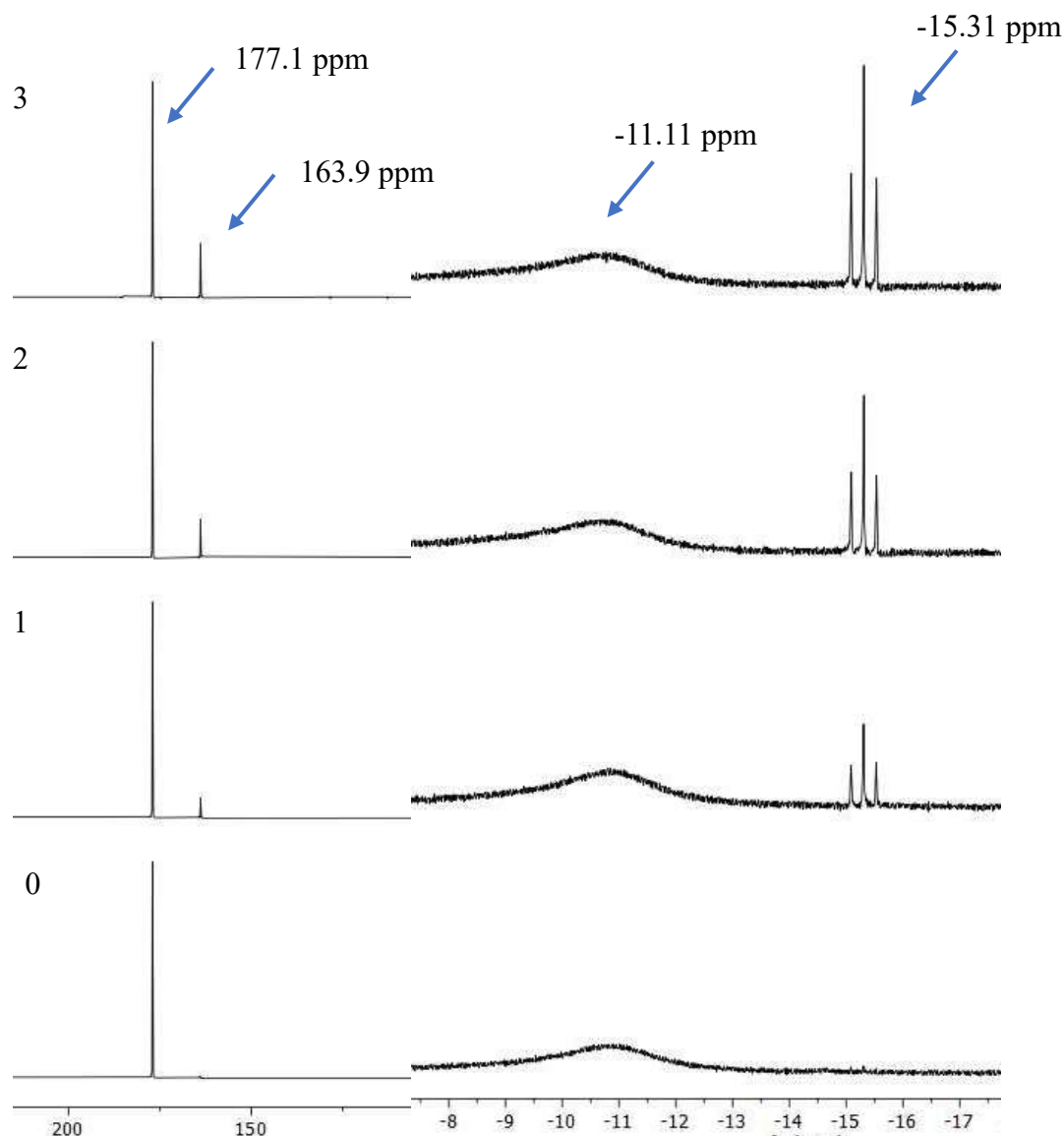


Figure 11. Gradual formation of **3-N₂** as observed in the $^{31}\text{P}\{^1\text{H}\}$ -NMR spectrum (left) and ^1H -NMR spectrum (right) by exposure of **3** to nitrogen gas. The numbers on the top left indicate the number of freeze-pump-thaw cycles and N_2 backflushes of the sample.

3-N₂ features a singlet in the $^{31}\text{P}\{^1\text{H}\}$ -NMR spectrum at 163.9 ppm. The ^1H -NMR spectrum features a characteristic triplet at 5.85 ppm with a $^3J_{\text{PH}}$ coupling constant of 10.0 Hz, which is assignable to the hydrogen atom located on the silyl ligand.

The hydride ligand was observed at -15.31 ppm with a $^2J_{\text{PH}}$ coupling constant of 55.6 Hz. The stretching band of the coordinated dinitrogen ligand was observed in the ATR-IR spectrum at 2055 cm^{-1} . In comparison, the dinitrogen ligand of **Fe6-Si** was observed at 2032 cm^{-1} , indicating a slightly more electron rich iron center in the latter.⁶³

The solid-state structure of **3-N₂** was elucidated confirming a slightly distorted octahedral geometry of the complex. (Figure 12)

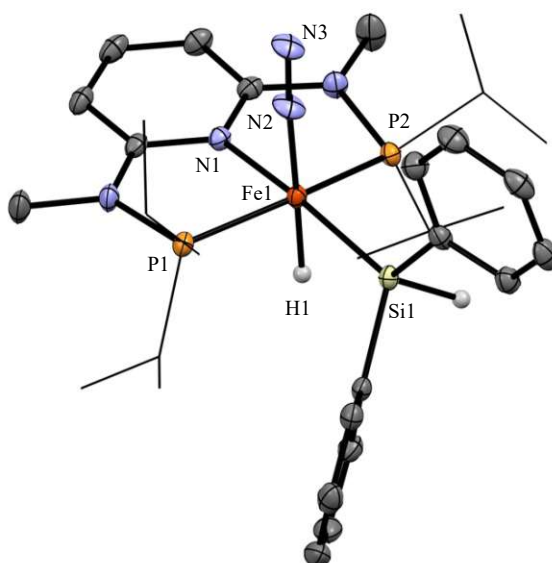
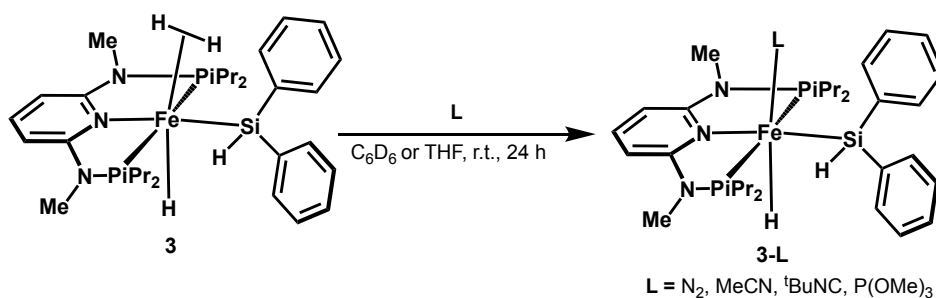


Figure 12. ORTEP view of [(PNP^{NMe})Fe(H)(SiPh₂H)(N₂)] (3-N₂) showing 50% thermal ellipsoids (most H omitted for clarity). Selected bond lengths (Å) and angles (deg): Fe1-N1 2.017(7), Fe1-P1 2.161(8), Fe1-P2 2.161(6), Fe1-Si1 2.279(1), Fe1-H1 1.44(4), Fe1-N2 1.885(4), N2-N3 1.135(1); N1-Fe1-Si1 169.22, P1-Fe1-P2 163.17.

The Fe1-Si1 bond distance of 2.279(1) Å is slightly shorter when compared to **3** (2.283(1) Å), while the Fe1-N2 bond distance of 1.885(4) Å and the N2-N3 bond distance of 1.135(1) Å are comparable to the distances observed in the isostructural complex **Fe6-Si**, which were reported as 1.8002(17) Å and 1.120(2) Å, respectively.⁶³

In a similar fashion, treatment of **3** with MeCN, ^tBuNC as well as P(OMe)₃ led to replacement of the η²-dihydrogen ligand and formation of the complexes[(PNP^{NMe})Fe(H)(SiPh₂H)(L)] (**3-L**) (L = MeCN, ^tBuNC, P(OMe)₃) (Scheme 31)



Scheme 31 Treatment of **3** with ancillary ligands **L** and formation of complexes **3-L**

In contrast to **3-^tBuNC** and **3-P(OMe)₃**, **3-MeCN** was only stable in solution and consequently difficult to characterize. All three complexes were studied *via* NMR spectroscopy and the characteristic spectroscopic shifts of the complexes **3-L** are listed in Table 4.

The solid structure of **3-P(OMe)₃** was additionally elucidated *via* single crystal X-Ray diffraction.

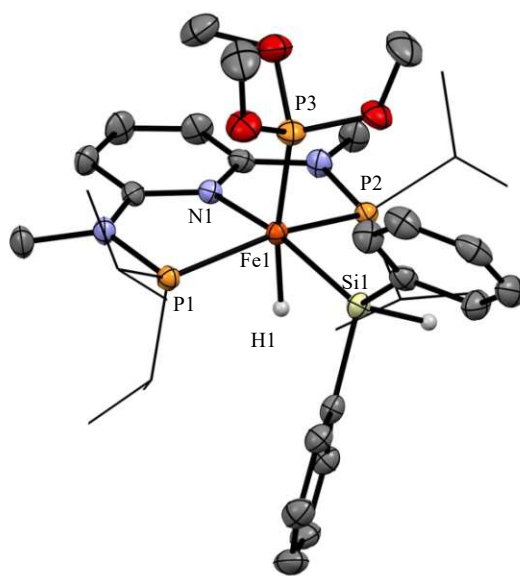
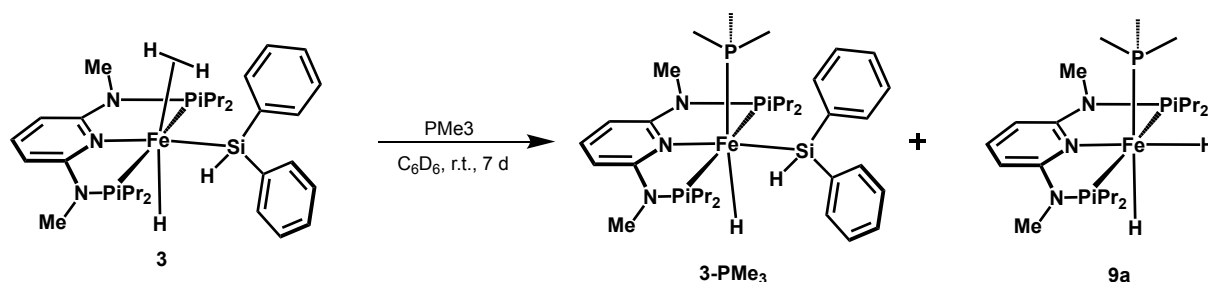


Figure 13. ORTEP view of $[(\text{PNP}^{\text{NMe}})\text{Fe}(\text{H})(\text{SiPh}_2\text{H})(\text{P}(\text{OMe})_3)]$ (**3-P(OMe)₃**) showing 50% thermal ellipsoids (most H and independent solvent molecule omitted for clarity). Selected bond lengths (Å) and angles (deg): Fe1-N1 2.037(2), Fe1-P1 2.1829(8), Fe1-P2 2.1982(8), Fe1-Si1 2.3094(7), Fe1-H1 1.44(3), Fe1-P3 2.125(1); N1-Fe1-Si1 164.15, P1-Fe1-P2 154.96, H1-Fe1-P3 165.77.

3-P(OMe) shows a distorted octahedral geometry, with the expected *trans* arrangement of the ancillary phosphite ester ligand and the hydride. The Fe1-Si1 bond distance of 2.3094(7) Å is slightly longer than in **3-N₂** (c.f. 2.279(1) Å). The Fe1-P3 distance of 2.125(1) Å is comparable to the iron-phosphorus bonds of the PNP moiety, which were measured as 2.1829(8) Å and 2.1982(8) Å, respectively. It is noteworthy, that the hydride ligand H1 is bend slightly towards the silyl ligand, which is illustrated by the H1-Fe1-P3 bond angle of 165.77°. The H1-Si1 distance of 2.270 Å is in the range of distances observed for complex **3**, indicative of secondary interaction between the silyl ligand and the hydride ligand.

Additionally, for **3-P(OMe)₃** an inverse gated decoupled $^{29}\text{Si}\{^1\text{H}\}$ -NMR measurement was carried out, where the coordinated silyl ligand was observed at 26.8 ppm as a quartet with a $^2J_{\text{SiP}}$ coupling constant of 35.9 Hz. Interestingly, instead of the expected triplet of doublets only a quartet could be observed, probably because of similar coupling constants of the

phosphine moieties on the PNP pincer ligand and the trimethylphosphite moiety to the silicon atom.



Scheme 32 Treatment of **3** with PMe_3 leads to the formation of **3- PMe_3** and **9a**

3 was also treated with the alkylphosphine ligand PMe_3 . However, compared to the reaction times observed with the previously mentioned ligands, the reaction was significantly slower. Even after seven days, no full conversion could be achieved, and additionally the formation of another diamagnetic species in addition to $[(\text{PNP}^{\text{NMe}})\text{Fe}(\text{H})(\text{SiPh}_2\text{H})(\text{PMe}_3)]$ (**3- PMe_3**) was observed during the experiment. This diamagnetic species was identified as $[(\text{PNP}^{\text{NMe}})\text{Fe}(\text{H})_2(\text{PMe}_3)]$ (**9a**). (Scheme 32) Formation of **9a** again suggests, that the silyl ligand on the metal center is also labile to substitution, indicating a possible equilibrium in **3** between the η^2 -dihydrogen structure and the η^2 -dialkylsilane structure observed in the crystal structures of **4** and **5**.

In a final ligand substitution reaction, complex **3** was also treated with pyridine, however even after reaction times of over a week, no conversion into a new diamagnetic species could be observed.

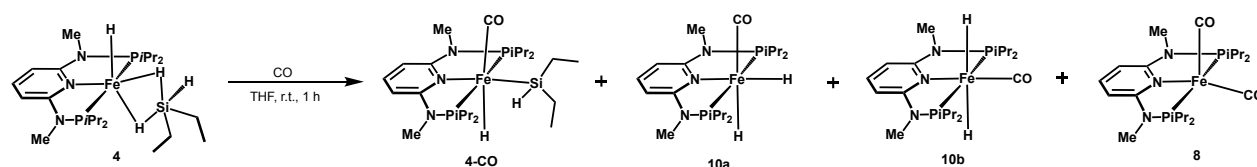
The characteristic NMR shifts and coupling constants of complexes **3-L** are listed in Table 4.

Table 4 Characteristic NMR shifts and coupling constants of complexes **3-L**

Complex	¹ H-NMR				³¹ P{ ¹ H}-NMR		²⁹ Si{ ¹ H}-NMR	
	hydride	² J _{PH}	silyl	³ J _{PH}		² J _{PP}		² J _{PSi}
	(ppm)	(Hz)	(ppm)	(Hz)	(ppm)	(Hz)	(ppm)	(Hz)
3-CO	-7.57 (t)	49.3	5.84 (t)	9.2	170.4	-	24.1	-
3-N ₂	-15.31 (t)	55.6	5.85 (t)	10.0	163.9	-	-	-
3-MeCN	-19.96 (t)	58.9	5.80 (t)	8.6	167.3	-	-	-
3- ^t BuNC	-10.62 (t)	58.8	5.78 (t)	8.0	172.3	-	-	-

3-P(OMe)₃	-9.70 (dt)	66.7	5.83 (q)	5.8	170.9 (d)	43.5	26.8 (q)	35.9
		61.8			164.9 (t)	43.5		
3-PMe₃	-13.21 (td)	72.1	5.81 (q)	8.2	170.6 (d)	25.5	-	-
		20.5			5.5 (t)	26.0		

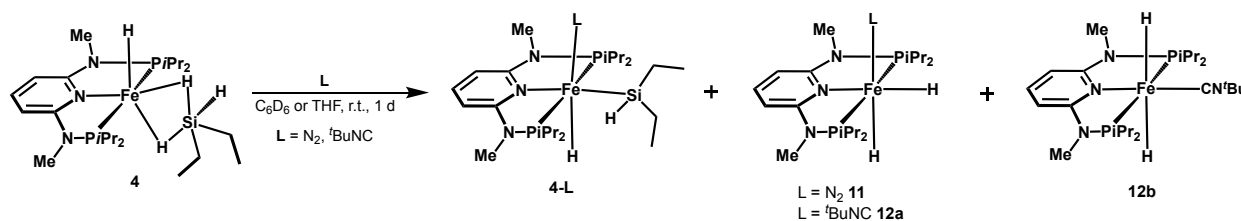
When carrying out the same ligand exchange reactions with **4** drastically different results were observed. Treatment of a THF solution of **4** with 1 bar of CO led to the formation of four diamagnetic species in an integral ratio of 70:7:14:9 as judged by $^{31}\text{P}\{^1\text{H}\}$ -NMR spectroscopy. The compounds were subsequently identified as $[(\text{PNP}^{\text{NMe}})\text{Fe}(\text{H})(\text{SiEt}_2\text{H})(\text{CO})]$ (**4-CO**), $[(\text{PNP}^{\text{NMe}})\text{Fe}(\text{CO})_2]$ (**8**) and the *cis* and *trans* isomers of $[(\text{PNP}^{\text{NMe}})\text{Fe}(\text{H})_2(\text{CO})]$ (**10a** and **10b**), respectively.¹¹⁹ (Scheme 33)



Scheme 33 Treatment of **4** with CO and formation of **4-CO**, the Fe(0) complex **8** and hydrides **10a** and **10b**

These results again indicate that both the silane of a Si-H σ -complex, affording **10a** and **10b**, as well as a η^2 -dihydrogen ligand, affording **4-CO** complex, can be substituted by CO, corroborating an equilibrium between the resonance structures in solution.

Treatment of a C_6D_6 solution of **4** in a Young-NMR tube with 1 bar of N_2 gas also rapidly led to the formation of two new diamagnetic species, which were tentatively assigned as $[(\text{PNP}^{\text{NMe}})\text{Fe}(\text{H})(\text{SiEt}_2\text{H})(\text{N}_2)]$ (**4-N₂**) and the *cis* isomer of the dihydride complex $[(\text{PNP}^{\text{NMe}})\text{Fe}(\text{H})_2(\text{N}_2)]$ (**11**), however rapid broadening of the ^1H -NMR spectra, indicative of rapid decomposition of the complexes, complicated their characterization. The presence of **11** in the sample was confirmed by preparing an authentic sample *via* treatment of **Fe20-NMe** with 1 bar of N_2 gas. In a similar fashion, treatment of a THF solution of **4** with 1 equiv of $t\text{BuNC}$ led to the formation of three new diamagnetic species, characterized as **4-*t*BuNC** and the *cis* and *trans* isomers of the dihydride complexes **12a** and **12b**. (Scheme 34)



Scheme 33 Treatment of **4** with N_2 and $tBuNC$ and formation of **4-L**, the dihydride complexes **11**, **12a** and **12b**

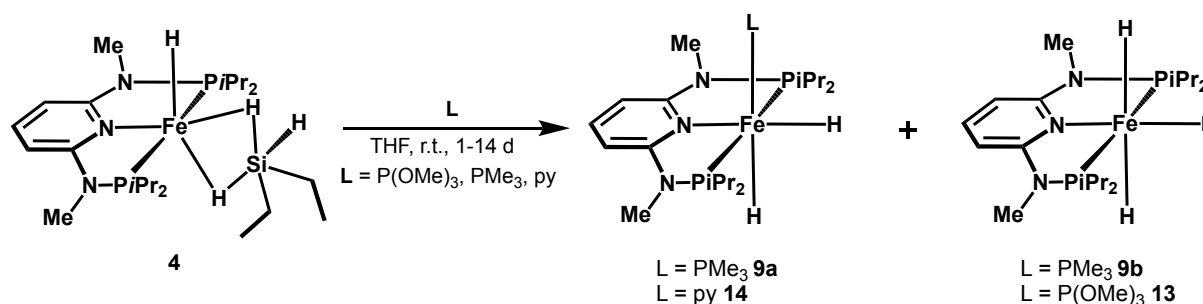
When treating a THF solution of **4** with an excess of MeCN, a rapid color change to intense red was observed, however spectroscopic analysis showed the formation of a multitude of new species, that could not be identified. Table 5 lists the characteristic spectroscopic shifts of the complexes **4-L**. A table of the characteristic spectroscopic shifts of the dihydride complexes **9-14** is given in chapter 2.6.

Table 5 Characteristic NMR shifts and coupling constants of complexes **4-L**

Complex	1H -NMR			$^{31}P\{^1H\}$ -NMR
	hydride (ppm)	$^2J_{PH}$ (Hz)	silyl (ppm)	(ppm)
4-CO	-8.26 (t)	51.0	4.23 (m)	172.2
4-N₂	-15.16 (t)	55.3	4.31 (m)	165.9
4-$tBuNC$	-11.05 (t)	57.7	4.24 (m)	174.5

In contrast to that, treatment of **4** with an excess of $P(OMe)_3$, PMe_3 or pyridine in THF led to the formation of only a single main product, which were identified as the dihydride complexes *trans*- $[(PNP^{NMe})Fe(H)_2(P(OMe)_3)]$ (**13**), *cis*- $[(PNP^{NMe})Fe(H)_2(PMe_3)]$ (**9a**) and *cis*- $[(PNP^{NMe})Fe(H)_2(py)]$ (**14**), respectively.

While **13** was the only product observed in the reaction of **4** with $P(OMe)_3$, in case of PMe_3 a second minor species identified as *trans*- $[(PNP^{NMe})Fe(H)_2(PMe_3)]$ (**9b**) was observed at a integral ratio of 7.5%. (Scheme 34) As for pyridine, even after prolonged reaction times of 2 weeks with 10 equiv pyridine, only a conversion of approximately 20 % to **14** was observed in the $^{31}P\{^1H\}$ -NMR spectrum. No evidence of formation of the putative complexes $[(PNP^{NMe})Fe(H)(SiEt_2H)(P(OMe)_3)]$ (**4-P(OMe)₃**), $[(PNP^{NMe})Fe(H)(SiEt_2H)(PMe_3)]$ (**4-PMe₃**) or $[(PNP^{NMe})Fe(H)(SiEt_2H)(py)]$ (**4-py**) were found, suggesting that the diethylsilyl moiety was cleanly substituted in all three cases.



Scheme 34 Treatment of **4** with P(OMe)_3 , PMe_3 and py form the dihydride complexes **9a**, **9b**, **13** and **14**

Crystals suitable for X-Ray diffraction analysis were grown from a concentrated *n*-pentane solution of **13** at -30°C . The solid-state structure of **13** is depicted in Figure 14, confirming the trans arrangement of the two hydride ligands. The structure is best described as slightly distorted octahedron, with the P1-Fe1-P2 plane showing the biggest deviation from linearity at 166.65° .

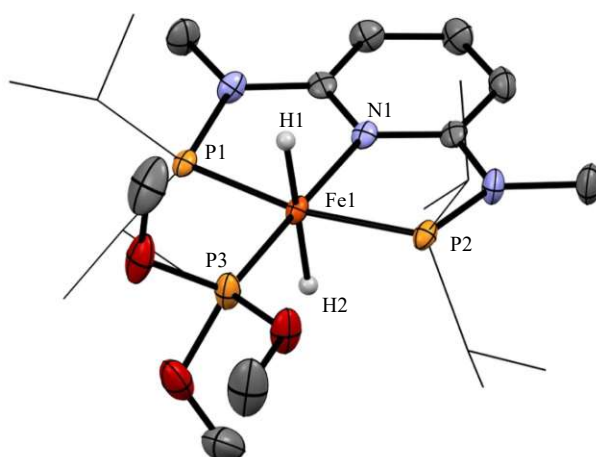
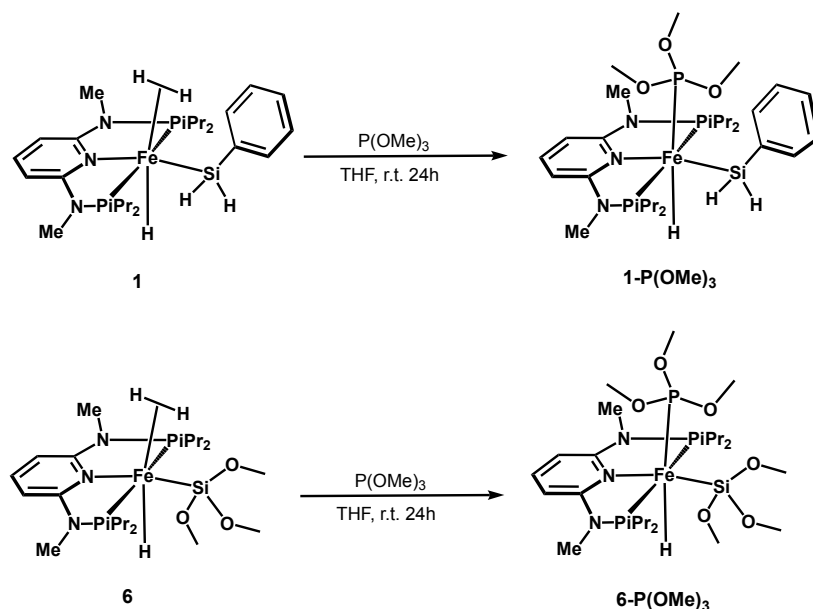


Figure 13. ORTEP view of *trans*-[PNP^{NMe}Fe(H)₂(P(OMe)₃)] (**13**) showing 50% thermal ellipsoids (most H omitted for clarity). Selected bond lengths (Å) and angles (deg): Fe1-N1 2.010(3), Fe1-P1 2.145(1), Fe1-P2 2.151(1), Fe1-P3 2.072(1), Fe1-H1 1.46(4), Fe1-H2 1.47(4); N1-Fe1-P3 177.98, P1-Fe1-P2 166.65, H1-Fe1-H2 175.42.

The P3-Fe1 bond distance of the trimethylphosphite ligand is with 2.072(1) Å slightly shorter than the phosphorus iron bonds of the PNP ligand, that were measured at 2.145(1) Å and 2.151(1) Å, respectively. It is also shorter than the phosphorus iron bond distance of the P(OMe)_3 ligand in **3-P(OMe)₃** of 2.125(1) Å.

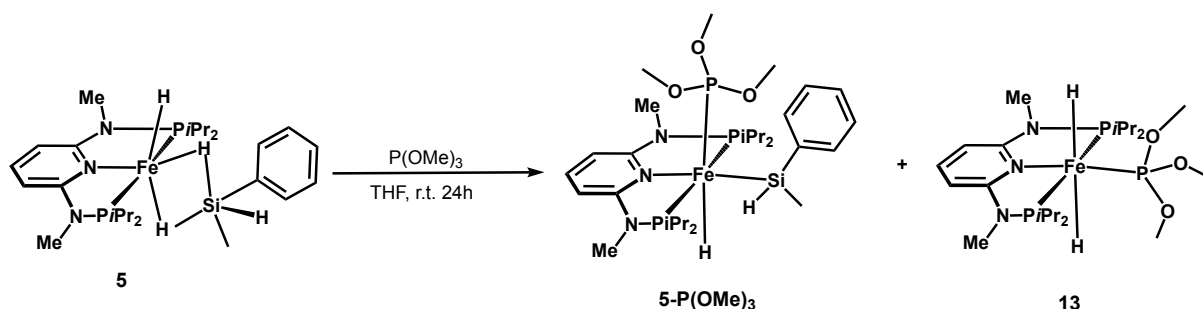
Due to the differences in reactivity of the above-mentioned ligand substitution reactions of **3** and **4**, it was decided to also study the substitution behavior of complexes **1**, **5** and **6** with

$\text{P}(\text{OMe})_3$. Treatment of THF solutions of **1** and **6** with the ancillary ligand selectively afforded the complexes **1-P(OMe)₃** and **6-P(OMe)₃**, closely mirroring the reactivity of **3** in substituting a η^2 -dihydrogen ligand. Both complexes were isolated as yellow solids in near quantitative yields and characterized with multinuclear NMR spectroscopy. (Scheme 35)



Scheme 35 Treatment of **1** and **6** with $\text{P}(\text{OMe})_3$ and formation of complexes **1-P(OMe)₃** and **6-P(OMe)₃**

When treating a THF solution of **5**, however, a mixture of 83 % **5-P(OMe)₃** and 17 % **13** was obtained, again underpinning the fact that **5** can be seen as an intermediate state between **3** and **4**. (Scheme 36)



Scheme 36 Treatment of **5** with $\text{P}(\text{OMe})_3$ and formation of complexes **5-P(OMe)₃** and **13**

In contrast to its congeneric complexes, the phosphine donors in the PNP ligand of **5-P(OMe)₃** do not exhibit the expected doublet resonance in the $^{31}\text{P}\{^1\text{H}\}$ -NMR spectrum, but rather two distinct doublet of doublets resonances are observed. This indicates that the phosphine moieties are not equivalent anymore. This is also contrasted by the spectrum of **5**, where only one singlet resonance can be observed in the $^{31}\text{P}\{^1\text{H}\}$ -NMR spectrum. The

inequivalence of the phosphine moieties can conceivably be explained by the slow rotation of the unsymmetrically substituted secondary silane ligand in the NMR time scale, creating a different chemical environment for both phosphine donor atoms. Interestingly, the coordinated trimethyl phosphite ligand exhibits the expected triplet resonance, indicating similar coupling constants of the inequivalent phosphorus atoms to the phosphite donor.

When comparing the $^2J_{PP}$ -coupling constants of the three distinct signals in the $^{31}\text{P}\{^1\text{H}\}$ -NMR spectrum, the two *trans*-phosphine atoms show an analogous $^2J_{PP}$ coupling constant of 83.3 Hz, while the coupling constants to the apical phosphite moiety vary and were measured as 43.9 Hz and 42.6 Hz, respectively. The NMR signal of the phosphite ligand features a $^2J_{PP}$ coupling constant of 43.0 Hz which is approximately the average of the two similar coupling constants observed in the signals of the phosphine donors. A similar effect can be observed in the ^1H -NMR and $^{13}\text{C}\{^1\text{H}\}$ -NMR spectra of the complex, which feature a doubling of the resonances assignable to the substituents of the phosphine donors compared to the symmetrically substituted congeners, hinting a loss of a mirror plane in the complex. The characteristic spectroscopic shifts of complexes **1-P(OMe)₃** - **6-P(OMe)₃** are listed in Table 6.

Table 6 Characteristic NMR shifts and coupling constants of complexes **1-P(OMe)₃** - **6-P(OMe)₃**

Complex	^1H -NMR				$^{31}\text{P}\{^1\text{H}\}$ -NMR		$^{29}\text{Si}\{^1\text{H}\}$ -NMR	
	hydride (ppm)	$^2J_{PH}$ (Hz)	silyl (ppm)	$^3J_{PH}$ (Hz)	(ppm)	$^2J_{PP}$ (Hz)	(ppm)	$^2J_{PSi}$ (Hz) _i
1-P(OMe)₃	-10.05 (q)	64.7	5.01 (q)	4.9	173.4 (d)	43.3	-3.0 (dt)	78.8
					164.1 (t)	42.1		47.2
3-P(OMe)₃	-9.70 (dt)	66.7	5.83 (q)	5.8	170.9 (d)	43.5	26.8 (q)	35.9
		61.8			164.9 (t)	43.5		
5-P(OMe)₃	-9.90 (q)	61.8	5.34 (m)	-	172.9 (dd)	83.3	11.3 (m)	-
						42.6		
					169.5 (dd)	83.3		
						43.9		
6-P(OMe)₃	-10.01 (q)	63.5	-	-	164.9 (t)	43.0	24.8 (q)	53.7
					177.0 (d)	42.7		
					169.3 (t)	41.9		

The ligand exchange studies indicated, that in the complexes containing secondary silane ligands, substitution of both, the η^2 -dihydrogen as well as the silane moiety can occur. To gain

further insight into this behavior DFT calculations were carried out for both **3** and **4**, comparing the energy profiles of the rearrangement of the η^2 -dihydrogen structure into the structure of the η^2 -dialkylsilane σ -Si-H complex.

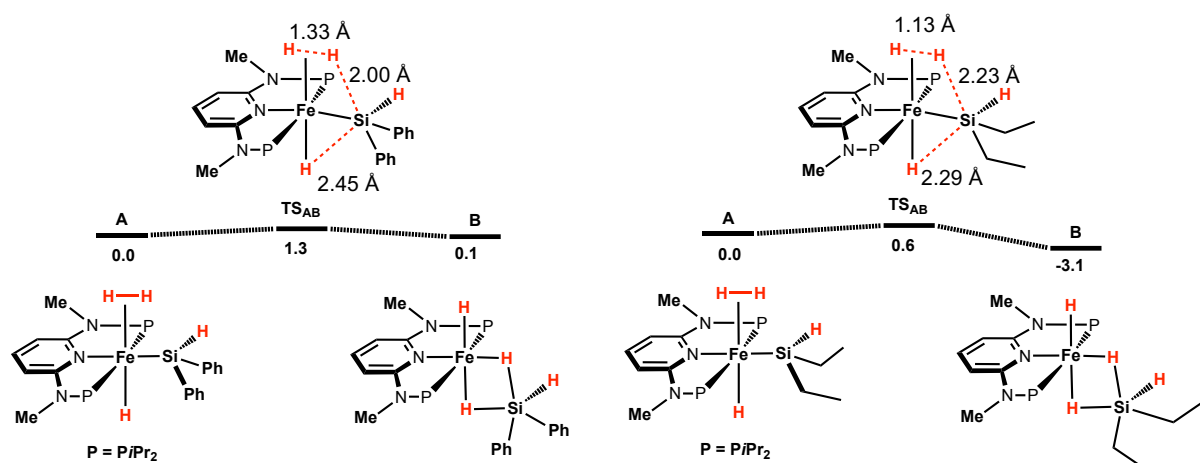


Figure 14. Gibbs free energy profile of the equilibria observed in complexes **3** (left) and **4** (right) with energies given in kcal/mol and selected bond lengths in the transition state given in Ångström.

As can be seen in Figure 14, the rearrangement of the bonds between the η^2 -dihydrogen **A** and the η^2 -dialkylsilane **B** resonance structures has a very low barrier for both complexes. It is noteworthy however, that for **4**, the barrier from **B** via the transition state **TS_{AB}** to **A** features a barrier of 3.1 kcal/mol, while a barrier of merely 0.1 kcal/mol was calculated for the same reaction in **3**. This suggests that while likely both structures are present at room temperature for both complexes, the η^2 -dialkylsilane structure is slightly favored in **4**, explaining the more facile substitution of the silyl ligand in this complex.

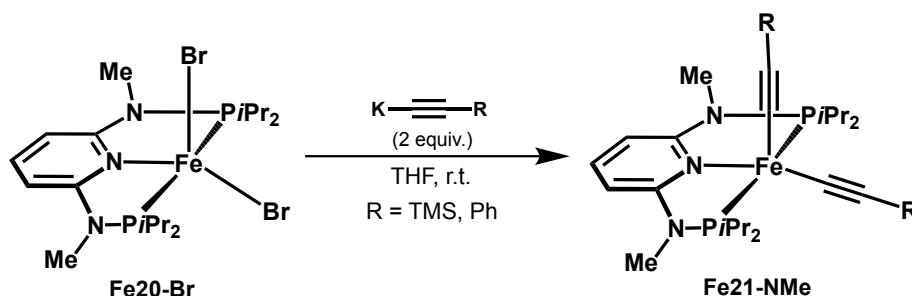
These studies further indicate that ligands such as alkenes can indeed substitute the silyl ligand on complexes **3** – **5**, making a classical Chalk-Harrod mechanism for the hydrosilylation of alkenes feasible. However, all complexes also show the potential for substitution of the η^2 -dihydrogen ligand facilitating subsequent migratory insertion into the Fe-Si bond, thus opening pathways for the modified Chalk-Harrod mechanism which can be associated with side reactions such as dehydrogenative hydrosilylation processes.

These calculations as well as the results of the experiments described above reasonably demonstrate that the increased catalytic activity of **4** can be rationalized by a more Si-H σ -complex character in the complex, thus facilitating substitution reactions of the silane moiety and creating pathways towards a classical Chalk-Harrod mechanism.

2.5. Fe PNP Acetylide Complexes and their Role in the Dimerization of Alkynes

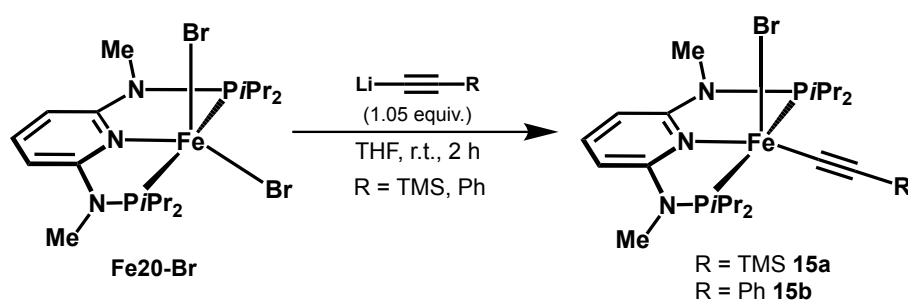
As described in Chapter 1.4, the Fe (II) bis(acetylide) PNP pincer complexes (**Fe21**) were determined to be the catalytically active species for the *Z*-selective dimerization of alkynes as well as the *Z*-selective hydroboration of alkynes by the polyhydride complexes **Fe20**. Complex **Fe21-NMe** was also successfully synthesized by treating the dihalide complex **Fe20-Br** with 2 equivalents of KHMDS in the presence of an excess of alkyne. (Scheme 37)

99



Scheme 37 Treatment of **Fe20-Br** with 2 equivalents of potassium acetylide and synthesis of **Fe21-NMe**

In the same manner it was anticipated that similar complexes, bearing only one acetylide moiety could be accessible when utilizing only one equivalent of alkali acetylide reagent. Consequently, treatment of **Fe20-Br** with a slight excess of lithium TMS-acetylide or lithium phenylacetylide, freshly prepared by reacting the corresponding acetylene with 1.05 eq of *n*-BuLi in THF, gave intensely dark colored solutions. Workup of the solution afforded in both cases yellow powder, that were characterized as the paramagnetic mono(acetylide) complexes [(PNP^{NMe})Fe(Br)(C≡C-TMS)] (**15a**) and [(PNP^{NMe})Fe(Br)(C≡C-Ph)] (**15b**) in a yield of 61 % and 63 % respectively. (Scheme 38)



Scheme 38 Treatment of **Fe20-Br** with 1.05 equivalents of potassium acetylide and synthesis of **15a** and **15b**

Solution magnetic susceptibility studies of **15a** and **15b** were conducted, indicating magnetic moments of $4.9(3) \mu_B$ and $4.9(1) \mu_B$, respectively, which is indicative of four unpaired electrons and thus 5-coordinate high-spin Fe(II) complexes in a quintet spin state ($S = 2$). Furthermore, IR spectroscopy was carried out and the stretching bands of the acetylide ligands were found at 1989 cm^{-1} for **15a** and 2045 cm^{-1} for **15b**, respectively. Additionally, high resolution mass spectrometry studies were conducted, where both complexes were observed as the $[(\text{PNP}^{\text{NMe}})\text{Fe}(\text{C}\equiv\text{C-R})]^+ [\text{M-Br}]^+$ ion at 522.2292 m/z (**15a**) and 526.2204 m/z (**15b**), respectively.

To unequivocally elucidate the solid state structures single crystals were grown of **15a** and X-Ray diffraction was carried out, indicating a slightly distorted square-pyramidal geometry ($\tau_5 = 0.13$), where the pyridine donor of the PNP backbone is located in *trans* position to the acetylide moiety. (Figure 15) A Fe1-C1 distance of $1.909(5) \text{ \AA}$ was measured, while the C1-C2 bond distance of the acetylide ligand was found to be $1.228(7) \text{ \AA}$, which is slightly elongated compared to free alkynes. (c.f. acetylene 1.203 \AA)¹²⁰ For comparison, in Figure 15, the structure of the previously reported intermediate spin ($S = 1$) complex $[(\text{PNP}^{\text{NMe}})\text{Fe}(\text{C}\equiv\text{C-TMS})_2]$ (**Fe21-NMe**) is also shown.

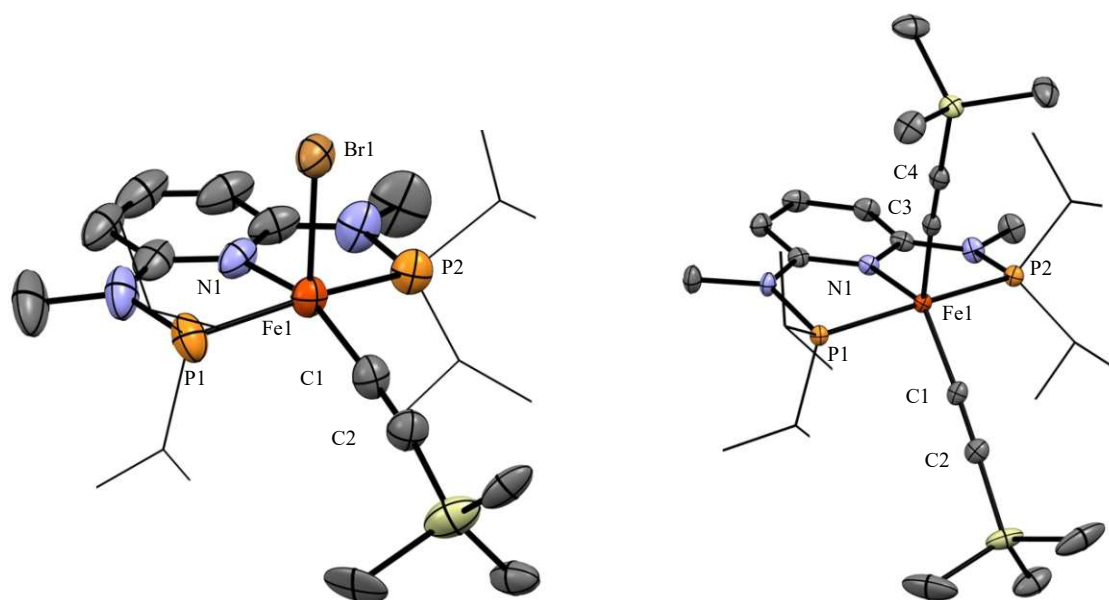
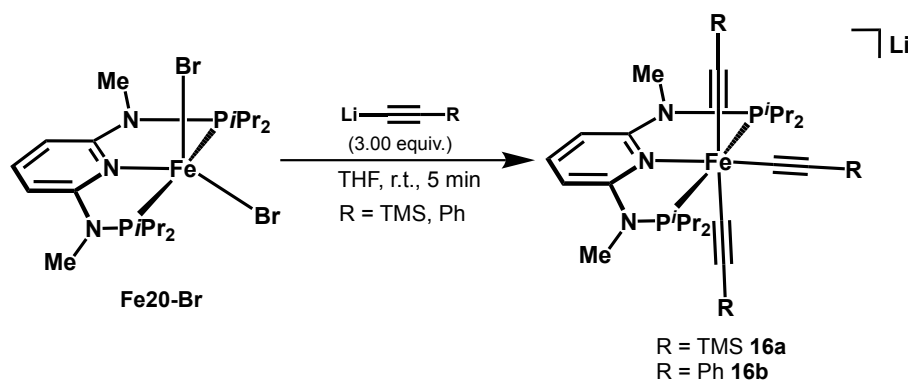


Figure 15. left: ORTEP view of $[(\text{PNP}^{\text{NMe}})\text{Fe}(\text{Br})(\text{C}\equiv\text{C-TMS})]$ (**15a**) showing 50% thermal ellipsoids (H omitted for clarity). Selected bond lengths (\AA) and angles ($^\circ$): Fe1-N1 2.019(4), Fe1-P1 2.214(1), Fe1-P2 2.209(2), Fe1-Br1 2.5467(9), Fe1-C1 1.909(5), C1-C2 1.228(7); N1-Fe1-C1 154.50 , P1-Fe1-P2 162.41 . right: ORTEP view of $[(\text{PNP}^{\text{NMe}})\text{Fe}(\text{C}\equiv\text{C-TMS})_2]$ (**Fe21-NMe**)⁹⁹ showing 50% thermal ellipsoids (H omitted for clarity). Selected bond lengths (\AA) and angles ($^\circ$): Fe1-N1 2.027(2), Fe1-P1 2.1936(6), Fe1-P2 2.2143(7), Fe1-C1 1.928(2), Fe1-C3 1.982(3), C1-C2 1.225(3), C3-C4 1.225(4); N1-Fe1-C1 134.15 , P1-Fe1-P2 163.08 .

In contrast to **15a**, the solid structure of **Fe21-NMe** is best described as an intermediate between the square-pyramidal and trigonal-bipyramidal geometries. ($\tau_5 = 0.48$) The carbon-iron bond lengths of 1.928(3) Å for the basal and 1.982(3) Å for the axial acetylide ligands is comparable, but slightly longer than the value obtained in **15a**. (1.909(5) Å). The -C≡C- bond lengths are with 1.225(3) Å and 1.225(4) Å very similar and marginally shorter than the one observed in **15a**. (1.228(7) Å)

When treating THF solutions of **Fe20-Br** with three or more equivalents of Li-C≡C-R (R = TMS, Ph), an instant color change from orange to golden yellow was observed. $^{31}\text{P}\{^1\text{H}\}$ -NMR spectroscopy indicated that in both cases a sole diamagnetic species was formed, featuring a singlet resonance at 147.2 ppm (**16a**) and 148.2 ppm (**16b**), respectively.

Complex **16a**, prepared by the addition of lithium TMS-acetylide, features two distinct singlet resonances in the ^1H -NMR spectrum at -0.03 ppm (9H) and -0.16 ppm (18H) which can be assigned to the TMS groups of two sets of inequivalent acetylide ligands. These data indicate the formation of the diamagnetic ($S = 0$) octahedral anionic complexes $\text{Li}[(\text{PNP}^{\text{NMe}})\text{Fe}(\text{C}\equiv\text{C-TMS})_3]$ (**16a**) and $\text{Li}[(\text{PNP}^{\text{NMe}})\text{Fe}(\text{C}\equiv\text{C-Ph})_3]$ (**16b**). (Scheme 39)



Scheme 39 Treatment of **Fe20-Br** with 3 equivalents of potassium acetylide and synthesis of **16a** and **16b**

Both complexes were found to only be stable in solution in etheric solvents, and removal of the solvent led to broadening of the signals, indicative of product degradation.

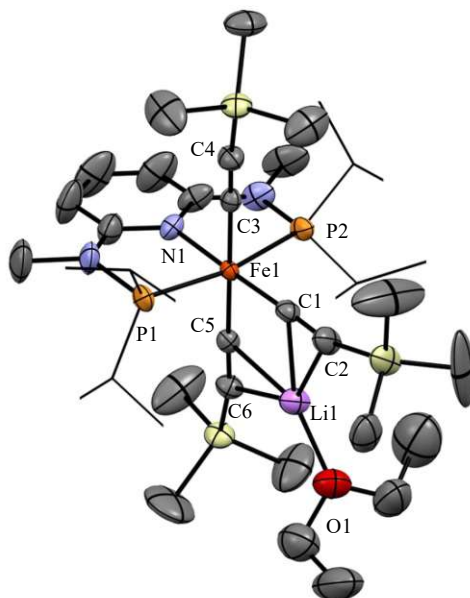
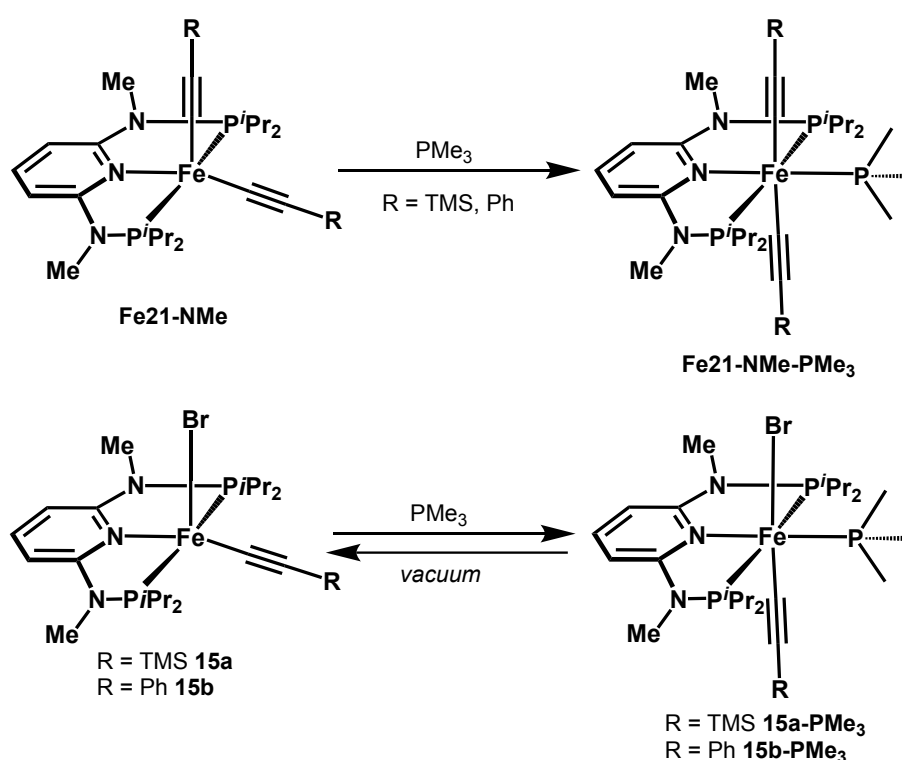


Figure 16. ORTEP view of $[\text{Li}\cdot\text{OEt}_2][(\text{PNP}^{\text{NMe}})\text{Fe}(\text{C}\equiv\text{C-TMS})_3]$ (**16a**) showing 50% thermal ellipsoids (H omitted for clarity). Selected bond lengths (Å) and angles (deg): Fe1-N1 1.992(3), Fe1-P1 2.199(1), Fe1-P2 2.179(1), Fe1-P3 2.072(1), Fe1-C1 1.888(4), Fe1-C3 1.931(3), Fe1-C5 1.918(3), C1-C2 1.225(6), C3-C4 1.220(5), C5-C6 1.223(5); N1-Fe1-C1 176.71., P1-Fe1-P2 167.84, C3-Fe1-C5 179.04.

Fortunately, single crystals of **16a** could be grown from a concentrated solution in diethyl ether. Single crystal X-Ray diffraction analysis confirms the nearly perfect octahedral geometry of the complex. The Li cation is embedded between the basal and one of the apical acetylide ligands and is further stabilized by a coordinating diethyl ether moiety. The lack of stabilization of the cation may be responsible for the degradation of the complex observed after evaporation of the solvent. The iron carbon distances of the acetylide ligands diverge, showing the shortest bond length in the basal ligand (1.888(4) Å) and the longest Fe-C distance observed on the apical ligand, without cation embedment, which was measured at 1.931(3) Å. Interestingly, the C≡C triple bond distances of the three acetylides is similar, but they vary between 1.220(5) Å and 1.225(6) Å, with the shortest again observed in the acetylide ligand without interaction to the cation and the longest observed in the basal acetylide ligand.

In analogy to the previously reported ligand exchange experiments with the (bis)acetylide complexes **Fe21-NMe**, the unsaturated $16e^-$ complexes **15a** and **15b** were treated with 1 equivalent of PMe_3 in THF. Analogously to **Fe21-NMe**, the color of the solutions immediately changed from yellow to red and spectroscopic analyses confirmed the formation of the diamagnetic complexes $[(\text{PNP}^{\text{NMe}})\text{Fe}(\text{Br})(\text{C}\equiv\text{C-TMS})(\text{PMe}_3)]$ (**15a-PMe₃**) and $[(\text{PNP}^{\text{NMe}})\text{Fe}(\text{Br})(\text{C}\equiv\text{C-Ph})(\text{PMe}_3)]$ (**15b-PMe₃**). (Scheme 40)



Scheme 40 Treatment of **15a** with PMe_3 and synthesis of the diamagnetic complexes **15a-PMe3** and **15b-PMe3**

However, in contrast to the complexes $[(\text{PNP}^{\text{NMe}})\text{Fe}(\text{C}\equiv\text{C-TMS})_2(\text{PMe}_3)]$ and $[(\text{PNP}^{\text{NMe}})\text{Fe}(\text{C}\equiv\text{C-Ph})_2(\text{PMe}_3)]$ (**Fe21-NMe-PMe3**) that were synthesized by reacting the Fe-bis(acetylide) complexes **Fe21-NMe** with PMe_3 , the coordination of the trimethylphosphine ligand is reversible in **15a** and **15b** under vacuum.

Evaporation of the solvent and prolonged exposure to vacuum of **15a-PMe3** and **15b-PMe3** led to the general regeneration of the unsaturated 5-coordinated complexes **15a** and **15b**, which coincided with a color shift of the complexes from red back to yellow. The reversible coordination of the PMe_3 ligand can possibly explained by the difference in spin state between the intermediate-spin ($S = 1$) complexes **Fe21-NMe** and the high-spin ($S = 2$) complexes **15a** and **15b**.

Interestingly however, treatment of the high-spin dihalide complex **Fe20-Br** with PMe_3 did not yield a diamagnetic species. The lability of PMe_3 in **15a** and **15b**, as well as the lack of reaction of **Fe20-Br** with the phosphine might be attributed to the weaker ligand field in the dibromide as well as bromide/acetylide complexes compared to the stronger donor ability of the bis(acetylide) ligand environment.

These findings are underpinned by DFT calculations on the spin state splitting of the paramagnetic compounds (Figure 17). Calculations were carried out at the TPSSh / 6-31G** / SDDAll (Fe) level of theory.

In the dibromide complex **Fe20-Br**, a quintet ($S = 2$) ground state appears to be the by far most stable spin state, lying 28.1 kcal/mol lower than the singlet ($S = 0$) and 10.5 kcal/mol lower than the respective triplet ($S = 1$) state. A quintet multiplicity was also found to be the most stable ground state for **15a**, 20.5 kcal/mol lower than the respective singlet state. Interestingly, the quintet and triplet states are almost equal in energy ($\Delta G_{\text{triplet}} = -19.4$ kcal/mol relative to $\Delta G_{\text{singlet}}$). Calculations on the bis(acetylide) complex **Fe20-NMe** suggest that the triplet ground state, in contrast to the dibromide and mono(acetylide) complexes, appears to be much closer to the singlet energy surface ($\Delta G_{\text{singlet}} - \Delta G_{\text{triplet}} = 6.2$ kcal/mol).

The decreasing spin state splitting across the series (**Fe20-Br** > **15a** > **Fe21-NMe**) reflects the observed binding affinity to an exogenous donor ligand such as trimethyl phosphine.

The seeming reluctance of **15a** to accommodate an additional ligand in the coordination sphere might thus also have impacts on its catalytic prowess for the dimerization of alkynes.

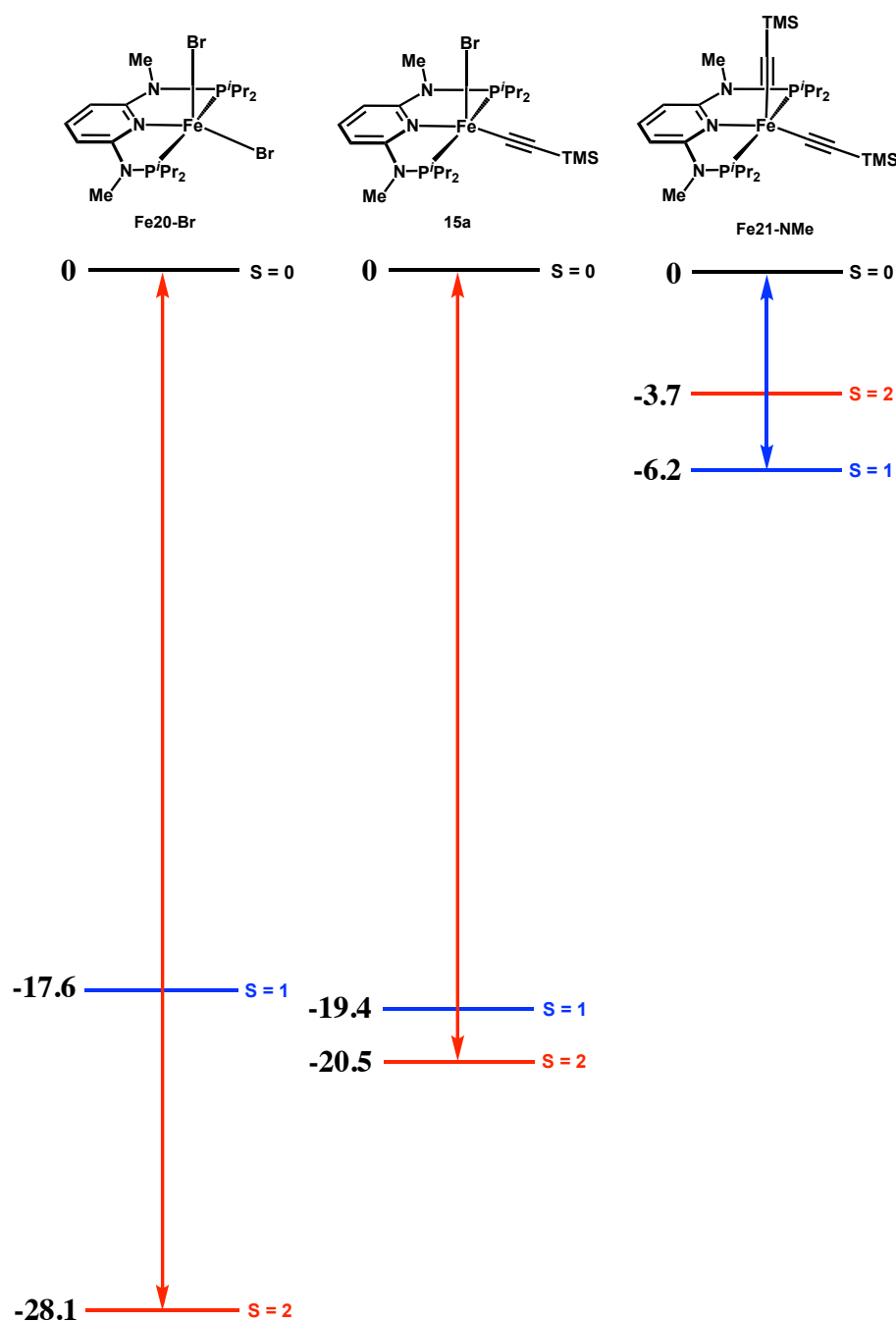


Figure 17 Calculated spin-state gaps in kcal/mol for complexes **Fe20-Br**, **15a** and **3a**. Gibbs free energies for quintet (S=2, red) and triplet (S=1, blue) relative to singlet (S=0, black) spin-states.

For this purpose, the catalytic competence of the complexes **15b** and **16b** was investigated by employing them in the Z-selective dimerization of terminal alkynes and subsequent comparison of the results with the catalytic performance of **Fe21-NMe**. The coordinatively saturated tris(acetylide) complex **16b** was chosen to test the lability of the third acetylide ligand, which can feasibly dissociate as $\text{LiC}\equiv\text{CPh}$. To judge if increased amounts of $\text{LiC}\equiv\text{CPh}$

influence the performance of the catalyst, the reaction was also performed utilizing the dihalide complex **Fe20-Br** in presence of 3, 5 and 10 equivalents of LiHMDS.

The reactions were carried out at room temperature using a 0.7 M solution of phenyl acetylene and 1 mol % of the respective catalyst. The reactions were continuously monitored by ^1H -NMR spectroscopy and the conversion and reaction times of the entries were plotted in Figure 18.

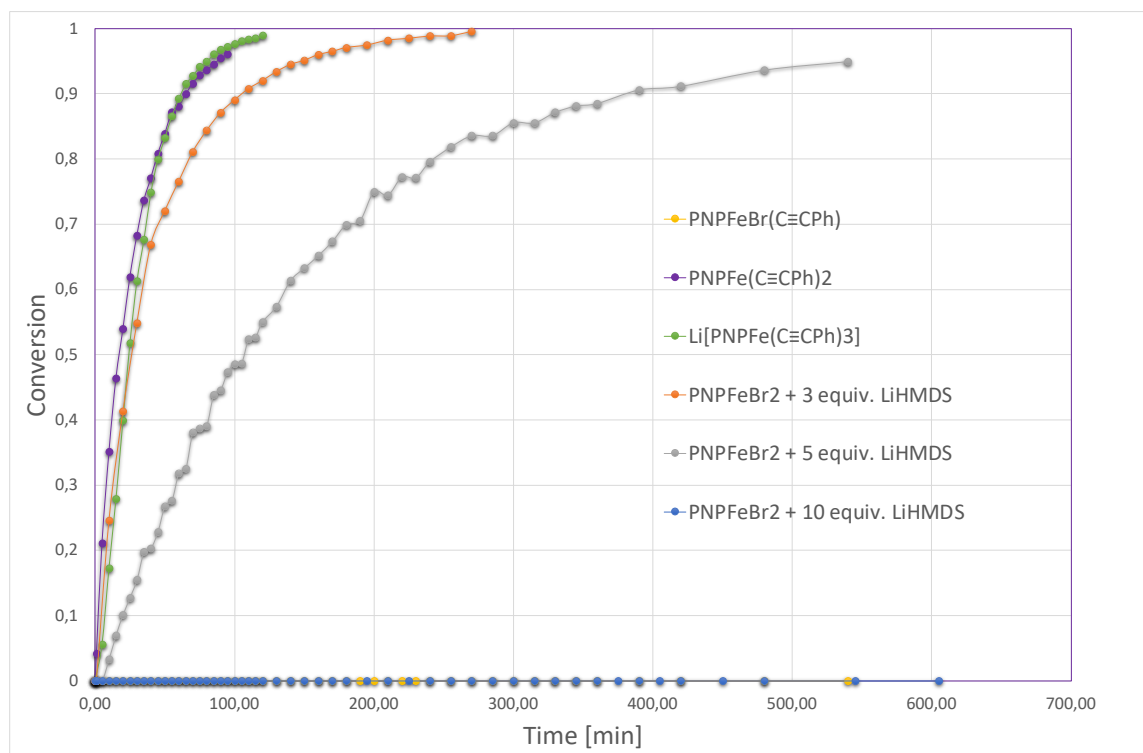


Figure 18 Kinetics of the Z- selective dimerization of alkynes catalyzed by Fe acetylide complexes

To compare the catalytic activities of complexes **15b** and **16b** and the bis(acetylide) complex **Fe21-NMe**, it was decided to calculate the turnover frequency after 50 % conversion (TOF_{50}) of the starting material which are shown in Figure 19.

Additionally, for comparison purposes, the TOF_{50} values of the experiments employing the dihalide complex **Fe20-Br** with the addition of base are also graphed in Figure 19.

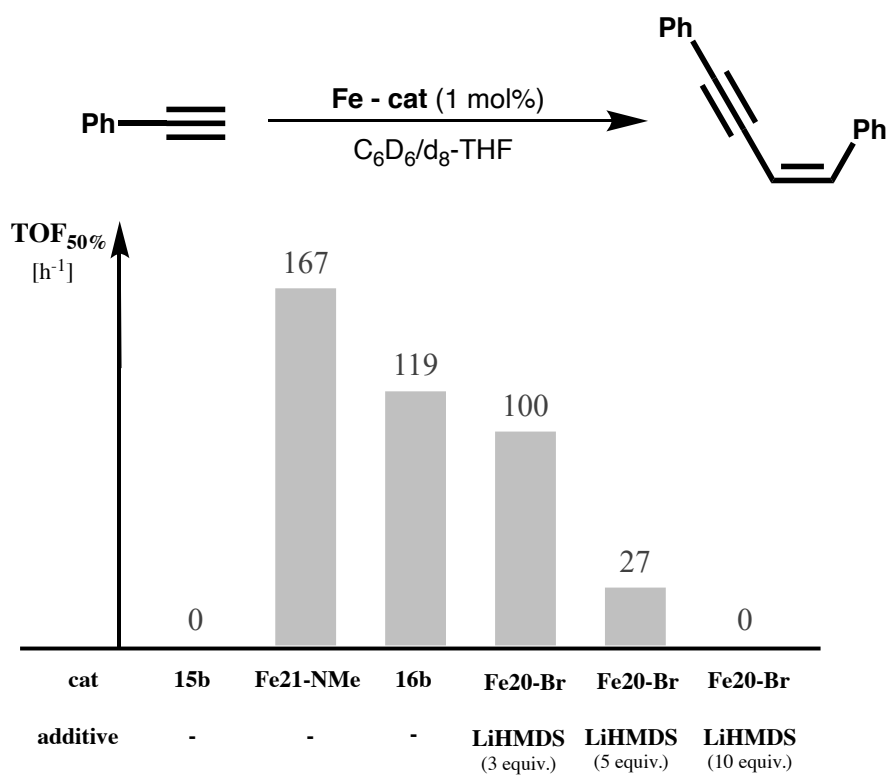


Figure 19 Calculated TOF₅₀ of the Z- selective dimerization of alkenes catalyzed by Fe acetylide complexes

No catalytic activity was observed for the mono(acetylide) complex **15b** whereas the bis(acetylide) complex **Fe21-NMe** quantitatively converted phenylacetylene into the respective Z-ene-yne within 90 min (TOF₅₀ = 167/h).

The tris(acetylide) complex **16b** was also found to promote the reaction but showed a lower catalytic activity than the **Fe21-NMe** (TOF₅₀ = 119/h). The reactivity of **16b** might be attributed to labile nature of the third acetylide ligand which can dissociate from the complex as LiC≡CPh. A similar catalytic activity (TOF₅₀ = 100/h) was obtained in a test reaction in which **16b** was generated in situ by the addition of 3 equivalents of LiC≡CPh to the dibromide complex **Fe20-Br**. Increasing the amount of added LiC≡CPh to 5 equivalents however resulted in a diminished catalytic activity (TOF₅₀ = 27/h), and the reaction completely ceased when the amount was increased to 10 equivalents, apparently completely preventing dissociation of the acetylide ligand. In these cases, ³¹P{¹H}-NMR spectra show the tris(acetylide) complex **16b** as the only organometallic species in the reaction solution.

In conclusion, the experimental data confirms, that the spin state of the acetylide complexes seems to greatly influence their catalytic performance. While the high-spin (S = 2) (mono)acetylide complex **15b** did not show any reactivity in the Z-selective dimerization of

alkynes, it was further corroborated that the intermediate spin ($S = 1$) (bis)acetylide complex **Fe21-NMe** is indeed the catalytically active species in this transformation. The coordinatively saturated, diamagnetic ($S = 0$) complex **16b**, showed slightly reduced catalytic performance which can be explained by an induction period due to the need of dissociation of an acetylide ligand during the catalytic reaction, again affording the catalytically active species **Fe21-NMe**. Increasing the amount of $\text{LiC}\equiv\text{CPh}$ in the reaction mixture, drastically decreases the catalytic proficiency of **16b**, which can be explained by gradual inhibition of the dissociation of the third acetylide ligand, that completely stops at the presence of 10 mol% $\text{LiC}\equiv\text{CPh}$ in the reaction mixture.

2.6. Fe PNP Pincer Hydride Complexes for the Activation of Carbon Dioxide

Transition metal hydride complexes are an important class of compounds and are of great interest in homogenous catalysis.¹²¹ In recent years, many catalysts based on Fe PNP pincer complexes were employed in catalysis, however with few exceptions, most published catalysts utilized carbonyls as ancillary ligands.^{22,122}

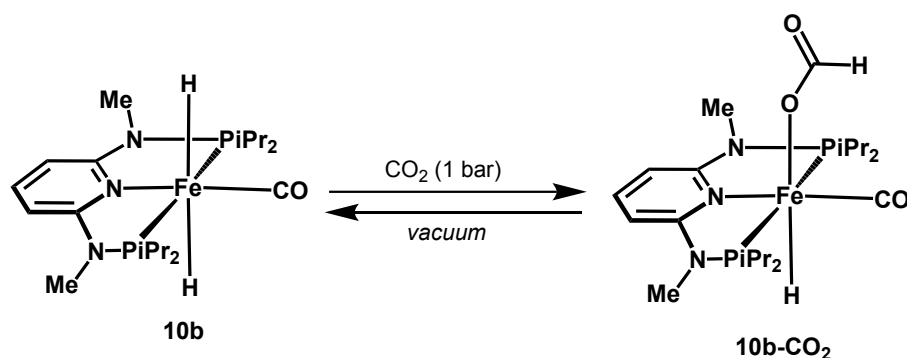
While carbon monoxide is known as an excellent π -acceptor ligand, utilizing ligands with weaker acceptor properties might, due to higher electron density on the metal center, benefit the catalytic activity in some transformations.

As described in chapter 2.4, one way to synthesize a series of novel dihydride complexes from PNP hydrido silyl compounds with various ancillary ligands was demonstrated. Furthermore, the mono(acetylide) complexes **15a** and **15b** described in chapter 2.4 present intriguing platforms for the synthesis of acetylide hydride complexes, which can also be tested in catalysis.

It is known that the reactivity of a transition-metal hydride is mainly influenced by the co-ligand located in *trans* position.^{119,123} Thus, it was expected that a mutually *trans* arrangement of hydrides, as well as a *trans* arrangement of the hydride and the acetylide ligand, would, due to their strong *trans*-influence, afford the catalytically most active species.

As a test reaction to study the reactivity of the novel PNP-Fe hydride complexes, the insertion of CO_2 into the metal hydride bond was chosen. This reaction was already conducted with the isomeric mixture of the carbonyl dihydride complexes *cis*- and *trans*- $[(\text{PNP}^{\text{NMe}})\text{Fe}(\text{H})_2(\text{CO})]$ **10a-b**, and cleanly afforded the hydrido-formate complex $[(\text{PNP}^{\text{NMe}})\text{Fe}(\text{H})(\eta^1\text{-CO}_2\text{H})(\text{CO})]$

10b-CO₂. This full conversion of the isomer mixture **10a-b** to **10b-CO₂** is likely caused by the mutual interconversion of the *cis*-complex **10a** and the *trans*-complex **10b** in solution and subsequent reaction of **10b** with CO₂, thus removing **10a** out of the equilibrium. **10b-CO₂** was only stable under CO₂ atmosphere as exposure of the complex to vacuum led to gradual reformation of **10a** and **10b**, showing the reversibility of the reaction¹²⁴ (Scheme 41)



Scheme 41 Treatment of **10b** with CO₂, formation of the formate complex **10b-CO₂** and reversibility under vacuum

In this context a correlation was calculated for a series of dihydride and acetylide-hydride complexes with various ancillary ligands. Figure 20 shows this correlation, graphing the Gibbs free energy (ΔG^0) of the formation of the formate complexes with the NPA (Natural Population Analysis) charges of the hydride ligands, obtained from NBO (Natural Bond Order) calculations.

It can also be seen in Figure 20, that the Gibbs free energy and the NPA charges of the hydrides give a good correlation, indicating that by increase of the σ -donor strength and decrease of the π -acceptor strength of the ancillary ligand, the insertion reaction should be more exergonic. Furthermore, it can be concluded that the hydride as *trans* ligand compared to the acetylide also seems to favor the insertion of the carbon dioxide into the metal hydride bond, as only the acetylide hydride complexes bearing trimethylphosphine ligands feature an exergonic formation of the formate. Although the dihydride complex with pyridine *cis*-[(PNP^{NMe})Fe(H)₂(py)] (**14**) was characterized as solely containing the *cis*-dihydride isomer, it was kept in the correlation as a benchmark due to its almost pure σ -donor ligand properties, with only weak π -accepting capabilities.

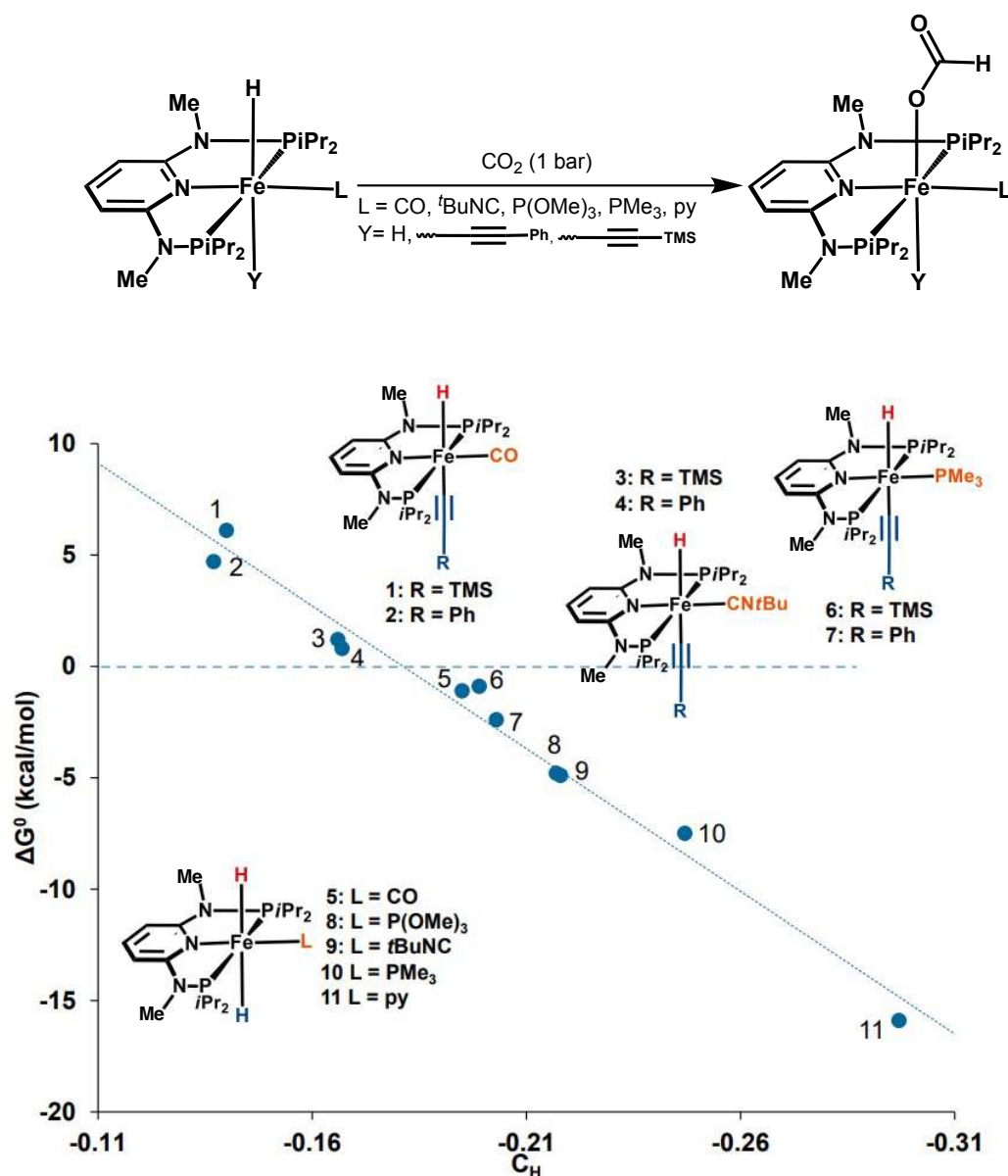
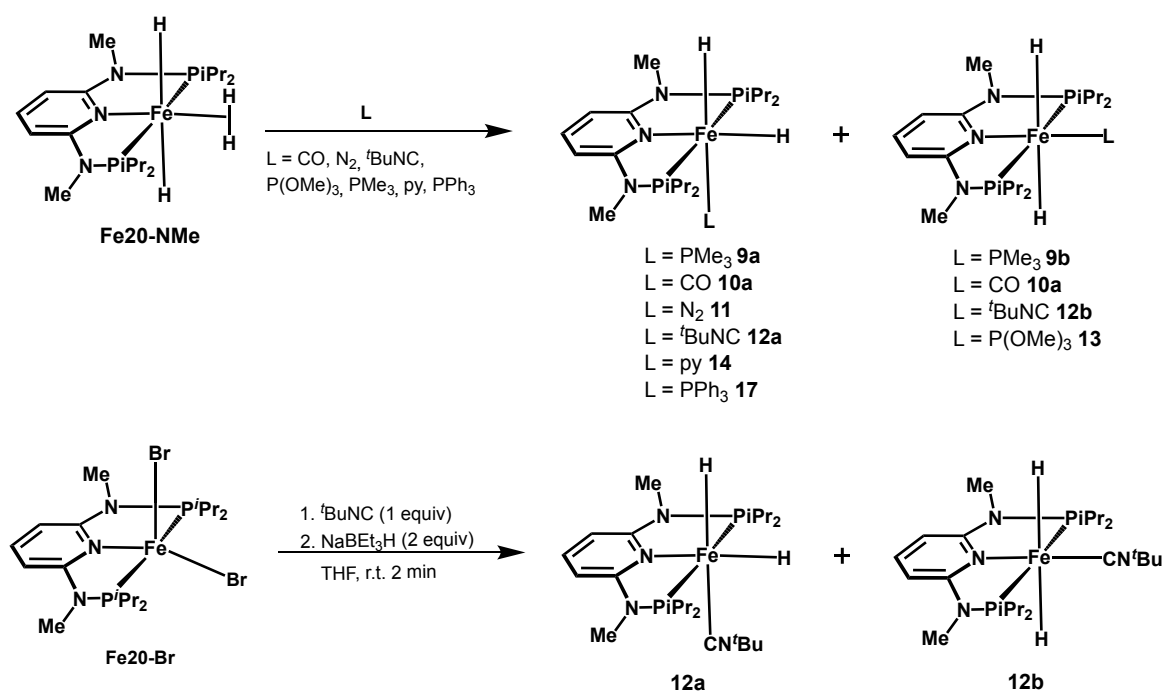


Figure 20 Correlation of the Gibbs free energy of the formation of the formate complexes with the NPA charges of the hydride ligands.

Initially, the corresponding dihydride complexes were synthesized by directly treating the polyhydride complex **Fe20-NMe** with the respective ancillary ligands. The dihydride complexes *cis*-[(PNP^{NMe})Fe(H)₂(^tBuNC)] **12a** and *trans*-[(PNP^{NMe})Fe(H)₂(^tBuNC)] **12b**, featuring ^tBuNC as spectator ligand, can additionally be prepared by treating a THF solution of the dibromide complex **Fe20-Br** with 2 equivalents of NaBEt₃H in presence of 1 equivalent of the isocyanide. In addition to the complexes featured in Figure 20, the dihydride complexes utilizing PPh₃, *cis*-[(PNP^{NMe})Fe(H)₂(PPh₃)] (**17**) and N₂, *cis*-[(PNP^{NMe})Fe(H)₂(N₂)] (**11**) as co-ligands, were also synthesized, however as they only were obtained as the respective *cis* isomers, they were not included in the correlation. (Scheme 42)



Scheme 42 General scheme for the synthesis of the dihydride complexes **9-17**

All dihydride complexes were characterized *via* multinuclear NMR spectroscopy. Complex **11** was only stable under nitrogen atmosphere, showing rapid decomposition to intractable side-products when exposed to an argon atmosphere. Furthermore, complex **14** could also not be isolated, due to it being only stable for short time periods in THF solutions containing an excess of pyridine. Evaporation of the solvent led to rapid discoloration of the intensely blue complex to grey, yielding only intractable side products. The characteristic spectroscopic shifts and coupling constants, as well as the ratio of the respective *cis*- and *trans*-isomers are listed in Table 7.

Table 7 Characteristic NMR shifts, coupling constants and ratio of the dihydride complexes **12 - 17**

Entry	Co-ligand	¹ H-NMR			³¹ P{ ¹ H}-NMR		Ratio
		hydrides (ppm)	² J _{HP} (Hz)	² J _{HH} (Hz)	(ppm)	² J _{PP} (Hz)	
10a	<i>cis</i>	CO	-13.02 (br)	-	-	191.9	57 %
10b	<i>trans</i>	CO	-8.76 (t)	42.9	-	189.6	43 %
11	<i>cis</i>	N ₂	-15.71 (td)	61.8	19.2	184.9	100 %
			-16.56 (td)	48.8	18.7		
12a	<i>cis</i>	tBuNC	-14.27 (br)	-	-	192.6	22 %

12b	<i>trans</i>	^t BuNC	-9.10 (t)	43.7	-	188.0	-	78 %
13	<i>trans</i>	P(OMe) ₃	-9.76 (dt)	59.6	-	183.9 (d)	76.0	100 %
				42.6	-	209.4 (t)	76.1	
9a	<i>cis</i>	PMe ₃	-13.46 (br)	-	-	184.4 (d)	29.0	93 %
			-18.57 (br)	-	-	13.4 (t)	29.1	
9b	<i>trans</i>	PMe ₃	-10.94 (dt)	55.2	-	182.1 (d)	43.3	7 %
				44.7	-	27.0 (t)	43.3	
14	<i>cis</i>	py	-16.91 (dt)	50.7	20.6	181.7	-	100 %
			-23.65 (dt)	66.7	20.6			
17	<i>cis</i>	PPh ₃	-13.02 (br)	-	-	182.7 (d)	22.9	100 %
			-17.49 (br)	-	-	65.1 (t)	23.0	

In addition to the spectroscopic characterization, single crystals suitable for X-Ray diffraction were grown from an *n*-pentane solution of the isocyanide complexes **12a** and **12b**. However, the measured crystal only contained the *trans*-isomer **12b**.

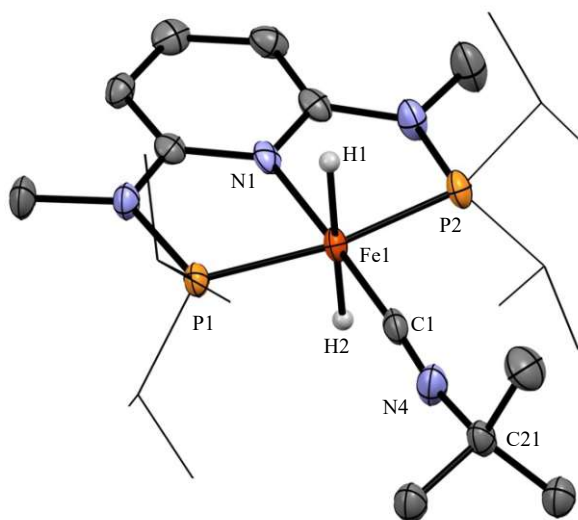
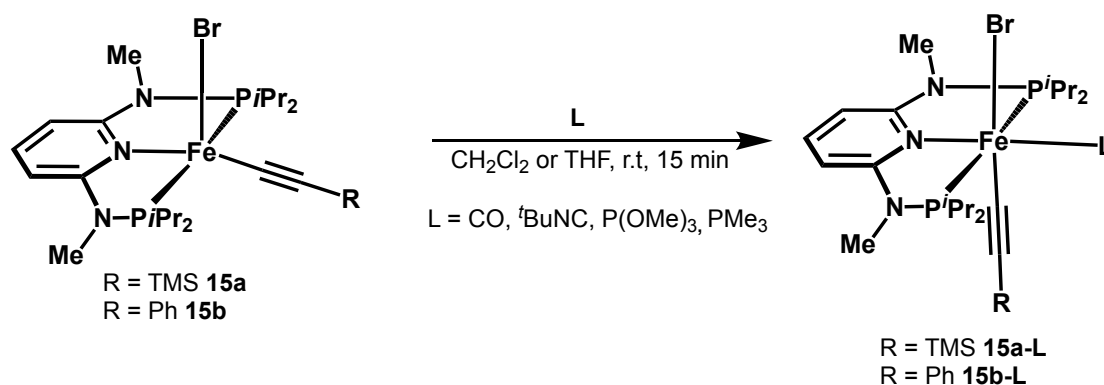


Figure 21. ORTEP view of *trans*-[(PNP^{NMe})Fe(H)₂(^tBuNC)] (**12b**) showing 50% thermal ellipsoids (most H omitted for clarity). Selected bond lengths (Å) and angles (deg): Fe1-N1 1.993(3), Fe1-P1 2.119(1), Fe1-P2 2.126(1), Fe1-C1 1.788(4), Fe1-H1 1.56(3), Fe1-H2 1.63(4), C1-N4 1.176(5); N1-Fe1-C1 177.81, P1-Fe1-P2 168.01, H1-Fe1-H1 176.90, C1-N4-C21 166.60.

As can be seen in Figure 21, **12b** features a slightly distorted octahedral geometry. The Fe1-C1 bond distance of 1.788(4) Å is comparable to other reported Fe-isocyanide complexes^{22,122,125} and longer than the carbon-iron bond distance of the isostructural complex *trans*-[(PNP^{NMe})Fe(H)₂(^tBuNC)] (**10b**), which was determined to be 1.683(3) Å.¹¹⁹ This is in line

with the weaker π -accepting properties of isocyanides compared to carbonyl ligands. The *t*BuNC also features a slightly bend structure, with a C1-N4-C21 bond angle of 166.40° , which is typical for isonitrile ligands functioning as acceptor ligands. Additionally, ATR-IR spectroscopy was conducted, where a $\text{C}\equiv\text{N}$ stretching band at 2040 cm^{-1} for the coordinated isocyanide ligand was observed.

To synthesize the hydrido-acetylide complexes, the 16 e^- -complexes $[(\text{PNP}^{\text{NMe}})\text{Fe}(\text{Br})(\text{C}\equiv\text{C-TMS})]$ (**15a**) and $[(\text{PNP}^{\text{NMe}})\text{Fe}(\text{Br})(\text{C}\equiv\text{C-Ph})]$ (**15b**), were, in a first step, treated with one equivalent of the respective spectator ligands, affording the saturated 18 e^- -complexes $[(\text{PNP}^{\text{NMe}})\text{Fe}(\text{Br})(\text{C}\equiv\text{C-Ph})(\text{L})]$ (**15a-b L**) ($\text{L} = \text{CO}, \text{tBuNC}, \text{P}(\text{OMe})_3, \text{PMe}_3$) in good yields. (Scheme 43)



Scheme 43 General scheme for the synthesis of the bromo-acetylide complexes **15a-L** and **15b-L**

Treating dichloromethane solutions of $[(\text{PNP}^{\text{NMe}})\text{Fe}(\text{Br})(\text{C}\equiv\text{C-TMS})]$ (**15a**) and $[(\text{PNP}^{\text{NMe}})\text{Fe}(\text{Br})(\text{C}\equiv\text{C-Ph})]$ (**15b**) with 1 bar of CO, led to the formation of the carbonyl complexes $[(\text{PNP}^{\text{NMe}})\text{Fe}(\text{Br})(\text{C}\equiv\text{C-TMS})(\text{CO})]$ (**15a-CO**) and $[(\text{PNP}^{\text{NMe}})\text{Fe}(\text{Br})(\text{C}\equiv\text{C-Ph})(\text{CO})]$ (**15b-CO**) in 86 % and 92 % respective yield. In contrast to the previously observed lability of the PMe_3 ligand of **15a-PMe₃** and **15b-PMe₃**, no evidence for the loss of the carbonyl ligand under vacuum was observed.

In the ATR-IR spectra of the complexes both the acetylide and the carbonyl ligands give strong bands, which are assignable the $\text{C}\equiv\text{O}$ and $\text{C}\equiv\text{C}$ stretching vibrations, respectively. The carbonyl bands were located at 1951 cm^{-1} (**15a-CO**) and 1941 cm^{-1} (**15b-CO**), while the $\text{C}\equiv\text{C}$ bands were observed at 2009 cm^{-1} (**15a-CO**) and 2083 cm^{-1} (**15b-CO**), respectively. In the $^{31}\text{P}\{^1\text{H}\}$ -NMR the complexes gave singlets at 148.4 ppm (**15a-CO**) and 147.9 ppm (**15b-CO**) can be observed, while in the $^{13}\text{C}\{^1\text{H}\}$ -NMR spectrum the carbonyl ligands give rise to triplet

signals at 222.7 ppm ($^2J_{\text{CP}} = 22.2$ Hz) (**15a-CO**) and 222.2 ppm ($^2J_{\text{CP}} = 22.2$ Hz) (**15b-CO**). The coordinated carbon atoms of the acetylides can also be observed as triplets located at 139.8 ppm ($^2J_{\text{CP}} = 30.9$ Hz) (**15a-CO**) and 112.0 ppm ($^2J_{\text{CP}} = 34.3$ Hz) (**15a-CO**), respectively.

Single crystals were grown from **15b-CO**, and the solid-state structure confirms the octahedral geometry of the complex with the acetylide ligand, and the bromide ligand being located mutually *trans* to each other. (Figure 22)

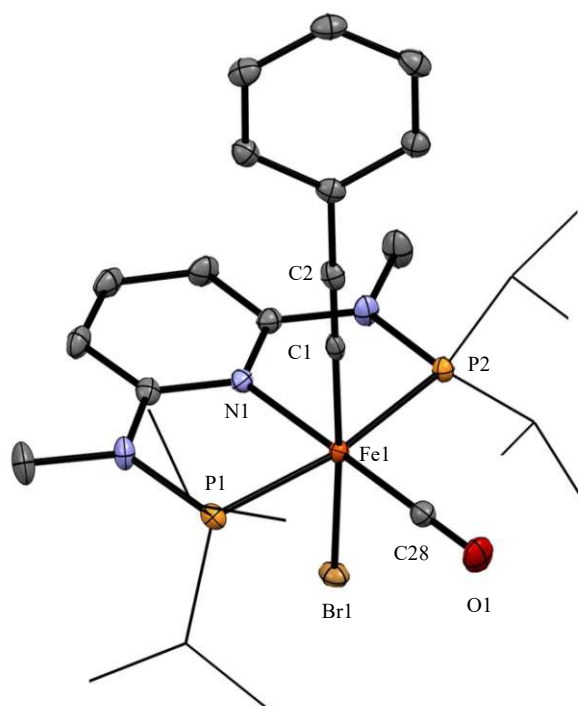


Figure 22. ORTEP view of $[(\text{PNP}^{\text{NMe}})\text{Fe}(\text{Br})(\text{C}\equiv\text{C-Ph})(\text{CO})]$ (**15b-CO**) showing 50% thermal ellipsoids (H omitted for clarity). Selected bond lengths (Å) and angles (deg): Fe1-N1 1.997(3), Fe1-P1 2.226(1), Fe1-P2 2.230(1), Fe1-C1 1.920(3), Fe1-C28 1.747(3), Fe1-Br1 2.4848(5), C1-C2 1.212(4), C28-O1 1.153(4); N1-Fe1-C28 179.26, P1-Fe1-P2 168.49, C1-Fe1-Br1 173.00.

The iron carbon σ -bond distance of the phenyl acetylide ligand was measured to be 1.920(3) Å, while the iron carbon bond of the carbonyl ligand was found to be 1.747(3) Å. The $\text{C}\equiv\text{C}$ bond distance was measured as 1.212(4) Å, which is similar to the distance observed in the acetylide complexes **15a**, **Fe21-NMe** and **16a**. The carbon oxygen triple bond of the carbonyl ligand has a bond distance of 1.153(4) Å.

In a similar fashion, treatment of **15a** and **15b** with 1 equivalent of $t\text{BuNC}$ in THF leads to the clean formation of the respective octahedral complexes $[(\text{PNP}^{\text{NMe}})\text{Fe}(\text{Br})(\text{C}\equiv\text{C-TMS})(t\text{BuNC})]$ (**15a- $t\text{BuNC}$**) and $[(\text{PNP}^{\text{NMe}})\text{Fe}(\text{Br})(\text{C}\equiv\text{C-Ph})(t\text{BuNC})]$ (**15b- $t\text{BuNC}$**) in good yields

of 88 % and 81 % respectively. Again, no evidence for the lability of the isocyanide spectator ligand were observed. In the ATR-IR spectrum, two sharp bands at 2105 cm^{-1} and 1986 cm^{-1} (**15a-^tBuNC**) and 2110 cm^{-1} and 2058 cm^{-1} (**15b-^tBuNC**), assignable to the $\text{C}\equiv\text{N}$ and $\text{C}\equiv\text{C}$ stretching frequency of the isocyanide ligand and the acetylide ligand respectively. In both cases, the wavenumbers observed for the $\text{C}\equiv\text{C}$ stretch are redshifted compared to the isostructural carbonyl complexes, hinting to stronger π -backbonding interactions of the acetylide ligands facilitated by the decreased π -acidity of the isocyanides in comparison to carbonyl ligands.

The $^{13}\text{C}\{^1\text{H}\}$ -NMR spectrum of the complexes features broad triplet resonances for the carbon atom of the isocyanide ligand at 173.6 ppm (**15a-^tBuNC**) and 173.8 ppm (**15b-^tBuNC**), respectively. The coordinated carbon of the acetylide complexes is also observed as triplets at 151.4 ppm ($^2J_{\text{CP}} = 32.0\text{ Hz}$) (**15a-^tBuNC**) and 124.0 ppm ($^2J_{\text{CP}} = 32.8\text{ Hz}$) (**15b-^tBuNC**), respectively, which indicates a significant downfield shift compared to the resonances observed in the carbonyl complexes **15a-CO** and **15b-CO**.

Single crystals of sufficient quality for X-Ray diffraction could be obtained of **15a-^tBuNC**, by slow evaporation of a concentrated CH_2Cl_2 solution of the complex.

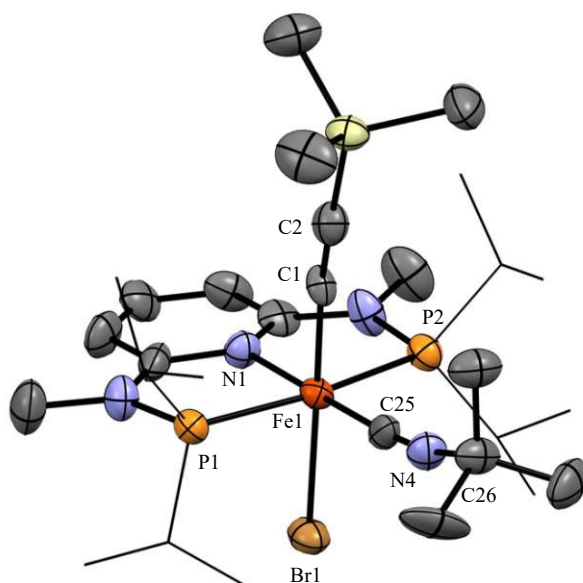


Figure 23. ORTEP view of $[(\text{PNP}^{\text{NMe}})\text{Fe}(\text{Br})(\text{C}\equiv\text{C-TMS})(^t\text{BuNC})]$ (**15a-^tBuNC**) showing 50% thermal ellipsoids (H and independent solvent molecule omitted for clarity). Selected bond lengths (Å) and angles (deg): Fe1-N1 2.013(6), Fe1-P1 2.229(3), Fe1-P2 2.234(2), Fe1-C1 1.927(8), Fe1-C25 1.829(8), Fe1-Br1 2.549(2), C1-C2 1.19(1), C25-N4 1.16(1); N1-Fe1-C24 179.29, P1-Fe1-P2 167.96, C1-Fe1-Br1 179.15, C25-N4-C26 167.76.

As shown in Figure 23, **15a-^tBuNC** features an octahedral geometry, where the bromide ligand and the acetylide are mutually trans to each other. The carbon-iron bond distance of the

acetylide ligand of 1.927(8) Å is similar to the one observed in **15b-CO**, while the C≡C bond (1.19(1) Å) is slightly shorter than in the isostructural carbonyl complex. The iron-carbon bond of the isocyanide of 1.829(8) Å is longer than the corresponding iron-carbon bond of the carbonyl in **15b-CO**, again underpinning the weaker π -acceptor properties of the isonitrile ligand. The C≡N triple bond of the isocyanide has a bond distance of 1.16(1) Å.

Treatment of complexes **15a** and **15b** with P(OMe)₃ in THF yielded the diamagnetic complexes [(PNP^{NMe})Fe(Br)(C≡C-TMS)(P(OMe)₃)] (**15a-P(OMe)₃**) and [(PNP^{NMe})Fe(Br)(C≡C-Ph)(P(OMe)₃)] (**15b-P(OMe)₃**) in near quantitative yields. While **15a-P(OMe)₃** was stable under vacuum, the phosphite ligand in **15b-P(OMe)₃** showed lability when kept under fine vacuum for longer periods, cleanly reforming **15b**. ATR-IR spectroscopy of **15a-P(OMe)₃** was performed and the characteristic band of the C≡C stretching frequency of the acetylide ligand was found at 1983 cm⁻¹. In the ¹³C{¹H}-NMR spectrum, the carbon of the acetylide ligand bonded to the iron center of **15a-P(OMe)₃** was observed as a doublet of triplets at 150.3 ppm, with ²J_{CP} coupling constants of 47.0 Hz to the phosphite ligand, and 29.1 Hz to the phosphine donors of the PNP ligand, respectively. For comparison, the carbon of the Fe-C bond in **15a-PMe₃** was found as doublet of triplets at 155.1 ppm, with ²J_{CP} coupling constants of 36.7 Hz to the trimethylphosphine spectator ligand and 30.7 Hz to the phosphine donors, again showing a trend of deshielding of this resonance, in correlation with decreased π -acceptor strength of the ancillary ligand. The stretching frequency of the triple bond of the phenylacetylide ligand of **15b-P(OMe)₃** was detected at 2058 cm⁻¹ in the ATR-IR spectrum.

The solid structure of **15a-P(OMe)₃** was elucidated *via* single crystal X-Ray diffraction analysis, again indicating an octahedral geometry of the complex with a mutual *trans* arrangement of the bromide ligand and the acetylide ligand (Figure 24)

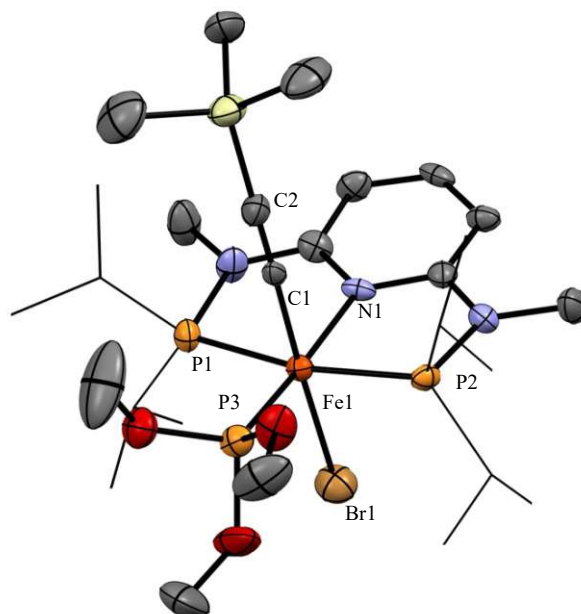
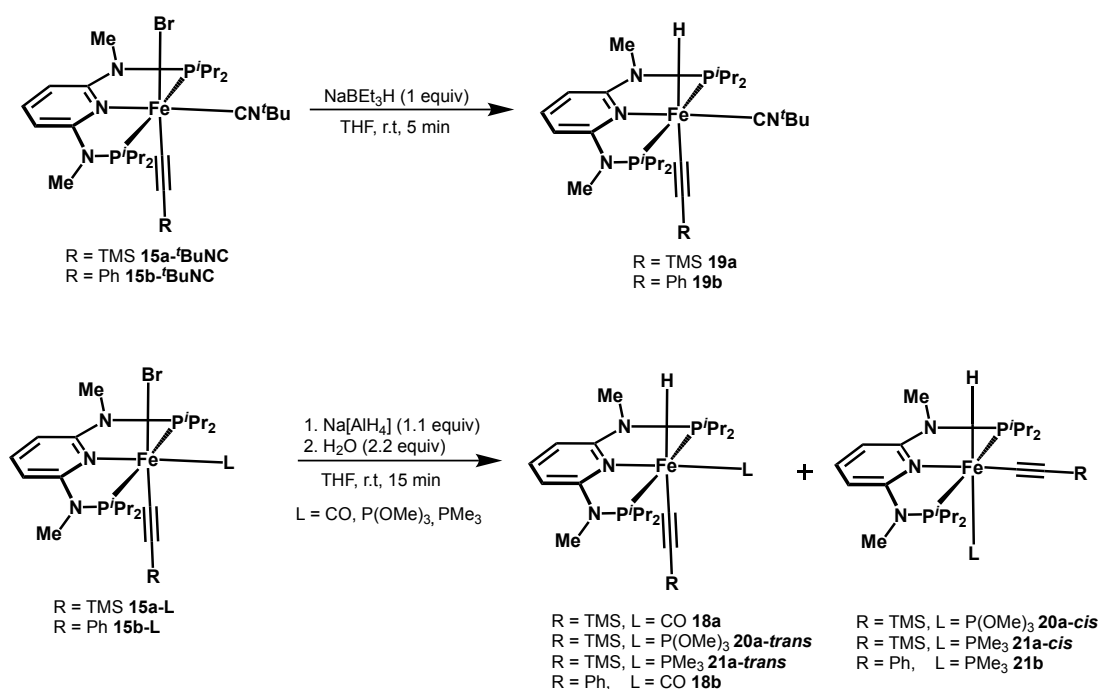


Figure 24. ORTEP view of $[(\text{PNP}^{\text{NMe}})\text{Fe}(\text{Br})(\text{C}\equiv\text{C-TMS})(\text{P}(\text{OMe})_3)]$ (**15a-P(OMe)₃**) showing 50% thermal ellipsoids (H omitted for clarity). Selected bond lengths (Å) and angles (deg): Fe1-N1 2.044(9), Fe1-P1 2.253(6), Fe1-P2 2.277(5), Fe1-C1 1.915(9), Fe1-P3 2.168(5), Fe1-Br1 2.474(6), C1-C2 1.24(1); N1-Fe1-P3 174.36, P1-Fe1-P2 166.64, C1-Fe1-Br1 176.49.

The iron-carbon bond of the acetylide ligand was determined to be 1.915(9) Å, which is in range of the previously described isostructural complexes. The Fe1-P3 bond distance of the ancillary ligand was measured to be 2.168(5) Å, which is longer than the value obtained in the structure of the dihydride complex **13** of 2.072(1) Å. The C≡C triple bond distance was measured to be 1.24(1) Å, which is longer than in the previously described complexes **15b-CO** and **15a-tBuNC**, which, in combination to the decreased wavenumber in the ATR-IR spectrum, is indicative of increased π -backbonding into the acetylide ligand.

With the bromido-acetylide complexes **15a-L** and **15b-L** in hand, the synthesis of the corresponding hydrido-acetylide complexes was attempted by treating a THF solution of the complexes with 1 equivalent of NaBEt_3H . This method worked well for the complexes utilizing tBuNC as co-ligand, however for the carbonyl, $\text{P}(\text{OMe})_3$ and PMe_3 congeners the reaction did not proceed in a clean fashion and various side products were formed during the reaction.

To circumvent side reactions, these complexes were instead synthesized by treating **15a-L** and **15b-L** with a small excess of $\text{Na}[\text{AlH}_4]$ and subsequent quenching with degassed water (Scheme 44)



Scheme 44 General scheme for the synthesis of the hydrido-acetylide complexes **18-21a** and **18-21b**

While the complexes $[(\text{PNP}^{\text{NMe}})\text{Fe}(\text{H})(\text{C}\equiv\text{C-TMS})(\text{CO})]$ (**18a**), $[(\text{PNP}^{\text{NMe}})\text{Fe}(\text{H})(\text{C}\equiv\text{C-Ph})(\text{CO})]$ (**18b**), $[(\text{PNP}^{\text{NMe}})\text{Fe}(\text{H})(\text{C}\equiv\text{C-TMS})(^t\text{BuNC})]$ (**19a**), $[(\text{PNP}^{\text{NMe}})\text{Fe}(\text{H})(\text{C}\equiv\text{C-Ph})(^t\text{BuNC})]$ (**19b**) and $[(\text{PNP}^{\text{NMe}})\text{Fe}(\text{H})(\text{C}\equiv\text{C-Ph})(\text{PMe}_3)]$ (**21b**) only yielded a single species, the complexes $[(\text{PNP}^{\text{NMe}})\text{Fe}(\text{H})(\text{C}\equiv\text{C-TMS})(\text{P(OMe)}_3)]$ (**20a**) and $[(\text{PNP}^{\text{NMe}})\text{Fe}(\text{H})(\text{C}\equiv\text{C-TMS})(\text{PMe}_3)]$ (**21a**) were obtained as mixture of isomers. Based on the spectral data, and by careful study of the $^2J_{\text{HP}}$ and $^2J_{\text{PP}}$ coupling constants, these isomers were identified as **20a-trans**, **21a-trans**, where the hydride and the acetylide ligands are mutually trans, and **20a-cis**, **21a-cis**, where the hydride and the ancillary ligands are mutually trans. (Scheme 44)

In the ^1H -NMR spectrum of complex **18a**, the hydride ligand gives rise to a resonance at -12.37 ppm and a $^2J_{\text{PH}}$ coupling constant of 49.9 Hz is obtained. The equivalent phosphine donors of the PNP backbone are found at 175.0 ppm. In the $^{13}\text{C}\{^1\text{H}\}$ -NMR spectrum the carbonyl ligand gives rise to a triplet at 222.2 ppm, with a $^2J_{\text{CP}}$ coupling constant of 25.0 Hz, which is similar to the resonance observed in **15b-CO**. The coordinated carbon atom, of the acetylide ligand is found at 156.8 ppm as a triplet with a $^2J_{\text{CP}}$ coupling constant of 25.0 Hz. This again corroborates the trend of a deshielding of the signal, when the electron density on the metal center is increased, in this case by substituting the π -donor halide ligand with the strong σ -donor hydride. The increase in electron density on the metal center is further underpinned by the redshift of the carbonyl band, which now can be observed at 1914 cm^{-1} as

well as the $\text{C}\equiv\text{C}$ stretching frequency of the TMS-acetylide ligand which was now located at 1998 cm^{-1} . The hydride ligand of **18b** gives rise to a triplet at -12.25 ppm with a $^2J_{\text{PH}}$ coupling constant of 49.9 Hz . In the $^{31}\text{P}\{^1\text{H}\}$ -NMR the complex features a singlet at 174.9 ppm . In the ATR-IR spectrum the carbonyl stretch is located at 1913 cm^{-1} , and the $\text{C}\equiv\text{C}$ stretching frequency phenylacetylide ligand is located at 2066 cm^{-1} . To elucidate the solid structure of **18a**, single crystal X-Ray diffraction was performed, confirming an octahedral geometry of the complex. (Figure 25)

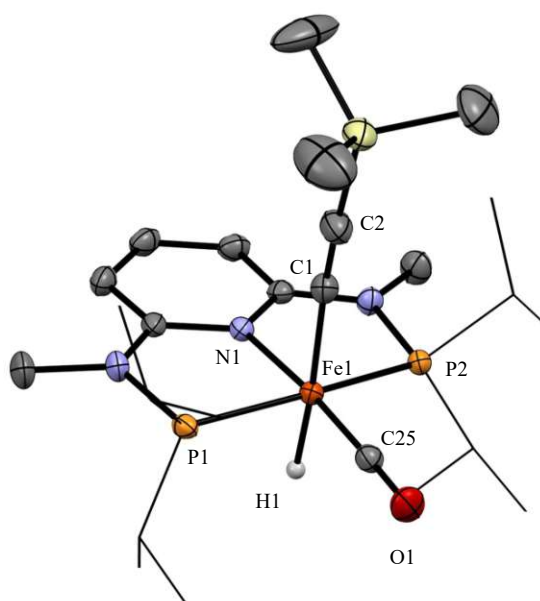


Figure 25. ORTEP view of $[(\text{PNP}^{\text{NMc}})\text{Fe}(\text{H})(\text{C}\equiv\text{C-TMS})(\text{CO})]$ (**18a**) showing 50% thermal ellipsoids (most H omitted for clarity). Selected bond lengths (Å) and angles (deg): Fe1-N1 2.024(2), Fe1-P1 2.178(1), Fe1-P2 2.171(1), Fe1-C1 1.966(2), Fe1-C25 1.731(2), Fe1-H1 1.48(3), C1-C2 1.220(3), C25-O1 1.168(3); N1-Fe1-C25 173.32, P1-Fe1-P2 164.37, C1-Fe1-H1 176.00.

Interestingly, the Fe-C bond of the acetylide ligand of **18a** ($1.966(2)\text{ Å}$) is longer compared to the bond length obtained from the solid structure of the halide precursor **15b-CO** ($1.920(3)\text{ Å}$). This fact can be explained by the stronger *trans*-influence of the hydride ligand, in comparison to the bromide. The $\text{C}\equiv\text{C}$ bond length of $1.220(3)\text{ Å}$ is in the range observed for **15b-CO**. Additionally, compared to **15b-CO**, the Fe-C bond of the carbonyl ligand is slightly shortened to $1.731(2)\text{ Å}$, indicating stronger back bonding of the carbonyl ligand, which is consistent with a more electron rich metal center in **18a** than in **15b-CO**.

Furthermore, the isocyanide congeners **19a** and **19b** were fully characterized by multinuclear NMR spectroscopy. The hydride signals, as the most characteristic resonances in the ^1H -NMR spectrum, were detected as triplets at -12.76 ppm ($^2J_{\text{PH}} = 51.4\text{ Hz}$) for **19a** and -12.63 ppm

($^2J_{\text{PH}} = 51.5$ Hz) for **19b**, respectively. The coordinated carbons of the isocyanide ligands only gave broad resonances in the $^{13}\text{C}\{^1\text{H}\}$ -NMR spectrum at 182.6 ppm (**19a**) and 181.9 ppm (**19b**), respectively. However, sharp triplets assignable to the carbon atoms attached to the metal center at 163.4 ppm ($^2J_{\text{PC}} = 11.3$ Hz) for **19a** and 140.1 ppm ($^2J_{\text{PC}} = 20.5$ Hz) for **19b** again show a significant downfield shift of the signals compared to the halide complexes **15a**-**t**BuNC (c.f. 151.4 ppm) and **15b**-**t**BuNC (c.f. 124.0 ppm). In the ATR-IR spectrum, two respective intense bands for the C \equiv N stretch of the isocyanide ligands and C \equiv C stretch of the acetylide ligands were observed in the complexes. The wavenumbers of 2044 cm^{-1} (**19a**) and 2054 cm^{-1} (**19b**) for the isocyanide ligands, and 1977 cm^{-1} (**19a**) and 2032 cm^{-1} (**19a**) for the acetylide ligands again are indicative of a more electron rich metal center in the hydride complexes, compared to the respective bromide precursors. To gain further insight into the properties of the isocyanide ligands, 2D $\{^{15}\text{N}-^1\text{H}\}$ HMBC NMR (c.f. free **t**BuNC: 195.6 ppm) spectroscopy was performed with all complexes containing isocyanide ligands and a comparison between the NMR data, and the angle of the C-N \equiv C carbon bonds of the ligands, as determined by X-Ray diffraction are listed in Table 8. Interestingly, the C \equiv N stretching frequencies of the isocyanide ligand seem to correlate well with the observed ^{15}N -NMR shifts and may be used as an additional tool to quantify π -backbonding interactions of metal centers into isocyanide ligands.

Table 8 Spectroscopic data and bond angle of the isocyanide ligands

Complex	^{13}C -NMR (ppm)	^{15}N -NMR (ppm)	IR (cm^{-1})	Angle (deg)
12b	196.5	190.3	2040	166.60
15a - t BuNC	173.6	200.3	2105	167.76
15b - t BuNC	173.8	200.9	2110	-
19a	182.6	190.7	2044	154.46
19b	181.9	191.8	2054	-

Moreover, single crystals of **19b** were grown from a cooled concentrated solution of the complex in *n*-pentane. Again, due to the strong *trans*-influence of the hydride ligand the Fe-C bond of the acetylide ligand of 1.9459(8) Å is significantly elongated compared to the halide complex **15a**-**t**BuNC (c.f. 1.927(8) Å). Similarly, the increase in C \equiv C bond length of 1.236(1) Å hints to increased π -backbonding interactions of the acetylide. Analogously, the shortening of the Fe-C bond of the isocyanide to 1.7919(8) Å, in combination with the

elongation of the C≡N bond to 1.186(1) Å and a C-N≡C bond angle of 154.46° is indicative of increased π -backbonding into the 'BuNC ligand. (Figure 26)

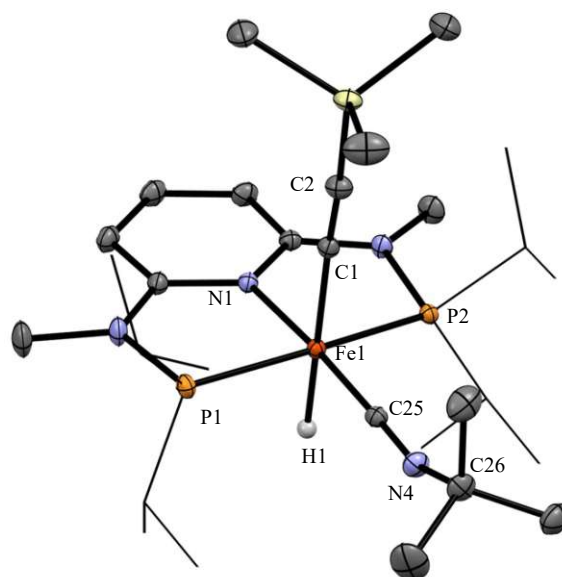


Figure 26. ORTEP view of $[(\text{PNP}^{\text{NMe}})\text{Fe}(\text{H})(\text{C}\equiv\text{C-TMS})(\text{'BuNC})]$ (**19a**) showing 50% thermal ellipsoids (most H and independent solvent molecule omitted for clarity). Selected bond lengths (Å) and angles (deg): Fe1-N1 2.0191(8), Fe1-P1 2.1563(5), Fe1-P2 2.1574(5), Fe1-C1 1.9459(8), Fe1-C25 1.7919(8), Fe1-H1 1.49(1), C1-C2 1.236(1), C25-N4 1.186(1); N1-Fe1-C25 174.58, P1-Fe1-P2 164.10, C1-Fe1-Br1 177.96, C25-N4-C26 154.46.

Treatment of **15a-P(OMe)₃** with Na[AlH₄] and subsequent quenching with water, led to the formation of a 72:28 mixture of the isomers **20a-trans** and **20a-cis**, as judged by $^{31}\text{P}\{^1\text{H}\}$ and ^1H -NMR spectroscopy. Similarly, treatment of **15a-PMe₃** with the hydride reagent, led to the formation of a mixture of **21a-trans** and **21b-cis** in a ratio of 5:95. In contrast, the reaction of **15b-PMe₃** with the alanate only gave one apparent isomer, however the reaction also yielded various side products making the characterization of a putative trans isomer in the reaction mixture difficult. The characteristic NMR shifts of the complexes are given in Table 9.

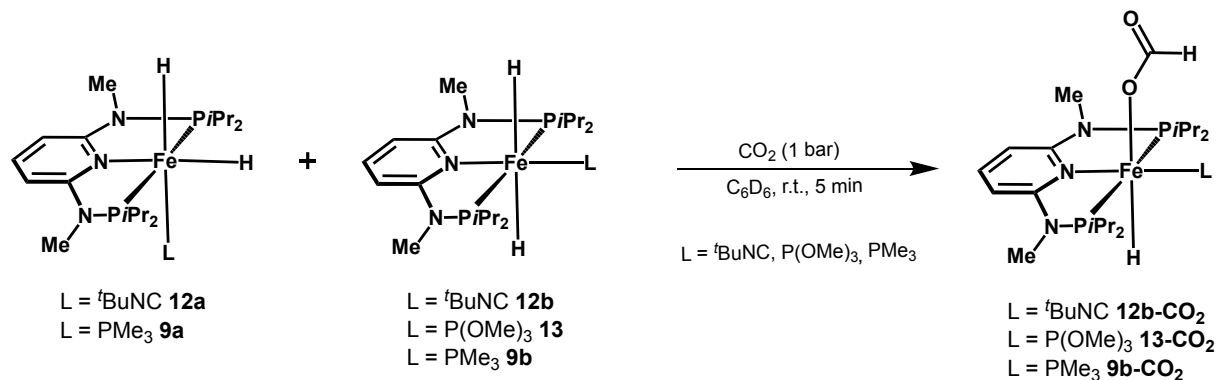
Table 8 Characteristic NMR shifts, coupling constants and ratio of hydrido-acetylide complexes **20- 21**

Entry	Co-ligand	^1H -NMR		$^{31}\text{P}\{^1\text{H}\}$ -NMR		Ratio	
		hydrides (ppm)	$^2J_{\text{HP}}$ (Hz)	(ppm)	$^2J_{\text{PP}}$ (Hz)		
20a	<i>trans</i>	P(OMe) ₃	-13.31 (dt)	66.9	169.8	73.9	72 %
				52.2	192.0	74.3	
20a	<i>cis</i>	P(OMe) ₃	-8.90 (dt)	83.9	165.3	37.3	28 %

				65.4	172.7	37.5	
21a	<i>trans</i>	PMe ₃	-13.16 (dt)	56.6	173.8	41.0	5 %
				52.2	22.2	40.9	
21a	<i>cis</i>	PMe ₃	-11.29 (td)	70.5	165.1	26.3	95 %
				35.5	15.5	28.1	
21b	<i>cis</i>	PMe ₃	-11.50 (td)	69.5	165.1	25.6	100 %
				36.4	10.7	26.3	

2.7. Reaction of the Fe PNP Hydride Complexes with Carbon Dioxide

To verify the calculations of the previous chapter, the novel hydride complexes were subsequently tested for the insertion of carbon dioxide into the Fe-H bonds. In a first step, the dihydride complexes **9a-b**, **12a-b** and **13** were dissolved in C₆D₆ and transferred into a Young NMR-tube. Freeze-pump-thawing and subsequent backflushing with 1 bar of CO₂ was performed.

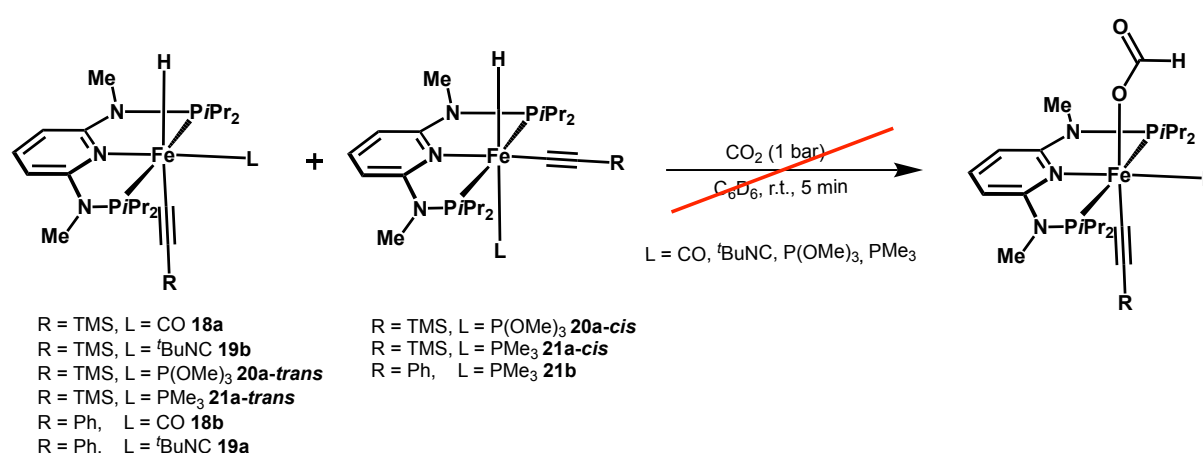


Scheme 45 General scheme for the reaction of the dihydride complexes **9-12** with CO₂

Treating a brown solution of the isomer mixture *cis-trans*[(PNP^{NMe})Fe(H)₂(^tBuNC)] (**12a-b**) with CO₂ led to an immediate change of the reaction mixture to yellow, and spectroscopically full conversion to [(PNP^{NMe})Fe(H)(η¹-CO₂H)(^tBuNC)] (**12b-CO₂**) was observed. In the ¹H-NMR spectrum, the hydride was observed as a triple with a chemical shift of -27.16 ppm relative to TMS, and a coupling constant of 57.8 Hz was measured. Furthermore, the formate species was observed as a singlet at 8.56 ppm. In the ATR-IR spectrum, the C≡N stretching band of the isocyanide ligand was observed at 2048 cm⁻¹, while the carbonyl stretch of the formate ligand was located at 1586 cm⁻¹.

The reaction of **13** with CO₂ afforded a light orange solution, which was spectroscopically identified as [(PNP^{NMe})Fe(H)(η¹-CO₂H)(P(OMe)₃)] (**13-CO₂**). In the hydride region of the ¹H-NMR a new doublet of triplets was observed at -29.07 ppm, with ²J_{PH} coupling constants of 76.1 Hz and 53.4 Hz respectively. The formate ligand was observed as a singlet at 9.44 ppm. The phosphite ligand gave rise to a triplet in the ³¹P{¹H}-NMR at 186.7 ppm (²J_{PP} = 70.7 Hz), while the phosphines of the PNP ligand were located as a doublet at 159.4 ppm. (²J_{PP} = 71.7 Hz). However, while **12b-CO₂** only slowly reacts back to **12a-b** when the CO₂ atmosphere is removed, **13-CO₂** rapidly reverts to **13** and other intractable side products are formed in absence of carbon dioxide.

In case of **9a-b**, backflushing with CO₂ caused an immediate color change of the reaction mixture from dark red to light red yielding a new complex as observed in NMR-spectroscopy. This complex, identified as [(PNP^{NMe})Fe(H)(η¹-CO₂H)(PMe₃)] (**9b-CO₂**), however is extremely unstable and rapid precipitation of intractable side products occurs, even when kept under CO₂ atmosphere. This severely hampers its spectroscopic characterization. Nonetheless, ¹H as well as ³¹P{¹H}-NMR spectroscopy were successfully conducted. The hydride ligand *trans* to the formate moiety can be observed as a doublet of triplets at -29.46 ppm with ²J_{PH} coupling constants of 60.6 Hz and 54.0 Hz and the formate ligand can be detected as a singlet at 8.67 ppm. In the ³¹P-NMR the phosphine donors of the PNP ligand, are observed as a doublet at 163.1 ppm (²J_{PP} = 39.3 Hz), while the PMe₃ ligand gives rise to a triplet at 19.5 ppm. (²J_{PP} = 39.5 Hz). (Scheme 45)



Scheme 46 Treatment of the hydrido-acetylide complexes **18-21** with CO₂ yielded no reaction

Encouraged by these results, in a next step the hydrido-acetylide complexes were also probed for their reactivity with CO₂. However, exchange of the atmosphere from argon to CO₂ in a

Young NMR tube containing d_6 -benzene solutions of the complexes utilizing CO, t BuNC and $P(OMe)_3$ as spectator ligands did not lead to any reaction, and only the starting materials were recovered. These results are in line with the calculations above, where only the complexes utilizing PMe_3 as spectator ligand showed exergonic formation of the formate complexes.

While the treatment of **21a-b** with CO_2 immediately caused a color change of the solution from red to yellow, unfortunately, no formate complex could be identified in the reaction mixture and only precipitation of intractable side products was observed. (Scheme 46)

In conclusion, the experimental data described above, show an excellent agreement with the calculated correlation of Figure 20. All the dihydride complexes that were considered in this study did indeed show, with exception for the exclusively *cis* complex *cis*- $[(PNP^{NMe})Fe(H)_2(py)]$ (**14**), the anticipated reaction with carbon dioxide, readily affording the respective formate complexes **9b-13b**. Furthermore, as calculated, the hydrido-acetylide complexes **18-20** did not show any reactivity towards CO_2 . On the other hand, while the hydrido-acetylide complexes $[(PNP^{NMe})Fe(Br)(C\equiv C-R)(PMe_3)]$ ($R = TMS, Ph$) (**21a, 21b**) were predicted to form the formate complexes, and a reaction with CO_2 took place, no main product could be characterized in the reaction mixture. This was probably caused by the instability of the formed products.

3. Conclusion

In conclusion, utilizing primary, secondary, and tertiary silanes, a series of novel Iron PNP silyl complexes was synthesized and fully characterized. Depending on the silane, either complexes featuring η^2 -dihydrogen ligands are formed, or in case of secondary silanes containing alkyl substituents, a η^2 -SiH₃R₂ coordination mode is obtained. It was further shown, that for secondary silanes, these two coordination modes are in equilibrium which was demonstrated by ligand substitution experiments. The complexes [(PNP^{NMe})Fe(H)(SiPh₂H)(η^2 -H₂)] (**3**), [(PNP^{NMe})Fe(H)(η^2 -SiEt₂H₃)] (**4**) and [(PNP^{NMe})Fe(H)(η^2 -SiMePhH₂)(H)] (**5**) were shown to be catalytically active for the hydrosilylation of alkenes. Complex **4** was determined to be the most prolific catalyst for this transformation, and after optimization, used for the catalytic hydrosilylation of allyl compounds and aliphatic alkenes with Et₂SiH₂. Studies were conducted to gain insight into the mechanism of the reaction, indicating that the high η^2 -SiH bond character of **4** facilitates substitution of the silyl ligand, allowing a classical Chalk-Harrod mechanism.

Furthermore, novel PNP Fe mono(acetylide) and tris(acetylide) complexes were synthesized and their reactivity was compared to the literature known bis(acetylide) complexes previously employed for the Z-selective hydroboration and Z-selective dimerization of alkynes. It was shown that these three species exist in three different spin-states. This was further underpinned by DFT-calculations. The difference of spin-states was demonstrated to drastically alter the catalytic proficiency of the complexes. Experiments were conducted, that establish the bis(acetylide) complex as the only catalytically active species for the Z-selective dimerization of alkynes.

Finally, to test the influence of spectator ligands as well as the effect of the donor ligands located *trans* to the hydride, DFT calculations were performed. As test reaction, the insertion of CO₂ into the Fe-H bond of PNP pincer complexes was chosen, and a correlation between the NPA charge of the hydride of a series of PNP pincer complexes with the Gibbs free energy of the formation of the respective formate complexes was observed. The calculations suggested that decrease in the π -acceptor ability of the ancillary ligand and increase in *trans*-influence of the ligand opposite of the hydride should make the insertion reaction more exergonic. To test this hypothesis, a series of Iron-PNP dihydride as well as Iron-PNP hydrido-acetylide complexes were synthesized and their reactivity towards CO₂ was probed, confirming the findings of the theoretical calculations.

4. Experimental

All manipulations were performed under an inert atmosphere of argon by using Schlenk techniques or in a MBraun inert-gas glovebox. Solvents were purified according to standard procedures.¹²⁶ Deuterated solvents were purchased from euriso-top and dried over 3 Å molecular sieves. Phenylsilane, diphenylsilane, diethylsilane, methylphenylsilane and trimethoxysilane were obtained from commercial sources and used as received. Complexes **Fe20-Br**, **Fe20-NMe** and **Fe21-NMe** were prepared according to literature procedures.^{98,99,127} ^1H , $^{13}\text{C}\{^1\text{H}\}$, ^{15}N , $^{19}\text{F}\{^1\text{H}\}$, $^{29}\text{Si}\{^1\text{H}\}$ and $^{31}\text{P}\{^1\text{H}\}$ NMR spectra were recorded on Bruker AVANCE-250, AVANCE-400 and ASCEND-600 spectrometers. ^1H $^{13}\text{C}\{^1\text{H}\}$ NMR and $^{29}\text{Si}\{^1\text{H}\}$ NMR spectra were referenced internally to residual protio-solvent, and solvent resonances, respectively, and are reported relative to tetramethylsilane ($\delta = 0$ ppm). $^{31}\text{P}\{^1\text{H}\}$ NMR spectra were referenced externally to H_3PO_4 (85%) ($\delta = 0$ ppm), ^{15}N NMR were referenced externally to NH_3 (l) and $^{19}\text{F}\{^1\text{H}\}$ NMR were referenced externally to CFCl_3 .

Infrared spectra were recorded in attenuated total reflection (ATR) mode on a PerkinElmer Spectrum Two FT-IR spectrometer.

GC–MS analysis was conducted on an ISQ LT Single quadrupole MS (Thermo Fisher) directly interfaced to a TRACE 1300 Gas Chromatographic systems (Thermo Fisher), using a Rxi-5Sil MS (30 m, 0.25mm ID) crossbonded dimethyl polysiloxane capillary column.

High resolution-accurate mass data mass spectra were recorded on a hybrid Maxis Qq-aoTOF mass spectrometer (Bruker Daltonics, Bremen, Germany) fitted with an ESI-source. Measured accurate mass data of the $[\text{M}]^+$ ions for confirming calculated elemental compositions were typically within ± 5 ppm accuracy. The mass calibration was done with a commercial mixture of perfluorinated trialkyl-triazines (ES Tuning Mix, Agilent Technologies, Santa Clara, CA, USA).

X-ray diffraction data for **1**, **3**, **3-P(OMe)₃** were collected at $T=100$ K in a dry stream of nitrogen on a STOE STADIVARI diffractometer system equipped with a Dectris Eiger CdTe hybrid photon counting detector using $\text{Cu-K}\alpha$ radiation ($\lambda=1.54186$ Å). Data were reduced with X-Area and an absorption correction was applied with the multi-scan approach implemented in LANA.¹²⁸ X-ray diffraction data of all other complexes were collected at $T=100$ K in a dry stream of nitrogen on a Bruker Kappa APEX II diffractometer system using $\text{Mo-K}\alpha$ radiation ($\lambda=0.71073$ Å). Data were reduced to intensity values with SAINT and an absorption correction was applied with the multi-scan approach implemented in SADABS.¹²⁹ The crystal structures were solved by the dual-space approach implemented in

SHELXT¹³⁰ and refined against F^2 with SHELXL.¹³¹ Non-H atoms were refined with anisotropic atomic displacement parameters. H atoms connected to C were placed in calculated positions and refined as riding on the parent atom. The hydride Hs as well as H atoms connected to Si were refined freely. Molecular graphics were generated with the program MERCURY.¹³²

4.1. General Procedure for the Hydrosilylation of Alkenes

Inside an argon-flushed glovebox, a screwcap-vial (8 mL) was charged with catalyst (1-2 mol%), alkene substrate (0.21 mmol, 1 equiv.), 0.25 mL THF (if used) and diethylsilane (0.53 mmol, 2.5 equiv.) in this order. A stirring bar was added, the vial was sealed, transferred outside the glovebox and the reaction mixture was heated to 50 °C and stirred for reaction was quenched by exposure to air. 1 μ l of the sample was taken for GC-MS analysis.

Isolation of product

After exposing the sample to air for 1 h, the solvent of the reaction was removed in vacuo and the residue was purified by filtration through a pad of silica (approx. 1.5 g, silica 60 μ m) followed by elution with diethylether (5 mL) and removal of the solvent.

4.2. General Procedure for the Dimerization of Alkynes

An NMR tube, fitted with a septum, was charged with a solution of 76.8 μ l (0.7 mmol) of phenylacetylene in 0.5 ml of C_6D_6 . Subsequently, the catalysts **Fe20-Br**, **Fe21-NMe 15b** and **16b** (1 mol%) and (if used) LiHMDS (3 – 10 mol%) were dissolved in 0.5 ml of d_8 -THF and transferred into a syringe. After locking and shimming, a 1H -NMR spectrum of the phenylacetylene solution was measured and immediately afterwards the catalyst solution was injected into the NMR tube and the sample was shaken. Subsequently, 1H -NMR measurements of the mixture were conducted every 5 minutes over a period of six hours.

4.3. Syntheses of PNP Fe Silyl Complexes



Method A

To a solution of **Fe-20Br** (30 mg, 0.051 mmol) in 2 ml THF was added Na[AlH₄] (6.0 mg, 0.111 mmol) resulting in a color change from yellow to orange. While stirring the reaction mixture, a stock solution of H₂O (2.0 M in THF, 33.4 μ L, 0.668 mmol) was added resulting in severe gas evolution. After stirring for 10 minutes, the dark orange suspension was filtered using a syringe filter (polytetrafluoroethylene, 0.2 μ m) and phenylsilane (1.0 M in THF, 52 μ L, 0.052 mmol) was added and stirred for 30 minutes affording a dark-yellow solution. The solvent was evaporated under reduced pressure, yielding **2** (26 mg, 0.049 mmol, 96 %) as brown solid.

Method B:

To a solution of **Fe20-Br** (30 mg, 0.051 mmol) in 3 ml THF was added phenylsilane (1 mol in THF, 52 μ L, 0.052 mmol). The yellow solution was treated with NaBEt₃H (1 M solution in THF, 110 μ L, 0.110 mmol) whereupon the color of the solution turned brown. The mixture was stirred for 5 min and subsequently filtered using a syringe filter (polytetrafluoroethylene, 0.2 μ m). The solvent was removed under reduced pressure and the residue was washed twice with 0.2 ml *n*-pentane. After drying **2** was afforded as a brown solid. (21 mg, 0.039 mmol, 77 %). Crystallization from a concentrated solution in *n*-pentane at -30 °C afforded yellow single crystals suitable for X-ray diffraction.

¹H NMR (400 MHz, C₆D₆, 20 °C): δ = 8.23 (d, J=6.9 Hz, 2H, Ph^{2,6}), 7.35 (t, J = 7.4 Hz, 2H, Ph^{3,5}), 7.22 (t, J=7.3 Hz, 1H, Ph⁴), 7.01 (t, J = 8.1 Hz, 1H, py⁴), 5.54 (d, J = 8.1 Hz, 2H, py^{3,5}), 5.42 (t, J_{PH} = 6.5 Hz, 2H, PhSiH₂), 2.61 (m, 2H, PCH(CH₃)₂), 2.42 (t, J = 1.7 Hz, 6H, N(CH₃)), 2.15 (m, 2H, PCH(CH₃)₂), 1.28 (app q 6 H, PCH(CH₃)₂), 1.02 (m 18 H, PCH(CH₃)₂), - 8.20 (br 1H, (Fe-HSiPhH₂), - 10.75 (br 2H, FeH) ppm; ¹³C{¹H} NMR (101 MHz, C₆D₆, 20 °C): δ = 163.4 (t, J = 10.6 Hz, py^{2,6}), 149.0 (Ph¹), 136.0 (Ph^{2,6}), 135.4 (py⁴), 127.3 (Ph^{3,5}), 127.0 (Ph⁴), 94.9 (t, J = 3.2 Hz, py^{3,5}), 33.2 (t, J = 3.0 Hz, N(CH₃)), 28.6 (t, J=9.2 Hz PCH(CH₃)₂), 25.1 (t, J=11.7 Hz, PCH(CH₃)₂), 18.3 (br, PCH(CH₃)₂), 18.1 (br,

$\text{PCH}(\text{CH}_3)_2$ 18.0 (br, $\text{PCH}(\text{CH}_3)_2$) 17.6 (br, $\text{PCH}(\text{CH}_3)_2$) ppm; $^{31}\text{P}\{^1\text{H}\}$ NMR (162 MHz, C_6D_6 , 20 °C): $\delta = 178.3$ ppm $^{29}\text{Si}\{^1\text{H}\}$ (79 MHz, C_6D_6 , 20 °C) $\delta = -8.9$ (t, $J_{\text{Si-P}}=25.2$ Hz) ppm



This complex was synthesized analogously to **1** using 30 mg **Fe-20Br** (0.051 mmol), *n*-butylsilan (1 mol in THF, 52 μl , 0.052 mmol) and NaBEt_3H (1M solution in THF, 110 μl , 0.110 mmol) in 3 ml THF. The yellow-brown suspension was filtered with a syringe filter (polytetrafluoroethylene, 0.2 μm), the solvent was evaporated, and the residue was washed with 0.5 ml cold *n*-pentane, affording **2b** as purple solid (20 mg, 0.038 mmol, 75%).

^1H NMR (600 MHz, C_6D_6 , 20 °C): $\delta = 7.00$ (t, $J = 8.0$ Hz, 1H, py^4), 5.53 (d, $J = 8.1$ Hz, 2H, $\text{py}^{3,5}$), 4.73 (m, 2H, BuSiH_2), 2.70 (m, 2H, $\text{PCH}(\text{CH}_3)_2$), 2.43 (s, 6H, $\text{N}(\text{CH}_3)$), 2.20 (m, 2H, $\text{PCH}(\text{CH}_3)_2$), 1.90 (m, 2H, $\text{CH}_3\text{CH}_2\text{CH}_2\text{CH}_2\text{Si-}$), 1.66 (m, 2H, $\text{CH}_3\text{CH}_2\text{CH}_2\text{CH}_2\text{Si-}$), 1.27 (m, 2H, $\text{CH}_3\text{CH}_2\text{CH}_2\text{CH}_2\text{Si-}$), 1.21 (m, 12 H, $\text{PCH}(\text{CH}_3)_2$), 1.23 (m, 6 H, $\text{PCH}(\text{CH}_3)_2$), 1.08 (t, $J = 7.34$ Hz, 3H, $\text{CH}_3\text{CH}_2\text{CH}_2\text{CH}_2\text{Si-}$), 1.00 (m, 6 H, $\text{PCH}(\text{CH}_3)_2$), -8.20 (br 1H, (Fe-HSiPhH_2), -11.02 (br 2H, FeH) ppm; $^{13}\text{C}\{^1\text{H}\}$ NMR (151 MHz, C_6D_6 , 20 °C): $\delta = 163.2$ (t, $J = 11.1$ Hz, $\text{py}^{2,6}$), 135.2 (py^4), 94.6 (t, $J = 3.1$ Hz, $\text{py}^{3,5}$), 33.2 (t, $J = 3.0$ Hz, $\text{N}(\text{CH}_3)$), 31.1 (Bu), 28.4 (br, $\text{PCH}(\text{CH}_3)_2$), 27.0 (Bu), 25.0 (br, $\text{PCH}(\text{CH}_3)_2$), 18.4-18.0 (br, $\text{PCH}(\text{CH}_3)_2$) ppm; 14.6 (Bu), 1.4 (Bu) $^{31}\text{P}\{^1\text{H}\}$ NMR (243 MHz, C_6D_6 , 20 °C): $\delta = 179.3$ ppm. $^{29}\text{Si-}^1\text{H}$ HMBC (119 MHz, C_6D_6 , 20 °C) $\delta = -14.5$ ppm



This complex was synthesized analogously to **1** using 30 mg of **Fe20-Br** (0.051 mmol) and 20 μl diphenylsilane (0.108 mmol) and NaBEt_3H (1M solution in THF, 110 μl , 0.110 mmol) in 3 ml THF. The dark yellow suspension was filtered with a syringe filter (polytetrafluoroethylene, 0.2 μm). The solvent was evaporated and the residue was washed twice with 0.5 ml cold *n*-pentane, affording **3** as dark yellow solid (24 mg, 0.040 mmol, 78 %). Dark-orange crystals of **3** were grown by storing a concentrated solution in *n*-pentane at -30 °C.

^1H NMR (400 MHz, C_6D_6 , 20 °C): $\delta = 8.00$ (m, 4H, $\text{Ph}^{2,6}$), 7.24 (t, $J = 7.3$ Hz, 4H, $\text{Ph}^{3,5}$), 7.10 (m, 2H, Ph^4), 6.99 (t, $J = 8.2$ Hz, 1H, py^4), 6.20 (t, $J_{\text{PH}} = 9.6$ Hz, 1H, Ph_2SiH), 5.51 (d,

$J = 8.1$ Hz, 2H, $\text{py}^{3,5}$), 2.40 (t, $J = 1.7$ Hz, 6H, $\text{N}(\text{CH}_3)$), 2.11 (m, 4H, $\text{PCH}(\text{CH}_3)_2$), 1.08 (app q 12 H, $\text{PCH}(\text{CH}_3)_2$), 1.05-0.83 (m 12 H, $\text{PCH}(\text{CH}_3)_2$), -11.11 (br 3H, $\text{Fe}(\text{H}_2)$, FeH) ppm; $^{13}\text{C}\{^1\text{H}\}$ NMR (101 MHz, C_6D_6 , 20 °C): $\delta = 163.5$ (t, $J = 10.4$ Hz, $\text{py}^{2,6}$), 149.2 (Ph^1), 136.8 ($\text{Ph}^{2,6}$), 135.5 (py^4), 127.0 ($\text{Ph}^{3,5}$), 127.0 (Ph^4) 94.7 (t, $J = 3.1$ Hz, $\text{py}^{3,5}$), 33.5 (t, $J = 3.0$ Hz, $\text{N}(\text{CH}_3)$), 28.0 (br., $\text{PCH}(\text{CH}_3)_2$), 25.0 (br, $\text{PCH}(\text{CH}_3)_2$), 18.1 (br, $\text{PCH}(\text{CH}_3)_2$) ppm; $^{31}\text{P}\{^1\text{H}\}$ NMR (162 MHz, C_6D_6 , 20 °C): $\delta = 177.1$ ppm $^{29}\text{Si}-^1\text{H}$ HMBC (79 MHz, C_6D_6 , 20 °C) $\delta = 15.2$ ppm

$[(\text{PNP}^{\text{NMe}})\text{Fe}(\text{H})(\eta^2\text{-SiEt}_2\text{H}_3)]$ (**4**)

This complex was synthesized analogously to **1** using 30 mg of **Fe20-Br** (0.051 mmol) and 27 μl diethylsilane (0.208 mmol) and NaBEt_3H (1M solution in THF, 110 μl , 0.110 mmol) in 3 ml THF. The brown suspension was filtered with a syringe filter (polytetrafluoroethylene, 0.2 μm). The solvent was removed under reduced pressure and the orange solid was recrystallized from a concentrated solution in *n*-pentane at -30 °C affording **4** as orange crystals. (20 mg, 0.038 mmol, 75 %)

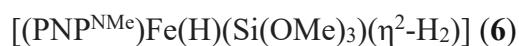
^1H NMR (600 MHz, C_6D_6 , 20 °C): $\delta = 6.98$ (t, $J = 8.1$ Hz, 1H, py^4), 5.50 (d, $J = 8.0$ Hz, 2H, $\text{py}^{3,5}$), 4.57 (br, 1H, $\text{CH}_3\text{CH}_2\text{SiH}$), 2.46 (m, 10H, $\text{N}(\text{CH}_3) + \text{PCH}(\text{CH}_3)_2$), 1.51 (t, 6H, $J = 7.7$ Hz, $\text{CH}_3\text{CH}_2\text{SiH}$), 1.32 (m, 2H, $\text{CH}_3\text{CH}_2\text{SiH}$), 1.24 (m 12 H, $\text{PCH}(\text{CH}_3)_2$), 1.09 (app. q 12 H, $\text{PCH}(\text{CH}_3)_2$), 0.92 (m, 2H, $\text{CH}_3\text{CH}_2\text{SiH}$), -11.00 (br 3H, $\text{Fe}-(\kappa^2\text{-Si-H})$, FeH) ppm; $^{13}\text{C}\{^1\text{H}\}$ NMR (151 MHz, C_6D_6 , 20 °C): $\delta = 163.2$ (t, $J = 10.9$ Hz, $\text{py}^{2,6}$), 135.1 (py^4), 94.4 (t, $J = 3.2$ Hz, $\text{py}^{3,5}$), 33.4 (t, $J = 3.2$ Hz, $\text{N}(\text{CH}_3)$), 31.6 (vt., $\text{PCH}(\text{CH}_3)_2$), 30.3 (vt, $\text{PCH}(\text{CH}_3)_2$), 18.3 ($\text{PCH}(\text{CH}_3)_2$), 18.1 (br, $\text{PCH}(\text{CH}_3)_2$), 17.8 ($\text{CH}_3\text{CH}_2\text{SiH}$), 17.7 ($\text{CH}_3\text{CH}_2\text{SiH}$), 12.5 ($\text{CH}_3\text{CH}_2\text{SiH}$), 12.5 ($\text{CH}_3\text{CH}_2\text{SiH}$) ppm; $^{31}\text{P}\{^1\text{H}\}$ NMR (243 MHz, C_6D_6 , 20 °C): $\delta = 179.0$ ppm, $^{29}\text{Si}-^1\text{H}$ HMBC (119 MHz, C_6D_6 , 20 °C) $\delta = 18.5$ ppm

$[(\text{PNP}^{\text{NMe}})\text{Fe}(\text{H})(\eta^2\text{-MePhH}_2)(\text{H})]$ (**5**)

This complex was synthesized analogously to **1** using 30 mg **Fe20-Br** (0.051 mmol) and 20 μl methylphenylsilane (0.145 mmol) and NaBEt_3H (1M solution in THF, 110 μl , 0.110 mmol) in 3 ml THF. The dark yellow suspension was filtered with a syringe filter (polytetrafluoroethylene, 0.2 μm), the solvent evaporated, and the residue was washed twice

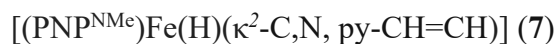
with 0.5 ml cold *n*-pentane, affording **5** as dark yellow solid (20 mg, 0.037 mmol, 72%). Yellow crystals of **5** were grown by storing a concentrated solution in *n*-pentane at -30 °C.

^1H NMR (400 MHz, C_6D_6 , 20 °C): δ = 8.07 (m, 2H, $\text{Ph}^{2,6}$), 7.33 (t, J = 7.4 Hz, 2H, $\text{Ph}^{3,5}$), 7.19 (m, 1H, Ph^4), 6.99 (t, J = 8.1 Hz, 1H, py^4), 5.59 (m, 1H, PhMeSiH), 5.51 (d, J = 8.1 Hz, 2H, $\text{py}^{3,5}$), 2.51 -2.41 (m, 2H, $\text{PCH}(\text{CH}_3)_2$), 2.41 (t, J = 1.6 Hz, 6H, $\text{N}(\text{CH}_3)$), 2.41 -2.24 (m, 2H, $\text{PCH}(\text{CH}_3)_2$), 1.24 (app q 6 H, $\text{PCH}(\text{CH}_3)_2$), 1.07-0.98 (m, 21 H, $\text{PCH}(\text{CH}_3)_2$ + MePhSiH), -10.07 (br 3H, FeH) ppm; $^{13}\text{C}\{^1\text{H}\}$ NMR (101 MHz, C_6D_6 , 20 °C): δ = 163.2 (t, J = 10.5 Hz, $\text{py}^{2,6}$), 152.6 (Ph^1), 135.3 (py^4), 135.2 ($\text{Ph}^{2,6}$), 127.2 ($\text{Ph}^{3,5}$), 126.7 (Ph^4), 94.6 (t, J = 3.2 Hz, $\text{py}^{3,5}$), 33.4 (t, J = 3.0 Hz, $\text{N}(\text{CH}_3)$), 31.2 (br., $\text{PCH}(\text{CH}_3)_2$), 30.2 (br, $\text{PCH}(\text{CH}_3)_2$), 18.2 (br, $\text{PCH}(\text{CH}_3)_2$), 9.6 (PhMeSiH) ppm; $^{31}\text{P}\{^1\text{H}\}$ NMR (162 MHz, C_6D_6 , 20 °C): δ = 177.9 ppm $^{29}\text{Si}-^1\text{H}$ HMBC (79 MHz, C_6D_6 , 20 °C) δ = 2.3 ppm



This complex was synthesized analogously to **1** using 30 mg **Fe20-Br** (0.051 mmol) and 10 μl trimethoxysilan (0.078 mmol) and NaBEt_3H (1M solution in THF, 110 μl , 0.110 mmol) in 3 ml THF. After stirring the purple mixture for 3h a color change to brown was observed. The brown suspension was filtered with a syringe filter (polytetrafluoroethylene, 0.2 μm) the solvent was evaporated and the residue was washed with 0.5 ml cold *n*-pentane, affording **6** as dark brown solid (21 mg, 0.038 mmol, 74%).

^1H NMR (400 MHz, C_6D_6 , 20 °C): δ = 6.94 (t, J = 8.0 Hz, 1H, py^4), 5.44 (d, J = 8.3 Hz, 2H, $\text{py}^{3,5}$), 3.38 (br, 9H, $(\text{MeO})_3\text{Si-}$), 2.82 (m, 2H, $\text{PCH}(\text{CH}_3)_2$), 2.38 (s, 6H, $\text{N}(\text{CH}_3)$), 2.23 (m, 2H, $\text{PCH}(\text{CH}_3)_2$), 1.38-0.98 (m, 24 H, $\text{PCH}(\text{CH}_3)_2$), -7.19 (t, J_{PH} = 23.3 Hz, 1H, Fe-H), -13.33 (t, J_{PH} = 36.8 Hz 2H, $\text{Fe}(\text{H})_2$) ppm; $^{13}\text{C}\{^1\text{H}\}$ NMR (101 MHz, C_6D_6 , 20 °C): δ = 163.2 (t, J = 10.5 Hz, $\text{py}^{2,6}$), 136.2 (py^4), 94.8 (t, J = 2.7 Hz, $\text{py}^{3,5}$), 49.0 (br, $\text{Si}(\text{OMe})_3$), 33.6 (t, 3.4 Hz, $\text{N}(\text{CH}_3)$), 30.0 (t, J = 8.7 Hz $\text{PCH}(\text{CH}_3)_2$), 24.4 (t, J = 13.0 Hz, $\text{PCH}(\text{CH}_3)_2$), 18.3 (br, $\text{PCH}(\text{CH}_3)_2$), 18.2 ($\text{PCH}(\text{CH}_3)_2$), 17.9 ($\text{PCH}(\text{CH}_3)_2$), 17.5 (t, J = 5.11 Hz, $\text{PCH}(\text{CH}_3)_2$) ppm; $^{31}\text{P}\{^1\text{H}\}$ NMR (162 MHz, C_6D_6 , 20 °C): δ = 180.0 ppm $^{29}\text{Si}\{^1\text{H}\}$ NMR (79 MHz, C_6D_6 , 20 °C) δ = -78.5 (br s) ppm



15 mg **4** (0.029 mmol) was dissolved in 2 ml THF and 6.6 μl 2-vinylpyridine (0.061 mmol, 2.1 eq) were added under stirring. The mixture was allowed to stir at r.t. for 24 hours, forming an intense dark red solution. The solvent was evaporated under reduced pressure and the dark residue was carefully washed twice with 0.2 ml of cold *n*-pentane. **7** was afforded after drying as a reddish-black solid. (10 mg, 0.019 mmol, 65%) Black crystals suitable for X-ray diffraction were obtained by cooling a saturated *n*-pentane solution of **7** at -30°C .

^1H NMR (600 MHz, C_6D_6 , 20°C): δ = 11.03 (dd, $J=8.1$ Hz, $J=3.2$ Hz, 1H, py^6), 7.66-7.62 (m, 2H, Fe-CH=CH-py), 7.25 (d, $J=8.00$ Hz, 1H, py^3), 7.07 (t, $J=8.1$ Hz, 1H, PNPpy^4), 6.96 (t, $J=7.4$ Hz, 1H, py), 6.09 (t, $J=6.4$ Hz, 1H, py), 5.72 (d, $J=8.0$ Hz, 2H, $\text{PNPpy}^{3,5}$), 2.51 (s, 6H, $\text{N}(\text{CH}_3)$), 2.03 (m, 2H, $\text{PCH}(\text{CH}_3)_2$), 1.91 (m, 2H, $\text{PCH}(\text{CH}_3)_2$), 1.48 (app q, 6H, $\text{PCH}(\text{CH}_3)_2$), 0.91-0.84 (m, 12H, $\text{PCH}(\text{CH}_3)_2$), 0.36 (app q, 6H, $\text{PCH}(\text{CH}_3)_2$), -16.62 (t, $J=72.5$ Hz, 1H, FeH) ppm; $^{13}\text{C}\{^1\text{H}\}$ NMR (151 MHz, C_6D_6 , 20°C): δ = 169.8 (py^2), 163.8 (t, $J=11.4$ Hz, $\text{PNPpy}^{2,6}$), 150.6 (py^6), 149.6 (br, Fe-CH=CH-py), 132.2 (PNPpy^4), 128.4 (py), 127.6 (Fe-CH=CH-py , superimposed by solvent peak, assigned via 2D-NMR), 119.0 (py), 112.2 (py), 94.6 (t, $J=3.5$ Hz, $\text{PNPpy}^{3,5}$), 32.4 (t, $J=5.2$ Hz, $\text{PCH}(\text{CH}_3)_2$), 32.2 (t, $J=3.1$ Hz, $\text{N}(\text{CH}_3)$), 31.2 (td, $J=13.2$ Hz, 5.2 Hz, $\text{PCH}(\text{CH}_3)_2$), 19.4 (t, $J=5.1$ Hz, $\text{PCH}(\text{CH}_3)_2$), 18.6 (br, $\text{PCH}(\text{CH}_3)_2$), 18.2 (br, $\text{PCH}(\text{CH}_3)_2$), 18.1 (t, $J=4.0$ Hz, $\text{PCH}(\text{CH}_3)_2$) ppm; $^{31}\text{P}\{^1\text{H}\}$ NMR (243 MHz, C_6D_6 , 20°C): δ = 162.9 (d, $J=58.9$ Hz) ppm



A solution of **3** (12 mg, 0.02 mmol) in 1.5 ml THF was stirred for 60 min under a CO atmosphere (1 bar) whereupon the color changed from orange to red. The solvent was removed under vacuum and a mixture of products of $[(\text{PNP}^{\text{NMe}})\text{Fe}(\text{H})(\text{SiPh}_2\text{H})(\text{CO})]$ (**3-CO**) and $[\text{Fe}(\text{PNP}^{\text{NMe}})(\text{CO})_2]$ (**8**) was obtained quantitatively in approximately a 8:1 ratio as determined by $^{31}\text{P}\{^1\text{H}\}$ NMR.

^1H NMR (600 MHz, C_6D_6 , 20°C): δ = 8.12 (m, 4H, $\text{Ph}^{2,6}$), 7.30 (app t., 4H, $\text{Ph}^{3,5}$), 7.18 (app t, 2H, Ph^4), 7.01 (t, $J=8.1$ Hz, 1H, py^4), 5.84 (t, $J_{\text{PH}}=9.2$ Hz, 1H, Ph_2SiH), 5.53 (d, $J=8.1$ Hz, 2H, $\text{py}^{3,5}$), 2.36 (m, 8H, $\text{N}(\text{CH}_3) + \text{PCH}(\text{CH}_3)_2$), 2.28 (m, 2H, $\text{PCH}(\text{CH}_3)_2$), 1.24 (app q, 6H, $\text{PCH}(\text{CH}_3)_2$), 1.18 (app q, 6H, $\text{PCH}(\text{CH}_3)_2$), 1.12 (app q, 6H, $\text{PCH}(\text{CH}_3)_2$), 0.86 (app q, 6H, $\text{PCH}(\text{CH}_3)_2$),

$\text{PCH}(\text{CH}_3)_2$), -7.57 (t, 1H, $J=49.3$ Hz, FeH) ppm; $^{13}\text{C}\{^1\text{H}\}$ NMR (151 MHz, C_6D_6 , 20 °C): δ = 217.4 (t, J = 17.3 Hz, CO), 162.5 (t, J = 9.4 Hz, $\text{py}^{2,6}$), 148.8 (Ph^1), 137.3 ($\text{Ph}^{2,6}$), 136.5 (py^4), 127.0 ($\text{Ph}^{3,5}$), 126.9 (Ph^4) 95.2 (t, J = 2.7 Hz, $\text{py}^{3,5}$), 33.5 (t, J = 3.6 Hz, $\text{N}(\text{CH}_3)$), 30.8 (t, $J=11.1$ Hz, $\text{PCH}(\text{CH}_3)_2$), 27.7 (t, $J=10.9$ Hz, $\text{PCH}(\text{CH}_3)_2$), 18.1 ($\text{PCH}(\text{CH}_3)_2$), 18.0 ($\text{PCH}(\text{CH}_3)_2$), 17.9 ($\text{PCH}(\text{CH}_3)_2$), 17.7 (t, $J=4.3$ Hz, $\text{PCH}(\text{CH}_3)_2$) ppm $^{31}\text{P}\{^1\text{H}\}$ NMR (243 MHz, C_6D_6 , 20 °C): δ = 170.4 ppm $^{29}\text{Si}-^1\text{H}$ HMBC (79 MHz, C_6D_6 , 20 °C) δ = 24.1 ppm. IR (ATR, cm^{-1}): 1889 (ν_{CO}).

$[(\text{PNP}^{\text{NMe}})\text{Fe}(\text{H})(\text{SiPh}_2\text{H})(\text{N}_2)]$ (**3-N₂**)

A solution of **3** (12 mg, 0.02 mmol) in 0.7 ml C_6D_6 was transferred into a Young-NMR tube and subjected to a freeze-pump-thaw cycle. After the cycle, the solution was backflushed with N_2 (1 bar). After shaking for 10 minutes the sample was again freeze-pump thawed and subsequently backflushed with N_2 (1 bar). This was repeated three times, whereupon the color of the solution changed from dark orange to yellow. $^{31}\text{P}\{^1\text{H}\}$ NMR measurements confirmed a 3:1 mixture of starting complex **3** and $[\text{Fe}(\text{PNP}^{\text{NMe}})(\text{H})(\text{N}_2)(\text{SiHPh}_2)]$ (**3-N₂**).

^1H NMR (250 MHz, C_6D_6 , 20 °C): δ = 8.06 (m, 4H, $\text{Ph}^{2,6}$), 7.32 (m, 4H, $\text{Ph}^{3,5}$), 7.15 (superimposed by solvent peak, 2H, Ph^4), 7.09 (t, 1H, py^4), 5.85 (t, $J=10.0$ Hz, 1H, Ph_2SiH), 5.64 (d, $J=8.1$ Hz, 2H, $\text{py}^{3,5}$), 2.46 (m, 8H, $\text{N}(\text{CH}_3)+\text{PCH}(\text{CH}_3)_2$), 2.13 (partially superimposed by **3**, 2H, $\text{PCH}(\text{CH}_3)_2$), 1.29 (app q. 6 H, $\text{PCH}(\text{CH}_3)_2$), 1.17 (m. 6 H, $\text{PCH}(\text{CH}_3)_2$), 1.00 (superimposed by **3**. 6 H, $\text{PCH}(\text{CH}_3)_2$), 0.86 (m. 6 H, $\text{PCH}(\text{CH}_3)_2$), -15.31 (t, 1H, $J=55.6$ Hz, FeH) ppm; $^{31}\text{P}\{^1\text{H}\}$ NMR (101 MHz, C_6D_6 , 20 °C): δ = 163.9 ppm. IR (ATR, cm^{-1}): 2055 (ν_{NN}).

$[(\text{PNP}^{\text{NMe}})\text{Fe}(\text{H})(\text{SiPh}_2\text{H})(\text{MeCN})]$ (**3-MeCN**)

To a solution of **3** (12 mg, 0.02 mmol) in 1.5 ml THF was added 5 μl of MeCN (0.096 mmol) and the reaction mixture was stirred for 2 h. The color of the solution gradually changed from orange to yellow. The complex was only stable in solution and in presence of an excess of MeCN.

^1H NMR (250 MHz, C_6D_6 , 20 °C): 8.14 (m, 4H, $\text{Ph}^{2,6}$), 7.45 (m., 4H, $\text{Ph}^{3,5}$), 7.23 (m, 2H, Ph^4), 6.85 (t, $J=8.1$ Hz, 1H, py^4), 5.80 (t, $J_{\text{PH}} = 8.6$ Hz, 1H, Ph_2SiH), 5.44 (d, $J=8.1$ Hz, 2H,

py^{3,5}), 2.44 (m, 8H, N(CH₃) + PCH(CH₃)₂), 2.23 (s, 3H, CH₃CN) 2.10 (m, 2H, PCH(CH₃)₂), 1.24 (app q. 6 H, PCH(CH₃)₂), 1.20 (app q. 6 H, PCH(CH₃)₂), 1.15 (app q. 6 H, PCH(CH₃)₂), 1.06 (app q. 6 H, PCH(CH₃)₂), -19.96 (t, 1H, J=58.9 Hz, FeH) ppm; ³¹P{¹H} NMR (101 MHz, C₆D₆, 20 °C): δ = 167.3 ppm.

[(PNP^{NMe})Fe(H)(SiPh₂H)(^tBuNC)] (**3-^tBuNC**)

A solution of **3** (12 mg, 0.02 mmol) in 1.5 ml THF was treated with 30 µl of ^tBuNC (0.096 mmol) and stirred for 24 h. The color of the solution changed from orange to yellowish brown. After evaporation of the solvent, **3-^tBuNC** was obtained as brown solid.

¹H NMR (250 MHz, C₆D₆, 20 °C): 8.09 (d, J=7.2 Hz, 4H, Ph^{2,6}), 7.28 (app t., 4H, Ph^{3,5}), 7.21 (app t, 2H, Ph⁴), 6.99 (t, J=8.1 Hz, 1H, py⁴), 5.78 (t, J_{PH} = 8.0 Hz, 1H, Ph₂SiH), 5.56 (d, J=8.0 Hz, 2H, py^{3,5}), 2.55 (m, 8H, N(CH₃) + PCH(CH₃)₂) 2.37 (m, 2H, PCH(CH₃)₂), 1.39 (app q. 6 H, PCH(CH₃)₂), 1.23 (m. 12 H, PCH(CH₃)₂), 1.10 (s, 9H, CNC(CH₃)₃), 0.96 (app q. 6 H, PCH(CH₃)₂), -10.62 (t, 1H, J=58.8 Hz, FeH) ppm; ³¹P{¹H} NMR (101 MHz, C₆D₆, 20 °C): δ = 172.3 ppm.

[(PNP^{NMe})Fe(H)(SiPh₂H)(P(OMe)₃)] (**3- P(OMe)₃**)

To a solution of **3** (12 mg, 0.02 mmol) in 1.5 ml THF was added P(OMe)₃ (4 µl, 0.034 mmol) and the reaction was stirred for 24 h. The solvent of the yellow solution was subsequently evaporated under reduced pressure and the dark yellow solid was washed twice with 0.3 ml *n*-pentane, yielding **3- P(OMe)₃** as a yellow solid. (12 mg, 0.016 mmol, 82 %)

¹H NMR (600 MHz, C₆D₆, 20 °C): δ = 8.13 (m, 4H, Ph^{2,6}), 7.28 (app t, 4H, Ph^{3,5}), 7.13 (m, 2H, Ph⁴), 6.94 (t, J=8.1 Hz 1H, py⁴), 5.83 (q, J=5.8 Hz, 1H, Ph₂SiH), 5.47 (d, J=8.0 Hz, 2H, py^{3,5}), 3.11 (d, J_{HP} = 9.7 Hz, 9H, P(OCH₃)₃), 2.73 (m, 2H, PCH(CH₃)₂), 2.49 (s, 6H, N(CH₃)), 2.47 (m, 2H, PCH(CH₃)₂) 1.34 (m. 12 H, PCH(CH₃)₂), 1.08 (app q. 6 H, PCH(CH₃)₂), 0.89 (app q. 6 H, PCH(CH₃)₂), -9.70 (dt 1H, J=66.7 Hz, J= 61.8 Hz, FeH) ppm; ¹³C{¹H} NMR (151 MHz, C₆D₆, 20 °C): δ = 163.9 (t, J=9.2 Hz, py^{2,6}), 152.4 (Ph¹), 137.1 (Ph^{2,6}), 136.1 (py⁴), 126.4 (Ph^{3,5}), 125.8 (Ph⁴) 94.1 (t, J = 3.0 Hz, py^{3,5}), 51.2 (d, J=8.1 Hz, P(OCH₃)₃), 35.0 (t, J = 3.4 Hz, N(CH₃)), 33.5 (m, PCH(CH₃)₂), 28.0 (vt, PCH(CH₃)₂), 19.3 (PCH(CH₃)₂), 19.1 (PCH(CH₃)₂), 18.3 (PCH(CH₃)₂), 18.3 (PCH(CH₃)₂) ppm ³¹P{¹H} NMR (243 MHz, C₆D₆,

20 °C): $\delta = 170.9$ (d, $J = 43.5$ Hz, $PCH(CH_3)_2$), 164.9 (t, $J = 43.5$ Hz, $P(OMe)_3$), $^{29}Si\{^1H\}$ (79 MHz, C_6D_6 , 20 °C) $\delta = 26.8$ (q, $J_{Si-P}=35.9$ Hz) ppm

$[(PNP^{NMe})Fe(H)(SiPh_2H)(PMe_3)]$ (3- PMe_3**)**

To a solution of **3** (12 mg, 0.02 mmol) in 1.5 ml THF was added PMe_3 (40 μ l, 0.04 mmol) and the reaction was stirred for 7 d, affording a red solution. The solvent of the solution was subsequently evaporated under reduced pressure and the red solid was characterized as a mixture of **3**, **3- PMe_3** and **9a**, in a ratio of 59/14/27 as determined by $^{31}P\{^1H\}$ -NMR.

1H NMR (250 MHz, C_6D_6 , 20 °C): $\delta = 8.01$ (m, 4H, $Ph^{2,6}$), 7.23 (m, 4H, $Ph^{3,5}$), 7.12 (m, 2H, Ph^4), 6.95 (t, $J=7.8$ Hz 1H, py^4), 5.81 (q, $J=8.2$ Hz, 1H, Ph_2SiH), 5.57 (m, partially superimposed by **3** and **9a**, 2H, $py^{3,5}$), 2.82 (m, 2H, $PCH(CH_3)_2$), 2.56 (s, 6H, $N(CH_3)$), 2.42 (m partially superimposed by **3** and **9a**, 2H, $PCH(CH_3)_2$) 1.34 - 0.76 (m, 33 H, $PCH(CH_3)_2$ + $P(CH_3)$ signals superimposed by **3** and **9a**), -13.21 (td, 1H, $J=71.1$ Hz, $J=20.5$ Hz, FeH) ppm; $^{31}P\{^1H\}$ NMR (101 MHz, C_6D_6 , 20 °C): 170.6 (d, $J = 25.5$ Hz, $PCH(CH_3)_2$), 5.5 (t, $J = 26.0$ Hz, PMe_3).

$[(PNP^{NMe})Fe(H)(SiEt_2H)(CO)]$ (4-CO**)**

A solution of **4** (20 mg, 0.038 mmol) in 1.5 ml THF was stirred for 60 min under a CO atmosphere (1 bar) whereupon the color changed from orange to red. The solvent was removed under vacuum and a mixture of products of $[Fe(PNP^{NMe})(H)(SiHEt_2)(CO)]$ (**4-CO**), $[Fe(PNP^{NMe})(CO)_2]$ (**8**) and the cis and trans isomer of $[Fe(PNP^{NMe})(H_2)(CO)]$ (**10a-b**) was obtained quantitatively in approximately a 70:7:14:9 ratio as determined by $^{31}P\{^1H\}$ -NMR.

1H NMR (400 MHz, C_6D_6 , 20 °C): $\delta = 7.00$ (app t, 1H, py^4), 5.54 (m, 2H, $py^{3,5}$), 4.23 (m, 1H, Et_2SiH), 2.65 (m, 2H, $PCH(CH_3)_2$), 2.54 (m, 2H, $PCH(CH_3)_2$), 2.42 (t, 6H, $N(CH_3)$), 1.52 (t, 6H, $J = 7.6$ Hz, CH_3CH_2SiH), 1.40 (app q. 6 H, $PCH(CH_3)_2$), 1.26 (m, 4H partially superimposed, CH_3CH_2SiH), 1.24 (m., 6 H, $PCH(CH_3)_2$), 1.15 (app q. 6 H, $PCH(CH_3)_2$), 1.02 (app q. 6 H, $PCH(CH_3)_2$), -8.26 (t, 1H, $J_{HP}=51.0$ Hz, FeH) ppm; $^{31}P\{^1H\}$ NMR (162 MHz, C_6D_6 , 20 °C): $\delta = 172.2$ ppm ^{29}Si - 1H HMBC (79 MHz, C_6D_6 , 20 °C) $\delta = 34.2$ ppm.

$[(\text{PNP}^{\text{NMe}})\text{Fe}(\text{H})(\text{SiEt}_2\text{H})(\text{N}_2)]$ (**4-N₂**)

A solution of **4** (12 mg, 0.02 mmol) in 0.7 ml C_6D_6 was transferred into a Young-NMR tube and treated to three freeze-pump-thaw cycles. Afterwards the solution was backflushed with N_2 (1 bar). After shaking for 10 minutes the sample was again freeze-pump thawed and subsequently backflushed with N_2 (1 bar). This was repeated two times, whereupon the color of the solution changed from dark orange to light orange. $^{31}\text{P}\{^1\text{H}\}$ NMR showed a 53:26:21 mixture of **4** and the tentative complexes $[\text{Fe}(\text{PNP}^{\text{Me}})(\text{H})_2(\text{N}_2)]$ (**4a**) and $[\text{Fe}(\text{PNP}^{\text{Me}})(\text{H})(\text{SiHPh}_2)(\text{N}_2)]$ (**4b**). Increased broadening of the ^1H NMR spectrum was observed with each freeze pump cycle, hindering the full characterization of the compounds.

^1H NMR (250 MHz): $\delta = 4.31$ (br, SiEt_2H), -15.16 (t, $J = 55.3$ Hz FeH); ^{31}P NMR (101 MHz): $\delta = 165.9$ ppm.

$[(\text{PNP}^{\text{NMe}})\text{Fe}(\text{H})(\text{SiEt}_2\text{H})(^t\text{BuNC})]$ (**4-^tBuNC**)

A solution of **3** (12 mg, 0.02 mmol) in 1.5 ml THF was treated with 30 μl of $^t\text{BuNC}$ (0.096 mmol) and stirred for 4 h. The color of the solution changed from orange to yellowish brown. After evaporation of the solvent a mixture of **4**, **4-^tBuNC** and **12a-b** in a product ratio of 40/34/5/21 as determined by $^{31}\text{P}\{^1\text{H}\}$ -NMR was obtained quantitatively as a brown solid.

^1H NMR (400 MHz, C_6D_6 , 20 °C): $\delta = 6.96$ (app t, 1H, py^4), 5.55 (br, 2H, $\text{py}^{3,5}$), 4.24 (m, 1H, Et_2SiH), 2.65 (m, 2H, $\text{PCH}(\text{CH}_3)_2$), 2.60 (m, 8H, $\text{N}(\text{CH}_3) + \text{PCH}(\text{CH}_3)_2$), 1.50 (br, 12H, $\text{PCH}(\text{CH}_3) + \text{CH}_3\text{CH}_2\text{SiH}$), 1.26 (m, 6 H, $\text{PCH}(\text{CH}_3)_2$), 1.13 (m, 19H partially superimposed, $\text{CH}_3\text{CH}_2\text{SiH} + \text{PCH}(\text{CH}_3)_2 + \text{CNC}(\text{CH}_3)_3$), 0.95 (br, 6 H, $\text{PCH}(\text{CH}_3)_2$), -11.05 (t, 1H, $J_{\text{HP}}=57.7$ Hz, FeH) ppm; $^{31}\text{P}\{^1\text{H}\}$ NMR (162 MHz, C_6D_6 , 20 °C): $\delta = 174.5$ ppm

trans- $[\text{Fe}(\text{PNP}^{\text{Me}})(\text{P}(\text{OMe})_3)(\text{H})_2]$ (**13**)

To a solution of **4** (13 mg, 0.025 mmol) in 1.5 ml benzene was added $\text{P}(\text{OMe})_3$ (4 μl , 0.034 mmol) and the solution was stirred for 24 h forming a brown solution. The solvent was evaporated to dryness and the brown residue was extracted with 2 ml *n*-pentane. The orange extract was filtered with a syringe filter (polytetrafluoroethylene, 0.2 μm) and after removing of the solvent, **13** was obtained as dark orange solid. (13 mg, 0.024 mmol, 94%) Crystals

suitable for X-ray diffraction analysis were obtained by evaporating a concentrated solution of **13** in *n*-pentane to dryness at -30°C.

^1H NMR (600 MHz, C_6D_6 , 20 °C): δ = 6.97 (t, J = 8.1 Hz, 1H, py^4), 5.53 (d, J = 8.0 Hz, 2H, $\text{py}^{3,5}$), 3.43 (d, J_{HP} = 10.5 Hz, 9H, $\text{P}(\text{OCH}_3)_3$), 2.62 (s, 6H, $\text{N}(\text{CH}_3)$), 2.58 (m, 4H, $\text{PCH}(\text{CH}_3)_2$), 1.45 (app. q 12 H, $\text{PCH}(\text{CH}_3)_2$), 1.28 (app. q 12 H, $\text{PCH}(\text{CH}_3)_2$), -9.76 (dt, J = 59.6 Hz, J = 42.6 Hz, 2H, FeH) ppm; $^{13}\text{C}\{^1\text{H}\}$ NMR (151 MHz, C_6D_6 , 20 °C): δ = 163.0 (t, J = 11.3 Hz, $\text{py}^{2,6}$), 133.3 (py^4), 93.9 (t, J = 3.3 Hz, $\text{py}^{3,5}$), 49.7 (d, J = 2.6 Hz, $\text{P}(\text{OCH}_3)_3$), 33.3 (t, J = 3.1 Hz, $\text{N}(\text{CH}_3)$), 28.6 (t, J = 9.2 Hz, $\text{PCH}(\text{CH}_3)_2$), 18.7 ($\text{PCH}(\text{CH}_3)_2$), 18.3 (t, J = 2.8 Hz, $\text{PCH}(\text{CH}_3)_2$) ppm; $^{31}\text{P}\{^1\text{H}\}$ NMR (243 MHz, C_6D_6 , 20 °C): δ = 209.4 (t, J = 76.1 Hz, $\text{P}(\text{OMe})_3$) 183.9 (d, J = 76.0 Hz, $\text{PCH}(\text{CH}_3)_2$), ppm.

[Fe(PNP^{Me})(H)₂(PMe₃)] (**9**)

This complex was analogously prepared to **13** with **4** (13 mg, 0.025 mmol) and 40 μl of PMe_3 (1M in THF, 0.04 mmol). After stirring for 24 h the solution turned intensely red. The solvent was evaporated in vacuo and the complex was washed with 0.5 ml TMS (-30°C). **9** was obtained as dark red solid in an isomeric ratio of *cis* 92.5 %/ *trans* 7.5 %. (10 mg, 0.02 mmol, 80 %)

cis-isomer

^1H NMR (600 MHz, C_6D_6 , 20 °C): δ = 6.94 (t, J = 7.5 Hz, 1H, py^4), 5.57 (d, J = 7.9 Hz, 2H, $\text{py}^{3,5}$), 2.73 (s, 6H, $\text{N}(\text{CH}_3)$), 2.40 (m, 2H, $\text{PCH}(\text{CH}_3)_2$), 2.25 (m, 2H, $\text{PCH}(\text{CH}_3)_2$), 1.56 (app q 6 H, $\text{PCH}(\text{CH}_3)_2$), 1.41 (app q, 6 H, $\text{PCH}(\text{CH}_3)_2$), 1.31 (m, 6 H, $\text{PCH}(\text{CH}_3)_2$), 1.01 (d, J = 5.3 Hz, 9 H, $\text{P}(\text{CH}_3)_3$), 0.80 (app q, 6 H, $\text{PCH}(\text{CH}_3)_2$) -13.46 (br, 1H, FeH), -18.57 (br, 1H, FeH) ppm; $^{13}\text{C}\{^1\text{H}\}$ NMR (151 MHz, C_6D_6 , 20 °C): δ = 164.1 (t, J = 10.5 Hz, $\text{py}^{2,6}$), 130.2 (py^4), 94.0 (t, J = 3.8 Hz, $\text{py}^{3,5}$), 33.6 (t, J = 3.4 Hz, $\text{N}(\text{CH}_3)$), 32.9 (m, $\text{PCH}(\text{CH}_3)_2$) 28.8 (m, $\text{PCH}(\text{CH}_3)_2$), 25.1 (t, J = 7.6 Hz, $\text{PCH}(\text{CH}_3)_2$), 23.3 (d, J = 14.3 Hz, $\text{P}(\text{CH}_3)_3$), 19.9 ($\text{PCH}(\text{CH}_3)_2$), 19.6 (t, J = 5.2 Hz, $\text{PCH}(\text{CH}_3)_2$), 18.0 ($\text{PCH}(\text{CH}_3)_2$) ppm; $^{31}\text{P}\{^1\text{H}\}$ NMR (162 MHz, C_6D_6 , 20 °C): δ = 184.4 (d, J = 29.0 Hz, $\text{PCH}(\text{CH}_3)_2$), 13.4 (t, J = 29.1 Hz, PMe_3) ppm.

characteristic chemical shifts of the *trans*-isomer

^1H NMR (600 MHz, C_6D_6 , 20 °C): δ = -10.94 (dt, J = 55.2 Hz, J = 44.7 Hz 2H, FeH) ppm;

$^{31}\text{P}\{^1\text{H}\}$ NMR (162 MHz, C_6D_6 , 20 °C): δ = 182.1 (d, J = 43.3 Hz, $\text{PCH}(\text{CH}_3)_2$), 27.0 (t, J = 43.3 Hz, PMe_3) ppm.

[Fe(PNP^{Me})(H)(P(OMe₃))(SiH₂Ph)] (**1-P(OMe)₃**)

A solution of **1** (12 mg, 0.02 mmol) in 1.5 ml THF was added P(OMe₃) (4 μl , 0.034 mmol) and the reaction was stirred for 24 h. The solvent of the yellow solution was subsequently evaporated under reduced pressure and the orange-yellow solid was washed twice with 0.3 ml *n*-pentane, yielding **1-P(OMe)₃** as a yellow solid. (10 mg, 0.016 mmol, 76 %)

^1H NMR (600 MHz, C_6D_6 , 20 °C): δ = 8.09 (d, J = 7.3 Hz, 2H, $\text{Ph}^{2,6}$), 7.32 (t, J = 7.4 Hz, 2H, $\text{Ph}^{3,5}$), 7.23 (t, J = 7.3 Hz 1H, Ph^4), 6.94 (t, J = 8.1 Hz 1H, py^4), 5.47 (d, J = 8.0 Hz, 2H, $\text{py}^{3,5}$), 5.01 (q, J = 4.9 Hz, 1H, PhSiH_2), 3.13 (d, J_{HP} = 9.9 Hz, 9H, $\text{P}(\text{OCH}_3)_3$), 3.04 (m, 2H, $\text{PCH}(\text{CH}_3)_2$), 2.54 – 2.48 (m, 8H, $\text{N}(\text{CH}_3) + \text{PCH}(\text{CH}_3)_2$) 1.46 (app q. 6H, $\text{PCH}(\text{CH}_3)_2$), 1.38 (app q. 6 H, $\text{PCH}(\text{CH}_3)_2$), 1.27 (app q. 6 H, $\text{PCH}(\text{CH}_3)_2$), 0.89 (app q. 6 H, $\text{PCH}(\text{CH}_3)_2$), -10.05 (q 1H, J = 64.7 Hz, FeH) ppm; $^{13}\text{C}\{^1\text{H}\}$ NMR (151 MHz, C_6D_6 , 20 °C): δ = 163.8 (t, J = 9.6 Hz, $\text{py}^{2,6}$), 151.0 (d, J = 4.1 Hz, Ph^1), 136.8 ($\text{Ph}^{2,6}$), 134.2 (py^4), 126.3 ($\text{Ph}^{3,5}$), 125.9 (Ph^4), 94.1 (t, J = 3.1 Hz, $\text{py}^{3,5}$), 51.3 (d, J = 7.2 Hz, $\text{P}(\text{OCH}_3)_3$), 34.9 (t, J = 3.3 Hz, $\text{N}(\text{CH}_3)$), 32.3 (app q, $\text{PCH}(\text{CH}_3)_2$), 28.6 (vt, $\text{PCH}(\text{CH}_3)_2$), 19.2 ($\text{PCH}(\text{CH}_3)_2$), 18.9 (vt, $\text{PCH}(\text{CH}_3)_2$), 18.9 ($\text{PCH}(\text{CH}_3)_2$), 18.6 ($\text{PCH}(\text{CH}_3)_2$) ppm $^{31}\text{P}\{^1\text{H}\}$ NMR (243 MHz, C_6D_6 , 20 °C): δ = 173.4 (d, J = 43.3 Hz, $\text{PCH}(\text{CH}_3)_2$), 164.1 (t, J = 42.1 Hz, $\text{P}(\text{OMe})_3$), $^{29}\text{Si}\{^1\text{H}\}$ (79 MHz, C_6D_6 , 20 °C) δ = - 3.0 (dt, $J_{\text{Si-P}}$ = 78.8 Hz, $J_{\text{Si-P}}$ = 47.2 Hz) ppm

[Fe(PNP^{Me})(H)(P(OMe₃))(SiHMePh)] (**5-P(OMe)₃**)

A solution of **5** (12 mg, 0.02 mmol) in 1.5 ml THF was added P(OMe₃) (4 μl , 0.034 mmol) and the reaction was stirred for 24 h. The solvent of the yellow solution was subsequently evaporated under reduced pressure and the dark yellow solid was washed twice with 0.3 ml *n*-pentane, yielding **5-P(OMe)₃** as a yellow solid. (12 mg, 0.016 mmol, 82 %)

^1H NMR (600 MHz, C_6D_6 , 20 °C): δ = 8.02 (dd, J = 7.7 Hz, J = 1.5 Hz 2H, $\text{Ph}^{2,6}$), 7.34 (t, J = 7.5 Hz, 2H, $\text{Ph}^{3,5}$), 7.21 (m, 1H, Ph^4), 6.94 (t, J = 8.0 Hz, 1H, py^4), 5.48 (dd, J = 15.5 Hz, J = 8.0 Hz, 2H, $\text{py}^{3,5}$), 5.34 (m, 1H, PhMeSiH), 3.16 (d, J_{HP} = 9.9 Hz, 9H, $\text{P}(\text{OCH}_3)_3$), 3.01-

2.92 (m, 2H, $PCH(CH_3)_2$), 2.51 (dd, $J = 35.7$ Hz, $J = 2.8$ Hz, 6H, $N(CH_3)$) 1.98 -1.86 (m, 2H, $PCH(CH_3)_2$), 1.54 (app dd, 3 H, $PCH(CH_3)_2$), 1.42 (app dd, 3 H, $PCH(CH_3)_2$), 1.33 (app dd, 3 H, $PCH(CH_3)_2$), 1.24-1.14 (m, 9 H, $PCH(CH_3)_2$), 1.08 (app dd, 3 H, $PCH(CH_3)_2$), 1.01 (d, $J=4.2$ Hz, 3 H, $MePhSiH$), 0.77 (app dd, 3 H, $PCH(CH_3)_2$) - 9.90 (q, $J=61.8$ Hz, 1H, FeH) ppm; $^{13}C\{^1H\}$ NMR (151 MHz, C_6D_6 , 20 °C): $\delta = 163.9$ (m, $py^{2,6}$), 155.5 (Ph^1), 135.8 ($Ph^{2,6}$), 134.1 (py^4), 126.4 ($Ph^{3,5}$), 125.8 (Ph^4) 94.0 (t, $J = 6.6$ Hz, $py^{3,5}$), 51.0 (d, $J=7.3$ Hz, $P(OCH_3)_3$), 35.1 (d, $J = 7.5$ Hz, $N(CH_3)$), 34.7 (d, $J = 7.3$ Hz, $N(CH_3)$) 34.5 (m, $PCH(CH_3)_2$), 33.1 (m, $PCH(CH_3)_2$) 28.6 (d, $J=14.1$ Hz, $PCH(CH_3)_2$), 26.9 (d, $J=15.6$ Hz, $PCH(CH_3)_2$), 19.7 (d, $J=3.3$ Hz, $PCH(CH_3)_2$), 19.0 (d, $J=3.5$ Hz, $PCH(CH_3)_2$) 18.8 (m, $PCH(CH_3)_2$) ,18.3–18.2 (m, $PCH(CH_3)_2$), 17.9 (d, $J=7.2$ Hz, $PCH(CH_3)_2$), 6.0 (d, $J=4.3$ Hz, $PhMeSiH$) ppm $^{31}P\{^1H\}$ NMR (243 MHz, C_6D_6 , 20 °C): $\delta = 172.9$ (dd, $J = 83.3$ Hz, $J = 43.9$ Hz, $PCH(CH_3)_2$), 169.5 (dd, $J = 83.3$ Hz, $J = 42.6$ Hz, $PCH(CH_3)_2$) 164.9 (t, $J = 43.0$ Hz, $P(OMe)_3$), $^{29}Si\{^1H\}$ (79 MHz, C_6D_6 , 20 °C) $\delta = 11.3$ (m) ppm

[Fe(PNP^{Me})(H)(P(OMe₃))(Si(OMe)₃)] (**6-P(OMe)₃**)

A solution of **6** (10.5 mg, 0.019 mmol) in 1.5 ml THF was added P(OMe₃) (4 μ l, 0.034 mmol) and the reaction was stirred for 24 h. The solvent of the dark solution was subsequently evaporated under reduced pressure and the dark residue was washed twice with 0.3 ml of cold *n*-pentane, yielding **6-P(OMe)₃** as a yellow solid. (9 mg, 0.014 mmol, 72 %)

1H NMR (400 MHz, C_6D_6 , 20 °C): $\delta=6.97$ (t, $J = 8.4$ Hz, 1H, py^4), 5.49 (d, $J = 7.9$ Hz, 2H, $py^{3,5}$), 3.76 (s, 9H, $(MeO)_3Si-$), 3.25 (d, $J_{HP} = 9.8$ Hz, 9H, $P(OCH_3)_3$), 2.82 (m, 2H, $PCH(CH_3)_2$), 2.57 (s, 6H, $N(CH_3)$), 2.25 (m, 2H, $PCH(CH_3)_2$), 1.57 (app q. 6H, $PCH(CH_3)_2$), 1.46 (app q. 6 H, $PCH(CH_3)_2$), 1.37 (app q. 6 H, $PCH(CH_3)_2$), 1.01 (app q. 6 H, $PCH(CH_3)_2$), -10.01 (q 1H, $J=63.5$ Hz, FeH) ppm; $^{13}C\{^1H\}$ NMR (101 MHz, C_6D_6 , 20 °C): $\delta = 163.8$ (t, $J=10.1$ Hz, $py^{2,6}$), 134.2 (py^4), 93.9 (t, $J = 2.6$ Hz, $py^{3,5}$), 51.0 (d, $J=7.1$ Hz, $P(OCH_3)_3$), 50.7 ($Si(OMe)_3$), 35.0 (t, 3.4 Hz, $N(CH_3)$), 33.0 (app q, $PCH(CH_3)_2$), 28.4 (vt, $PCH(CH_3)_2$), 19.4 ($PCH(CH_3)_2$), 18.9 ($PCH(CH_3)_2$), 18.8 ($PCH(CH_3)_2$), 18.8 (vt, $PCH(CH_3)_2$) ppm; $^{31}P\{^1H\}$ NMR (162 MHz, C_6D_6 , 20 °C): $\delta = 177.0$ (d, $J = 42.7$ Hz, $PCH(CH_3)_2$), 169.3 (t, $J = 41.9$ Hz, $P(OMe)_3$) ppm; $^{29}Si\{^1H\}$ NMR (79 MHz, C_6D_6 , 20 °C) $\delta = 24.8$ (q, $J_{Si-P}=53.7$ Hz) ppm

4.4. Syntheses of Fe PNP Mono- and Tris(acetylide) Complexes

$[(\text{PNP}^{\text{NMe}})\text{Fe}(\text{Br})(\text{C}\equiv\text{C-TMS})]$ (**15a**)

200 mg (0.34 mmol) of **Fe20-Br** were dissolved in 20 ml THF and a freshly prepared solution of lithium TMS- acetylide (prepared from 50 μl (0.36 mmol) TMS acetylene and 224 μl *n*-BuLi (0.36 mmol, 1.05 eq, 1.6 M in hexanes) in 2 ml THF) was added. The color of the solution changed from yellow to dark brown. The reaction mixture was stirred for 2 h at r.t. and subsequently concentrated to a volume of 2 ml. The crude product was then precipitated by addition of 10 ml *n*-pentane. After decantation of the supernatant solution the beige crude product was washed three times with 2 ml of cold Et_2O , affording **15a** as yellow solid. (125 mg, 0.21 mmol, 61 %).

Magnetic susceptibility (Evans' Method, THF): $\mu_{\text{eff}} = 4.9(3) \mu_{\text{B}}$. IR (ATR, $\nu_{\text{C}\equiv\text{C}}$, cm^{-1}): 1989. HRMS (ESI⁺, $\text{CH}_3\text{CN}/\text{MeOH} + 1\% \text{H}_2\text{O}$): m/z calcd for $\text{C}_{24}\text{H}_{46}\text{FeN}_3\text{P}_2\text{Si} [\text{M-Br}]^+$ 522.2280 found 522.2292.

$[(\text{PNP}^{\text{NMe}})\text{Fe}(\text{Br})(\text{C}\equiv\text{C-Ph})]$ (**15b**)

This complex was prepared analogously to **15a** starting from 200 mg (0.34 mmol) of **Fe20-Br** with 40 μl of phenyl acetylene (0.36 mmol) and 224 μl *n*-BuLi (0.36 mmol, 1.05 eq). **15b** was afforded as yellow powder (130 mg, 0.21 mmol, 63 %).

Magnetic susceptibility (Evans' Method, THF): $\mu_{\text{eff}} = 4.9(1) \mu_{\text{B}}$. IR (ATR, $\nu_{\text{C}\equiv\text{C}}$, cm^{-1}): 2045. HRMS (ESI⁺, $\text{CH}_3\text{CN}/\text{MeOH} + 1\% \text{H}_2\text{O}$): m/z calcd for $\text{C}_{27}\text{H}_{42}\text{FeN}_3\text{P}_2 [\text{M-Br}]^+$ 526.2197 found 526.2204.

$[(\text{PNP}^{\text{NMe}})\text{Fe}(\text{Br})(\text{C}\equiv\text{C-TMS})(\text{PMe}_3)]$ (**15a-PMe₃**)

15a (15 mg, 0.025 mmol) was suspended in 0.7 ml C_6D_6 and 3 μl of PMe_3 (0.029 mmol) was added and after stirring for 20 min affording a red solution was afforded. After filtration with a syringe filter (polytetrafluoroethylene, 0.2 μm) the red solution was characterized without further purification.

^1H NMR (600 MHz, C_6D_6 , 20 °C): δ = 6.97 (tt, J = 8.1 Hz J = 1.2 Hz, 1H, py^4), 5.62 (d, J = 8.1 Hz, 2H, $\text{py}^{3,5}$), 3.22 (m, 2H, $\text{PCH}(\text{CH}_3)_2$), 3.10 (m, 2H, $\text{PCH}(\text{CH}_3)_2$), 2.63 (s, 6H, $\text{N}(\text{CH}_3)$), 1.57 (d, J = 7.8 Hz 9H, $\text{P}(\text{CH}_3)_3$), 1.53 (app q 6 H, $\text{PCH}(\text{CH}_3)_2$), 1.48 (app q 6 H, $\text{PCH}(\text{CH}_3)_2$), 1.43 (app q 6 H, $\text{PCH}(\text{CH}_3)_2$), 1.35 (app q 6 H, $\text{PCH}(\text{CH}_3)_2$) 0.18 (s 9H, $\text{Si}(\text{CH}_3)_3$); $^{13}\text{C}\{^1\text{H}\}$ NMR (151 MHz, C_6D_6 , 20 °C): δ = 164.3 (t, J = 9.8 Hz, $\text{py}^{2,6}$), 155.1 (dt, J = 36.7 Hz, J = 30.7 Hz, $\text{C}\equiv\text{CSiMe}_3$), 137.3 (py^4), 125.9 ($\text{C}\equiv\text{CSiMe}_3$), 95.9 (t, J = 2.7 Hz, $\text{py}^{3,5}$), 37.6 (t, J = 2.7 Hz, $\text{N}(\text{CH}_3)$), 30.3 (t, J = 6.0 Hz, $\text{PCH}(\text{CH}_3)_2$), 29.7 (t, J = 7.9 Hz, $\text{PCH}(\text{CH}_3)_2$), 22.1 ($\text{PCH}(\text{CH}_3)_2$), 21.9 (br $\text{P}(\text{CH}_3)_3$), 21.8 ($\text{PCH}(\text{CH}_3)_2$), 21.7 ($\text{PCH}(\text{CH}_3)_2$) 20.3 ($\text{PCH}(\text{CH}_3)_2$), 2.3 ($\text{Si}(\text{CH}_3)_3$ ppm; $^{31}\text{P}\{^1\text{H}\}$ NMR (243 MHz, C_6D_6 , 20 °C): δ = 148.8 (d, J = 40.5 Hz, $\text{PCH}(\text{CH}_3)_2$), 13.4 (t, J = 40.1 Hz, $\text{P}(\text{Me}_3)_3$ ppm.

$[(\text{PNP}^{\text{NMe}})\text{Fe}(\text{Br})(\text{C}\equiv\text{C-Ph})(\text{PMe}_3)]$ (**15b-PMe₃**)

2b (15 mg, 0.025 mmol) was dissolved in 0.7 ml THF d_8 and 25 μl of PMe_3 (1M in THF- d_8) was added and a red solution was formed after stirring for 20 min. After filtration with a syringe filter (polytetrafluoroethylene, 0.2 μm) the red solution was characterized without further purification.

^1H NMR (400 MHz, THF- d_8 , 20 °C): δ = 7.34 (t, J = 8. Hz, 1H, py^4), 6.92 (m, 2H, Ph), 6.83 (m, 2H, Ph), 6.73 (m, 1H, Ph) 6.03 (d, J = 8.1 Hz, 2H, $\text{py}^{3,5}$), 3.36-3.23 (m, 4H, $\text{PCH}(\text{CH}_3)_2$), 3.15 (s, 6H, $\text{N}(\text{CH}_3)$) 1.60 (d, J = 7.7 Hz 9H, $\text{P}(\text{CH}_3)_3$), 1.56-1.33 (m 24 H, $\text{PCH}(\text{CH}_3)_2$) ppm; $^{13}\text{C}\{^1\text{H}\}$ NMR (151 MHz, THF- d_8 , 20 °C): δ = 165.2 (t, J = 9.8 Hz, $\text{py}^{2,6}$), 138.0 (py^4), 131.2 ($\text{C}\equiv\text{CPh}$), 130.7 (Ph), 128.2 (Ph), 126.5 (Ph C^1) 122.7 (Ph), 96.3 (t, J = 3.2 Hz, $\text{py}^{3,5}$), 38.2 (t, J = 3.2 Hz, $\text{N}(\text{CH}_3)$), 30.8 (t, J = 7.0 Hz, $\text{PCH}(\text{CH}_3)_2$), 30.4 (t, J = 7.7 Hz, $\text{PCH}(\text{CH}_3)_2$), 22.2 ($\text{PCH}(\text{CH}_3)_2$), 22.2 (d, J = 23.3 Hz, $\text{P}(\text{CH}_3)_3$), 22.0 ($\text{PCH}(\text{CH}_3)_2$) 21.1 ($\text{PCH}(\text{CH}_3)_2$), 20.1 ($\text{PCH}(\text{CH}_3)_2$) ppm (Fe- $\text{C}\equiv\text{CPh}$ signal not detected); $^{31}\text{P}\{^1\text{H}\}$ NMR (243 MHz, THF- d_8 , 20 °C): δ = 149.5 (d, J = 40.1 Hz, $\text{PCH}(\text{CH}_3)_2$), 15.1 (t, J = 40.1 Hz, $\text{P}(\text{Me}_3)_3$ ppm

$\text{Li}[(\text{PNP}^{\text{NMe}})\text{Fe}(\text{C}\equiv\text{C-TMS})_3]$ (**16a**)

LiHMDS (12.9 mg, 0.077 mmol) was dissolved in 0.4 ml THF- d_8 , treated with 12 μl TMS-acetylene (0.086 mmol) and stirred for 15 min. The solution was subsequently added to a

suspension of **Fe20-Br** (15 mg, 0.026 mmol) in 0.3 ml THF- d^8 creating an orange solution. The solution was filtered with a syringe filter (polytetrafluoroethylene, 0.2 μ m) into an NMR-tube and characterized without further purification.

^1H NMR (400 MHz, THF- d^8 , 20 °C): δ = 7.20 (tt, J = 8.1 Hz, J = 1.2 Hz, 1H, py^4), 5.87 (d, J = 8.2 Hz, 2H, $\text{py}^{3,5}$), 3.29 (br, 4H, $\text{PCH}(\text{CH}_3)_2$), 3.07 (t, J = 1.5 Hz, 6H, $\text{N}(\text{CH}_3)$), 1.58 (br, 24 H, $\text{PCH}(\text{CH}_3)_2$), -0.03 (s, 9H, $\text{Si}(\text{CH}_3)_3$), -0.16 (s, 18H, $\text{Si}(\text{CH}_3)_3$). $^{13}\text{C}\{^1\text{H}\}$ NMR (101 MHz, THF- d^8 , 20 °C): δ = 164.0 (t, J = 10.4 Hz, $\text{py}^{2,6}$), 136.1 (py^4), 125.8 ($\text{C}\equiv\text{CTMS}$), 125.1 ($\text{C}\equiv\text{CTMS}$), 96.3 (t, J = 3.3 Hz, $\text{py}^{3,5}$), 37.2 (t, J = 3.0 Hz, $\text{N}(\text{CH}_3)$), 32.4 (br, $\text{PCH}(\text{CH}_3)_2$), 20.8 (t, J = 2.2 Hz, $\text{PCH}(\text{CH}_3)_2$), 2.6 ($\text{Si}(\text{CH}_3)_3$), 2.4 ($\text{Si}(\text{CH}_3)_3$) ppm, (Fe- $\text{C}\equiv\text{CTMS}$ signals not detected); $^{31}\text{P}\{^1\text{H}\}$ NMR (162 MHz, THF- d^8 , 20 °C): δ = 147.2 ppm

Li[(PNP^{NMe})Fe($\text{C}\equiv\text{C}$ -Ph)₃] (**16b**)

This complex was analogously prepared to **16a** using 15 mg (0.026 mmol) **Fe20-Br**, 12.9 mg LiHMDS (0.077 mmol) and 8.7 μ l phenylacetylene (0.079 μ l) creating a red-orange solution that was filtered with a syringe filter (polytetrafluoroethylene, 0.2 μ m) into an NMR-tube and characterized without further purification.

^1H NMR (400 MHz, THF- d^8 , 20 °C): δ = 7.23 (tt, J = 8.1 Hz, J = 1.2 Hz, 1H, py^4), 7.07 (m, 2H, Ph), 7.02 – 6.90 (m, Ph, 10H), 6.81 (vt, 1H, Ph), 6.76 (vt, 2H, Ph), 5.92 (d, J = 8.1 Hz, 2H, $\text{py}^{3,5}$), 3.24 (m, 4H, $\text{PCH}(\text{CH}_3)_2$), 3.12 (t, J = 1.4 Hz, 6H, $\text{N}(\text{CH}_3)$), 1.66 (app q, 12 H, $\text{PCH}(\text{CH}_3)_2$), 1.58 (app q, 12 H, $\text{PCH}(\text{CH}_3)_2$). $^{13}\text{C}\{^1\text{H}\}$ NMR (101 MHz, THF- d^8 , 20 °C): δ = 164.3 (t, J = 10.3 Hz, $\text{py}^{2,6}$), 136.0 (py^4), 132.2 ($\text{C}\equiv\text{CPh}$), 132.0 ($\text{C}\equiv\text{CPh}$); 131.2 (Ph), 130.8 (Ph), 128.3 (Ph), 128.1 (Ph), 123.1 (Ph), 122.7 (Ph), 121.0 (Ph), 120.9 (Ph), 96.1 (t, J = 3.1 Hz, $\text{py}^{3,5}$), 36.7 (t, J = 2.9 Hz, $\text{N}(\text{CH}_3)$), 31.6 (t, J = 7.6 Hz, $\text{PCH}(\text{CH}_3)_2$), 21.2 ($\text{PCH}(\text{CH}_3)_2$), 20.5 (t, J = 2.4 Hz, $\text{PCH}(\text{CH}_3)_2$) ppm, (Fe- $\text{C}\equiv\text{CPh}$ signals not detected); $^{31}\text{P}\{^1\text{H}\}$ NMR (162 MHz, THF- d^8 , 20 °C): δ = 148.2 ppm

4.5 Synthesis of Fe PNP Acetylide Hydride Complexes

cis-[Fe(PNP^{Me})(H)₂(N₂)] (**11**)

To a solution of **Fe-20Br** (15 mg, 0.026 mmol) in 0.8 ml d₈-THF was added Na[AlH₄] (3.0 mg, 0.056 mmol) resulting in a color change from yellow to orange. While stirring the reaction mixture, a stock solution of H₂O (4.0 M in d₈-THF, 50 μL, 0.2 mmol) was added resulting in severe gas evolution. After stirring for 10 minutes, the dark orange suspension was filtered using a syringe filter (polytetrafluoroethylene, 0.2 μm) and transferred into a Young-NMR tube. The dark orange solution was subjected to three consecutive freeze-pump-thaw cycles with subsequent backflushing with 1 bar of N₂ gas, until showing full conversion and affording a light orange solution of **11**.

¹H NMR (250 MHz, d₈-THF, 20 °C): δ = 7.19 (t, *J* = 8.2 Hz, 1H, py⁴), 5.90 (d, *J* = 8.1 Hz, 2H, py^{3,5}), 3.06 (s, 6H, N(CH₃)), 2.64 (m, 2H, PCH(CH₃)₂), 2.30 (m, 2H, PCH(CH₃)₂), 1.47 (app q, 6 H, PCH(CH₃)₂), 1.29 (m, 6 H, PCH(CH₃)₂), 1.17 (m, 6 H, PCH(CH₃)₂), 0.70 (app q, 6 H, PCH(CH₃)₂) -15.71 (td, *J*_{HP}=61.8 Hz, *J*_{HH}=19.2 Hz 1H, FeH), -16.56 (td, *J*_{HP}=48.8 Hz, *J*_{HH}=18.7 Hz 1H, FeH) ppm; ³¹P NMR (101 MHz, d₈-THF, 20 °C): δ = 184.9 ppm

[Fe(PNP^{Me})(H)₂(^{*t*}BuNC)] (**12 a-b**)

To a solution of 30 mg **Fe20-Br** (0.051 mmol) in THF is added *tert*-Butyl isocyanide (51 μl, 1 M solution in THF, 0.051 mmol, 1 eq) affording a green solution. Immediately afterwards Na[HBET₃] (107 μl, 1.05 eq, 1 M solution in THF) was added whereupon the color of the solution changed to dark brown. The solution was stirred for 1 h at r.t. and subsequently filtered with a syringe filter (polytetrafluoroethylene, 0.2 μm). After evaporation of the solvent, the dark brown residue was carefully washed with cold *n*-pentane affording **12** as light orange solid. (18 mg, 0.035 mmol, 70 %) in a 4:1 ratio of the corresponding *trans* (**12b**) and *cis* (**12a**) dihydride complexes.

Spectroscopic analysis of **12b**

¹H NMR (600 MHz, C₆D₆, 20 °C): δ = 6.92 (t, *J* = 8.1 Hz, 1H, py⁴), 5.47 (d, *J* = 8.0 Hz, 2H, py^{3,5}), 2.55 (s, 6H, N(CH₃)), 2.29 (m, 4H, PCH(CH₃)₂), 1.55 (app q, 12 H, PCH(CH₃)₂), 1.29 (app q, 12 H, PCH(CH₃)₂), 1.14 (s, 9 H, CNC(CH₃)₃), -9.10 (t, *J* = 43.7 Hz, 2 H, Fe-H) ppm;

$^{13}\text{C}\{^1\text{H}\}$ NMR (151 MHz, C_6D_6 , 20 °C): δ = 196.5 (t, J = 26.0 Hz, $\text{CNC}(\text{CH}_3)_3$), 162.4 (t, J = 11.9 Hz, $\text{py}^{2,6}$), 133.6 (py^4), 93.7 (t, J = 4.1 Hz, $\text{py}^{3,5}$), 54.3 (s, $\text{CNC}(\text{CH}_3)_3$), 32.0 (t, (J = 9.9 Hz, $\text{PCH}(\text{CH}_3)_2$), 31.9 (t, J = 2.4 Hz, $\text{N}(\text{CH}_3)$), 31.4 ($\text{CNC}(\text{CH}_3)_3$), 19.7 (t, J = 5.4 Hz, $\text{PCH}(\text{CH}_3)_2$), 19.1 ($\text{PCH}(\text{CH}_3)_2$) ppm; $^{31}\text{P}\{^1\text{H}\}$ NMR (243 MHz, C_6D_6 , 20 °C): δ = 188.0 ppm, 2D $\{^{15}\text{N}-^1\text{H}\}$ HMBC NMR (60.8 MHz, C_6D_6 , 20 °C): δ = 190.3 ($\text{CNC}(\text{CH}_3)_3$) ppm. IR (ATR, cm^{-1}): 2040 ($\nu_{\text{N}=\text{C}}$), HRMS (ESI⁺, $\text{CH}_3\text{CN}/\text{MeOH}$ + 1% H_2O): m/z calcd for $\text{C}_{24}\text{H}_{48}\text{FeN}_4\text{P}_2$ $[\text{M}]^+$ 510.2704 found 510.2683.

Spectroscopic analysis of **12a**

^1H NMR (600 MHz, C_6D_6 , 20 °C): δ = 7.26 (t, J = 8.1 Hz, 1H, py^4), 5.57 (d, J = 8.0 Hz, 2H, $\text{py}^{3,5}$), 2.61 (s, 6H, $\text{N}(\text{CH}_3)$), superimposed by **12a** (m, 2H, $\text{PCH}(\text{CH}_3)_2$), 2.04 (m, 2H, $\text{PCH}(\text{CH}_3)_2$), 1.59 (m, partly superimposed by **12a**, 6 H, $\text{PCH}(\text{CH}_3)_2$), 1.43 (app q, 12 H, $\text{PCH}(\text{CH}_3)_2$), 1.37 (app q 12 H, $\text{PCH}(\text{CH}_3)_2$), 1.22 (s, 9 H, $\text{CNC}(\text{CH}_3)_3$), 0.92 (app q 12 H, $\text{PCH}(\text{CH}_3)_2$), -14.27 (br, 2 H, Fe- H) ppm; $^{13}\text{C}\{^1\text{H}\}$ NMR (151 MHz, C_6D_6 , 20 °C): δ = 163.5 (t, J = 10.9 Hz, $\text{py}^{2,6}$), 133.0 (py^4), 93.9 (t, J = 3.4 Hz, $\text{py}^{3,5}$), 54.1 (s, $\text{CNC}(\text{CH}_3)_3$), 32.6 (t, J = 7.2 Hz, $\text{PCH}(\text{CH}_3)_2$), 32.2 (app t, $\text{N}(\text{CH}_3)$), 31.7 ($\text{CNC}(\text{CH}_3)_3$), 28.5 (t, J = 8.4 Hz, $\text{PCH}(\text{CH}_3)_2$), 20.5 (t, J = 6.0 Hz, $\text{PCH}(\text{CH}_3)_2$), 20.0 (t, J = 5.6 Hz, $\text{PCH}(\text{CH}_3)_2$), 19.9 ($\text{PCH}(\text{CH}_3)_2$), 18.5 ($\text{PCH}(\text{CH}_3)_2$) ppm; $^{31}\text{P}\{^1\text{H}\}$ NMR (243 MHz, C_6D_6 , 20 °C): δ = 192.6 ppm

cis-[Fe(PNP^{Me})(H)₂(py)] (**14**)

15 mg **Fe20-Br** (0.026 mmol) was suspended in 0.8 ml d_8 -THF and 3.8 mg NaAlH_4 (0.07 mmol) was added in one portion affording an orange suspension. The suspension was stirred for 15 minutes and the filtered with a syringe filter (polytetrafluoroethylene, 0.2 μm) affording an orange solution. To the solution 50 μl H_2O (4M in d_8 -THF, 0.2 mmol) was added leading to vigorous gas evolution. The dark orange solution was stirred for 15 minutes and subsequently filtered with a syringe filter. (polytetrafluoroethylene, 0.2 μm) To the dark orange solution was then added 2.1 μl pyridine (0.026 mmol) leading to a rapid darkening of the solution. After stirring for 10 minutes a dark blue solution was obtained and transferred into an NMR tube and identified as a 75 %/25 % mixture of **14** and complex **Fe21-NMe**.

^1H NMR (250 MHz, d_8 -THF, 20 °C): δ = 9.19 (d, J = 5.8 Hz, 1H, pyridine), 7.55 (t, J = 7.9 Hz, 1H, pyridine), 7.08 (t, J = 8.2 Hz, 1H, py^4), 6.55 (br, 1H, pyridine), 6.35 (t, J = 6.7 Hz, 1H,

pyridine), 6.14 (t, $J=6.7$ Hz, 1H, pyridine), 5.72 (d, $J=8.0$ Hz, 2H, $\text{py}^{3,5}$), 2.97 (s, 6H, $\text{N}(\text{CH}_3)$), 2.60-2.31 (m, 4H, $\text{PCH}(\text{CH}_3)_2$), 1.30 (app q 6 H, $\text{PCH}(\text{CH}_3)_2$), 0.96 (m, 6 H, $\text{PCH}(\text{CH}_3)_2$ superimposed by polyhydride complex), 0.48 (app q, 6 H, $\text{PCH}(\text{CH}_3)_2$), 0.30 (app q, 6 H, $\text{PCH}(\text{CH}_3)_2$) -16.91 (td, $J_{\text{PH}} = 50.7$ Hz, $J_{\text{HH}} = 20.6$ Hz 1H, FeH), -23.65 (td, $J_{\text{PH}} = 66.7$ Hz, $J_{\text{HH}} = 20.6$ Hz 1H, FeH) ppm; $^{13}\text{C}\{^1\text{H}\}$ NMR (101 MHz, d_8 -THF, 20 °C): $\delta=166.2$ (pyridine), 164.4 (br, $\text{py}^{2,6}$), 153.5 (pyridine), 130.3 (py^4), 129.0 (pyridine), 122.9 (pyridine), 122.3 (pyridine), 94.2 (t, $J=3.2$ Hz, $\text{py}^{3,5}$), 34.3-34.0 (m, $\text{N}(\text{CH}_3)+\text{PCH}(\text{CH}_3)_2$), 32.7 (app t, $\text{PCH}(\text{CH}_3)_2$), 20.4 ($\text{PCH}(\text{CH}_3)_2$), 19.9 ($\text{PCH}(\text{CH}_3)_2$), 19.1 ($\text{PCH}(\text{CH}_3)_2$), 18.8 ($\text{PCH}(\text{CH}_3)_2$) ppm; $^{31}\text{P}\{^1\text{H}\}$ NMR (101 MHz, d_8 -THF, 20 °C): $\delta = 181.7$

cis-[Fe(PNP^{Me})(H)₂(PPh₃)] (**17**)

15 mg **Fe20-Br** (0.026 mmol) was dissolved in 1.5 ml THF and 3.8 mg NaAlH_4 (0.07 mmol) was added in one portion affording an orange suspension. The suspension was stirred for 15 minutes and the filtered with a syringe filter (polytetrafluoroethylene, 0.2 μm) affording an orange solution. To the solution 100 μl H_2O (2M in THF, 0.2 mmol) was added leading to vigorous gas evolution. The dark orange was stirred for 15 minutes and the filtered with a syringe filter. (polytetrafluoroethylene, 0.2 μm) To the dark orange solution was the added 26 μl triphenylphosphine (1 mol in THF, 0.026 mmol) and the solution was stirred for 1 h forming a red solution. The solvent was evaporated in vacuo affording **17** as dark red solid. (17 mg, 0.026 mmol, 98 %)

^1H NMR (400 MHz, C_6D_6 , 20 °C): $\delta=7.64$ (m, 6H, Ph), 7.26 (t, $J=8.1$ Hz, 1H, py^4), 7.01 (m, 9H, Ph), 5.66 (d, $J=8.1$ Hz, 2H, $\text{py}^{3,5}$), 2.59 (s, 6H, $\text{N}(\text{CH}_3)$), 2.30 (m, 2H, $\text{PCH}(\text{CH}_3)_2$), 1.98 (m, 2H, $\text{PCH}(\text{CH}_3)_2$), 1.33 (app q 6 H, $\text{PCH}(\text{CH}_3)_2$), 1.12 (app q, 6 H, $\text{PCH}(\text{CH}_3)_2$), 1.00 (m, 6 H, $\text{PCH}(\text{CH}_3)_2$), 0.81 (app q, 6 H, $\text{PCH}(\text{CH}_3)_2$) -13.02 (br, 1H, FeH), -17.49 (br, 1H, FeH) ppm; $^{13}\text{C}\{^1\text{H}\}$ NMR (101 MHz, C_6D_6 , 20 °C): $\delta=164.4$ (t, $J=10.5$ Hz, $\text{py}^{2,6}$), 144.0 (d, $J=20.33$ Hz, Ph^1), 135.1 (d, $J=10.4$ Hz, Ph), 134.2 (d, $J=19.8$ Hz, Ph), 131.4 (py^4), 126.8 (d, $J=7.2$ Hz, Ph), 94.7 (t, $J=2.9$ Hz, $\text{py}^{3,5}$), 34.0 (t, $J=3.6$ Hz, $\text{N}(\text{CH}_3)$), 30.2 (m, $\text{PCH}(\text{CH}_3)_2$) 28.1 (m, $\text{PCH}(\text{CH}_3)_2$), 24.4 (t, $J=5.5$ Hz, $\text{PCH}(\text{CH}_3)_2$), 19.9 ($\text{PCH}(\text{CH}_3)_2$), 19.4 ($\text{PCH}(\text{CH}_3)_2$), 18.1 ($\text{PCH}(\text{CH}_3)_2$) ppm; $^{31}\text{P}\{^1\text{H}\}$ NMR (101 MHz, C_6D_6 , 20 °C): $\delta = 182.7$ (d, $J=22.9$ Hz, $\text{PCH}(\text{CH}_3)_2$), 65.1 (t, $J=23.0$ Hz, PPh_3) ppm.

[(PNP^{NMe})Fe(Br)(C \equiv C-TMS)(CO)] (**15a-CO**)

A solution of **15a** (50 mg, 0.083 mmol) in 3 ml CH₂Cl₂ was stirred for 20 min under a CO atmosphere (1 bar) upon which the color of the solution turned from yellow to orange. The solvent was evaporated under vacuum and the orange solid was extracted with 5 ml benzene. After evaporation of the solvent the orange solid was washed twice with 1 mL of cold *n*-pentane affording an orange solid. (45 mg, 0.071 mmol, 86 %)

¹H NMR (600 MHz, C₆D₆, 20 °C): δ = 6.97 (t, *J* = 8.2 Hz, 1H, py⁴), 5.62 (d, *J* = 8.2 Hz, 2H, py^{3,5}), 3.06 (m, 4H, PCH(CH₃)₂), 2.54 (s, 6H, N(CH₃)), 1.56 (m 24 H, PCH(CH₃)₂), 0.12 (s 9H, Si(CH₃)₃) ppm; ¹³C{¹H} NMR (151 MHz, C₆D₆, 20 °C): δ = 222.7 (t, *J* = 22.2 Hz, CO), 162.5 (t, *J* = 10.3 Hz, py^{2,6}), 139.8 (t, *J* = 30.9 Hz, C≡CSiMe₃), 138.8 (py⁴), 128.3 (C≡CSiMe₃), 98.1 (t, *J* = 3.4 Hz, py^{3,5}), 36.9 (t, *J* = 3.1 Hz, N(CH₃)), 31.0 (t, *J* = 9.9 Hz, PCH(CH₃)₂), 30.4 (vt, PCH(CH₃)₂), 22.2 (PCH(CH₃)₂), 21.0 (PCH(CH₃)₂), 20.2 (PCH(CH₃)₂), 19.3 (PCH(CH₃)₂), 1.62 (Si(CH₃)₃) ppm; ³¹P{¹H} NMR (243 MHz, C₆D₆, 20 °C): δ = 148.4 ppm. IR (ATR, cm⁻¹): 2009 (ν_{C≡C}), 1951 (ν_{CO})

[(PNP^{NMe})Fe(Br)(C≡C-Ph)(CO)] (**15b-CO**)

This complex was analogously prepared to **15a-CO** using **15b** (50 mg, 0.083 mmol), yielding **15b-CO** as orange solid. (47 mg, 0.076 mmol, 92 %)

¹H NMR (600 MHz, CD₂Cl₂, 20 °C): δ = 7.59 (t, *J* = 8.2 Hz, 1H, py⁴), 7.06 (m, 2H, Ph), 6.93 (m, 3H, Ph), 6.21 (d, *J* = 8.2 Hz, 2H, py^{3,5}), 3.27 (m, 2 H, PCH(CH₃)₂), 3.21 (s, 6H, N(CH₃)), 3.13 (2 H, PCH(CH₃)₂), 1.63 (m 12H, PCH(CH₃)₂), 1.52 (app. q 6 H, PCH(CH₃)₂), 1.41 (app. q 6 H, PCH(CH₃)₂) ppm; ¹³C{¹H} NMR (151 MHz, CD₂Cl₂, 20 °C): δ = 222.2 (t, *J* = 22.1 Hz, CO), 162.5 (t, *J* = 10.2 Hz, py^{2,6}), 139.4 (py⁴), 130.4 (Ph), 129.1 (C≡CPh), 127.9 (Ph), 123.9 (Ph), 121.4 (Ph C¹), 112.0 (t, *J* = 34.3 Hz, C≡CPh), 98.1 (t, *J* = 3.5 Hz, py^{3,5}), 37.2 (t, *J* = 2.9 Hz, N(CH₃)), 31.3 (t, *J* = 9.8 Hz, PCH(CH₃)₂), 29.6 (t, *J* = 12.1 Hz, PCH(CH₃)₂), 21.8 (PCH(CH₃)₂), 19.9 (PCH(CH₃)₂), 19.8 (PCH(CH₃)₂), 18.9 (t, 2.53 Hz, PCH(CH₃)₂) ppm; ³¹P{¹H} NMR (243 MHz, CD₂Cl₂, 20 °C): δ = 147.9 ppm; IR (ATR, cm⁻¹): 2083 (ν_{C≡C}), 1941 (ν_{CO}).

[(PNP^{NMe})Fe(Br)(C≡C-TMS)(^tBuNC)] (**15a-^tBuNC**)

A solution of 15 mg (0.025 mmol) **15a** in 2 ml THF was treated with *tert*-Butyl isocyanide (25 μ l, 1 M solution in THF), whereupon the solution immediately turned orange. The solution was stirred for 15 min and the solvent was removed under vacuum. The orange residue was washed with cold *n*-pentane yielding **4a** as orange solid. (15 mg, 0.022 mmol, 88 %)

^1H NMR (600 MHz, C_6D_6 , 20 $^\circ\text{C}$): δ = 6.96 (t, J = 8.2 Hz, 1H, py^4), 5.65 (d, J = 8.1 Hz, 2H, $\text{py}^{3,5}$), 3.22 (m, 4H, $\text{PCH}(\text{CH}_3)_2$), 2.67 (s, 6H, $\text{N}(\text{CH}_3)$), 1.72-1.61 (m 24 H, $\text{PCH}(\text{CH}_3)_2$), 1.22 (s, 9H, $\text{CNC}(\text{CH}_3)_3$), 0.17 (s 9H, $\text{Si}(\text{CH}_3)_3$) ppm; $^{13}\text{C}\{^1\text{H}\}$ NMR (151 MHz, C_6D_6 , 20 $^\circ\text{C}$): δ = 173.6 (t, 25.7 Hz, $\text{CNC}(\text{CH}_3)_3$), 163.6 (t, J = 10.5 Hz, $\text{py}^{2,6}$), 151.4 (t, J = 32.0 Hz, $\text{C}\equiv\text{CSiMe}_3$), 137.5 (py^4), 125.9 ($\text{C}\equiv\text{CSiMe}_3$), 97.3 (t, J = 3.3 Hz, $\text{py}^{3,5}$), 55.9 (s, $\text{CNC}(\text{CH}_3)_3$), 36.8 (t, J = 2.7 Hz, $\text{N}(\text{CH}_3)$), 31.7 (t, J = 8.3 Hz, $\text{PCH}(\text{CH}_3)_2$), 30.7 ($\text{CNC}(\text{CH}_3)_3$), 30.6 (m, $\text{PCH}(\text{CH}_3)_2$), 23.0 ($\text{PCH}(\text{CH}_3)_2$), 21.4 ($\text{PCH}(\text{CH}_3)_2$), 20.5 ($\text{PCH}(\text{CH}_3)_2$), 19.4 (t, J = 2.5 Hz, $\text{PCH}(\text{CH}_3)_2$), 2.2 ($\text{Si}(\text{CH}_3)_3$) ppm; $^{31}\text{P}\{^1\text{H}\}$ NMR (243 MHz, C_6D_6 , 20 $^\circ\text{C}$): δ = 147.3 ppm; 2D $\{^{15}\text{N}-^1\text{H}\}$ HMBC NMR (60.8 MHz, C_6D_6 , 20 $^\circ\text{C}$): δ = 200.3 ($\text{CNC}(\text{CH}_3)_3$) ppm. IR (ATR, cm^{-1}): 2105 ($\nu_{\text{N}=\text{C}}$), 1986 ($\nu_{\text{C}=\text{C}}$)

$[(\text{PNP}^{\text{NMe}})\text{Fe}(\text{Br})(\text{C}\equiv\text{C-Ph})(^t\text{BuNC})]$ (**15b- $^t\text{BuNC}$**)

This complex was analogously prepared to **15a- $^t\text{BuNC}$** using **15b** (15 mg, 0.025 mmol) and *tert*-Butyl isocyanide (25 μ l, 1 M solution in THF), yielding **15b- $^t\text{BuNC}$** as red-orange solid. (14 mg, 0.020 mmol, 81 %)

^1H NMR (600 MHz, C_6D_6 , 20 $^\circ\text{C}$): δ = 7.21 (m, 2H, Ph), 7.06 (m, 3H, Ph), 6.85 (t, J = 7.4 Hz, 1H, py^4), 5.73 (d, J = 8.2 Hz, 2H, $\text{py}^{3,5}$), 3.29 (m, 2 H, $\text{PCH}(\text{CH}_3)_2$), 2.90 (m, 2 H, $\text{PCH}(\text{CH}_3)_2$), 2.67 (s, 6H, $\text{N}(\text{CH}_3)$), 1.72 (app. q 6 H, $\text{PCH}(\text{CH}_3)_2$), 1.64 (app. q 6 H, $\text{PCH}(\text{CH}_3)_2$), 1.60 (app. q 6 H, $\text{PCH}(\text{CH}_3)_2$), 1.52 (app. q 6 H, $\text{PCH}(\text{CH}_3)_2$), 1.24 (s, 9 H, $\text{CNC}(\text{CH}_3)_3$) ppm; $^{13}\text{C}\{^1\text{H}\}$ NMR (151 MHz, C_6D_6 , 20 $^\circ\text{C}$): δ = 173.8 (t, J = 22.1 Hz, $\text{CNC}(\text{CH}_3)_3$), 163.8 (t, J = 10.5 Hz, $\text{py}^{2,6}$), 137.6 (py^4), 130.8 (Ph), 128.0 (Ph), 125.9 ($\text{C}\equiv\text{CPh}$), 124.0 (t, J = 32.8 Hz, $\text{C}\equiv\text{CPh}$), 123.5 (Ph C^1), 123.0 (Ph), 97.2 (t, J = 3.3 Hz, $\text{py}^{3,5}$), 56.0 ($\text{CNC}(\text{CH}_3)_3$), 36.4 (t, J = 2.9 Hz, $\text{N}(\text{CH}_3)$), 32.5 (t, J = 8.2 Hz, $\text{PCH}(\text{CH}_3)_2$), 30.7 ($\text{CNC}(\text{CH}_3)_3$), 30.3 (m, $\text{PCH}(\text{CH}_3)_2$), 22.9 ($\text{PCH}(\text{CH}_3)_2$), 20.5 ($\text{PCH}(\text{CH}_3)_2$), 20.4 ($\text{PCH}(\text{CH}_3)_2$), 19.2 (t, 3.4 Hz, $\text{PCH}(\text{CH}_3)_2$) ppm; $^{31}\text{P}\{^1\text{H}\}$ NMR (243 MHz, C_6D_6 , 20 $^\circ\text{C}$):

$\delta = 147.9$ ppm; $2D\{^{15}\text{N}-^1\text{H}\}$ HMBC NMR (60.8 MHz, C_6D_6 , 20 °C): $\delta = 200.9$ ($\text{CNC}(\text{CH}_3)_3$) ppm. IR (ATR, cm^{-1}): 2110 ($\nu_{\text{N}=\text{C}}$), 2058 ($\nu_{\text{C}=\text{C}}$)

$[(\text{PNP}^{\text{NMe}})\text{Fe}(\text{Br})(\text{C}\equiv\text{C}-\text{TMS})(\text{P}(\text{OMe})_3)]$ (**15a-P(OMe)₃**)

15a (10 mg, 0.017 mmol) was dissolved in 1 ml THF and 2.5 μl of $\text{P}(\text{OMe})_3$ (0.019 mmol, 1.1 eq) was added affording a red solution. The solvent was removed under reduced pressure affording **15a-P(OMe)₃** as red solid. (11 mg, 0.016 mmol, 90 %)

^1H NMR (600 MHz, C_6D_6 , 20 °C): $\delta = 7.02$ (m, 1H, py^4), 5.68 (d, $J = 8.1$ Hz, 2H, $\text{py}^{3,5}$), 3.56 (d, $J = 9.5$ Hz, 9H, $\text{P}(\text{OCH}_3)_3$), 3.44 (m, 2H, $\text{PCH}(\text{CH}_3)_2$), 3.25 (m, 2H, $\text{PCH}(\text{CH}_3)_2$) (superimposed by $\text{P}(\text{OMe})_3$), 2.68 (t, $J = 1.54$ Hz, 6H, $\text{N}(\text{CH}_3)$), 1.66 (app q, 6 H, $\text{PCH}(\text{CH}_3)_2$), 1.54 (m 12 H, $\text{PCH}(\text{CH}_3)_2$), 1.43 (app q, 6 H, $\text{PCH}(\text{CH}_3)_2$) 0.15 (s 9H, $\text{Si}(\text{CH}_3)_3$) ppm; $^{13}\text{C}\{^1\text{H}\}$ NMR (151 MHz C_6D_6 , 20 °C): $\delta = 163.6$ (t, $J = 10.0$ Hz, $\text{py}^{2,6}$), 150.3 (dt, $J = 47.9$ Hz, $J = 29.1$ Hz, $\text{C}\equiv\text{CSiMe}_3$), 137.7 (py^4), 125.9 ($\text{C}\equiv\text{CSiMe}_3$), 96.4 (t, $J = 3.4$ Hz, $\text{py}^{3,5}$), 54.2 (d, $J = 10.9$ Hz, $\text{P}(\text{OCH}_3)_3$), 37.7 (t, $J = 3.4$ Hz, $\text{N}(\text{CH}_3)$), 30.2 (vt, $\text{PCH}(\text{CH}_3)_2$), 29.8 (vt, $\text{PCH}(\text{CH}_3)_2$), 22.0 ($\text{PCH}(\text{CH}_3)_2$), 21.9 ($\text{PCH}(\text{CH}_3)_2$), 21.3 (t, $J = 3.0$ Hz, $\text{PCH}(\text{CH}_3)_2$), 20.6 ($\text{PCH}(\text{CH}_3)_2$), 2.3 ($\text{Si}(\text{CH}_3)_3$) ppm; $^{31}\text{P}\{^1\text{H}\}$ NMR (243 MHz, C_6D_6 , 20 °C): $\delta = 171.0$ (t, $J = 71.3$ Hz, $\text{P}(\text{OMe})_3$), 151.7 (d, $J = 71.6$ Hz, $\text{PCH}(\text{CH}_3)_2$), ppm. IR (ATR, cm^{-1}): 1983 ($\nu_{\text{C}=\text{C}}$).

$[(\text{PNP}^{\text{NMe}})\text{Fe}(\text{Br})(\text{C}\equiv\text{C}-\text{Ph})(\text{P}(\text{OMe})_3)]$ (**15b-P(OMe)₃**)

15b (10 mg, 0.017 mmol) was dissolved in 1 ml THF and 2.5 μl of $\text{P}(\text{OMe})_3$ (0.019 mmol, 1.1 eq) was added affording a red solution. The solvent was removed under reduced pressure affording **15b-P(OMe)₃** as red solid. (11 mg, 0.016 mmol, 90 %)

^1H NMR (600 MHz, C_6D_6 , 20 °C): $\delta = 7.09$ (m, 4H, py^4 , Ph), 6.88 (m, 2H, Ph), 5.74 (d, $J = 8.0$ Hz, 2H, $\text{py}^{3,5}$), 3.58 (d, $J = 9.28$ Hz, 9H, $\text{P}(\text{OCH}_3)_3$), 3.30 (4H, $\text{PCH}(\text{CH}_3)_2$) (superimposed by $\text{P}(\text{OMe})_3$), assigned by HSQC), 2.68 (s, 6H, $\text{N}(\text{CH}_3)$), 1.67 (app. q 6 H, $\text{PCH}(\text{CH}_3)_2$), 1.55 (app. q 6 H, $\text{PCH}(\text{CH}_3)_2$), 1.50 (app. q 6 H, $\text{PCH}(\text{CH}_3)_2$), 1.34 (s, 9 H, $\text{CNC}(\text{CH}_3)_3$) ppm; $^{13}\text{C}\{^1\text{H}\}$ NMR (151 MHz, C_6D_6 , 20 °C): $\delta = 163.8$ (t, $J = 10.0$ Hz, $\text{py}^{2,6}$), 151.5 (br, $\text{C}\equiv\text{CPh}$), 137.8 (py^4), 131.1 ($\text{C}\equiv\text{CPh}$), 130.7 (Ph), 128.6 (Ph), 127.6 (Ph C^1), 122.8 (Ph), 96.4 ($\text{py}^{3,5}$), 54.1 (d, $J = 10.7$ Hz, $\text{P}(\text{OCH}_3)_3$), 37.4 ($\text{N}(\text{CH}_3)$), 30.3 (vt, $\text{PCH}(\text{CH}_3)_2$), 30.0 (vt, $\text{PCH}(\text{CH}_3)_2$), 21.9 ($\text{PCH}(\text{CH}_3)_2$), 21.3 ($\text{PCH}(\text{CH}_3)_2$), 20.9 ($\text{PCH}(\text{CH}_3)_2$), 20.2 ($\text{PCH}(\text{CH}_3)_2$) ppm; $^{31}\text{P}\{^1\text{H}\}$ NMR (243 MHz, C_6D_6 , 20 °C): $\delta = 171.0$

(t, $J = 71.6$ Hz, $P(\text{OMe}_3)_3$ 151.3 (d, $J = 71.7$ Hz, $P\text{CH}(\text{CH}_3)_2$), ppm. IR (ATR, cm^{-1}): 2058 ($\nu_{\text{C}\equiv\text{C}}$)

$[(\text{PNP}^{\text{NMe}})\text{Fe}(\text{H})(\text{C}\equiv\text{C-TMS})(\text{CO})]$ (**18a**)

15a-CO (17 mg, 1 eq, 0.027 mmol) were dissolved in 1 ml THF and treated with $\text{Na}[\text{AlH}_4]$ (1.6 mg, 0.03 mmol, 1.1 equiv) creating an orange suspension. The suspension was stirred for 15 min and then treated with H_2O (22 μl , 3M in THF) leading to vigorous gas evolution. The orange solution was treated with 1 ml of benzene and filtered with a syringe filter (polytetrafluoroethylene, 0.2 μm). After evaporation of the solvent the orange residue was washed with 0.2 ml of cold *n*-pentane (-30 °C) and dried in vacuo, affording **18a** as orange solid, (13 mg, 0.023 mmol, 85 %)

^1H NMR (600 MHz, C_6D_6 , 20 °C): $\delta = 6.83$ (t, $J = 8.1$ Hz, 1H, py^4), 5.40 (d, $J = 8.1$ Hz, 2H, $\text{py}^{3,5}$), 2.41 (s, 6H, $\text{N}(\text{CH}_3)$), 2.37 (m, 2H, $\text{PCH}(\text{CH}_3)_2$), 1.94 (m, 2H, $\text{PCH}(\text{CH}_3)_2$), 1.89 (app. q 6 H, $\text{PCH}(\text{CH}_3)_2$), 1.77 (app. q 6 H, $\text{PCH}(\text{CH}_3)_2$), 1.23 (app. q 6 H, $\text{PCH}(\text{CH}_3)_2$), 0.83 (app. q 6 H, $\text{PCH}(\text{CH}_3)_2$), 0.30 (s, 9H, $\text{Si}(\text{CH}_3)_3$), -12.37 (t, $J = 49.9$ Hz, Fe-*H*) ppm; $^{13}\text{C}\{^1\text{H}\}$ NMR (151 MHz, C_6D_6 , 20 °C): $\delta = 222.2$ (t, $J = 25.0$ Hz, CO), 161.6 (t, $J = 10.9$ Hz, $\text{py}^{2,6}$), 156.8 (t, $J = 20.9$ Hz, $\text{C}\equiv\text{CSiMe}_3$), 137.0 (py^4), 125.9 ($\text{C}\equiv\text{CSiMe}_3$), 95.7 (t, $J = 3.2$ Hz, $\text{py}^{3,5}$), 34.2 (t, $J = 10.2$ Hz, $\text{PCH}(\text{CH}_3)_2$), 32.9 (vt, $\text{N}(\text{CH}_3)$), 32.4 (t, $J = 13.1$ Hz, $\text{PCH}(\text{CH}_3)_2$), 21.1 ($\text{PCH}(\text{CH}_3)_2$), 20.3 (t, $J = 4.9$ Hz, $\text{PCH}(\text{CH}_3)_2$), 18.3 ($\text{PCH}(\text{CH}_3)_2$), 17.8 (t, $J = 4.6$ Hz, $\text{PCH}(\text{CH}_3)_2$), 2.4 ($\text{Si}(\text{CH}_3)_3$) ppm; $^{31}\text{P}\{^1\text{H}\}$ NMR (243 MHz, C_6D_6 , 20 °C): $\delta = 175.0$ (d, $J = 13$ Hz) ppm, IR (ATR, cm^{-1}): 1998 ($\nu_{\text{C}\equiv\text{C}}$), 1914 ($\nu_{\text{C}=\text{O}}$),

$[(\text{PNP}^{\text{NMe}})\text{Fe}(\text{H})(\text{C}\equiv\text{C-Ph})(\text{CO})]$ (**18b**)

18b was analogously prepared to **18a** with 20 mg (0.031 mmol) of **15b-CO** and 1.9 mg $\text{Na}[\text{AlH}_4]$ (0.035 mmol) and after quenching with 26 μl of degassed H_2O (3M in THF). After evaporation of the solvent, an orange residue was obtained, containing **18b** in a purity of about 70 %.

^1H NMR (250 MHz, C_6D_6 , 20 °C): $\delta = 7.46$ (m, 2H, Ph), 7.07 (m, 3H, Ph), 6.91 (t, $J = 8.0$ Hz, 1H, py^4), 5.49 (d, $J = 8.0$ Hz, 2H, $\text{py}^{3,5}$), 2.44 (m, 2 H, $\text{PCH}(\text{CH}_3)_2$), 2.41 (s, 6H, $\text{N}(\text{CH}_3)$), 2.10 (2H, $\text{PCH}(\text{CH}_3)_2$), 1.84 (app q, 6H, $\text{PCH}(\text{CH}_3)_2$), 1.67 (app. q, 6 H, $\text{PCH}(\text{CH}_3)_2$), 1.31 (m, 6 H,

$\text{PCH}(\text{CH}_3)_2$, 0.94 (m, 6 H, $\text{PCH}(\text{CH}_3)_2$) ppm; $^{31}\text{P}\{^1\text{H}\}$ NMR (C_6D_6 MHz, CD_2Cl_2 , 20 °C): $\delta = 174.9$ ppm; IR (ATR, cm^{-1}): 2066 ($\nu_{\text{C}=\text{C}}$), 1913 (ν_{CO}).

$[(\text{FePNP}^{\text{Me}})(\text{H})(\text{C}\equiv\text{C-TMS})(^t\text{BuNC})]$ (19a**)**

15a- $^t\text{BuNC}$ (12 mg, 1 eq, 0.017 mmol) were dissolved in 2 ml THF and cooled to 0 °C. Subsequently, $\text{Na}[\text{HBEt}_3]$ (18 μl , 0.018 mmol, 1.03 eq, 1 M solution in THF) was added affording a brown suspension. The reaction was brought to RT and stirred for 30 min. After filtration with a syringe filter (polytetrafluoroethylene, 0.2 μm) the solvent was evaporated to dryness. The brownish residue was washed with 0.2 ml of cold *n*-pentane (-30 °C) and dried in vacuo, affording **19a** as yellow solid, (8 mg, 0.013 mmol, 75 %)

^1H NMR (600 MHz, C_6D_6 , 20 °C): $\delta = 6.83$ (t, $J = 8.1$ Hz, 1H, py^4), 5.44 (d, $J = 8.0$ Hz, 2H, $\text{py}^{3,5}$), 2.53 (s, 6H, $\text{N}(\text{CH}_3)$), 2.51 (m, 2H, $\text{PCH}(\text{CH}_3)_2$), 2.09 (m, 2H, $\text{PCH}(\text{CH}_3)_2$), 1.91 (app. q 6 H, $\text{PCH}(\text{CH}_3)_2$), 1.85 (app. q 6 H, $\text{PCH}(\text{CH}_3)_2$), 1.28 (app. q 6 H, $\text{PCH}(\text{CH}_3)_2$), 1.16 (s, 9 H, $\text{CNC}(\text{CH}_3)_3$), 0.95 (app. q 6 H, $\text{PCH}(\text{CH}_3)_2$), 0.35 (s, 9H, $\text{Si}(\text{CH}_3)_3$), -12.76 (t, $J = 51.4$ Hz, Fe-*H*) ppm; $^{13}\text{C}\{^1\text{H}\}$ NMR (151 MHz, C_6D_6 , 20 °C): $\delta = 182.6$ (br, $\text{CNC}(\text{CH}_3)_3$), 167.0 (br, $\text{C}\equiv\text{CSiMe}_3$), 163.4 (t, 1 H, $J = 11.3$ Hz, $\text{py}^{2,6}$), 135.5 (py^4), 125.7 ($\text{C}\equiv\text{CSiMe}_3$), 94.8 (m, $\text{py}^{3,5}$), 55.0 (s, $\text{CNC}(\text{CH}_3)_3$), 35.1 (t, $J = 8.5$ Hz, $\text{PCH}(\text{CH}_3)_2$), 33.1 (t, $J = 11.8$ Hz, $\text{PCH}(\text{CH}_3)_2$), 32.8 (vt, $\text{N}(\text{CH}_3)$), 31.1 ($\text{CNC}(\text{CH}_3)_3$), 21.4 ($\text{PCH}(\text{CH}_3)_2$), 20.6 (t, $J = 5.2$ Hz, $\text{PCH}(\text{CH}_3)_2$), 18.6 ($\text{PCH}(\text{CH}_3)_2$), 18.5 (t, $J = 5.1$ Hz, $\text{PCH}(\text{CH}_3)_2$), 2.8 ($\text{Si}(\text{CH}_3)_3$) ppm; $^{31}\text{P}\{^1\text{H}\}$ NMR (243 MHz, C_6D_6 , 20 °C): $\delta = 174.4$ ppm, $2\text{D}\{^{15}\text{N}-^1\text{H}\}$ HMBC NMR (60.8 MHz, C_6D_6 , 20 °C): $\delta = 82.9$ ($\text{N}(\text{CH}_3)$), 190.7 ($\text{CNC}(\text{CH}_3)_3$) ppm. IR (ATR, cm^{-1}): 2044 ($\nu_{\text{N}=\text{C}}$), 1977 ($\nu_{\text{C}=\text{C}}$)

$[(\text{FePNP}^{\text{Me}})(\text{H})(\text{C}\equiv\text{C-Ph})(^t\text{BuNC})]$ (19b**)**

This complex was analogously prepared to **19a** using **15b- $^t\text{BuNC}$** (11 mg, 0.016 mmol) and, $\text{Na}[\text{HBEt}_3]$ (16.5 μl , 1.03 eq, 1 M solution in THF), yielding **19b** as yellow solid. (7 mg, 0.011 mmol, 72 %)

^1H NMR (600 MHz, C_6D_6 , 20 °C): $\delta = 7.49$ (dd, $J = 8.1$ Hz, $J = 1.4$ Hz, 2H, Ph), 7.12 (m, 3H, Ph), 6.88 (t, $J = 7.3$ Hz, 1H, py^4), 5.52 (d, $J = 8.0$ Hz, 2H, $\text{py}^{3,5}$), 2.54 (s, 6H, $\text{N}(\text{CH}_3)$), 2.48 (m, 2H, $\text{PCH}(\text{CH}_3)_2$), 2.11 (m, 2H, $\text{PCH}(\text{CH}_3)_2$), 1.89 (app. q 6 H, $\text{PCH}(\text{CH}_3)_2$), 1.78 (app. q 6 H, $\text{PCH}(\text{CH}_3)_2$), 1.32 (app. q 6 H, $\text{PCH}(\text{CH}_3)_2$), 1.16 (s, 9 H, $\text{CNC}(\text{CH}_3)_3$), 1.00 (app. q 6 H, $\text{PCH}(\text{CH}_3)_2$), -12.63 (t, $J = 51.5$ Hz, Fe-*H*) ppm; $^{13}\text{C}\{^1\text{H}\}$ NMR (151 MHz, C_6D_6 , 20 °C):

δ = 181.9 (br, $\text{CNC}(\text{CH}_3)_3$), 162.5 (t, J = 11.0 Hz, $\text{py}^{2,6}$), 140.1 (t, J = 20.5 Hz, $\text{C}\equiv\text{CPh}$), 135.9 (py^4), 131.8 ($\text{C}\equiv\text{CPh}$), 130.8 (Ph), 125.7 (Ph),), 122.5 (Ph C), 119.1 (Ph^1), 95.1 (m, $\text{py}^{3,5}$), 55.1 (s, $\text{CNC}(\text{CH}_3)_3$) 34.6 (t, J = 8.5 Hz, $\text{PCH}(\text{CH}_3)_2$), 33.0 (t, J = 11.7 Hz, $\text{PCH}(\text{CH}_3)_2$), 31.4 ($\text{CNC}(\text{CH}_3)_3$), 31.0 (vt, $\text{N}(\text{CH}_3)$), 20.6 ($\text{PCH}(\text{CH}_3)_2$), 20.5 (t, J = 5.2 Hz, $\text{PCH}(\text{CH}_3)_2$), 18.6 ($\text{PCH}(\text{CH}_3)_2$), 18.5 (vt, $\text{PCH}(\text{CH}_3)_2$ ppm; $^{31}\text{P}\{^1\text{H}\}$ NMR (243 MHz, C_6D_6 , 20 °C): δ = 174.2 ppm; 2D $\{^{15}\text{N}-^1\text{H}\}$ HMBC NMR (60.8 MHz, C_6D_6 , 20 °C): δ = 191.8 ($\text{CNC}(\text{CH}_3)_3$) ppm. IR (ATR, cm^{-1}): 2054 ($\nu_{\text{C}\equiv\text{C}}$), 2032 ($\nu_{\text{N}\equiv\text{C}}$)

$[(\text{FePNP}^{\text{Me}})(\text{H})(\text{C}\equiv\text{C-TMS})(\text{P}(\text{OMe})_3)]$ (**20a**)

15a-P(OMe)₃ (15 mg, 0.020 mmol) was dissolved in 1 ml THF and $\text{Na}[\text{AlH}_4]$ (1.2 mg, 0.022 mmol) was added in one portion, creating an orange suspension. The suspension was stirred for 15 min and then treated with H_2O (16 μl , 3M in THF) leading to vigorous gas evolution. The dark orange solution was treated with 1 ml of benzene and filtered with a syringe filter (polytetrafluoroethylene, 0.2 μm). After evaporation of the solvent the dark orange residue was washed with 0.2 ml of cold *n*-pentane (-30 °C) and dried in vacuo, affording an isomeric mixture of *cis*-**20a** (28 %) and *trans*-**20a** (72 %) as orange solid. (9 mg, 0.014 mmol, 68 %)

Spectroscopic analysis of *trans*-**20a**

^1H NMR (250 MHz, C_6D_6 , 20 °C): δ = 6.96 (t, J = 8.2 Hz 1H, py^4), 5.54 (d, J = 8.1 Hz, 2H, $\text{py}^{3,5}$), 3.55 (d, J = 10.2 Hz, 9H, $\text{P}(\text{OCH}_3)_3$), 2.80 (m, 2H, $\text{PCH}(\text{CH}_3)_2$), 2.63 (s, 6H, $\text{N}(\text{CH}_3)$), 2.41 (m, 2H, $\text{PCH}(\text{CH}_3)_2$), 1.79 (app q, 6 H, $\text{PCH}(\text{CH}_3)_2$), 1.68 (app q, 6 H, $\text{PCH}(\text{CH}_3)_2$) 1.23 (app q 6 H, $\text{PCH}(\text{CH}_3)_2$), 1.05 (m, 6 H, $\text{PCH}(\text{CH}_3)_2$) 0.23 (s 9H, $\text{Si}(\text{CH}_3)_3$), -13.31 (dt, J = 63.9, J = 52.2 Hz, Fe-*H*) ppm; $^{31}\text{P}\{^1\text{H}\}$ NMR (101 MHz, C_6D_6 , 20 °C): δ = 192.0 (t, J = 74.2 Hz, $\text{P}(\text{OMe})_3$) 169.8 (d, J = 73.9 Hz, $\text{PCH}(\text{CH}_3)_2$), ppm.

Spectroscopic analysis of *cis*-**20a**

^1H NMR (250 MHz, C_6D_6 , 20 °C): δ = 6.82 (t, J = 7.9 Hz 1H, py^4), 5.35 (d, J = 8.2 Hz, 2H, $\text{py}^{3,5}$), 3.43 (d, J = 9.6 Hz, 9H, $\text{P}(\text{OCH}_3)_3$), 2.55 (m, 2H, $\text{PCH}(\text{CH}_3)_2$), 2.51 (s, 6H, $\text{N}(\text{CH}_3)$), 2.41 (m, 2H, $\text{PCH}(\text{CH}_3)_2$, superimposed by *trans*-**20a**), superimposed by *trans*-**20a**), 1.79 (m, superimposed by *trans*-**20a** 6 H, $\text{PCH}(\text{CH}_3)_2$), 1.68 (m, 6 H, $\text{PCH}(\text{CH}_3)_2$), 1.30 (m, 6 H, $\text{PCH}(\text{CH}_3)_2$), 0.95 (m, 6 H, $\text{PCH}(\text{CH}_3)_2$), 0.29 (s 9H, $\text{Si}(\text{CH}_3)_3$), -8.90 (dt, J = 83.9, J = 65.4

Hz, Fe-*H*) ppm; $^{31}\text{P}\{^1\text{H}\}$ NMR (101 MHz, C_6D_6 , 20 °C): δ = 172.7 (t, J = 37.5 Hz, $P(\text{OMe}_3)_3$) 165.3 (d, J = 37.3 Hz, $P\text{CH}(\text{CH}_3)_2$), ppm.

$[(\text{FePNP}^{\text{Me}})(\text{H})(\text{C}\equiv\text{C-TMS})(\text{PMe}_3)]$ (**21a**)

15a (15 mg, 0.025 mmol) was dissolved in 1 ml THF and PMe_3 (30 μl , 1 M. in THF) was added forming a red solution. Subsequently the reaction mixture was treated with $\text{Na}[\text{AlH}_4]$ (1.5 mg, 0.027 mmol) creating a deep red suspension. The suspension was stirred for 15 min and then quenched with H_2O (18 μl , 3M in THF) leading to vigorous gas evolution. The dark red solution was diluted with 1 ml of benzene and filtered with a syringe filter (polytetrafluoroethylene, 0.2 μm). After evaporation of the solvent the dark residue was washed with 0.1 ml of cold TMS (-30 °C) and dried in vacuo, affording an isomeric mixture of *cis*-**21a** (95 %) and *trans*-**21a** (5 %) as dark red solid. (11 mg, 0.018 mmol, 74 %)

Spectroscopic analysis of *cis*-**21a**

^1H NMR (250 MHz, C_6D_6 , 20 °C): δ = 6.82 (t, J = 8.2 Hz 1H, py^4), 5.36 (d, J = 8.1 Hz, 2H, $\text{py}^{3,5}$), 2.55 (m, 2H, $P\text{CH}(\text{CH}_3)_2$), 2.52 (s, 6H, $\text{N}(\text{CH}_3)$), 2.39 (m, 2H, $P\text{CH}(\text{CH}_3)_2$), 1.83 (app q, 6 H, $P\text{CH}(\text{CH}_3)_2$), 1.64 (app q, 6 H, $P\text{CH}(\text{CH}_3)_2$) 1.34 (m 6 H, $P\text{CH}(\text{CH}_3)_2$), 1.08 (d, J = 5.5 Hz, 9H, $P(\text{CH}_3)_3$) 0.85 (app q, 6 H, $P\text{CH}(\text{CH}_3)_2$) 0.36 (s 9H, $\text{Si}(\text{CH}_3)_3$), -11.29 (td, J = 70.5, J = 35.5 Hz, Fe-*H*) ppm; $^{31}\text{P}\{^1\text{H}\}$ NMR (101 MHz, C_6D_6 , 20 °C): δ = 165.1 (d, J = 26.3 Hz, $P\text{CH}(\text{CH}_3)_2$), 15.5 (t, J = 28.1 Hz, $P(\text{Me}_3)_3$) ppm.

Spectroscopic analysis of *trans*-**21a**

^1H NMR (250 MHz, C_6D_6 , 20 °C): δ = 6.97 (t, J = 8.2 Hz 1H, py^4), 5.57 (d, J = 8.2 Hz, 2H, $\text{py}^{3,5}$), 2.67 (s, 6H, $\text{N}(\text{CH}_3)$), 0.30 (s 9H, $\text{Si}(\text{CH}_3)_3$), -13.16 (dt, J = 56.6, J = 52.2 Hz, Fe-*H*) ppm all other resonances superimposed by *cis*-**21a**; $^{31}\text{P}\{^1\text{H}\}$ NMR (101 MHz, C_6D_6 , 20 °C): δ = 173.8 (d, J = 41.0 Hz, $P\text{CH}(\text{CH}_3)_2$), 22.2 (t, J = 40.9 Hz, $P(\text{Me}_3)_3$) ppm.

$[(\text{FePNP}^{\text{Me}})(\text{H})(\text{C}\equiv\text{C-Ph})(\text{PMe}_3)]$ (**21b**)

21b was analogously prepared to **21a** with 15 mg (0.025 mmol) of **15b**, 30 μl PMe_3 (1 M. in THF) and 1.5 mg $\text{Na}[\text{AlH}_4]$ (0.027 mmol) and was quenched with 18 μl of degassed H_2O (3M

in THF). After evaporation of the solvent, a red residue was obtained, containing **18b** in a purity of about 50 %.

^1H NMR (400 MHz, d_8 -THF, 20 °C): δ = 7.89 (m, 2H, Ph), 7.22 (m, 3H, Ph), 6.78 (t, J = 7.4 Hz, 1H, py^4), 5.50 (d, J = 8.1 Hz, 2H, $\text{py}^{3,5}$), 3.01 (s, 6H, $\text{N}(\text{CH}_3)$), 2.52 (m, 2H, $\text{PCH}(\text{CH}_3)_2$), 2.30 (m, 2H, $\text{PCH}(\text{CH}_3)_2$), 1.51 (app q, 6 H, $\text{PCH}(\text{CH}_3)_2$), 1.39 (app q, 6 H, $\text{PCH}(\text{CH}_3)_2$), 1.23 (m 6 H, $\text{PCH}(\text{CH}_3)_2$), 0.83 (d, J = 4.9 Hz, 9H, $\text{P}(\text{CH}_3)_3$) 0.60 (app q, 6 H, $\text{PCH}(\text{CH}_3)_2$), -11.50 (td) (td, J = 69.5, J = 36.4 Hz, Fe- H) ppm; $^{31}\text{P}\{^1\text{H}\}$ NMR (162 MHz, d_8 -THF, 20 °C): δ = 165.1 (d, J = 25.6 Hz, $\text{PCH}(\text{CH}_3)_2$), 10.7 (t, J = 26.3 Hz, $\text{P}(\text{Me}_3)_3$) ppm.

$[(\text{PNP}^{\text{NMe}})\text{Fe}(\text{H})(\eta^1\text{-CO}_2\text{H})(\text{tBuNC})]$ (**12b-CO₂**)

A solution of **12a-b** (18 mg, 0.035 mmol) in C_6D_6 was treated with 1 bar of CO_2 and the color of the solution immediately turned from orange to yellow. After evaporation of the solvent **12b-CO₂** was washed with 1 ml of n-pentane and dried under vacuum affording **12b-CO₂** as yellow solid. (16 mg, 0.029 mmol, 82 %)

^1H NMR (600 MHz, C_6D_6 , 20 °C): δ = 8.56 (s, 1H, HCOO), 7.06 (t, J = 8.1 Hz, 1H, py^4), 5.61 (d, J = 7.9 Hz, 2H, $\text{py}^{3,5}$), 2.47 (s, 6H, $\text{N}(\text{CH}_3)$), 2.34 (m, 2H, $\text{PCH}(\text{CH}_3)_2$), 2.02 (m, 2H, $\text{PCH}(\text{CH}_3)_2$), 1.64 (m 6 H, $\text{PCH}(\text{CH}_3)_2$), 1.27 (m 6 H, $\text{PCH}(\text{CH}_3)_2$), 1.24 (s, 9 H, $\text{CNC}(\text{CH}_3)_3$), 1.17 (m 6 H, $\text{PCH}(\text{CH}_3)_2$), 0.73 (m 6 H, $\text{PCH}(\text{CH}_3)_2$), -27.16 (t, J = 57.8 Hz, 1 H, Fe- H) ppm; $^{13}\text{C}\{^1\text{H}\}$ NMR (151 MHz, C_6D_6 , 20 °C): δ = 172.6 (br, $\text{CNC}(\text{CH}_3)_3$), 164.0 (t, J = 11.3 Hz, $\text{py}^{2,6}$), 137.5 (py^4), 95.7 (t, J = 3.3 Hz, $\text{py}^{3,5}$), 56.0 (s, $\text{CNC}(\text{CH}_3)_3$), 32.4 ($\text{N}(\text{CH}_3)$), 32.2 (m, $\text{PCH}(\text{CH}_3)_2$), 31.3 (m, $\text{PCH}(\text{CH}_3)_2$), 30.9 ($\text{CNC}(\text{CH}_3)_3$), 20.1 (vt, $\text{PCH}(\text{CH}_3)_2$), 19.9 ($\text{PCH}(\text{CH}_3)_2$), 18.9 (vt, $\text{PCH}(\text{CH}_3)_2$), 18.6 ($\text{PCH}(\text{CH}_3)_2$), (Formate resonance not found) ppm; $^{31}\text{P}\{^1\text{H}\}$ NMR (243 MHz, C_6D_6 , 20 °C): δ = 162.9 ppm, 2D $\{^{15}\text{N}-^1\text{H}\}$ HMBC NMR (60.8 MHz, C_6D_6 , 20 °C): δ = 201.9 ($\text{CNC}(\text{CH}_3)_3$) ppm. IR (ATR, cm^{-1}): 2048 ($\nu_{\text{N}=\text{C}}$), 1587 (ν_{HCOO})

$[(\text{PNP}^{\text{NMe}})\text{Fe}(\text{H})(\eta^1\text{-CO}_2\text{H})(\text{P}(\text{OMe})_3)]$ (**13-CO₂**)

A solution of **13** (12 mg, 0.022 mmol) in C_6D_6 was treated with 1 bar of CO_2 and the color of the solution immediately turned from dark orange to light orange. Due to the low stability of

the compound, **13-CO₂** was not purified and immediately characterized *via* NMR spectroscopy.

¹H NMR (600 MHz, C₆D₆, 20 °C): δ = 9.44 (s, 1H, HCOO), 6.97 (t, J = 8.3 Hz, 1H, py⁴), 5.68 (d, J = 8.2 Hz, 2H, py^{3,5}), 3.40 (d, J = 10.2 Hz, 9H, P(OCH₃)₃), 2.72 (m, 2H, PCH(CH₃)₂), 2.57 (s, 6H, N(CH₃)), 2.22 (m, 2H, PCH(CH₃)₂), 1.50 (m 6 H, PCH(CH₃)₂), 1.32 (m 6 H, PCH(CH₃)₂), 0.97 (m 12 H, PCH(CH₃)₂), -29.07 (t, J = 76.1, J = 53.4 Hz, 1 H, Fe-*H*) ppm; ¹³C{¹H} NMR (151 MHz, C₆D₆, 20 °C): δ = 168.0 (HCOO⁻), 164.2 (t, J = 10.5 Hz, py^{2,6}), 137.9 (py⁴), 96.1 (br, py^{3,5}), 51.1 (d, J = 5.3 Hz, P(OCH₃)₃), 33.5 (t, J = 3.3 Hz, N(CH₃)), 31.0 (t, J = 11.9 Hz, PCH(CH₃)₂), 27.5 (t, J = 5.5 Hz, PCH(CH₃)₂), 19.9 (PCH(CH₃)₂), 19.8 (PCH(CH₃)₂), 18.4 (vt, PCH(CH₃)₂), 18.3 (PCH(CH₃)₂) ppm; ³¹P{¹H} NMR (243 MHz, C₆D₆, 20 °C): δ = 186.7 ppm (t, J = 70.7 Hz, P(OMe)₃), 159.4 ppm. (d, J = 71.7 Hz, PCH(CH₃)₂).

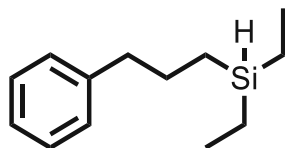
[(PNP^{NMe})Fe(H)(η^1 -CO₂H)(PMe₃)] (**9b-CO₂**)

A solution of **9a-b** (15 mg, 0.030 mmol) was treated with 1 bar of CO₂ and the color of the solution immediately turned from dark red to light red. Due to the low stability of the compound, **9b-CO₂** was not purified and immediately characterized *via* NMR spectroscopy.

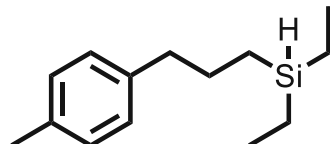
¹H NMR (250 MHz, C₆D₆, 20 °C): δ = 8.67 (s, 1H, HCOO), 7.26 (t, J = 8.1 Hz, 1H, py⁴), 5.56 (d, J = 8.1 Hz, 2H, py^{3,5}), 3.09 (s, 6H, N(CH₃)), 2.66 (m, 2H, PCH(CH₃)₂), 2.00 (m, 2H, PCH(CH₃)₂), 1.47 (m, 6 H, PCH(CH₃)₂), 1.33 (m, 6 H, PCH(CH₃)₂), 1.08 (d, J = 7.0 Hz, 9H, P(CH₃)₃), 0.99 (m, 12 H, PCH(CH₃)₂), -29.46 (dt, J = 60.6, J = 54.0 Hz, Fe-*H*) ppm; ³¹P{¹H} NMR (101 MHz, C₆D₆, 20 °C): δ = 163.1 (d, J = 39.3 Hz, PCH(CH₃)₂), 19.5 (t, J = 39.5 Hz, P(Me₃)₃) ppm.

4.6. Spectroscopic Data of Hydrosilylation Products

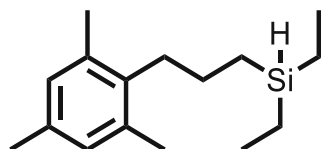
NMR spectra of organic products



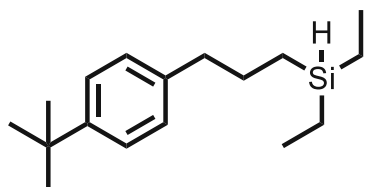
^1H NMR (400 MHz, CDCl_3 , 20 °C): δ = 7.30 (m, 2H, Ph), 7.21 (m, 3H, Ph), 3.69 (hept, $J_{\text{Si-H}}$ = 3.2 Hz, 1H, SiH), 2.67 (t, J = 7.7 Hz, $\text{ArCH}_2\text{CH}_2\text{CH}_2\text{Si}$, 2H), 1.71 (m, 2H, $\text{ArCH}_2\text{CH}_2\text{CH}_2\text{Si}$), 1.00 (t, J = 7.9 Hz, 6H, $-\text{SiHCH}_2\text{CH}_3$) 0.68 (m, 2H, $\text{ArCH}_2\text{CH}_2\text{CH}_2\text{Si}$), 0.62 (qd, 4H, J = 7.6 Hz, $J_{\text{Si-H}}$ = 3.1 Hz, J = 0.7 Hz, $-\text{SiHCH}_2\text{CH}_3$). $^{13}\text{C}\{^1\text{H}\}$ NMR (101 MHz, CDCl_3 , 20 °C): δ = 142.7 ($\text{Ar}^{\text{C-C}}$), 128.6 (Ph), 128.4 (Ph), 125.8 (Ph), 39.8 ($\text{ArCH}_2\text{CH}_2\text{CH}_2\text{Si}$), 26.9 ($\text{ArCH}_2\text{CH}_2\text{CH}_2\text{Si}$), 10.7 ($\text{ArCH}_2\text{CH}_2\text{CH}_2\text{Si}$) 8.4 ($-\text{SiHCH}_2\text{CH}_3$), 2.9 ($-\text{SiHCH}_2\text{CH}_3$), ^{29}Si -INEPT NMR (79 MHz, CDCl_3 , 20 °C): -2.1 ppm)



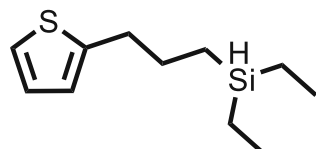
^1H NMR (400 MHz, CDCl_3 , 20 °C): δ = 7.11 (d, 4H, J = 2.5 Hz, Ph), 3.69 (hept, $J_{\text{Si-H}}$ = 3.2 Hz, 1H, SiH), 2.63 (t, J = 7.7 Hz, $\text{ArCH}_2\text{CH}_2\text{CH}_2\text{Si}$, 2H), 2.35 (s, 3H, $\text{CH}_3\text{-Ar}$), 1.68 (m, 2H, $\text{ArCH}_2\text{CH}_2\text{CH}_2\text{Si}$), 1.00 (t, J = 7.9 Hz, 6H, $-\text{SiHCH}_2\text{CH}_3$), 0.70-0.58 (m, 6H, $-\text{SiHCH}_2\text{CH}_3$ + $\text{ArCH}_2\text{CH}_2\text{CH}_2\text{Si}$). $^{13}\text{C}\{^1\text{H}\}$ NMR (101 MHz, CDCl_3 , 20 °C): δ = 139.7 ($\text{Ar}^{\text{C-Me}}$), 135.2 ($\text{Ar}^{\text{C-C}}$), 129.1 (Ph), 128.5 (Ph), 39.3 ($\text{ArCH}_2\text{CH}_2\text{CH}_2\text{Si}$), 27.0 ($\text{ArCH}_2\text{CH}_2\text{CH}_2\text{Si}$), 21.1 ($\text{CH}_3\text{-Ar}$), 10.7 ($\text{ArCH}_2\text{CH}_2\text{CH}_2\text{Si}$) 8.4 ($-\text{SiHCH}_2\text{CH}_3$), 2.9 ($-\text{SiHCH}_2\text{CH}_3$), ^{29}Si -INEPT NMR (79 MHz, CDCl_3 , 20 °C): -2.0 ppm



^1H NMR (400 MHz, CDCl_3 , 20 °C): δ = 6.87 (s, 2H, Ph), 3.73 (hept, $J_{\text{Si-H}} = 3.2$ Hz, 1H, SiH), 2.65 (m, $\text{ArCH}_2\text{CH}_2\text{CH}_2\text{Si}$, 2H), 2.30 (s, 6H, $\text{CH}_3\text{-Ar}$), 2.28 (s, 3H, $\text{CH}_3\text{-Ar}$), 1.54 (m, 2H, $\text{ArCH}_2\text{CH}_2\text{CH}_2\text{Si}$), 1.02 (t, $J = 7.9$ Hz, 6H, $-\text{SiHCH}_2\text{CH}_3$), 0.79 (m, 2H, $\text{ArCH}_2\text{CH}_2\text{CH}_2\text{Si}$), 0.64 (qd, 4H, $J = 8.1$ Hz, $J_{\text{Si-H}} = 3.2$ Hz, $-\text{SiHCH}_2\text{CH}_3$) $^{13}\text{C}\{^1\text{H}\}$ NMR (101 MHz, CDCl_3 , 20 °C): δ = 136.7 ($\text{Ar}^{\text{C-Me}}$), 136.6 ($\text{Ar}^{\text{C-Me}}$), 136.0 ($\text{Ar}^{\text{C-Me}}$), 135.0 ($\text{Ar}^{\text{C-C}}$), 129.0 (Ph), 33.5 ($\text{ArCH}_2\text{CH}_2\text{CH}_2\text{Si}$), 24.6 ($\text{ArCH}_2\text{CH}_2\text{CH}_2\text{Si}$), 20.9 ($\text{CH}_3\text{-Ar}$), 19.9 ($\text{CH}_3\text{-Ar}$), 11.7 ($\text{ArCH}_2\text{CH}_2\text{CH}_2\text{Si}$), 8.4 ($-\text{SiHCH}_2\text{CH}_3$), 3.0 ($-\text{SiHCH}_2\text{CH}_3$), ^{29}Si -INEPT NMR (79 MHz, CDCl_3 , 20 °C): -2.4 ppm

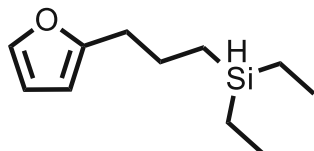


^1H NMR (400 MHz, CDCl_3 , 20 °C): δ = 7.32 (d, 2H, $J = 8.3$ Hz, Ph), 7.14 (m, 2H, Ph), 3.68 (hept, $J_{\text{Si-H}} = 3.3$ Hz, 1H, SiH), 2.63 (t, $J = 8.1$ Hz, $\text{ArCH}_2\text{CH}_2\text{CH}_2\text{Si}$, 2H), 1.69 (m, 2H, $\text{ArCH}_2\text{CH}_2\text{CH}_2\text{Si}$), 1.33 (s, 9H, $(\text{CH}_3)_3\text{C-Ar}$), 0.99 (t, $J = 7.86$ Hz, 6H, $-\text{SiHCH}_2\text{CH}_3$), 0.69 (m, 2H, $\text{ArCH}_2\text{CH}_2\text{CH}_2\text{Si}$), 0.61 (qd, 4H, $J = 7.6$ Hz, $J_{\text{Si-H}} = 3.1$ Hz, $J = 0.65$ Hz, $-\text{SiHCH}_2\text{CH}_3$). $^{13}\text{C}\{^1\text{H}\}$ NMR (101 MHz, CDCl_3 , 20 °C): δ = 148.5 ($\text{Ar}^{\text{C-}t\text{Bu}}$), 139.7 ($\text{Ar}^{\text{C-C}}$), 128.2 (Ph), 125.3 (Ph), 39.3 ($\text{ArCH}_2\text{CH}_2\text{CH}_2\text{Si}$), 34.5 ($(\text{CH}_3)_3\text{C-Ar}$), 31.6 ($(\text{CH}_3)_3\text{CAr}$), 26.9 ($\text{ArCH}_2\text{CH}_2\text{CH}_2\text{Si}$), 10.8 ($\text{ArCH}_2\text{CH}_2\text{CH}_2\text{Si}$), 8.4 ($-\text{SiHCH}_2\text{CH}_3$), 2.9 ($-\text{SiHCH}_2\text{CH}_3$), ^{29}Si -INEPT NMR (79 MHz, CDCl_3 , 20 °C): -2.1 ppm



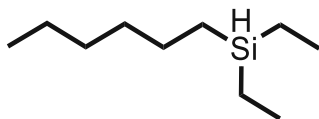
^1H NMR (400 MHz, CDCl_3 , 20 °C): δ = 7.12 (dd, $J = 5.1$ Hz, $J = 1.2$ Hz, 1H, Ar), 6.93 (dd, $J = 5.1$ Hz, $J = 3.4$ Hz, 1H, Ar), 6.80 (m, 1H, Ar), 3.68 (hept, $J_{\text{Si-H}} = 3.2$ Hz, 1H, SiH), 2.87 (t,

$J=7.5$ Hz, $\text{ArCH}_2\text{CH}_2\text{CH}_2\text{Si}$, 2H), 1.75 (m, 2H, $\text{ArCH}_2\text{CH}_2\text{CH}_2\text{Si}$), 0.99 (t, $J=7.9$ Hz, 6H, - $\text{SiHCH}_2\text{CH}_3$), 0.70 (m, 2H, $\text{ArCH}_2\text{CH}_2\text{CH}_2\text{Si}$). 0.61 (qdd, 4H, $J=7.7$ Hz, $J_{\text{Si-H}}=3.2$ Hz, $J=0.7$ Hz, - $\text{SiHCH}_2\text{CH}_3$). $^{13}\text{C}\{^1\text{H}\}$ NMR (101 MHz, CDCl_3 , 20 °C): δ = 145.6 ($\text{Ar}^{\text{C-C}}$), 126.8 (Ar), 124.2 (Ar), 123.0 (Ar), 33.6 ($\text{ArCH}_2\text{CH}_2\text{CH}_2\text{Si}$), 27.2 ($\text{ArCH}_2\text{CH}_2\text{CH}_2\text{Si}$), 10.5 ($\text{ArCH}_2\text{CH}_2\text{CH}_2\text{Si}$) 8.3 (- $\text{SiHCH}_2\text{CH}_3$), 2.9 (- $\text{SiHCH}_2\text{CH}_3$), ^{29}Si -INEPT NMR (79 MHz, CDCl_3 , 20 °C): -2.2 ppm

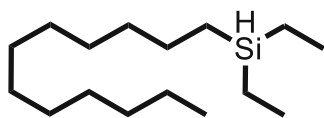


^1H NMR (400 MHz, CDCl_3 , 20 °C): δ = 7.30 (dd, $J=1.9$ Hz, $J=0.9$ Hz, 1H, Ar), 6.28 (dd, $J=3.2$ Hz, $J=1.9$ Hz, 1H, Ar), 5.99 (dd, $J=3.2$ Hz, $J=0.9$ Hz, 1H, Ar), 3.67 (hept, $J_{\text{Si-H}}=3.2$ Hz, 1H, SiH), 2.66 (t, $J=7.5$ Hz, $\text{ArCH}_2\text{CH}_2\text{CH}_2\text{Si}$, 2H), 1.71 (m, 2H, $\text{ArCH}_2\text{CH}_2\text{CH}_2\text{Si}$), 0.98 (t, $J=7.9$ Hz, 6H, - $\text{SiHCH}_2\text{CH}_3$), 0.68-0.57 (m, 6H, - $\text{SiHCH}_2\text{CH}_3$ + $\text{ArCH}_2\text{CH}_2\text{CH}_2\text{Si}$). $^{13}\text{C}\{^1\text{H}\}$ NMR (101 MHz, CDCl_3 , 20 °C): δ = 156.4 ($\text{Ar}^{\text{C-C}}$), 140.8 (Ar), 110.1 (Ar), 104.9 (Ar), 31.6 ($\text{ArCH}_2\text{CH}_2\text{CH}_2\text{Si}$), 23.6 ($\text{ArCH}_2\text{CH}_2\text{CH}_2\text{Si}$), 10.5 ($\text{ArCH}_2\text{CH}_2\text{CH}_2\text{Si}$) 8.3 (- $\text{SiHCH}_2\text{CH}_3$), 2.9 (- $\text{SiHCH}_2\text{CH}_3$), ^{29}Si -INEPT NMR (79 MHz, CDCl_3 , 20 °C): -2.2 ppm

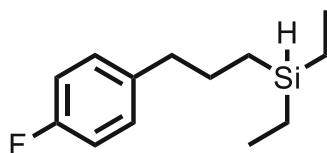
Yellow oil!



^1H NMR (400 MHz, C_6D_6 , 20 °C): δ = 3.96 (hept, $J_{\text{Si-H}}=3.2$ Hz, 1H, SiH), 1.41-1.23 (m, 8H, CH_2), 1.01 (t, $J=7.9$ Hz, 6H, - $\text{SiHCH}_2\text{CH}_3$), 0.91 (t, $J=6.9$ Hz, 3H, CH_3CH_2), 0.65-0.55 (m, 6H, $\text{R-CH}_2\text{CH}_2\text{Si}$ + - $\text{SiHCH}_2\text{CH}_3$) $^{13}\text{C}\{^1\text{H}\}$ NMR (101 MHz, C_6D_6 , 20 °C): δ = 33.5 (- CH_2 -), 31.2 (- CH_2 -), 25.0 (- CH_2 -), 23.0 (- CH_2 -), 14.4 (CH_3CH_2 -), 11.0 (- $\text{CH}_2\text{CH}_2\text{Si}$ -) 8.5 (- $\text{SiHCH}_2\text{CH}_3$), 3.2 (- $\text{SiHCH}_2\text{CH}_3$), ^{29}Si -INEPT NMR (79 MHz, C_6D_6 , 20 °C): -2.1 ppm

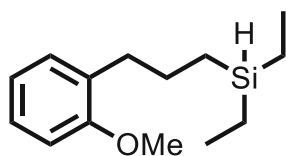


^1H NMR (400 MHz, C_6D_6 , 20 °C): δ = 3.96 (hept, J =3.2 Hz, 1H, SiH), 1.46-1.28 (m, 20H, CH_2), 1.02 (t, J =7.9 Hz, 6H, $-\text{SiHCH}_2\text{CH}_3$), 0.91 (t, J =7.1 Hz, 3H, CH_3CH_2), 0.66-0.56 (m, 6H, $\text{R}-\text{CH}_2\text{CH}_2\text{Si} + -\text{SiHCH}_2\text{CH}_3$) $^{13}\text{C}\{^1\text{H}\}$ NMR (101 MHz, C_6D_6 , 20 °C): δ = 33.9 ($-\text{CH}_2-$), 32.4 ($-\text{CH}_2-$), 30.3 ($-\text{CH}_2-$), 30.2 ($-\text{CH}_2$), 30.2 ($-\text{CH}_2$), 30.2 ($-\text{CH}_2$), 29.9 ($-\text{CH}_2$), 29.9 ($-\text{CH}_2$), 25.2 ($-\text{CH}_2$), 23.2 ($-\text{CH}_2-$), 14.4 (CH_3CH_2-), 11.1 ($-\text{CH}_2\text{CH}_2\text{Si}-$) 8.5 ($-\text{SiHCH}_2\text{CH}_3$), 3.3 ($-\text{SiHCH}_2\text{CH}_3$), ^{29}Si -INEPT NMR (79 MHz, C_6D_6 , 20 °C): -2.2 ppm



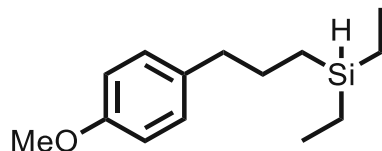
^1H NMR (400 MHz, CDCl_3 , 20 °C): δ = 7.12 (m, 2H, Ph), 6.97 (m, 2H, Ph), 3.66 (hept, $J_{\text{Si-H}}$ = 3.2 Hz, 1H, SiH), 2.61 (t, J =7.6 Hz, $\text{ArCH}_2\text{CH}_2\text{CH}_2\text{Si}$, 2H), 1.65 (m, 2H, $\text{ArCH}_2\text{CH}_2\text{CH}_2\text{Si}$), 0.97 (t, J =7.9 Hz, 6H, $-\text{SiHCH}_2\text{CH}_3$) 0.66-0.56 (m, 6H, $-\text{SiHCH}_2\text{CH}_3 + \text{ArCH}_2\text{CH}_2\text{CH}_2\text{Si}$) $^{13}\text{C}\{^1\text{H}\}$ NMR (101 MHz, CDCl_3 , 20 °C): δ = 161.3 (d, $^1J_{\text{F-C}}$ = 242.8 Hz, $\text{Ar}^{\text{C-F}}$), 138.3 (d, $^4J_{\text{F-C}}$ = 3.2 Hz, $\text{Ar}^{\text{C-C}}$), 129.9 (d, $^3J_{\text{F-C}}$ = 7.7 Hz, Ph), 115.1 (d, $^2J_{\text{F-C}}$ = 21.0 Hz, Ph) 38.9 ($\text{ArCH}_2\text{CH}_2\text{CH}_2\text{Si}$), 27.0 ($\text{ArCH}_2\text{CH}_2\text{CH}_2\text{Si}$), 10.5 ($\text{ArCH}_2\text{CH}_2\text{CH}_2\text{Si}$) 8.3 ($\text{SiHCH}_2\text{CH}_3$), 2.9 ($\text{SiHCH}_2\text{CH}_3$).

$^{19}\text{F}\{^1\text{H}\}$ NMR (376 MHz, CDCl_3 , 20 °C): -118.1 ppm; ^{29}Si -INEPT NMR (79 MHz, CDCl_3 , 20 °C): -2.1 ppm

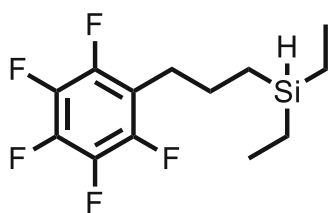


^1H NMR (400 MHz, CDCl_3 , 20 °C): δ = 7.21-7.14 (m, 2H, Ph), 6.93-6.85 (m, 2H, Ph), 3.84 (s, 3H, $\text{CH}_3\text{O-Ar}$), 3.68 (hept, $J_{\text{Si-H}}$ = 3.3 Hz, 1H, SiH), 2.67 (t, J =7.8 Hz, $\text{ArCH}_2\text{CH}_2\text{CH}_2\text{Si}$, 2H), 1.65 (m, 2H, $\text{ArCH}_2\text{CH}_2\text{CH}_2\text{Si}$), 1.00 (t, J =7.9 Hz, 6H, $-\text{SiHCH}_2\text{CH}_3$) 0.70 (m, 2H, $\text{ArCH}_2\text{CH}_2\text{CH}_2\text{Si}$). 0.61 (qd, 4H, J =7.9 Hz, $J_{\text{Si-H}}$ =3.1 Hz, $-\text{SiHCH}_2\text{CH}_3$) $^{13}\text{C}\{^1\text{H}\}$ NMR (101 MHz, CDCl_3 , 20 °C): δ = 157.5 ($\text{Ar}^{\text{C-OMe}}$), 131.1 ($\text{Ar}^{\text{C-C}}$), 130.0 (Ph), 126.9 (Ph), 120.4

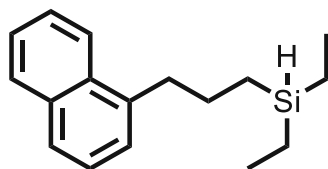
(Ph), 110.3 (Ph), 54.9 ($\text{CH}_3\text{O-Ar}$) 34.0 ($\text{ArCH}_2\text{CH}_2\text{CH}_2\text{Si}$), 25.0 ($\text{ArCH}_2\text{CH}_2\text{CH}_2\text{Si}$), 10.8 ($\text{ArCH}_2\text{CH}_2\text{CH}_2\text{Si}$) 8.3 ($-\text{SiHCH}_2\text{CH}_3$), 2.9 ($-\text{SiHCH}_2\text{CH}_3$), ^{29}Si -INEPT NMR (79 MHz, CDCl_3 , 20 °C): -2.1 ppm



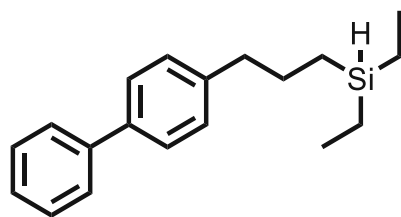
^1H NMR (400 MHz, CDCl_3 , 20 °C): δ = 7.10 (d, 2H, $J=8.6$ Hz, Ph), 6.84 (d, 2H, $J=8.6$ Hz, Ph), 3.80 (s, 3H, $\text{CH}_3\text{O-Ar}$), 3.67 (hept, $J_{\text{Si-H}}=3.2$ Hz, 1H, SiH), 2.59 (t, $J=7.6$ Hz, $\text{ArCH}_2\text{CH}_2\text{CH}_2\text{Si}$, 2H), 1.65 (m, 2H, $\text{ArCH}_2\text{CH}_2\text{CH}_2\text{Si}$), 0.98 (t, $J=7.9$ Hz, 6H, $-\text{SiHCH}_2\text{CH}_3$), 0.68-0.56 (m, 6H, $-\text{SiHCH}_2\text{CH}_3 + \text{ArCH}_2\text{CH}_2\text{CH}_2\text{Si}$). $^{13}\text{C}\{^1\text{H}\}$ NMR (101 MHz, CDCl_3 , 20 °C): δ = 157.8 ($\text{Ar}^{\text{C-OMe}}$), 134.8 ($\text{Ar}^{\text{C-C}}$), 129.5 (Ph), 113.8 (Ph), 55.4 ($\text{CH}_3\text{O-Ar}$) 38.8 ($\text{ArCH}_2\text{CH}_2\text{CH}_2\text{Si}$), 27.1 ($\text{ArCH}_2\text{CH}_2\text{CH}_2\text{Si}$), 10.6 ($\text{ArCH}_2\text{CH}_2\text{CH}_2\text{Si}$) 8.4 ($-\text{SiHCH}_2\text{CH}_3$), 2.9 ($-\text{SiHCH}_2\text{CH}_3$), ^{29}Si -INEPT NMR (79 MHz, CDCl_3 , 20 °C): -2.1 ppm



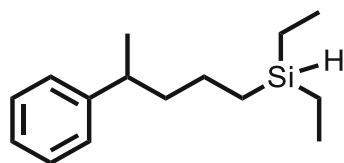
^1H NMR (400 MHz, CDCl_3 , 20 °C): δ = 3.65 (hept, $J_{\text{Si-H}}=3.2$ Hz, 1H, SiH), 2.73 (tt, $J=7.7$, $J=1.7$ Hz, $\text{ArCH}_2\text{CH}_2\text{CH}_2\text{Si}$, 2H), 1.64 (m, 2H, $\text{ArCH}_2\text{CH}_2\text{CH}_2\text{Si}$), 0.97 (t, $J=7.9$ Hz, 6H, $-\text{SiHCH}_2\text{CH}_3$) 0.68-0.56 (m, 6H, $-\text{SiHCH}_2\text{CH}_3 + \text{ArCH}_2\text{CH}_2\text{CH}_2\text{Si}$). $^{13}\text{C}\{^1\text{H}\}$ NMR (101 MHz, CDCl_3 , 20 °C): δ = 146.6-146.3 + 144.2-143.8 (m, $^1J_{\text{F-C}}=245.0$ Hz, $\text{Ar}^{\text{C-F}}$), 141.0-140.7 + 138.5-138.2 (m, $^1J_{\text{F-C}}=251.2$ Hz, $\text{Ar}^{\text{C-F}}$), 139.0-138.6 + 136.5-136.1 (m, $^1J_{\text{F-C}}=251.8$ Hz, $\text{Ar}^{\text{C-F}}$) 115.6- 115.1 (m $\text{Ar}^{\text{C-C}}$), 25.9 ($\text{ArCH}_2\text{CH}_2\text{CH}_2\text{Si}$), 24.9 ($\text{ArCH}_2\text{CH}_2\text{CH}_2\text{Si}$), 10.7 ($\text{ArCH}_2\text{CH}_2\text{CH}_2\text{Si}$), 8.2 ($\text{SiHCH}_2\text{CH}_3$), 2.8 ($\text{SiHCH}_2\text{CH}_3$). $^{19}\text{F}\{^1\text{H}\}$ NMR (376 MHz, CDCl_3 , 20°C): -144.4 - -144.5 (m), -158.4 (t, $J=21.5$ Hz), -163.1 - 163.5 (m) ppm; ^{29}Si -INEPT NMR (79 MHz, CDCl_3 , 20 °C): -2.3 ppm



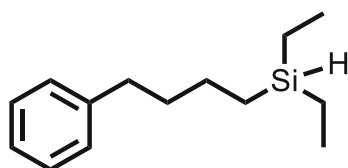
^1H NMR (400 MHz, CDCl_3 , 20 °C): δ = 8.03 (m, 1H, Ph), 7.82 (m, 1H, Ph), 7.68 (m, 1H, Ph), 7.46 (m, 2H, Ph), 7.37 (m, 1H, Ph), 7.30 (m, 1H, Ph), 3.68 (hept, $J_{\text{Si-H}} = 3.1$ Hz, 1H, SiH), 3.09 (t, $J = 7.8$ Hz, $\text{ArCH}_2\text{CH}_2\text{CH}_2\text{Si}$, 2H), 1.80 (m, 2H, $\text{ArCH}_2\text{CH}_2\text{CH}_2\text{Si}$), 0.95 (t, $J = 7.9$ Hz, 6H, $-\text{SiHCH}_2\text{CH}_3$), 0.75 (m, 2H, $\text{ArCH}_2\text{CH}_2\text{CH}_2\text{Si}$), 0.59 (m, 4H, $\text{SiHCH}_2\text{CH}_3$). $^{13}\text{C}\{^1\text{H}\}$ NMR (101 MHz, CDCl_3 , 20 °C): δ = 138.8 ($\text{Ar}^{\text{C-C}}$), 134.0 ($\text{Ar}^{\text{C-C}}$), 132.1 ($\text{Ar}^{\text{C-C}}$), 128.9 (Ph), 126.6 (Ph), 126.1 (Ph), 125.8 (Ph), 125.6 (Ph), 125.5 (Ph), 124.0 (Ph), 36.9 ($\text{ArCH}_2\text{CH}_2\text{CH}_2\text{Si}$), 26.2 ($\text{ArCH}_2\text{CH}_2\text{CH}_2\text{Si}$), 11.2 ($\text{ArCH}_2\text{CH}_2\text{CH}_2\text{Si}$), 8.3 ($-\text{SiHCH}_2\text{CH}_3$), 2.9 ($-\text{SiHCH}_2\text{CH}_3$), ^{29}Si -INEPT NMR (79 MHz, CDCl_3 , 20 °C): -2.1 ppm



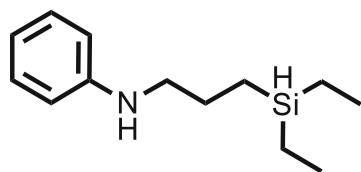
^1H NMR (400 MHz, CDCl_3 , 20 °C): δ = 7.56 (m, 2H, Ph), 7.49 (d, $J = 8.2$ Hz, 2H, Ph), 7.40 (t, $J = 7.5$ Hz, 2H, Ph), 7.30 (m, 1H, Ph), 7.23 (d, $J = 8.2$ Hz, 2H, Ph), 3.67 (hept, $J_{\text{Si-H}} = 3.17$ Hz, 1H, SiH), 2.66 (t, $J = 7.7$ Hz, $\text{ArCH}_2\text{CH}_2\text{CH}_2\text{Si}$, 2H), 1.69 (m, 2H, $\text{ArCH}_2\text{CH}_2\text{CH}_2\text{Si}$), 0.96 (t, $J = 7.9$ Hz, 6H, $-\text{SiHCH}_2\text{CH}_3$), 0.67 (m, 2H, $\text{ArCH}_2\text{CH}_2\text{CH}_2\text{Si}$), 0.59 (m, 4H, $\text{SiHCH}_2\text{CH}_3$). $^{13}\text{C}\{^1\text{H}\}$ NMR (101 MHz, CDCl_3 , 20 °C): δ = 141.8 ($\text{Ar}^{\text{C-C}}$), 141.3 ($\text{Ar}^{\text{C-C}}$), 138.8 ($\text{Ar}^{\text{C-C}}$), 129.0 (Ph), 128.8 (Ph), 127.1 (Ph), 127.1 (Ph), 127.0 (Ph), 39.4 ($\text{ArCH}_2\text{CH}_2\text{CH}_2\text{Si}$), 26.8 ($\text{ArCH}_2\text{CH}_2\text{CH}_2\text{Si}$), 10.7 ($\text{ArCH}_2\text{CH}_2\text{CH}_2\text{Si}$), 8.0 ($-\text{SiHCH}_2\text{CH}_3$), 2.9 ($-\text{SiHCH}_2\text{CH}_3$), ^{29}Si -INEPT NMR (79 MHz, CDCl_3 , 20 °C): -2.0 ppm



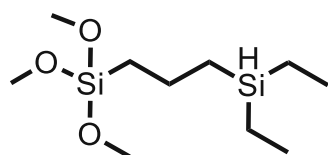
^1H NMR (400 MHz, CDCl_3 , 20 °C): δ = 7.31 (m, 2H, Ph), 7.20 (m, 3H, Ph), 3.63 (hept, $J_{\text{Si-H}}$ = 3.1 Hz, 1H, SiH), 2.73 (m, $\text{ArCH}(\text{CH}_3)\text{CH}_2\text{CH}_2\text{CH}_2\text{Si}$, 1H), 1.63 (m, 2H, $\text{ArCH}(\text{CH}_3)\text{CH}_2\text{CH}_2\text{CH}_2\text{Si}$), 1.44 (m, 2H, $\text{ArCH}_2\text{CH}_2\text{CH}_2\text{CH}_2\text{Si}$), 1.31 (m, 2H, $\text{ArCH}(\text{CH}_3)\text{CH}_2\text{CH}_2\text{CH}_2\text{Si}$), 1.26 (d, J = 7.00 Hz, 3H, $\text{ArCH}(\text{CH}_3)\text{CH}_2\text{CH}_2\text{CH}_2\text{Si}$), 0.97 (td, J = 7.9 Hz, J = 1.6 Hz, 6H, $-\text{SiHCH}_2\text{CH}_3$), 0.72-0.53 (m, 6H, $-\text{SiHCH}_2\text{CH}_3$ + $\text{ArCH}(\text{CH}_3)\text{CH}_2\text{CH}_2\text{CH}_2\text{Si}$) $^{13}\text{C}\{^1\text{H}\}$ NMR (101 MHz, CDCl_3 , 20 °C): δ = 148.0 ($\text{Ar}^{\text{C-C}}$), 128.4 (Ph), 127.1 (Ph), 125.9 (Ph), 42.2 ($\text{ArCH}(\text{CH}_3)\text{CH}_2\text{CH}_2\text{CH}_2\text{Si}$), 39.7 ($\text{ArCH}(\text{CH}_3)\text{CH}_2\text{CH}_2\text{CH}_2\text{Si}$), 22.8 ($\text{ArCH}(\text{CH}_3)\text{CH}_2\text{CH}_2\text{CH}_2\text{Si}$), 22.4 ($\text{ArCH}(\text{CH}_3)\text{CH}_2\text{CH}_2\text{CH}_2\text{Si}$), 10.4 ($\text{ArCH}(\text{CH}_3)\text{CH}_2\text{CH}_2\text{CH}_2\text{Si}$) 8.3 (d, J = 1.6 Hz, $-\text{SiHCH}_2\text{CH}_3$), 2.9 (d, J = 1.6 Hz, $-\text{SiHCH}_2\text{CH}_3$), ^{29}Si -INEPT NMR (79 MHz, CDCl_3 , 20 °C): -2.1 ppm



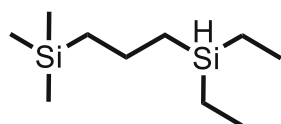
^1H NMR (400 MHz, CDCl_3 , 20 °C): δ = 7.30 (m, 2H, Ph), 7.20 (m, 3H, Ph), 3.67 (hept, $J_{\text{Si-H}}$ = 3.1 Hz, 1H, SiH), 2.64 (t, J = 7.9 Hz, $\text{ArCH}_2\text{CH}_2\text{CH}_2\text{CH}_2\text{Si}$, 2H), 1.69 (m, 2H, $\text{ArCH}_2\text{CH}_2\text{CH}_2\text{CH}_2\text{Si}$), 1.44 (m, 2H, $\text{ArCH}_2\text{CH}_2\text{CH}_2\text{CH}_2\text{Si}$), 1.00 (t, J = 7.9 Hz, 6H, $-\text{SiHCH}_2\text{CH}_3$), 0.69-0.57 (m, 6H, $-\text{SiHCH}_2\text{CH}_3$ + $\text{ArCH}_2\text{CH}_2\text{CH}_2\text{CH}_2\text{Si}$) $^{13}\text{C}\{^1\text{H}\}$ NMR (101 MHz, CDCl_3 , 20 °C): δ = 143.0 ($\text{Ar}^{\text{C-C}}$), 128.5 (Ph), 128.4 (Ph), 125.7 (Ph), 35.8 ($\text{ArCH}_2\text{CH}_2\text{CH}_2\text{CH}_2\text{Si}$), 35.3 ($\text{ArCH}_2\text{CH}_2\text{CH}_2\text{CH}_2\text{Si}$), 24.5 ($\text{ArCH}_2\text{CH}_2\text{CH}_2\text{CH}_2\text{Si}$), 10.6 ($\text{ArCH}_2\text{CH}_2\text{CH}_2\text{CH}_2\text{Si}$) 8.4 ($-\text{SiHCH}_2\text{CH}_3$), 2.9 ($-\text{SiHCH}_2\text{CH}_3$), ^{29}Si -INEPT NMR (79 MHz, CDCl_3 , 20 °C): -2.0 ppm



^1H NMR (400 MHz, CDCl_3 , 20 °C): δ = 7.20 (m, 2H, Ph), 6.72 (m, 1H, Ph), 6.64 (m, 2H, Ph), 3.72 (hept, $J_{\text{Si-H}} = 3.2$ Hz, 1H, SiH), 3.65 (br, 1H, ArNH), 3.14 (t, $J = 7.2$ Hz, ArNHCH₂CH₂CH₂Si, 2H), 1.69 (m, 2H, ArNHCH₂CH₂CH₂Si), 1.02 (t, $J = 7.9$ Hz, 6H, -SiHCH₂CH₃), 0.71 (m, 2H, ArCH₂CH₂CH₂Si). 0.65 (m, 4H, SiHCH₂CH₃) ppm. $^{13}\text{C}\{^1\text{H}\}$ NMR (101 MHz, CDCl_3 , 20 °C): δ = 148.6 (Ar^{C-C}), 129.4 (Ph), 117.2 (Ph), 112.8 (Ph), 47.1 (ArNHCH₂CH₂CH₂Si), 24.9 (ArNHCH₂CH₂CH₂Si), 8.3 (-SiHCH₂CH₃), 8.2 (ArNHCH₂CH₂CH₂Si) 2.9 (-SiHCH₂CH₃), ^{29}Si -INEPT NMR (79 MHz, CDCl_3 , 20 °C): -1.8 ppm

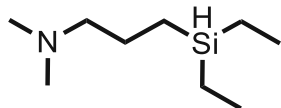


^1H NMR (400 MHz, CDCl_3 , 20 °C): δ = 3.64 (hept, $J_{\text{Si-H}} = 3.2$ Hz, 1H, SiH), 3.57 (s, 9H, -Si(OCH₃)), 1.51 (m, 2H, (MeO)₃SiCH₂CH₂CH₂Si), 0.97 (t, $J = 7.9$ Hz, 6H, -SiHCH₂CH₃) 0.76-0.55 (m, 8H, -SiHCH₂CH₃ + (MeO)₃SiCH₂CH₂CH₂Si + (MeO)₃SiCH₂CH₂CH₂Si) ppm. $^{13}\text{C}\{^1\text{H}\}$ NMR (101 MHz, CDCl_3 , 20 °C): δ = 50.6 (Si(OCH₃)), 18.2 ((MeO)₃SiCH₂CH₂CH₂Si), 14.9((MeO)₃SiCH₂CH₂CH₂Si), 13.5 ((MeO)₃SiCH₂CH₂CH₂Si), 8.3 (SiHCH₂CH₃), 2.9 (SiHCH₂CH₃). ppm; ^{29}Si -INEPT NMR (79 MHz, CDCl_3 , 20 °C): -2.8 (-SiHEt₂), -42.0 ((MeO)₃Si-) ppm.



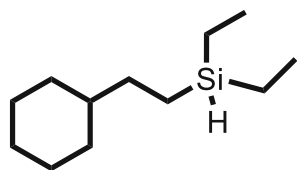
^1H NMR (400 MHz, CDCl_3 , 20 °C): δ = 3.64 (hept, $J_{\text{Si-H}} = 3.4$ Hz, 1H, SiH), 1.41 (m, 2H, Me₃SiCH₂CH₂CH₂Si), 0.98 (t, $J = 7.9$ Hz, 6H, -SiHCH₂CH₃) 0.69-0.55 (m, 8H, -SiHCH₂CH₃ + Me₃SiCH₂CH₂CH₂Si + Me₃SiCH₂CH₂CH₂Si), - 0.02 (s, 9H, (CH₃)₃Si) ppm. $^{13}\text{C}\{^1\text{H}\}$ NMR (101 MHz, CDCl_3 , 20 °C): δ = 21.2 (Me₃SiCH₂CH₂CH₂Si), 19.3(Me₃SiC

H₂CH₂CH₂Si), 15.3 (MeSiCH₂CH₂CH₂Si), 8.4 (SiHCH₂CH₃), 3.0 (SiHCH₂CH₃), -1.44 ((CH₃)₃Si-) ppm; ²⁹Si-INEPT NMR (79 MHz, CDCl₃, 20 °C): 0.62 (Me₃Si-), -2.8 (-SiHEt₂) ppm.

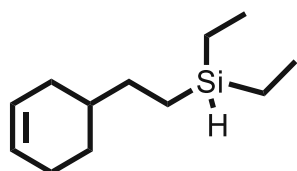


¹H NMR (400 MHz, CDCl₃, 20 °C): δ = 3.65 (hept, J_{Si-H} = 3.2 Hz, 1H, SiH), 2.25 (t, J = 7.6 Hz, 2H, Me₂NCH₂CH₂CH₂Si), 2.22 (s, 6H, (CH₃)₂NCH₂CH₂CH₂Si), 1.51 (m, 2H, Me₂NCH₂CH₂CH₂Si) 0.97 (t, J = 7.9 Hz, 6H, -SiHCH₂CH₃) 0.74 (m, 2H, Me₂CH₂CH₂CH₂Si). 0.59 (m, 4H, SiHCH₂CH₃) ppm.

¹³C{¹H} NMR (101 MHz, CDCl₃, 20 °C): δ = 63.3 (Me₂NCH₂CH₂CH₂Si), 45.6 ((CH₃)₂N -) 22.9 (Me₃SiCH₂CH₂CH₂Si), 8.3 (SiHCH₂CH₃), 8.3 (Me₂NCH₂CH₂CH₂Si), 2.9 (SiHCH₂CH₃) ppm; ²⁹Si-INEPT NMR (79 MHz, CDCl₃, 20 °C): -1.8 ppm.

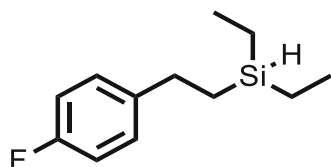


¹H NMR (400 MHz, C₆D₆, 20 °C): δ = 3.95 (hept, J = 3.2 Hz, 1H, SiH), 1.76-1.63 (m, 5H), 1.31-1.10 (m, 6H), 1.02 (t, J = 7.9 Hz, 6H, -SiHCH₂CH₃), 0.89-0.78 (m, 2H), 0.62-0.56 (m, 6H, R-CH₂CH₂Si + -SiHCH₂CH₃) ¹³C{¹H} NMR (101 MHz, C₆D₆, 20 °C): δ = 40.1 ((CH₂)₂-CH-CH₂), 33.3 (-CH₂-), 32.6 (-CH₂-), 27.2 (-CH₂), 26.9 (-CH₂), 8.5 (-SiHCH₂CH₃), 7.9 (-CH₂CH₂Si-), 3.2 (-SiHCH₂CH₃), ²⁹Si-INEPT NMR (79 MHz, C₆D₆, 20 °C): -1.5 ppm

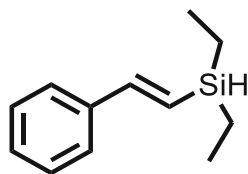


¹H NMR (400 MHz, C₆D₆, 20 °C): δ = 5.75-5.65 (m, 2H, -CH=CH-), 3.93 (hept, J = 3.3 Hz, 1H, SiH), 2.11-1.91 (m, 3H), 1.71-1.66 (m, 1H), 1.65-1.56 (m, 1H), 1.49-1.40 (m, 1H), 1.34-1.27 (m, 2H), 1.23-1.15 (m, 1H), 1.00 (t, J = 7.9 Hz, 6H, -SiHCH₂CH₃), 0.61-0.54 (m, 6H, R-

$\text{CH}_2\text{CH}_2\text{Si} + \text{-SiHCH}_2\text{CH}_3$ $^{13}\text{C}\{^1\text{H}\}$ NMR (101 MHz, C_6D_6 , 20 °C): δ = 127.3 (-CH=CH-), 126.9 (-CH=CH-), 36.8 ((CH₂)₂-CH-CH₂), 32.0 (-CH₂-), 31.8 (-CH₂-), 28.9 (-CH₂), 25.7 (-CH₂), 8.5 (-SiHCH₂CH₃), 7.9 (-CH₂CH₂Si-), 3.1 (-SiHCH₂CH₃), ^{29}Si -INEPT NMR (79 MHz, C_6D_6 , 20 °C): -1.6 ppm



^1H NMR (400 MHz, CD_2Cl_2 , 20 °C): δ = 7.17 (m, 2H, Ph), 6.96 (m, 2H, Ph), 3.68 (p, $J_{\text{Si-H}} = 3.2$ Hz 1H, SiH), 2.66 (m, 2H, $\text{ArCH}_2\text{CH}_2\text{Si}$), 1.06-0.93 (m, 8H, $\text{ArCH}_2\text{CH}_2\text{Si} + \text{-SiHCH}_2\text{CH}_3$), 0.62 (qdd, $J = 7.7$ Hz, $J_{\text{Si-H}} = 6.2$ Hz, $J = 0.7$ Hz 6H, -SiHCH₂CH₃). $^{13}\text{C}\{^1\text{H}\}$ NMR (101 MHz, CD_2Cl_2 , 20 °C): δ = 161.5 (d, $^1J_{\text{F-C}} = 242.0$ Hz, $\text{Ar}^{\text{C-F}}$), 141.3 (d, $^4J_{\text{F-C}} = 3.1$ Hz, $\text{Ar}^{\text{C-C}}$), 129.6 (d, $^3J_{\text{F-C}} = 7.8$ Hz, Ph), 115.2 (d, $^2J_{\text{F-C}} = 21.1$ Hz, Ph), 30.3 ($\text{ArCH}_2\text{CH}_2\text{Si}$), 13.3 ($\text{ArCH}_2\text{CH}_2\text{Si}$), 8.3 (-SiHCH₂CH₃), 3.1 (-SiHCH₂CH₃), $^{19}\text{F}\{^1\text{H}\}$ NMR (376 MHz, CD_2Cl_2 , 20 °C): -119.1 ppm



^1H NMR (400 MHz, CDCl_3 , 20 °C): δ = 7.45-7.42 (m, 2H, Ph), 7.35-7.24 (m, 3H, Ph), 7.01 (d, $J = 19.2$ Hz, 1H, Ar-CH=CH-Si), 6.42 (dd, $J = 19.1$ Hz, $J_{\text{Si-H}} = 3.4$ Hz, 1H, Ar-CH=CH-Si), 4.00 (p, $J_{\text{Si-H}} = 3.2$ Hz 1H, SiH), 2.66 (m, 2H, $\text{ArCH}_2\text{CH}_2\text{Si}$), 1.03 (t, $J = 7.86$ Hz, 6H, -SiHCH₂CH₃), 0.74 (m, 4H, SiHCH₂CH₃). $^{13}\text{C}\{^1\text{H}\}$ NMR (101 MHz, CD_2Cl_2 , 20 °C): δ = 147.2 (Ar-CH=CH-Si), 137.4 ($\text{Ar}^{\text{C-C}}$), 128.6 (Ph), 128.2 (Ph), 126.5 (Ph), 123.8 (Ar-CH=CH-Si), 8.2 (-SiHCH₂CH₃), 3.4 (-SiHCH₂CH₃), ^{29}Si -INEPT NMR (79 MHz, CDCl_3 , 20 °C): -8.4 ppm

5. References

- 1 Leach, B. E. *Applied Industrial Catalysis*, 1st ed.; Elsevier Science, 1983.
- 2 Hayler, J. D.; Leahy, D. K.; Simmons, E. M. A Pharmaceutical Industry Perspective on Sustainable Metal Catalysis. *Organometallics* **2019**, *38* (1), 36–46. <https://doi.org/10.1021/acs.organomet.8b00566>.
- 3 Nuss, P.; Eckelman, M. J. Life Cycle Assessment of Metals: A Scientific Synthesis. *PLoS One* **2014**, *9* (7), e101298-.
- 4 Bauer, I.; Knölker, H.-J. Iron Catalysis in Organic Synthesis. *Chem Rev* **2015**, *115* (9), 3170–3387. <https://doi.org/10.1021/cr500425u>.
- 5 Benito-Garagorri, D.; Lagoja, I.; Veiros, L. F.; Kirchner, K. A. Reactivity of Coordinatively Unsaturated Iron Complexes towards Carbon Monoxide: To Bind or Not to Bind? *Dalton Trans.* **2011**, *40* (18), 4778–4792. <https://doi.org/10.1039/C0DT01636E>.
- 6 Chirik, P.; Morris, R. Getting Down to Earth: The Renaissance of Catalysis with Abundant Metals. *Acc Chem Res* **2015**, *48* (9), 2495. <https://doi.org/10.1021/acs.accounts.5b00385>.
- 7 Langer, R.; Leitus, G.; Ben-David, Y.; Milstein, D. Efficient Hydrogenation of Ketones Catalyzed by an Iron Pincer Complex. *Angewandte Chemie International Edition* **2011**, *50* (9), 2120–2124. <https://doi.org/10.1002/anie.201007406>.
- 8 Langer, R.; Iron, M. A.; Konstantinovski, L.; Diskin-Posner, Y.; Leitus, G.; Ben-David, Y.; Milstein, D. Iron Borohydride Pincer Complexes for the Efficient Hydrogenation of Ketones under Mild, Base-Free Conditions: Synthesis and Mechanistic Insight. *Chemistry – A European Journal* **2012**, *18* (23), 7196–7209. <https://doi.org/10.1002/chem.201200159>.
- 9 Gorgas, N.; Stöger, B.; Veiros, L. F.; Pittenauer, E.; Allmaier, G.; Kirchner, K. Efficient Hydrogenation of Ketones and Aldehydes Catalyzed by Well-Defined Iron(II) PNP Pincer Complexes: Evidence for an Insertion Mechanism. *Organometallics* **2014**, *33* (23), 6905–6914. <https://doi.org/10.1021/om5009814>.
- 10 Gorgas, N.; Stöger, B.; Veiros, L. F.; Kirchner, K. Highly Efficient and Selective Hydrogenation of Aldehydes: A Well-Defined Fe(II) Catalyst Exhibits Noble-Metal Activity. *ACS Catal* **2016**, *6* (4), 2664–2672. <https://doi.org/10.1021/acscatal.6b00436>.

- 11 Lagaditis, P. O.; Sues, P. E.; Sonnenberg, J. F.; Wan, K. Y.; Lough, A. J.; Morris, R. H. Iron(II) Complexes Containing Unsymmetrical P–N–P' Pincer Ligands for the Catalytic Asymmetric Hydrogenation of Ketones and Imines. *J Am Chem Soc* **2014**, *136* (4), 1367–1380. <https://doi.org/10.1021/ja4082233>.
- 12 Gorgas, N.; Brünig, J.; Stöger, B.; Vanicek, S.; Tilset, M.; Veiros, L. F.; Kirchner, K. Efficient Z-Selective Semihydrogenation of Internal Alkynes Catalyzed by Cationic Iron(II) Hydride Complexes. *J Am Chem Soc* **2019**, *141* (43), 17452–17458. <https://doi.org/10.1021/jacs.9b09907>.
- 13 Schratzberger, H.; Stöger, B.; Veiros, L. F.; Kirchner, K. Selective Transfer Semihydrogenation of Alkynes Catalyzed by an Iron PCP Pincer Alkyl Complex. *ACS Catal* **2023**, *13* (21), 14012–14022. <https://doi.org/10.1021/acscatal.3c04156>.
- 14 Pandey, D. K.; Khaskin, E.; Pal, S.; Fayzullin, R. R.; Khusnutdinova, J. R. Efficient Fe-Catalyzed Terminal Alkyne Semihydrogenation by H₂: Selectivity Control via a Bulky PNP Pincer Ligand. *ACS Catal* **2023**, *13* (1), 375–381. <https://doi.org/10.1021/acscatal.2c04274>.
- 15 Thompson, C. V.; Arman, H. D.; Tonzetich, Z. J. Investigation of Iron Silyl Complexes as Active Species in the Catalytic Hydrosilylation of Aldehydes and Ketones. *Organometallics* **2022**, *41* (4), 430–440. <https://doi.org/10.1021/acs.organomet.1c00682>.
- 16 Chakraborty, S.; Bhattacharya, P.; Dai, H.; Guan, H. Nickel and Iron Pincer Complexes as Catalysts for the Reduction of Carbonyl Compounds. *Acc Chem Res* **2015**, *48* (7), 1995–2003. <https://doi.org/10.1021/acs.accounts.5b00055>.
- 17 Nakajima, K.; Kato, T.; Nishibayashi, Y. Hydroboration of Alkynes Catalyzed by Pyrrolide-Based PNP Pincer–Iron Complexes. *Org Lett* **2017**, *19* (16), 4323–4326. <https://doi.org/10.1021/acs.orglett.7b01995>.
- 18 Narro, A. L.; Arman, H. D.; Tonzetich, Z. J. Mechanistic Studies of Alkyne Hydroboration by a Well-Defined Iron Pincer Complex: Direct Comparison of Metal-Hydride and Metal-Boryl Reactivity. *Inorg Chem* **2022**, *61* (27), 10477–10485. <https://doi.org/10.1021/acs.inorgchem.2c01325>.
- 19 Zell, T.; Butschke, B.; Ben-David, Y.; Milstein, D. Efficient Hydrogen Liberation from Formic Acid Catalyzed by a Well-Defined Iron Pincer Complex under Mild Conditions. *Chemistry – A European Journal* **2013**, *19* (25), 8068–8072. <https://doi.org/https://doi.org/10.1002/chem.201301383>.

- 20 Bielinski, E. A.; Lagaditis, P. O.; Zhang, Y.; Mercado, B. Q.; Würtele, C.; Bernskoetter, W. H.; Hazari, N.; Schneider, S. Lewis Acid-Assisted Formic Acid Dehydrogenation Using a Pincer-Supported Iron Catalyst. *J Am Chem Soc* **2014**, *136* (29), 10234–10237. <https://doi.org/10.1021/ja505241x>.
- 21 Mellone, I.; Gorgas, N.; Bertini, F.; Peruzzini, M.; Kirchner, K.; Gonsalvi, L. Selective Formic Acid Dehydrogenation Catalyzed by Fe-PNP Pincer Complexes Based on the 2,6-Diaminopyridine Scaffold. *Organometallics* **2016**, *35* (19), 3344–3349. <https://doi.org/10.1021/acs.organomet.6b00551>.
- 22 Curley, J. B.; Smith, N. E.; Bernskoetter, W. H.; Hazari, N.; Mercado, B. Q. Catalytic Formic Acid Dehydrogenation and CO₂ Hydrogenation Using Iron PNP Pincer Complexes with Isonitrile Ligands. *Organometallics* **2018**, *37* (21), 3846–3853. <https://doi.org/10.1021/acs.organomet.8b00534>.
- 23 Curley, J. B.; Bernskoetter, W. H.; Hazari, N. Additive-Free Formic Acid Dehydrogenation Using a Pincer-Supported Iron Catalyst. *ChemCatChem* **2020**, *12* (7), 1934–1938. <https://doi.org/10.1002/cctc.202000066>.
- 24 Pandey, B.; Krause, J. A.; Guan, H. Methyl Effects on the Stereochemistry and Reactivity of PPP-Ligated Iron Hydride Complexes. *Inorg Chem* **2023**, *62* (2), 967–978. <https://doi.org/10.1021/acs.inorgchem.2c03803>.
- 25 Pandey, B.; Krause, J. A.; Guan, H. On the Demise of PPP-Ligated Iron Catalysts in the Formic Acid Dehydrogenation Reaction. *Inorg Chem* **2023**, *62* (45), 18714–18723. <https://doi.org/10.1021/acs.inorgchem.3c03125>.
- 26 Kuriyama, S.; Kato, T.; Tanaka, H.; Konomi, A.; Yoshizawa, K.; Nishibayashi, Y. Catalytic Reduction of Dinitrogen to Ammonia and Hydrazine Using Iron–Dinitrogen Complexes Bearing Anionic Benzene-Based PCP-Type Pincer Ligands. *Bull Chem Soc Jpn* **2022**, *95* (4), 683–692. <https://doi.org/10.1246/bcsj.20220048>.
- 27 Nakajima, Y.; Shimada, S. Hydrosilylation Reaction of Olefins: Recent Advances and Perspectives. *RSC Adv* **2015**, *5* (26), 20603–20616. <https://doi.org/10.1039/C4RA17281G>.
- 28 Sommer, L. H.; Pietrusza, E. W.; Whitmore, F. C. PEROXIDE-CATALYZED ADDITION OF TRICHLOROSILANE TO 1-OCTENE. *J Am Chem Soc* **1947**, *69* (1), 188. <https://doi.org/10.1021/ja01193a508>.
- 29 Speier, J. L.; Webster, J. A.; Barnes, G. H. The Addition of Silicon Hydrides to Olefinic Double Bonds. Part II. The Use of Group VIII Metal Catalysts. *J Am Chem Soc* **1957**, *79* (4), 974–979. <https://doi.org/10.1021/ja01561a054>.

- 30 Karstedt, B. D. Platinum Complexes of Unsaturated Siloxanes and Platinum Containing Organopolysiloxanes. US3775452A, 1973.
- 31 Obligacion, J. V.; Chirik, P. J. Earth-Abundant Transition Metal Catalysts for Alkene Hydrosilylation and Hydroboration. *Nat Rev Chem* **2018**, 2 (5), 15–34. <https://doi.org/10.1038/s41570-018-0001-2>.
- 32 Nihala, R.; Hisana, K. N.; Afsina, C. M. A.; Anilkumar, G. Applications of Iron Pincer Complexes in Hydrosilylation Reactions. *RSC Adv* **2022**, 12 (37), 24339–24361. <https://doi.org/10.1039/D2RA04239H>.
- 33 Chalk, A. J.; Harrod, J. F. Homogeneous Catalysis. II. The Mechanism of the Hydrosilation of Olefins Catalyzed by Group VIII Metal Complexes¹. *J Am Chem Soc* **1965**, 87 (1), 16–21. <https://doi.org/10.1021/ja01079a004>.
- 34 McGrady, G. S.; Sirsch, P.; Chatterton, N. P.; Ostermann, A.; Gatti, C.; Altmannshofer, S.; Herz, V.; Eickerling, G.; Scherer, W. Nature of the Bonding in Metal-Silane σ -Complexes. *Inorg Chem* **2009**, 48 (4), 1588–1598. <https://doi.org/10.1021/ic8019777>.
- 35 Corey, J. Y. Reactions of Hydrosilanes with Transition Metal Complexes. *Chem Rev* **2016**, 116 (19), 11291–11435. <https://doi.org/10.1021/acs.chemrev.5b00559>.
- 36 Nikonov, G. I. Recent Advances in Nonclassical Interligand Si...H Interactions. *Advances in Organometallic Chemistry*. 2005, pp 217–309. [https://doi.org/10.1016/S0065-3055\(05\)53006-5](https://doi.org/10.1016/S0065-3055(05)53006-5).
- 37 Waterman, R. σ -Bond Metathesis: A 30-Year Retrospective. *Organometallics* **2013**, 32 (24), 7249–7263. <https://doi.org/10.1021/om400760k>.
- 38 Perutz, R. N.; Sabo-Etienne, S. The σ -CAM Mechanism: σ Complexes as the Basis of σ -Bond Metathesis at Late-Transition-Metal Centers. *Angewandte Chemie International Edition* **2007**, 46 (15), 2578–2592. <https://doi.org/https://doi.org/10.1002/anie.200603224>.
- 39 Crabtree, R. H. Transition Metal Complexation of σ Bonds. *Angewandte Chemie International Edition in English* **1993**, 32 (6), 789–805. <https://doi.org/https://doi.org/10.1002/anie.199307891>.
- 40 Luo, X.-L.; Crabtree, R. H. Synthesis and Spectroscopic Characterization of [ReH₅(Triphos)] and [ReH₆(Triphos)]+[Triphos = PPh(CH₂CH₂PPh₂)₂]. *Journal of the Chemical Society, Dalton Transactions* **1991**, No. S, 587–590. <https://doi.org/10.1039/DT9910000587>.
- 41 Perutz, R. N.; Sabo-Etienne, S.; Weller, A. S. Metathesis by Partner Interchange in σ -Bond Ligands: Expanding Applications of the σ -CAM Mechanism. *Angewandte*

- Chemie International Edition* **2022**, *61* (5), e202111462. <https://doi.org/https://doi.org/10.1002/anie.202111462>.
- 42 Atheaux, I.; Delpech, F.; Donnadieu, B.; Sabo-Etienne, S.; Chaudret, B.; Hussein, K.; Barthelat, J. C.; Braun, T.; Duckett, S. B.; Perutz, R. N. Exchange Processes in Complexes with Two Ruthenium (H₂-Silane) Linkages: Role of the Secondary Interactions between Silicon and Hydrogen Atoms. *Organometallics* **2002**, *21* (24), 5347–5357. <https://doi.org/10.1021/om0206148>.
- 43 Hussein, K.; J. Marsden, C.; Barthelat, J.-C.; Rodriguez, V.; Conejero, S.; Sabo-Etienne, S.; Donnadieu, B.; Chaudret, B. X-Ray Structure and Theoretical Studies of RuH₂(H₂-H₂)(H₂-H-SiPh₃)(PCy₃)₂, a Complex with Two Different H₂-Coordinated σ Bonds. *Chemical Communications* **1999**, No. 14, 1315–1316. <https://doi.org/10.1039/A901558B>.
- 44 Delpech, F.; Sabo-Etienne, S.; Daran, J.-C.; Chaudret, B.; Hussein, K.; Marsden, C. J.; Barthelat, J.-C. Ruthenium Complexes Containing Two Ru–(H₂-Si-H) Bonds: Synthesis, Spectroscopic Properties, Structural Data, Theoretical Calculations, and Reactivity Studies. *J Am Chem Soc* **1999**, *121* (28), 6668–6682. <https://doi.org/10.1021/ja990199j>.
- 45 Scherer, W.; Meixner, P.; Barquera-Lozada, J. E.; Hauf, C.; Obenhuber, A.; Brück, A.; Wolstenholme, D. J.; Ruhland, K.; Leusser, D.; Stalke, D. A Unifying Bonding Concept for Metal Hydrosilane Complexes. *Angewandte Chemie International Edition* **2013**, *52* (23), 6092–6096. <https://doi.org/https://doi.org/10.1002/anie.201210224>.
- 46 Ignatov, S. K.; Rees, N. H.; Tyrrell, B. R.; Dubberley, S. R.; Razuvaev, A. G.; Mountford, P.; Nikonov, G. I. Nonclassical Titanocene Silyl Hydrides. *Chemistry – A European Journal* **2004**, *10* (20), 4991–4999. <https://doi.org/https://doi.org/10.1002/chem.200400230>.
- 47 Kawachi, A.; Tanaka, Y.; Tamao, K. Synthesis and Structures of Tris[2-(Dimethylamino)Phenyl]Silane and -Germane Compounds. *Organometallics* **1997**, *16* (23), 5102–5107. <https://doi.org/10.1021/om970548n>.
- 48 Lachaize, S.; Sabo-Etienne, S. σ -Silane Ruthenium Complexes: The Crucial Role of Secondary Interactions. *Eur J Inorg Chem* **2006**, *2006* (11), 2115–2127. <https://doi.org/https://doi.org/10.1002/ejic.200600151>.
- 49 Nesmeyanov, A. N.; Freidlina, R. Kh.; Chukovskaya, E. C.; Petrova, R. G.; Belyavsky, A. B. Addition, Substitution, and Telomerization Reactions of Olefins in the Presence

- of Metal Carbonyls or Colloidal Iron. *Tetrahedron* **1962**, *17* (1), 61–68. [https://doi.org/https://doi.org/10.1016/S0040-4020\(01\)99004-0](https://doi.org/https://doi.org/10.1016/S0040-4020(01)99004-0).
- 50 A. Schroeder, M.; S. Wrighton, M. Pentacarbonyliron(0) Photocatalyzed Reactions of Trialkylsilanes with Alkenes. *J Organomet Chem* **1977**, *128* (3), 345–358. [https://doi.org/https://doi.org/10.1016/S0022-328X\(00\)92207-1](https://doi.org/https://doi.org/10.1016/S0022-328X(00)92207-1).
- 51 Mitchener, J. C.; Wrighton, M. S. Photogeneration of Very Active Homogeneous Catalysts Using Laser Light Excitation of Iron Carbonyl Precursors. *J Am Chem Soc* **1981**, *103* (4), 975–977. <https://doi.org/10.1021/ja00394a060>.
- 52 Small, B. L.; Brookhart, M.; Bennett, A. M. A. Highly Active Iron and Cobalt Catalysts for the Polymerization of Ethylene. *J Am Chem Soc* **1998**, *120* (16), 4049–4050. <https://doi.org/10.1021/ja9802100>.
- 53 Bart, S. C.; Lobkovsky, E.; Chirik, P. J. Preparation and Molecular and Electronic Structures of Iron(0) Dinitrogen and Silane Complexes and Their Application to Catalytic Hydrogenation and Hydrosilation. *J Am Chem Soc* **2004**, *126* (42), 13794–13807. <https://doi.org/10.1021/ja046753t>.
- 54 Stieber, S. C. E.; Milsman, C.; Hoyt, J. M.; Turner, Z. R.; Finkelstein, K. D.; Wieghardt, K.; Debeer, S.; Chirik, P. J. Bis(Imino)Pyridine Iron Dinitrogen Compounds Revisited: Differences in Electronic Structure between Four- and Five-Coordinate Derivatives. *Inorg Chem* **2012**, *51* (6), 3770–3785. <https://doi.org/10.1021/ic202750n>.
- 55 Tondreau, A. M.; Atienza, C. C. H.; Weller, K. J.; Nye, S. A.; Lewis, K. M.; Delis, J. G. P.; Chirik, P. J. Iron Catalysts for Selective Anti-Markovnikov Alkene Hydrosilylation Using Tertiary Silanes. *Science (1979)* **2012**, *335* (6068), 567–570. <https://doi.org/10.1126/science.1214451>.
- 56 Russell, S. K.; Darmon, J. M.; Lobkovsky, E.; Chirik, P. J. Synthesis of Aryl-Substituted Bis(Imino) Pyridine Iron Dinitrogen Complexes. *Inorg Chem* **2010**, *49* (6), 2782–2792. <https://doi.org/10.1021/ic902162z>.
- 57 Greenhalgh, M. D.; Thomas, S. P. Chemo-, Regio-, and Stereoselective Iron-Catalysed Hydroboration of Alkenes and Alkynes. *Chemical Communications* **2013**, *49* (95), 11230–11232. <https://doi.org/10.1039/C3CC46727A>.
- 58 Challinor, A. J.; Calin, M.; Nichol, G. S.; Carter, N. B.; Thomas, S. P. Amine-Activated Iron Catalysis: Air- and Moisture-Stable Alkene and Alkyne Hydrofunctionalization. *Adv Synth Catal* **2016**, *358* (15), 2404–2409. <https://doi.org/10.1002/adsc.201600570>.

- 59 Docherty, J. H.; Peng, J.; Dominey, A. P.; Thomas, S. P. Activation and Discovery of Earth-Abundant Metal Catalysts Using Sodium Tert-Butoxide. *Nat Chem* **2017**, *9* (6), 595–600. <https://doi.org/10.1038/nchem.2697>.
- 60 Tondreau, A. M.; Atienza, C. C. H.; Darmon, J. M.; Milsman, C.; Hoyt, H. M.; Weller, K. J.; Nye, S. A.; Lewis, K. M.; Boyer, J.; Delis, J. G. P.; Lobkovsky, E.; Chirik, P. J. Synthesis, Electronic Structure, and Alkene Hydrosilylation Activity of Terpyridine and Bis(Imino)Pyridine Iron Dialkyl Complexes. *Organometallics* **2012**, *31* (13), 4886–4893. <https://doi.org/10.1021/om3004527>.
- 61 Kamata, K.; Suzuki, A.; Nakai, Y.; Nakazawa, H. Catalytic Hydrosilylation of Alkenes by Iron Complexes Containing Terpyridine Derivatives as Ancillary Ligands. *Organometallics* **2012**, *31* (10), 3825–3828. <https://doi.org/10.1021/om300279t>.
- 62 Toya, Y.; Hayasaka, K.; Nakazawa, H. Hydrosilylation of Olefins Catalyzed by Iron Complexes Bearing Ketimine-Type Iminobipyridine Ligands. *Organometallics* **2017**, *36* (9), 1727–1735. <https://doi.org/10.1021/acs.organomet.7b00087>.
- 63 Trovitch, R. J.; Lobkovsky, E.; Chirik, P. J. Bis(Diisopropylphosphino)Pyridine Iron Dicarboxyl, Dihydride, and Silyl Hydride Complexes. *Inorg Chem* **2006**, *45* (18), 7252–7260. <https://doi.org/10.1021/ic0608647>.
- 64 Peng, D.; Zhang, Y.; Du, X.; Zhang, L.; Leng, X.; Walter, M. D.; Huang, Z. Phosphinite-Iminopyridine Iron Catalysts for Chemoselective Alkene Hydrosilylation. *J Am Chem Soc* **2013**, *135* (51), 19154–19166. <https://doi.org/10.1021/ja404963f>.
- 65 Du, X.; Zhang, Y.; Peng, D.; Huang, Z. Base-Metal-Catalyzed Regiodivergent Alkene Hydrosilylations. *Angewandte Chemie International Edition* **2016**, *55* (23), 6671–6675. <https://doi.org/10.1002/anie.201601197>.
- 66 Kamitani, M.; Kusaka, H.; Toriyabe, T.; Yuge, H. Facile Entry to Iron Complexes Supported by Quinoline-Based PNN Pincer Ligand. *Bull Chem Soc Jpn* **2018**, *91* (9), 1429–1435. <https://doi.org/10.1246/bcsj.20180124>.
- 67 Kamitani, M.; Kusaka, H.; Yuge, H. Iron-Catalyzed Versatile and Efficient C(Sp²)-H Borylation. *Chem Lett* **2019**, *48* (8), 898–901. <https://doi.org/10.1246/cl.190345>.
- 68 Pappas, I.; Treacy, S.; Chirik, P. J. Alkene Hydrosilylation Using Tertiary Silanes with α -Diimine Nickel Catalysts. Redox-Active Ligands Promote a Distinct Mechanistic Pathway from Platinum Catalysts. *ACS Catal* **2016**, *6* (7), 4105–4109. <https://doi.org/10.1021/acscatal.6b01134>.

- 69 Schuster, C. H.; Diao, T.; Pappas, I.; Chirik, P. J. Bench-Stable, Substrate-Activated Cobalt Carboxylate Pre-Catalysts for Alkene Hydrosilylation with Tertiary Silanes. *ACS Catal* **2016**, *6* (4), 2632–2636. <https://doi.org/10.1021/acscatal.6b00304>.
- 70 Kamitani, M.; Kusaka, H.; Yuge, H. Development of Activator-Free Iron Pincer Complexes for Alkene Hydrosilylation and Elucidation of Its Activation Mechanism. *Chem Lett* **2019**, *48* (10), 1196–1198. <https://doi.org/10.1246/cl.190521>.
- 71 Kamitani, M.; Yujiri, K.; Yuge, H. Hemisphere and Distance-Dependent Steric Analysis of PNN Iron Pincer Complexes Using SambVca 2.1 and Its Influence on Alkene Hydrosilylation. *Organometallics* **2020**, *39* (19), 3535–3539. <https://doi.org/10.1021/acs.organomet.0c00512>.
- 72 Zhang, L.; Zuo, Z.; Wan, X.; Huang, Z. Cobalt-Catalyzed Enantioselective Hydroboration of 1,1-Disubstituted Aryl Alkenes. *J Am Chem Soc* **2014**, *136* (44), 15501–15504. <https://doi.org/10.1021/ja5093908>.
- 73 Chen, J.; Cheng, B.; Cao, M.; Lu, Z. Iron-Catalyzed Asymmetric Hydrosilylation of 1,1-Disubstituted Alkenes. *Angewandte Chemie International Edition* **2015**, *54* (15), 4661–4664. <https://doi.org/https://doi.org/10.1002/anie.201411884>.
- 74 Sun, W.; Li, M.-P.; Li, L.-J.; Huang, Q.; Hu, M.-Y.; Zhu, S.-F. Phenanthroline-Imine Ligands for Iron-Catalyzed Alkene Hydrosilylation. *Chem Sci* **2022**, *13* (9), 2721–2728. <https://doi.org/10.1039/d1sc06727c>.
- 75 Buschbeck, R.; Low, P. J.; Lang, H. Homoleptic Transition Metal Acetylides. *Coord Chem Rev* **2011**, *255* (1), 241–272. <https://doi.org/https://doi.org/10.1016/j.ccr.2010.07.004>.
- 76 Lichtenberger, D. L.; Renshaw, S. K.; Bullock, R. M. Metal-Acetylide Bonding in $(\eta^5\text{-C}_5\text{H}_5)\text{Fe}(\text{CO})_2\text{C}\equiv\text{C}\cdot\text{R}$ Compounds. Measures of Metal-d.Pi.-Acetylide-Pi. Interactions from Photoelectron Spectroscopy. *J Am Chem Soc* **1993**, *115* (8), 3276–3285. <https://doi.org/10.1021/ja00061a028>.
- 77 McGrady, J. E.; Lovell, T.; Stranger, R.; Humphrey, M. G. Bonding of H1-Acetylide Ligands to Electron-Rich Ruthenium Centers: Can Electron-Withdrawing Ligands Induce Significant Metal-to-Ligand Back-Bonding? *Organometallics* **1997**, *16* (18), 4004–4011. <https://doi.org/10.1021/om970212d>.
- 78 Yang, E. S.; Combey, E.; Goicoechea, J. M. Putting Cyaphide in Its Place: Determining the Donor/Acceptor Properties of the KC-Cyaphido Ligand. *Chem Sci* **2023**, *14* (17), 4627–4632. <https://doi.org/10.1039/d3sc01126g>.

- 79 Rosenthal, U. Transition Metal Acetylides. In *Acetylene Chemistry*; 2004; pp 139–171. <https://doi.org/https://doi.org/10.1002/3527605487.ch4>.
- 80 Sasaki, Y.; Horita, Y.; Zhong, C.; Sawamura, M.; Ito, H. Copper(I)-Catalyzed Regioselective Monoborylation of 1,3-Enynes with an Internal Triple Bond: Selective Synthesis of 1,3-Dienylboronates and 3-Alkynylboronates. *Angewandte Chemie International Edition* **2011**, *50* (12), 2778–2782. <https://doi.org/https://doi.org/10.1002/anie.201007182>.
- 81 Zhou, H.; Moberg, C. Regio- and Stereoselective Hydrosilylation of 1,3-Enynes Catalyzed by Palladium. *Org Lett* **2013**, *15* (7), 1444–1447. <https://doi.org/10.1021/ol4001334>.
- 82 Daly, J. W.; Witkop, B.; Tokuyama, T.; Nishikawa, T.; Karle, I. L. Gephyrotoxins, Histrionicotoxins and Pumiliotoxins from the Neotropical Frog *Dendrobates histrionicus*. *Helv Chim Acta* **1977**, *60* (3), 1128–1140. <https://doi.org/https://doi.org/10.1002/hlca.19770600336>.
- 83 Leyden, J. Pharmacokinetics and Pharmacology of Terbinafine and Itraconazole. *J Am Acad Dermatol* **1998**, *38* (5, Supplement 2), S42–S47. [https://doi.org/https://doi.org/10.1016/S0190-9622\(98\)70483-9](https://doi.org/https://doi.org/10.1016/S0190-9622(98)70483-9).
- 84 Stork, G.; Zhao, K. Total Syntheses of (-)-Histrionicotoxin and (-)-Histrionicotoxin 235A. *J Am Chem Soc* **1990**, *112* (15), 5875–5876. <https://doi.org/10.1021/ja00171a035>.
- 85 Trost, B. M.; Masters, J. T. Transition Metal-Catalyzed Couplings of Alkynes to 1,3-Enynes: Modern Methods and Synthetic Applications. *Chem Soc Rev* **2016**, *45* (8), 2212–2238. <https://doi.org/10.1039/C5CS00892A>.
- 86 García-Garrido, S. E. Catalytic Dimerization of Alkynes. In *Modern Alkyne Chemistry*; 2014; pp 299–334. <https://doi.org/https://doi.org/10.1002/9783527677894.ch11>.
- 87 Weber, S. M.; Hilt, G. Late 3d Metal-Catalyzed (Cross-) Dimerization of Terminal and Internal Alkynes. *Front Chem* **2021**, *9*. <https://doi.org/10.3389/fchem.2021.635826>.
- 88 Liang, Q.; Hayashi, K.; Song, D. Catalytic Alkyne Dimerization without Noble Metals. *ACS Catal* **2020**, *10* (9), 4895–4905. <https://doi.org/10.1021/acscatal.0c00988>.
- 89 Weber, S.; Veiros, L. F.; Kirchner, K. Selective Manganese-Catalyzed Dimerization and Cross-Coupling of Terminal Alkynes. *ACS Catal* **2021**, *11* (11), 6474–6483. <https://doi.org/10.1021/acscatal.1c01137>.

- 90 Midya, G. C.; Paladhi, S.; Dhara, K.; Dash, J. Iron Catalyzed Highly Regioselective Dimerization of Terminal Aryl Alkynes. *Chemical Communications* **2011**, 47 (23), 6698–6700. <https://doi.org/10.1039/c1cc10346f>.
- 91 Midya, G. C.; Parasar, B.; Dhara, K.; Dash, J. Ligand Mediated Iron Catalyzed Dimerization of Terminal Aryl Alkynes: Scope and Limitations. *Org. Biomol. Chem.* **2014**, 12 (11), 1812–1822. <https://doi.org/10.1039/C3OB42365D>.
- 92 Xue, F.; Song, X.; Lin, T. T.; Munkerup, K.; Albawardi, S. F.; Huang, K. W.; Hor, T. S. A.; Zhao, J. Dimerization of Terminal Aryl Alkynes Catalyzed by Iron(II) Amine-Pyrazolyl Tripodal Complexes with E/ Z Selectivity Controlled by Tert-Butoxide. *ACS Omega* **2018**, 3 (5), 5071–5077. <https://doi.org/10.1021/acsomega.8b00539>.
- 93 Bhunia, M.; Sahoo, S. R.; Vijaykumar, G.; Adhikari, D.; Mandal, S. K. Cyclic (Alkyl)Amino Carbene Based Iron Catalyst for Regioselective Dimerization of Terminal Arylalkynes. *Organometallics* **2016**, 35 (21), 3775–3780. <https://doi.org/10.1021/acs.organomet.6b00703>.
- 94 Liang, Q.; Osten, K. M.; Song, D. Iron-Catalyzed Gem -Specific Dimerization of Terminal Alkynes . *Angewandte Chemie* **2017**, 129 (22), 6414–6417. <https://doi.org/10.1002/ange.201700904>.
- 95 Liang, Q.; Sheng, K.; Salmon, A.; Zhou, V. Y.; Song, D. Active Iron(II) Catalysts toward Gem-Specific Dimerization of Terminal Alkynes. *ACS Catal* **2019**, 9 (2), 810–818. <https://doi.org/10.1021/acscatal.8b03552>.
- 96 Liang, Q.; Hayashi, K.; Rabeda, K.; Jimenez-Santiago, J. L.; Song, D. Piano-Stool Iron Complexes as Precatalysts for Gem-Specific Dimerization of Terminal Alkynes. *Organometallics* **2020**, 39 (12), 2320–2326. <https://doi.org/10.1021/acs.organomet.0c00271>.
- 97 Rivada-Wheelaghan, O.; Chakraborty, S.; Shimon, L. J. W.; Ben-David, Y.; Milstein, D. Z-Selective (Cross-)Dimerization of Terminal Alkynes Catalyzed by an Iron Complex. *Angewandte Chemie International Edition* **2016**, 55 (24), 6942–6945. <https://doi.org/https://doi.org/10.1002/anie.201601382>.
- 98 Gorgas, N.; Alves, L. G.; Stöger, B.; Martins, A. M.; Veiros, L. F.; Kirchner, K. Stable, Yet Highly Reactive Nonclassical Iron(II) Polyhydride Pincer Complexes: Z-Selective Dimerization and Hydroboration of Terminal Alkynes. *J Am Chem Soc* **2017**, 139 (24), 8130–8133. <https://doi.org/10.1021/jacs.7b05051>.

- 99 Gorgas, N.; Stöger, B.; Veiros, L. F.; Kirchner, K. Iron(II) Bis(Acetylide) Complexes as Key Intermediates in the Catalytic Hydrofunctionalization of Terminal Alkynes. *ACS Catal* **2018**, 8 (9), 7973–7982. <https://doi.org/10.1021/acscatal.8b01942>.
- 100 Thompson, C. V.; Narro, A. L.; Arman, H. D.; Tonzetich, Z. J. Synthesis and Reactivity of Iron(II) Acetylide Complexes Relevant to Alkyne Dimerization. *Organometallics* **2022**, 41 (16), 2291–2300. <https://doi.org/10.1021/acs.organomet.2c00265>.
- 101 Garhwal, S.; Fridman, N.; de Ruiter, G. Z-Selective Alkyne Functionalization Catalyzed by a Trans-Dihydride N-Heterocyclic Carbene (NHC) Iron Complex. *Inorg Chem* **2020**, 59 (19), 13817–13821. <https://doi.org/10.1021/acs.inorgchem.0c02057>.
- 102 Stevens, J. E.; Miller, J. D.; Fitzsimmons, M. C.; Moore, C. E.; Thomas, C. M. Z-Selective Dimerization of Terminal Alkynes by a (PNNP)FeII Complex. *Chemical Communications* **2024**. <https://doi.org/10.1039/d4cc00469h>.
- 103 Smith, A. D.; Saini, A.; Singer, L. M.; Phadke, N.; Findlater, M. Synthesis, Characterization and Reactivity of Iron- and Cobalt-Pincer Complexes. *Polyhedron* **2016**, 114, 286–291. <https://doi.org/10.1016/j.poly.2015.12.037>.
- 104 Thompson, C. V.; Arman, H. D.; Tonzetich, Z. J. Square-Planar Iron(II) Silyl Complexes: Synthesis, Characterization, and Insertion Reactivity. *Organometallics* **2019**, 38 (15), 2979–2989. <https://doi.org/10.1021/acs.organomet.9b00335>.
- 105 Schubert, U. η -2 Coordination of Si–H σ Bonds to Transition Metals. In *Advances in Organometallic Chemistry*; Stone, F. G. A., West, R., Eds.; Academic Press, 1990; Vol. 30, pp 151–187.
- 106 Thomas, C. M.; Peters, J. C. An H₃-H₂SiR₂ Adduct of [$\{\text{PhB}(\text{CH}_2\text{PiPr}_2)_3\}\text{FeIIH}$]. *Angewandte Chemie - International Edition* **2006**, 45 (5), 776–780. <https://doi.org/10.1002/anie.200502527>.
- 107 Murphy, L. J.; Ferguson, M. J.; McDonald, R.; Lumsden, M. D.; Turculet, L. Synthesis of Bis(Phosphino)Silyl Pincer-Supported Iron Hydrides for the Catalytic Hydrogenation of Alkenes. *Organometallics* **2018**, 37 (24), 4814–4826. <https://doi.org/10.1021/acs.organomet.8b00807>.
- 108 Stevens, J. E.; Moore, C. E.; Thomas, C. M. Si-H Bond Activation and Dehydrogenative Coupling of Silanes across the Iron-Amide Bond of a Bis(Amido)Bis(Phosphine) Iron(II) Complex. *J Am Chem Soc* **2023**, 145 (2), 794–799. <https://doi.org/10.1021/jacs.2c12157>.

- 109 Freeman, S. T. N.; Petersen, J. L.; Lemke, F. R. The Chloride Effect: Structural Dependence of Ruthenium Silyl Complexes on Phosphorus and Silicon Substituents. *Organometallics* **2004**, *23* (5), 1153–1156. <https://doi.org/10.1021/om034226x>.
- 110 Thompson, C. V.; Arman, H. D.; Tonzetich, Z. J. Investigation of Iron Silyl Complexes as Active Species in the Catalytic Hydrosilylation of Aldehydes and Ketones. *Organometallics* **2022**, *41* (4), 430–440. <https://doi.org/10.1021/acs.organomet.1c00682>.
- 111 Bader, R. F. W. A Quantum Theory of Molecular Structure and Its Applications. *Chem Rev* **1991**, *91* (5), 893–928. <https://doi.org/10.1021/cr00005a013>.
- 112 Claisen, L. Über Umlagerung von Phenol-Allylthern in C-Allyl-Phenole. *Berichte der deutschen chemischen Gesellschaft* **1912**, *45* (3), 3157–3166. <https://doi.org/https://doi.org/10.1002/cber.19120450348>.
- 113 Gorgas, N.; Stadler, B.; White, A. J. P.; Crimmin, M. R. Vinylic C–H Activation of Styrenes by an Iron–Aluminum Complex. *J Am Chem Soc* **2024**, *146* (6), 4252–4259. <https://doi.org/10.1021/jacs.3c14281>.
- 114 Stoutland, P. O.; Bergman, R. G. Insertion of Iridium into the Carbon-Hydrogen Bonds of Alkenes: The π -Complex Cannot Be an Intermediate. *J Am Chem Soc* **1985**, *107* (15), 4581–4582. <https://doi.org/10.1021/ja00301a052>.
- 115 Stoutland, P. O.; Bergman, R. G. Carbon-Hydrogen Insertion and π -Complex Formation Reactions of $(\eta^5\text{-C}_5\text{Me}_5)(\text{PMe}_3)\text{Ir}$ with Ethylene: An Intra- and Intermolecular Isotope Effect Study. *J Am Chem Soc* **1988**, *110* (17), 5732–5744. <https://doi.org/10.1021/ja00225a025>.
- 116 Baker, M. V; Field, L. D. Reaction of Sp^2 Carbon-Hydrogen Bonds in Unactivated Alkenes with Bis(Diphosphine) Complexes of Iron. *J Am Chem Soc* **1986**, *108* (23), 7433–7434. <https://doi.org/10.1021/ja00283a062>.
- 117 Baker, M. V; Field, L. D. Reaction of Ethylene with a Coordinatively Unsaturated Iron Complex $\text{Fe}(\text{DEPE})_2$: Sp^2 Carbon-Hydrogen Bond Activation without Prior Formation of a π -Complex. *J Am Chem Soc* **1986**, *108* (23), 7436–7438. <https://doi.org/10.1021/ja00283a065>.
- 118 Glatz, M.; Gorgas, N.; Stöger, B.; Pittenauer, E.; Ferreira, L.; Veiros, L. F.; Calhorda, M. J.; Kirchner, K. Structural and Electronic Properties of Iron(0) PNP Pincer Complexes. *Z Anorg Allg Chem* **2021**, *647* (14), 1429–1435. <https://doi.org/https://doi.org/10.1002/zaac.202100015>.

- 119 Gorgas, N.; Stöger, B.; Veiros, L. F.; Kirchner, K. Highly Efficient and Selective Hydrogenation of Aldehydes: A Well-Defined Fe(II) Catalyst Exhibits Noble-Metal Activity. *ACS Catal* **2016**, 6 (4), 2664–2672. <https://doi.org/10.1021/acscatal.6b00436>.
- 120 Overend, J. The Equilibrium Bond Lengths in Acetylene and HCN. *Trans. Faraday Soc.* **1960**, 56 (0), 310–314. <https://doi.org/10.1039/TF9605600310>.
- 121 Babón, J. C.; Esteruelas, M. A.; López, A. M. Homogeneous Catalysis with Polyhydride Complexes. *Chem. Soc. Rev.* **2022**, 51 (23), 9717–9758. <https://doi.org/10.1039/D2CS00399F>.
- 122 Smith, N. E.; Bernskoetter, W. H.; Hazari, N.; Mercado, B. Q. Synthesis and Catalytic Activity of PNP-Supported Iron Complexes with Ancillary Isonitrile Ligands. *Organometallics* **2017**, 36 (20), 3995–4004. <https://doi.org/10.1021/acs.organomet.7b00602>.
- 123 Eisenstein, O.; Crabtree, R. H. Outer Sphere Hydrogenation Catalysis. *New J. Chem.* **2013**, 37 (1), 21–27. <https://doi.org/10.1039/C2NJ40659D>.
- 124 Bertini, F.; Gorgas, N.; Stöger, B.; Peruzzini, M.; Veiros, L. F.; Kirchner, K.; Gonsalvi, L. Efficient and Mild Carbon Dioxide Hydrogenation to Formate Catalyzed by Fe(II) Hydrido Carbonyl Complexes Bearing 2,6-(Diaminopyridyl)Diphosphine Pincer Ligands. *ACS Catal* **2016**, 6 (5), 2889–2893. <https://doi.org/10.1021/acscatal.6b00416>.
- 125 Nguyen, D. H.; Merel, D.; Merle, N.; Trivelli, X.; Capet, F.; Gauvin, R. M. Isonitrile Ruthenium and Iron PNP Complexes: Synthesis, Characterization and Catalytic Assessment for Base-Free Dehydrogenative Coupling of Alcohols. *Dalton Trans.* **2021**, 50 (29), 10067–10081. <https://doi.org/10.1039/D1DT01722E>.
- 126 Perrin, D. D.; Armarego, W. L. F. *Purification of Laboratory Chemicals*, 3rd ed.; Elsevier Science & Technology, 1988.
- 127 Glatz, M.; Holzhacker, C.; Bichler, B.; Mastalir, M.; Stöger, B.; Mereiter, K.; Weil, M.; Veiros, L. F.; Mösch-Zanetti, N. C.; Kirchner, K. FeII Carbonyl Complexes Featuring Small to Bulky PNP Pincer Ligands – Facile Substitution of K2P,N-Bound PNP Ligands by Carbon Monoxide. *Eur J Inorg Chem* **2015**, 2015 (30), 5053–5065. <https://doi.org/10.1002/ejic.201500646>.
- 128 STOE & Cie GmbH. X-Area 1.31.175.0, LANA 2.6.2.0. Darmstadt, Germany 2021.
- 129 Bruker AXS Inc. Bruker Computer Programs: APEX3, SAINT and SADABS. Madison, WI 2020.

- 130 Sheldrick, G. M. SHELXT – Integrated Space-Group and Crystal-Structure Determination. *Acta Crystallographica Section A* **2015**, *71* (1), 3–8. <https://doi.org/10.1107/S2053273314026370>.
- 131 Sheldrick, G. M. Crystal Structure Refinement with SHELXL. *Acta Crystallographica Section C* **2015**, *71* (1), 3–8. <https://doi.org/10.1107/S2053229614024218>.
- 132 Macrae, C. F.; Edgington, P. R.; McCabe, P.; Pidcock, E.; Shields, G. P.; Taylor, R.; Towler, M.; van de Streek, J. Mercury: Visualization and Analysis of Crystal Structures. *J Appl Crystallogr* **2006**, *39* (3), 453–457. <https://doi.org/10.1107/S002188980600731X>.

6. List of Abbreviations

Å	Ångström
Ar	aryl
ATR	attenuated total reflection
Cy	cyclohexyl
DFT	density functional theory
ee	enantiomeric excess
equiv.	equivalents
Et	ethyl
GC	gas chromatography
HMBC	heteronuclear multiple-bond correlation spectroscopy
HSQC	heteronuclear single quantum correlation
<i>i</i>Pr	<i>iso</i> -propyl
IR	infrared
KOtBu	potassium <i>tert</i> -butoxide
LiHMDS	lithium hexamethyldisilazide
Me	methyl
MeCN	acetonitrile
Mes	mesityl
MS	mass spectrometry
NaBEt₃H	sodium triethylborohydride
NaOtBu	sodium <i>tert</i> -butoxide
NHC	N-heterocyclic carbene

NMR	nuclear magnetic resonance
OTf	triflate
Ph	phenyl
ppm	parts per million
Pr	propyl
PTFE	polytetrafluoroethylene
py	pyridine
Pyr	pyrrole
QTAIM	quantum theory of atoms in molecules
r.t.	room temperature
<i>t</i>Bu	<i>tert</i> -butyl
<i>t</i>BuNC	<i>tert</i> -butylisocyanide
TEMPO	(2,2,6,6-Tetramethylpiperidin-1-yl)oxyl
THF	tetrahydrofuran
TMS	trimethylsilyl; tetramethylsilane
TOF	turnover frequency
TON	turnover number
UV	ultraviolet

7. Curriculum Vitae

Personal Data

Name: Wolfgang Eder

Date of Birth: [REDACTED]

Nationality: [REDACTED]

E-Mail: wolfgang.eder@tuwien.ac.at

ORCID-ID: 0000-0001-7494-1098

Education

November 2018 - present

PhD student at the Institute of Applied Synthetic Chemistry (IAS) *Vienna*
TU Wien, Vienna, Austria

May 2016 – November 2018

Master studies in technical chemistry at TU Wien graduated with distinction
Thesis title: *Base metal complexes with PCP pincer ligands, TU Wien,*
Vienna, Austria

September 2010 - May 2016

B.Sc. Technical Chemistry *TU Wien*
Vienna, Austria

September 2008 - September 2010

Diplomstudium Pharmazie
University of Vienna, Vienna, Austria

September 1999 - July 2007

Higher secondary school BG Tamsweg

Tamsweg, Austria

September 1995 - July 1999

Elementary School Mauterndorf

Mauterndorf, Austria

Experience**April 2023 - present**

Project assistant (FWF Österreich) at *TU Wien*

Vienna, Austria

April 2019 - April 2023

University Assistant for academic research and teaching in student laboratories

TU Wien, Vienna, Austria

March 2015 -January 2019

Tutor in synthetic chemistry student laboratory *TU*

Wien, Vienna, Austria

Languages

- German: Native
- English: Fluent
- Spanish: Intermediate
- French: Basic
- Japanese: Basic

Technical Skills

- **Laboratory** Extensive experience in synthesis of organic and organometallic compounds under air and moisture free conditions with Schlenk technique and glovebox; Catalytic Transformations including high pressure reactions; Characterization of organic and organometallic compounds *via* TLC, HPLC, GC, NMR (multinuclear spectroscopy and Evans method), IR, EPR, X-Ray single crystal analysis.
- **Computational** Extended experience in softwares needed for chemical research, including, ChemDraw, ChemDoodle, MestreNova, TopSpin, APEX II, ShelXle; Extended experience in Microsoft Office (Word, Excel, PowerPoint)

8. Published Papers and Conference Contributions

Stöger, B.; Weil, M.; Bichler, B.; Eder, W.; Kirchner, K. Crystal Structure of N,N'-Bis(Diisopropylphosphanyl)-4-Methylpyridine-2,6-Diamine. *Acta Crystallogr Sect E Struct Rep Online* **2014**, 70 (9). <https://doi.org/10.1107/S1600536814010976>.

Eder, W.; Stöger, B.; Kirchner, K. Synthesis and Characterization of Xylene-Based Group-Six Metal PCP Pincer Complexes. *Monatsh Chem* **2019**, 150 (7). <https://doi.org/10.1007/s00706-019-02422-6>.

Pecak, J.; Eder, W.; Stöger, B.; Realista, S.; Martinho, P. N.; Calhorda, M. J.; Linert, W.; Kirchner, K. Synthesis, Characterization, and Catalytic Reactivity of {CoNO}⁸PCP Pincer Complexes. *Organometallics* **2020**, 39 (14). <https://doi.org/10.1021/acs.organomet.0c00167>.

Eder, W.; Himmelbauer, D.; Stöger, B.; Veiros, L. F.; Pignitter, M.; Kirchner, K. Manganese and Iron PCP Pincer Complexes - The Influence of Sterics on Structure and Reactivity. *Dalton Transactions* **2021**, 50 (39). <https://doi.org/10.1039/d1dt02407h>.

Pecak, J.; Eder, W.; Tomsu, G.; Stöger, B.; Pignitter, M.; Kirchner, K. Synthesis and Characterization of Cobalt NCN Pincer Complexes. *Eur J Inorg Chem* **2021**, 2021 (41). <https://doi.org/10.1002/ejic.202100643>.

Schratzberger, H.; Himmelbauer, D.; Eder, W.; Weiser, M.; Stöger, B.; Kirchner, K. Solvothermal Synthesis of Cobalt PCP Pincer Complexes from $[\text{Co}_2(\text{CO})_8]$. *Monatsh Chem* **2023**, 154 (11). <https://doi.org/10.1007/s00706-023-03123-x>.

Käfer, M. G.; Eder, W.; Pecak, J.; Stöger, B.; Pignitter, M.; Veiros, L. F.; Kirchner, K. Cr(II) and Cr(III) NCN Pincer Complexes: Synthesis, Structure, and Catalytic Reactivity. *Monatsh Chem* **2023**, 154 (11). <https://doi.org/10.1007/s00706-023-03128-6>.

Oral Presentation: 10th Workshop Inorganic Chemistry in Graz, Austria “Synthesis of Group Six PCP Complexes via Oxidative Addition under Solvothermal Conditions” (2018)

Poster-Presentation: 28th International Conference of Organometallics Chemistry (ICOMC) in Florence, Italy “Synthesis of Novel Base Metal PCP Complexes under Solvothermal Conditions” (2018)

Poster-Presentation: 5th CHAOS-Meeting (COST, European Cooperation in Science and Technology) in Ayia Napa, Cyprus “Synthesis of Novel Base Metal PCP Complexes under Solvothermal Conditions” (2019)

Poster-Presentation: 18th Austrian Chemistry Days in Linz, Austria “Synthesis of Novel Base Metal PCP Complexes under Solvothermal Conditions” (2019)

Poster-Presentation: 44th International Conference on Coordination Chemistry (ICCC) in Rimini, Italy “Novel PNP Pincer Complexes for the Activation of Carbon Dioxide” (2022)

Poster-Presentation: Dalton 2023 in Coventry, UK “Novel PNP Pincer Complexes for the Activation of Carbon Dioxide” (2023)